NEDG-24817
ORNL/SUB-7537/14
Class I
~~December 1979~~
June 1980

SAFETY ANALYSIS OF THORIUM-BASED FUELS IN THE GENERAL ELECTRIC STANDARD BWR

PRINCIPAL AUTHORS

M. J. Colby
D. B. Townsend
C. L. Kunz

CONTRIBUTORS

R. J. Bodily
R. L. Crowther
K. M. Hu
R. B. Linford
G. N. Marrotte
G. A. Potts
S. H. Slivinsky
R. A. Wolters
S. Young

Approved: R. A. Wolters
R. A. Wolters, Manager
Special Nuclear Programs

Approved: R. L. Crowther
R. L. Crowther, Manager
Reactor Physics Technology

Report Prepared by

GENERAL ELECTRIC COMPANY
NUCLEAR ENGINEERING DIVISION
175 Curtner Avenue
San Jose, California 95125

for

OAK RIDGE NATIONAL LABORATORY
Oak Ridge, Tennessee 37830

Operated by

UNION CARBIDE CORPORATION

for the

DEPARTMENT OF ENERGY
CONTRACT NO. W-7405-eng-26

DISCLAIMER

NOTICE

This report was prepared by the General Electric Company under a subcontract with Union Carbide Corporation (No. 7537) for the account of DOE. No person acting on behalf of DOE, Union Carbide Corporation or General Electric Company will:

(1) Make any warranty or representation, express or implied, with respect to the accuracy, completeness, or usefulness of the information contained in this report, or that information, apparatus, method or process disclosed in this report may not infringe privately owned rights, or

(2) Assumes any liabilities with respect to the use of, or for damages resulting from the use of any information, apparatus, method, or process disclosed in this report.

This report was prepared as an account of work sponsored by an agency of the United States Government. Neither the United States Government nor any agency thereof, nor any of their employess, contractors, subcontractors, or their employees, makes any warranty, express or implied, nor assumes any legal liability of responsibility for any third party's use or the results of such use of any information, apparatus, product or process disclosed in this report, nor represents that its use by such third party would not infringe privately owned rights.

TABLE OF CONTENTS

TABLE OF CONTENTS (Continued)

TABLE OF CONTENTS (Continued)

LIST OF ILLUSTRATIONS

LIST OF ILLUSTRATIONS (Continued)

LIST OF ILLUSTRATIONS (Continued)

LIST OF ILLUSTRATIONS (Continued)

LIST OF TABLES

LIST OF TABLES (Continued)

ABSTRACT

A denatured (U-233/Th)O_2 fuel assembly has been designed which is energy equivalent to and hardware interchangeable with a modern boiling water reactor (BWR) reference reload assembly. Relative to the reference UO_2 fuel, the thorium fuel design shows better performance during normal and transient reactor operation for the BWR/6 product line and will meet or exceed current safety and licensing criteria. Power distributions are flattened and thermal operating margins are increased by reduced steam void reactivity coefficients caused by U-233. However, a (U-233/Th)O_2-fueled BWR will likely have reduced operating flexibility.

A (U-235/Th)O_2-fueled BWR should perform similar to a UO_2-fueled BWR under all operating conditions. A (Pu/Th)O_2-fueled BWR may have reduced thermal margins and similar accident response and be less stable than a UO_2-fueled BWR. The assessment is based on comparisons of point model and infinite lattice predictions of various nuclear reactivity parameters, including void reactivity coefficients, Doppler reactivity coefficients, and control blade worths.

The cost of a comprehensive program to implement thorium-based fuels in BWRs would range between 60 and 260 million dollars, depending on the amount of effort required for each phase of research, development and demonstration. The requirements would include Lead Test Assemblies with segmented rods for ramp testing, manufacturing development ($20 to $200M), nuclear measurements, licensing, and a full-scale demonstration of four successive reloads to measure core transient and pressure response.

ACKNOWLEDGMENT

The authors would like to express their deep appreciation to Miss Brenda J. LefFall for typing a difficult manuscript and incorporating numerous revisions.

1. INTRODUCTION, PURPOSE AND SCOPE

1.1 INTRODUCTION

As part of the Nonproliferation Alternative Systems Assessment Program (NASAP), alternate fuel cycles other than the present UO_2-based cycle are being evaluated for their nonproliferation potential. A list of alternative nuclear energy systems has been developed by the Department of Energy (DOE) based upon their potential to reduce the risk of proliferation and ability to use uranium resources more efficiently than the current light water once-through cycle. Systems having reduced proliferation risk are defined as those which do not permit access to clean, separated fissile material. Reliable and consistent information is required for these systems in order to perform a valid assessment of their comparative merits.

Thorium-based fuels offer potentially reduced proliferation risks. If the fissile U-233 material is diluted by adding large quantities of fertile U-238 (denaturing the fuel), then the U-233 cannot be chemically separated from the U-238. Furthermore, the use of thorium as a fertile material for the production of U-233 will enlarge the United States' domestic fissionable resources in light water reactor (LWR) spent fuel.

1.2 PURPOSE

The purpose of the work performed under this project is to develop a reliable data base on selected nuclear energy systems for use by DOE in comparative assessments and evaluations as part of the NASAP program. A large, 1200-MWe (net) BWR/6 plant has been chosen as the basis for these evaluations.

Practical implementation requirements and preliminary estimates of research, development, and demonstration (RD&D) requirements are presented for the thorium fuel cycle alternatives being evaluated. The primary effort is focused on the denatured (U-233+U-238)ThO_2 fuel cycle. Differential and less detailed studies also were performed for (Pu/Th)O_2 and (U-235/U-238/Th)O_2 fuels.

1.3 SCOPE

This effort is intended to assess the safety and licensability of LWRs loaded with the denatured (U-233/U-238/Th)O_2-based fuel type. Based on previous scoping studies[1,2] of both the denatured (U-235/U-238-Th)O_2 and (Pu/Th)O_2 fuel types, these two additional designs are evaluated to identify potential changes in plant characteristics and potential impact on safety and licensing characteristics. A conservative objective is to develop designs which minimize licensing requirements by making maximum use of existing technology and by minimizing performance differences relative to the large data base on UO_2 fuel and existing operational reactors.

Three dimensional, coupled nuclear-thermal-hydraulic fuel cycle methods[3] are used in the nuclear and core performance analyses. Fuel assembly design is performed with 98 group spectral determinations,[4] involving various one-dimensional integral transport theory corrected diffusion theory. Safety and transient analyses are carried out with standard methods[5,6,7] that have been approved by the Nuclear Regulatory Commission for boiling water reactor (BWR) application.

In evaluating the design and performance of the structures, systems and components of the plant from a licensing standpoint, the common types of anticipated operational occurrences, design basis accidents, and transients are considered. In addition to these evaluations, the results applicable to Section 15 of a Safety Analysis Report (SAR)[8] are presented in the Section 15 format as an Appendix.

2. SUMMARY AND CONCLUSIONS

A denatured (U-233/Th)O_2 fuel assembly has been designed which is energy equivalent to and hardware interchangeable with a BWR reference UO_2 reload fuel assembly. Relative to the reference UO_2 fuel, the thorium fuel design shows better performance during normal and transient reactor operation for the BWR/6 product line and will meet or exceed current safety and licensing criteria. However, uncertainties still remain in the basic nuclear data and material properites of thorium based fuels compared to the extensive data base available for uranium based fuels. Additional research will be required to reduce these uncertainties and demonstrate the validity of this program's results and conclusions. Required thorium nuclear data and material properties could be determined through a combination of Lead Test Assembly (LTA) and Segmented Rod Programs (SRPs) that would involve both nondestructive (gamma scans, eddy current, etc.) and destructive (power ramps, isotopics, etc.) testing. A critical assembly benchmark program also may be needed to reduce uncertainties in the basic nuclear properties of the particular U/Th fuel combinations utilized for design in the current study. Any such critical assembly program would probably include fuel rods of pure ThO_2 and various combinations of (U-233/U-238/Th)O_2 fashioned into critical configurations.

The denatured (U-233/Th)O_2 design reduces local peak-to-average power by 5%, reduces peak kw/ft by 10%, and increases minimum critical power ratio (MCPR) by 5% as compared to the UO_2 reload bundle. The (U-233/Th)O_2 design also improves cold shutdown margin by a factor of four and has an improved scram reactivity shape.

Analyses have shown that a denatured (U-233/Th)O_2-fueled BWR will meet or exceed design basis safety criteria for a loss-of-coolant-accident (LOCA), rod withdrawal error, and rod drop accident. Response to limiting abnormal operating trasients, including load rejection without bypass, feedwater controller failure, pressure regulator downscale failure, and loss of feedwater heater, is equal to or superior to that of the reference UO_2 BWR.

The only identified adverse impact of denatured (U-233/Th)O_2 fuel on the BWR is a reduction in operating flexibility. Indications are that a (U-233/Th)O_2-fueled BWR will have a flatter flow control line and reduced stability relative to the reference UO_2 plant. This will likely impact BWR load following and startup capabilities.

A qualitative assessment of the impact on BWR safety of a denatured (U-235/Th)O_2 fuel design has been made. The assessment is based on comparisons of point model and infinite lattice predictions of various nuclear reactivity parameters, including void reactivity coefficients, Doppler reactivity coefficients and control blade worths. Indications are that a (U-235/Th)O_2-fueled BWR should behave in a manner similar to the reference UO_2 BWR under normal, accident, and abnormal operating transient conditions. The (Pu/Th)O_2-fueled BWR will probably have reduced thermal margins, similar accident condition response, and poorer abnormal transient response than the reference UO_2 BWR. The impact of (Pu/Th)O_2 fuel on BWR stability could be important due to its significantly more negative dynamic void reactivity coefficient relative to the reference UO_2 design.

A summary of the major conclusions is given in Table 2-1.

Table 2-1

SUMMARY AND CONCLUSIONS

Denatured (U-233/Th)O_2 Fuel vs. BWR/6 UO_2 Design

BWR Operating Characteristics

- Reduces local peak-to-average by 5%
- Reduces peak kW/ft by 10%
- Increases MCPR margin by 5%
- Increases cold shutdown by a factor of 4
- Hardware interchangeable with standard UO_2 assembly
- Flatter flow control line reduces flexibility in load following

Accident Analyses

- Compliance to design basis LOCA
- Meets rod withdrawal error criteria
- Rod drop more favorable

Abnormal Operational Transients

- Within designed safety limit critical power ratio for limiting transients:
  - (a) Feedwater control failure
  - (b) Load rejection without bypass
  - (c) Pressure regulator downscale failure
  - (d) Loss of feedwater heater

BWR Stability

- Reduced, but controlled by restricting the flow control operating range

Denatured (U-235/Th)O_2 Fuel vs. Standard UO_2 - Qualitative Assessment

- Similar to reference UO_2 under normal, accident and abnormal operating transient conditions

(Pu/Th)O_2 Fuel vs. Standard UO_2 - Qualitative Assessment

- Significantly more negative dynamic void coefficient could cause major stability problems.
- Reduced thermal margins, similar accident condition response, poorer abnormal transient response

3. REFERENCE BWR/6 DESCRIPTION

3.1 GENERAL DESCRIPTION

The 748 bundle BWR/6 plant design[8] was selected for this study. General characteristics of the 3579 MWt/1200 MWe nuclear steam supply system (NSSS) are given in Table 3-1. The pressure vessel measures 238 inches across its ID and is designed to safely sustain a peak internal pressure of 1375 psig. The reactor pressure is nominally 1060 psig while the reactor is operating at 100% power (54.071 kW/l) and 100% flow (104×10^6 lb/hr).

3.2 CORE AND LATTICE DESIGN

The equilibrium reactor fuel core is loaded with 748 standard reload fuel assemblies. Each reload assembly consists of 55 low enriched $(U\text{-}235/U\text{-}238)O_2$ fuel rods, seven $(U\text{-}235/U\text{-}238)O_2\text{-}Gd_2O_3$ burnable poison rods, and two water rods fashioned into an 8x8 square array surrounded by a channel. The reactor core active fuel length is 150 inches, composed of 3.0 wt% U-235 bundle average enrichment for 138 inches and natural uranium on each end (6 inches).

3.3 FUEL CYCLE CHARACTERISTICS

Equilibrium fuel cycle characteristics were used for all evaluations in this study. The equilibrium fuel cycle is based on the reference UO_2 fuel shuffling and reload procedure. The plant is designed for an annual cycle with a 75% capacity factor and a 25% reload batch fraction. A typical equilibrium cycle end exposure is 16.5 GWd/MT (~15 GWd/ST).

Table 3-1

PLANT CHARACTERISTICS

Type	Standard BWR/6
No. of Fuel Bundles	748
Dimensions	238-inch reactor pressure vessel inside diameter
Rating	
Thermal	3579 MW
Electrical	1200 MW
Capacity Factor	75%
Reload Cycle	Annual
Power Density	54.071 kW/l
Reactor Pressure	1055 psia
Total Core Flow	104.0×10^6 lb/hr

4. ANALYSIS METHODS

4.1 LATTICE PHYSICS AND METHODS VERIFICATION

4.1.1 Lattice Physics

BWR lattice physics methods[4] consist of multigroup mixed one- and two-dimensional transport theory and transport corrected diffusion theory techniques. The epithermal spectrum is computed in 68 groups with determination of spatial weighting of the fuel, cladding, and moderator and evaluation of the two-dimensional Dancoff interaction between individual pins in the resolved resonance region. Resolved resonances are evaluated using the intermediate resonance (IR) approximation. The space-dependent thermal spectrum is computed by use of 30-group integral transport theory. Gadolinia rods are specially represented to include greater local spatial neutron spectrum detail and to permit space-dependent depletion calculations within the fuel pins.

4.1.2 Methods Verification

BWR reactor physics methods have been maintained with capability to predict fuel containing Th-232 and mixed Th-232/U-233 fertile materials. However, these methods and their current neutron cross-section libraries had not been benchmarked against available thorium lattice measurements. A few such benchmark comparisons[1] for simple geometry as well as benchmarks against full spectrum Monte Carlo predictions have been completed. These benchmark comparisons indicated that existing BWR lattice methods reasonably predict physical characteristics of uniform oxide lattices fueled with Th-232/U-235 and Th-232/U-233. However, the more complex thorium design lattices, particularly those utilizing rods containing ThO_2 in peripheral fuel rod positions and rods of Gadolinia, have unique physical characteristics. The ability to predict more complex design lattice characteristics was not confirmed by the uniform lattice benchmarks.

4.2 THREE-DIMENSIONAL BWR SIMULATOR

Core physics calculations were performed using a three-dimensional coupled nuclear-thermal-hydraulic simulator[3] which represents the BWR core exclusive of the external flow loop. The calculational model consists of coarse mesh, one group, static diffusion theory coupled to static parallel channel thermal-hydraulics. The simulator is used to predict detailed three-dimensional design thermal performance as a function of control rod position, refueling pattern, coolant flow, reactor pressure, and other operational and design variables.

4.3 THERMAL/MECHANICAL PERFORMANCE

The model[9] employed to determine the thermal/mechanical performance of the fuel designs incorporates the effects of fuel/cladding thermal expansion, fuel/cladding creep and fuel irradiation swelling, densification, relocation, and fission gas release as they affect pellet-cladding thermal conductance, fuel rod internal pressure, and pellet/cladding mechanical interaction. Including are the effects of fuel-cladding axial slip, cladding creepdown, clad irradiation growth, pellet and cladding plasticity, work hardening, creep and relaxation, and pellet hot pressing.

4.4 TRANSIENT MODELING (EXCEPT FOR LOSS OF FEEDWATER HEATER)

The transient performance model[6] consists of an integrated one-dimensional reactor core model which is coupled to the recirculation loop through the core exit pressure and core inlet flow. The core exit quality and pressure drop are computed by the core model, which, in turn, interacts with the loop parameters. The model also includes a nodalized description of the mass and momentum balances in the steamline and is capable of predicting the wave phenomenon present in the steamline during transients such as turbine trips.

Some of the significant features of the model include the following:

a. A one-dimensional 24 axial node kinetic model is assumed with reactivity feedbacks from control rods (absorption), voids (moderation), and Doppler (capture) effects.

b. At each axial location, the average fuel element is represented by seven cylindrical nodes encased in a cladding node. This element is used to represent core average power and fuel temperature conditions, providing the source of Doppler feedback.

c. Thirty-four primary system pressure nodes are simulated:

1. Upper plenum pressure
2. Vessel dome pressure
3. Eight steamline nodal pressures
4. Twenty-four reactor core nodal pressures

d. One-dimensional nuclear parameters are obtained from the steady-state three-dimensional BWR core simulator. Axial void variation is determined from multinodal transient core calculations. Heat fluxes are obtained from the average fuel temperature model and transient nuclear solution.

e. Principle controller functions such as feedwater flow, recirculation flow, reactor water level, pressure, and load demand are represented together with their dominant nonlinear characteristics.

f. The ability to simulate necessary reactor protection system functions is provided.

4.5 LOSS OF FEEDWATER HEATER (LFWH) TRANSIENT MODELING

The detailed, non-linear dynamic model[7] described below was used to evaluate the LFWH transient, because the one-dimensional transient model discussed in Section 4.3 is not essential to phenomologically simulate this event. Some of the significant features of the model include the following:

a. A point kinetic model is assumed with reactivity feedbacks from control rods (absorption), voids (moderation) and Doppler (capture) effects.

b. The fuel is represented by a four-node cylindrical element, enclosed in a cladding node. One cylindrical element is used to represent core average power and fuel temperature conditions, providing the source of Doppler feedback.

c. Four primary system pressure nodes are simulated:

1. Core average pressure

2. Vessel dome pressure

3. Steamline pressure (at a point representative of the relief/safety valve location)

4. Turbine inlet pressure

d. The active core void fraction is calculated from a relationship between core exit quality, inlet subcooling, and pressure. This relationship is generated from multinode core steady-state calculations. A second-order void dynamic model with the void boiling sweep time calculated as a function of core flow and void conditions is also utilized. Pressurization effects on void fraction are assumed to occur instantaneously.

e. Principal controller functions, such as feedwater flow, recirculation flow, reactor water level, pressure and load demand, are represented together with their dominant nonlinear characteristics.

f. The ability to simulate necessary reactor protection system functions is provided.

4.6 LOSS-OF-COOLANT SIMULATION

Loss-of-coolant calculations were performed using standard methods.[5] The methods utilize a multi-rod core model whose primary purpose is to analytically determine the transient response of the reactor core to a loss-of-coolant

accident (LOCA). In particular, the core temperatures and the extent of metal-water reaction are calculated. Secondary purposes of the program include correlation of core cooling system test data and calculation of core response to any power transient in which fuel heat generation rates and cladding-to-coolant heat transfer coefficients are known.

The following phenomena are considered:

a. Inter-rod and rod-to-channel thermal radiation
b. Metal-water reaction
c. Bundle dryout heat transfer
d. Core spray and/or flooding
e. Temperature dependence of material properties
f. Nucleate boiling and pool film boiling heat transfer
g. Gamma-smeared heat generation
h. Transient gap heat conductance
i. Fuel rod cladding swelling and rupture
j. Rod and channel wall wetting
k. Various types of fuel rod geometry and material

4.7 STABILITY MODELING

The mathematical model[10] representing the reactor core examines the linearized reactivity response of a reactor system with density-dependent reactivity feedback caused by hydraulics effects. In addition, the hydrodynamics of various hydraulically coupled reactor channels, or regions, are examined separately on an axially multi-noded basis by grouping various channels that are thermodynamically and hydraulically similar. This interchannel hydrodynamic interaction, or coupling, exists through pressure variations in the inlet pluenum, such as can be caused by disturbances in flow distribution between regions or channels. This approach provides a reasonably accurate, three-dimensional representation of the reactor's hydrodynamics and kinetics response.

5. THORIUM FUEL ASSEMBLY DESIGN

5.1 GENERAL DESCRIPTION

A denatured (U-233/Th)O_2 fuel assembly has been designed which is energy equivalent to and hardware interchangeable with the BWR reference UO_2 reload fuel assembly discussed in Section 3. The final design utilizes U-233 and Th-232 nuclear characteristics to increase thermal margins during normal, steady-state full power operation and expected accidents and transients, relative to the reference UO_2 fuel. Because of the reduced delayed neturon fraction of U-233, the thorium fuel design has a 9% more negative dynamic void reactivity coefficient. However, its dynamic Doppler coefficient is two to three times greater and its scram response is better; thus, the net effect on fast transients is an increase in the (U-233/Th)O_2 fuel design thermal margins, relative to the reference UO_2 reactor.

5.2 LATTICE DESIGN

The (U-233/Th)O_2 fuel assembly design shown in Figure 5-1 is identical in all respects to the reference UO_2 fuel assembly except for the composition of the fuel rods. The thorium bundle employs two water rods, as does the reference UO_2 design, but has one less burnable posion rod. Assembly fuel is composed of various concentrations of uranium in a thorium matrix. The uranium consists of 12 wt % U-233 to total uranium. The U/Th ratios are determined by the required fissile content necessary for each fuel rod type to maintain the maximum local peak-to-average power below the 1.13 limit.

5.3 NUCLEAR CHARACTERISTICS

Various nuclear parameters for the (U-233/Th)O_2 and reference UO_2 fuel assembly designs were determined using the standard nuclear design methods discussed in Subsections 4.1 and 4.2. Comparisons of the dynamic void and dynamic Doppler coefficients for the fuel designs are given in Table 5-1; advantages and disadvantages of the parameters are noted. These parameters directly impact accidents, abnormal transient responses, and BWR operability.

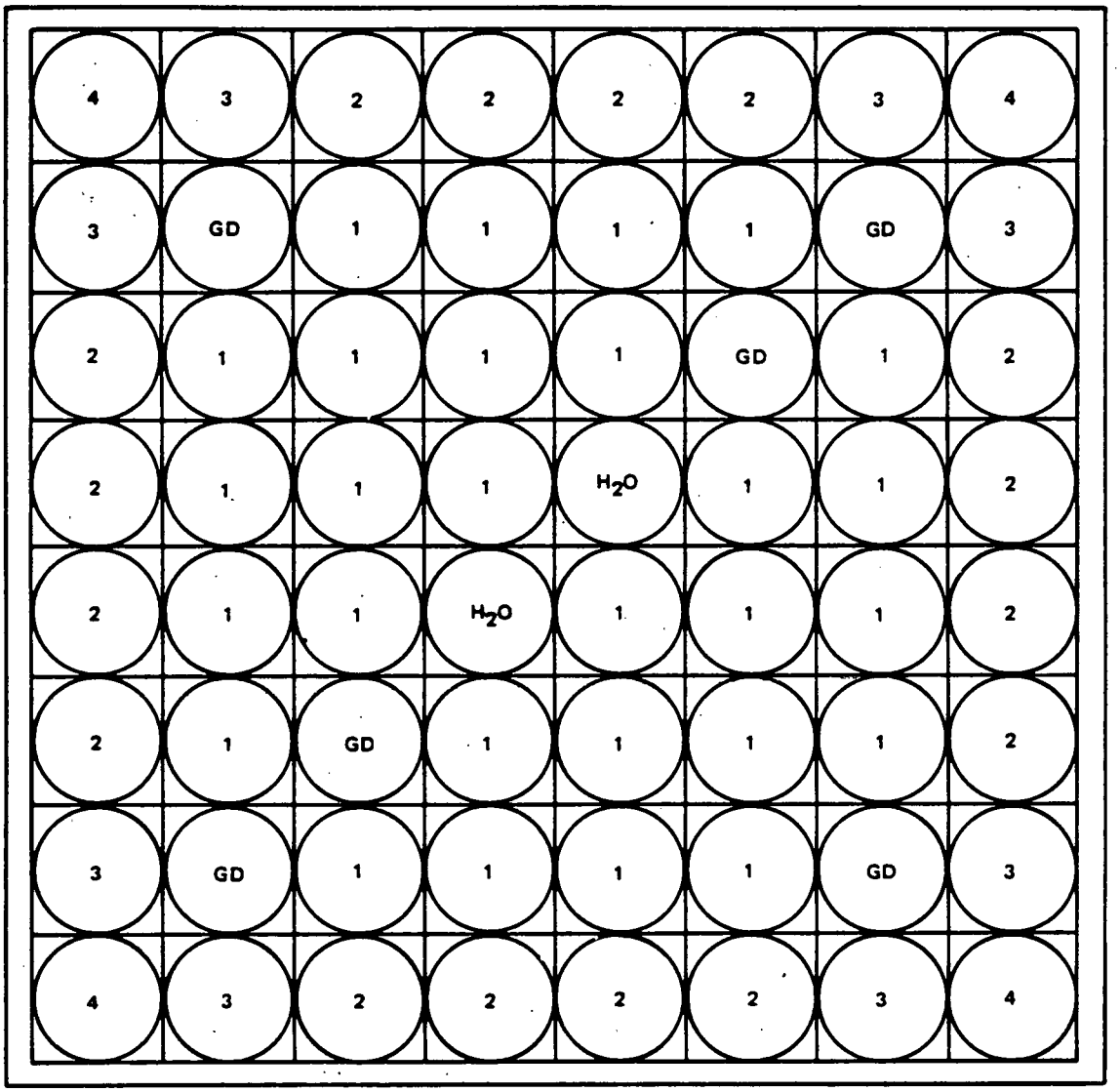

ROD ID	Wt% U	Wt% Th	Wt% FISSILE
1	27.8	72.2	3.34
2	21.5	78.5	2.58
3	20.2	79.8	2.42
4	16.6	83.4	1.99
Gd	20.9	76.1	2.51

Figure 5-1. Denatured U233/Th Fuel Assembly Design

Table 5-1

EQUILIBRIUM CYCLE DYNAMIC COEFFICIENTS*

	Reference UO_2	Denatured $(U\text{-}233/Th)O_2$	% Advantage Over UO_2 Fuel
Dynamic void coefficient, ¢/°C	-11	-12	-9
Dynamic Doppler coefficient, ¢/%V	-0.41	-0.87	112

*At core average voids.

The abnormal transients will result in the largest decrease in thermal and vessel overpressure margins if they occur at the end-of-equilibrium cycle (EOEC) and the most unstable reactor operating conditions occur where the dynamic void coefficient (DVC) assumes its maximum value. Therefore, important nuclear parameters were determined as functions of exposure during the equilibrium cycle for both fuels. Parameters for both fuels are compared at EOEC (16.5 GWd/MT) and the cycle maximum DVC for each fuel is determined.

5.3.1 Delayed Neutron Fraction

Figure 5-2 shows the variation of the core average delayed neutron fraction (β) as a function of exposure in the $(U\text{-}233/Th)O_2$ and reference UO_2 fuel bundles. The $(U\text{-}233/Th)O_2$ β value remains lower than the reference UO_2 β throughout the entire equilibrium cycle. The reference UO_2 fuel β decreases slightly with increasing exposure as Pu-239, which has a 0.003 β value as compared to the 0.006 U-235 β value, is generated by U-238 neutron capture and decay. However, the denatured thorium fuel's β, which is initially equal to 0.0032, remains at about that value as exposure increases since the main fissile products (U-233 and Pu-239) of fertile absorption in the fuel have similar delayed neutron fractions.

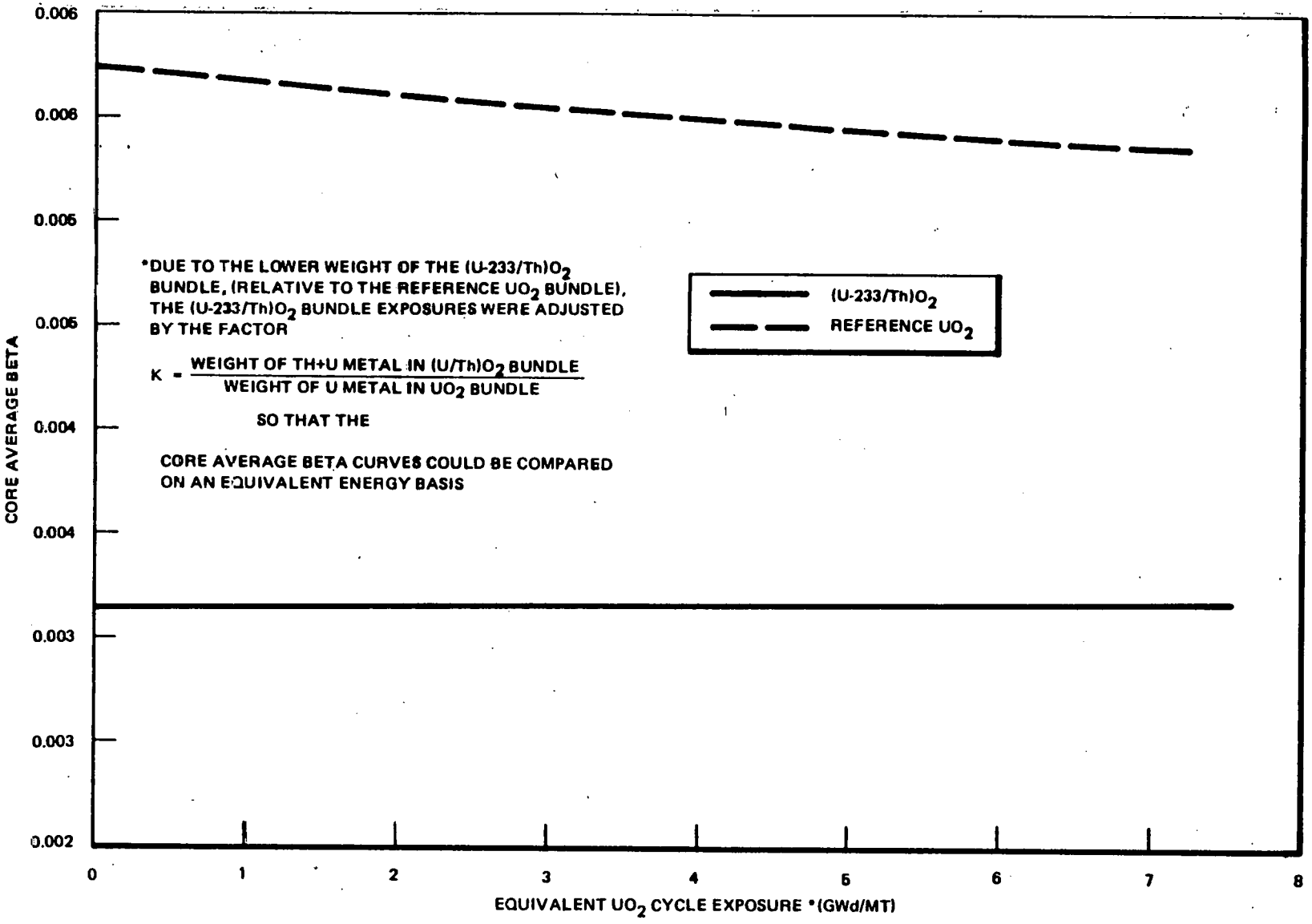

Figure 5-2. Equilibrium Cycle Core Average Beta

The thorium fuel's smaller β results in faster time response during reactivity insertions than for the reference UO_2 fuel. The smaller value creates a larger dynamic void coefficient and dynamic Doppler coefficient, relative to those for UO_2 fuel. These reactivity feedbacks determine the reactor power response to changes in reactor conditions, in the absence of scram reactivity. Also, the smaller β increases the speed and magnitude of scram reactivity insertions, as is shown by Figure 5-3.

The scram reactivity curves were generated at the all control blade out, EOEC, 100% power condition. This condition is chosen because it is the only point in the cycle when the reactor is critical with all blades removed and because the blades will be worth the least at this point. At time zero, a scram is initiated and all control blades are inserted at a specified rate with the scram worth being determined as $(\Delta k/k)/\beta$, where k is the effective neutron multiplication factor of the core. As seen in Figure 5-3, for the same core conditions and scram insertion rate, the $(U\text{-}233/Th)O_2$ has a substantially larger scram worth. This improved scram reactivity will result in improved transient performance for the $(U\text{-}233/Th)O_2$ design relative to that of the UO_2 design.

5.3.2 Steam Void Reactivity Coefficient

The steam void reactivity coefficient is defined as:

$$\text{Steam void coefficient} = \left(\frac{dk/k}{dv}\right) v$$

where:

$\left(\frac{dk/k}{dv}\right) v$ = net reactivity change per percent change in void fraction at void fraction, v;

v = void fraction, and

k = infinite lattice neutron multiplication factor.

The void coefficient is a measure of reactivity change due to void fraction change.

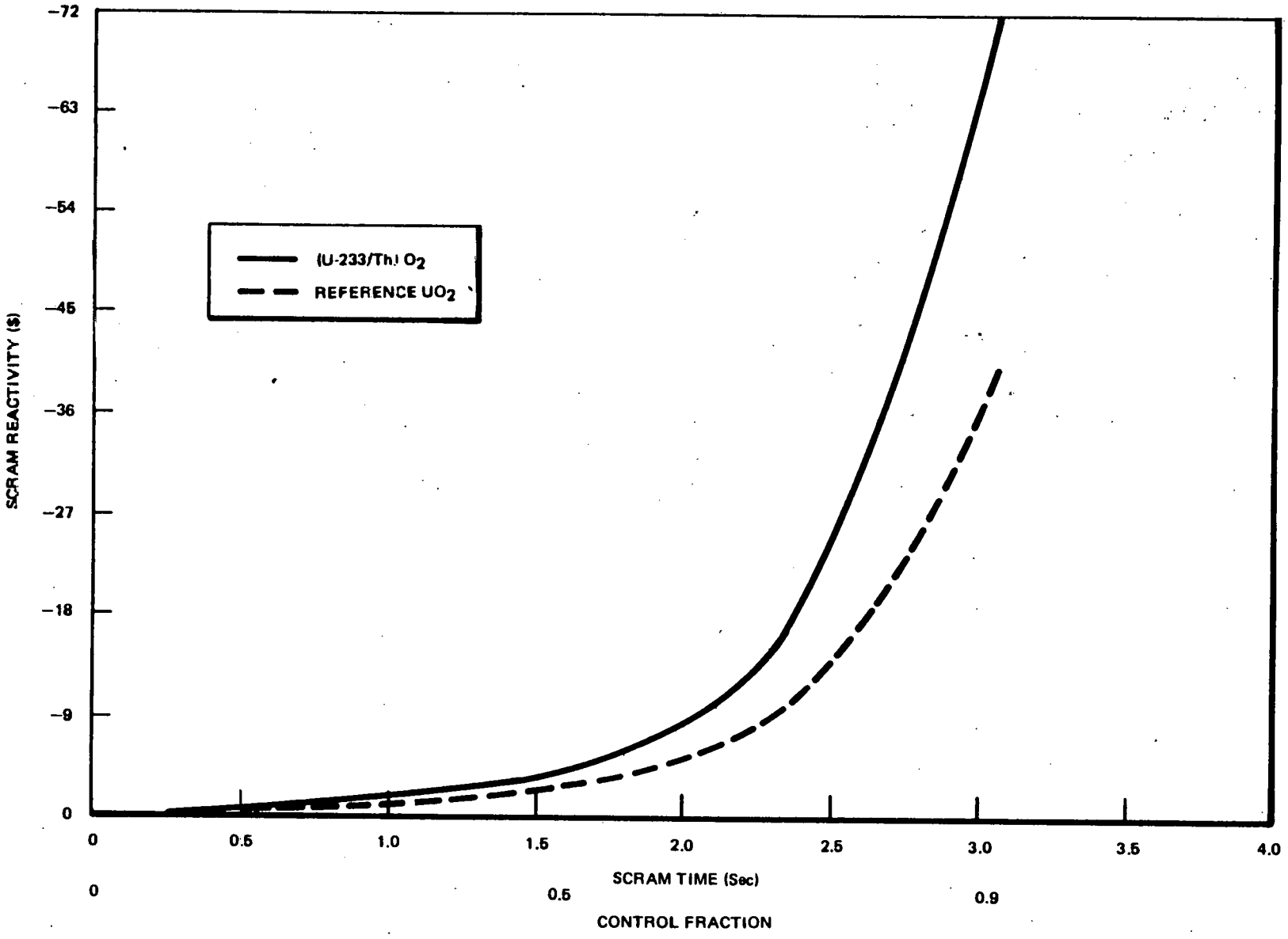

Figure 5-3. Scram Reactivity vs. Scram Time

Figure 5-4 gives the point model and three-dimensional steam void coefficients (SVCs) as a function of void fraction for both the (U-233/Th)O_2 and reference UO_2 fuels near the end of their respective equilibrium cycles (16.5 GWd/MT). The point model gives the relative dependence of the SVCs on voids while the three-dimensional values indicate magnitudes of the coefficients at core average voids. The thorium fuel power response is less dependent on steam void variations than that of the reference UO_2 fuel due to U-233's smaller thermal and larger intermediate fission cross-sections relative to U-235, shown in Table 5-2. Diminished void dependence flattens the axial power shape, reduces the local power peaking, and increases thermal margins relative to the reference UO_2-fueled reactor.

Figure 5-5 shows the variation of the SVCs of the two reactor fuels at 40% voids as a function of exposure during the equilibrium cycle. The (U-233/Th)O_2 fuel SVC remains approximately 40% below that of the reference UO_2 fuel during the equilibrium cycle.

Table 5-2
FISSILE MATERIAL PROPERTIES[11]

	U-233	U-235	PU-239	PU-241
Thermal (2200 m/s)				
σ_γ	47.7	98.6	269	369
σ_f	531	582	743	1009
ν	2.492	2.418	2.871	2.927
η	2.287	2.068	2.108	2.145
Epithermal				
I_γ	140	144	200	162
I_f	764	275	301	570
η	2.106	1.587	1.725	2.279
First level, ev	1.55	1.14	7.82	4.28

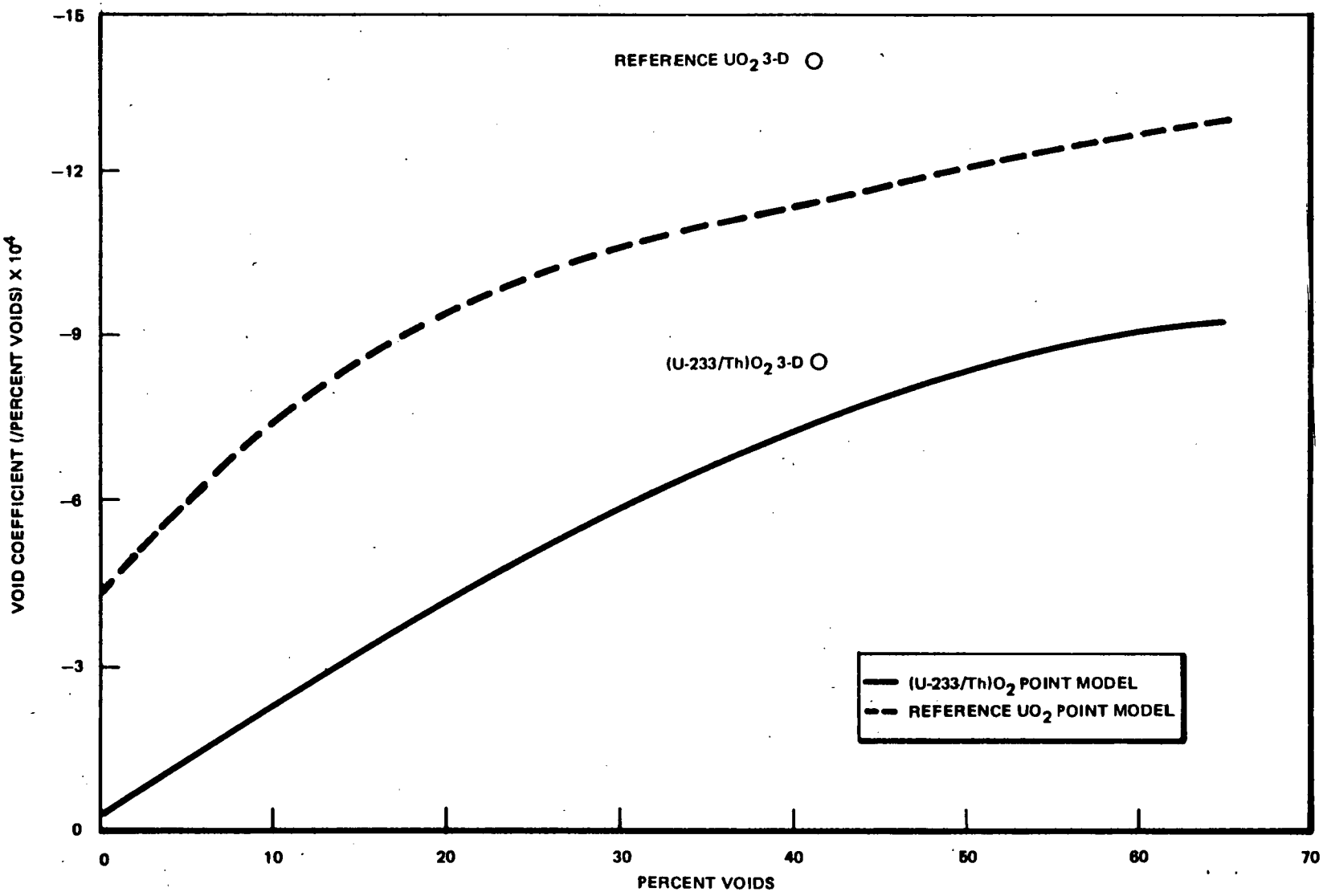

Figure 5-4. Steam Void Reactivity Coefficient versus Percent Voids at End of Equilibrium Cycle

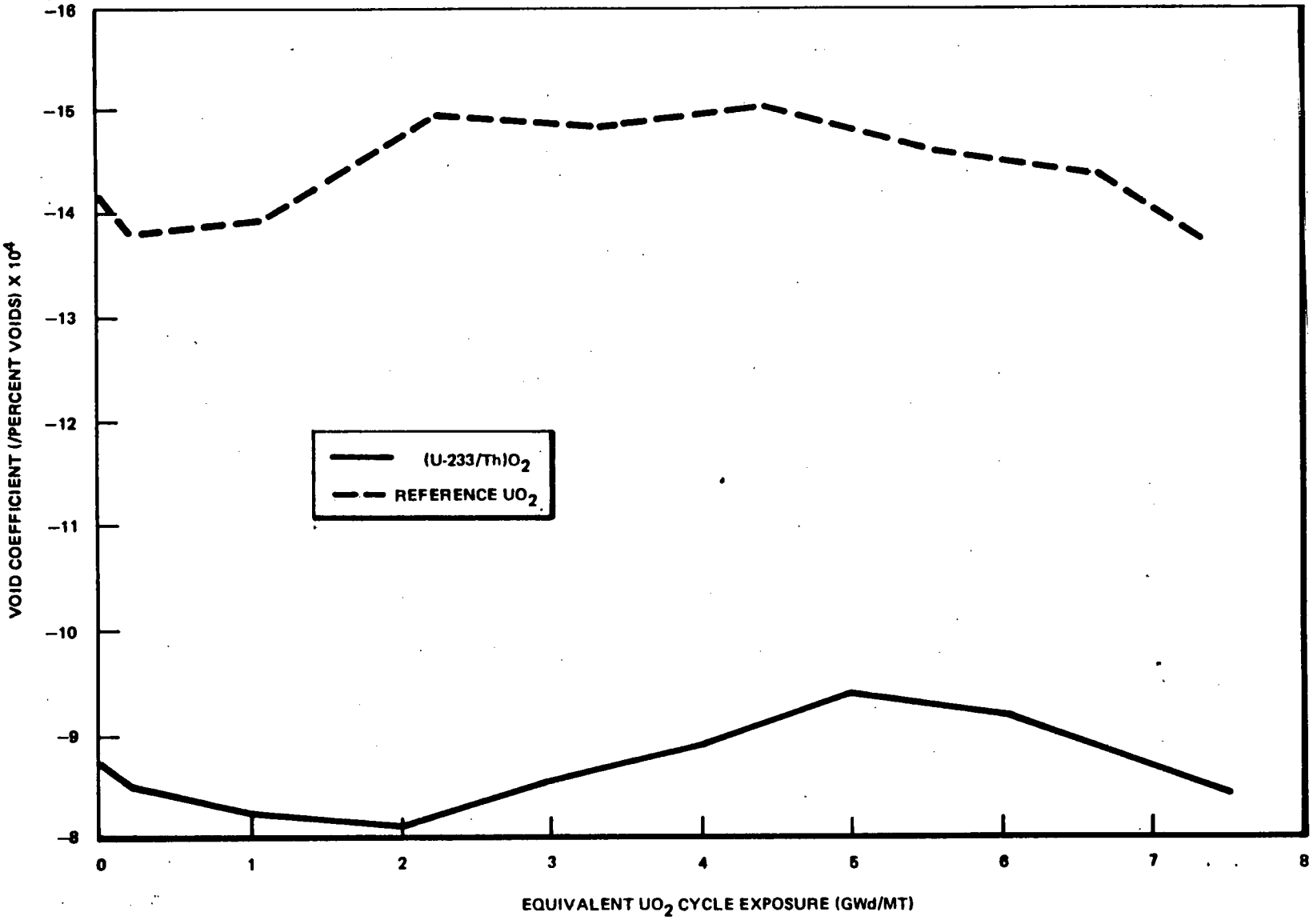

Figure 5-5. Equilibrium Cycle Steam Void Reactivity Coefficient at Core Average Voids

5.3.3 Dynamic Void Coefficient

The dynamic void coefficient of reactivity is defined as:

$$\text{Dynamic Void Coefficient} = \left(\frac{dk/k}{dv}\right)_v \times \frac{v}{\beta}$$

where

$\left(\frac{dk/k}{dv}\right)_v$ = net reactivity change per percent change in void fraction at void fraction, v;

v = void fraction;

β = effective delayed neutron fraction; and

k = infinite lattice neutron multiplication factor.

The dynamic void coefficient is a measure of reactivity change due to void fraction change. The effective delayed neutron fraction, β, is an important parameter influencing the magnitude of the dynamic void coefficient. By including β, the parameter also gives an indication of the speed of the system response due to a reactivity (void) perturbation.

The BWR operates in a partially voided condition with power increases tending to increase voids. Thus, a negative void reactivity coefficient is desirable for inherent limitation of power transients. The size of the void coefficient is nearly as important as its sign. It should be large and negative enough to quickly damp positive reactivity insertions and to provide inherent self-damping of spatial xenon perturbations. However, too large a negative dynamic void coefficient of reactivity can cause excessive power increases due to low probability, accident basis, pressure transients which reduce steam voids. Large negative dynamic void reactivity coefficients also can decrease reactor stability when the reactor is operating at natural circulation or near the bottom of the flow control range.

Figure 5-6 gives the point model and three-dimensional determination of the dynamic void coefficient (DVC) as a function of voids at the end of the

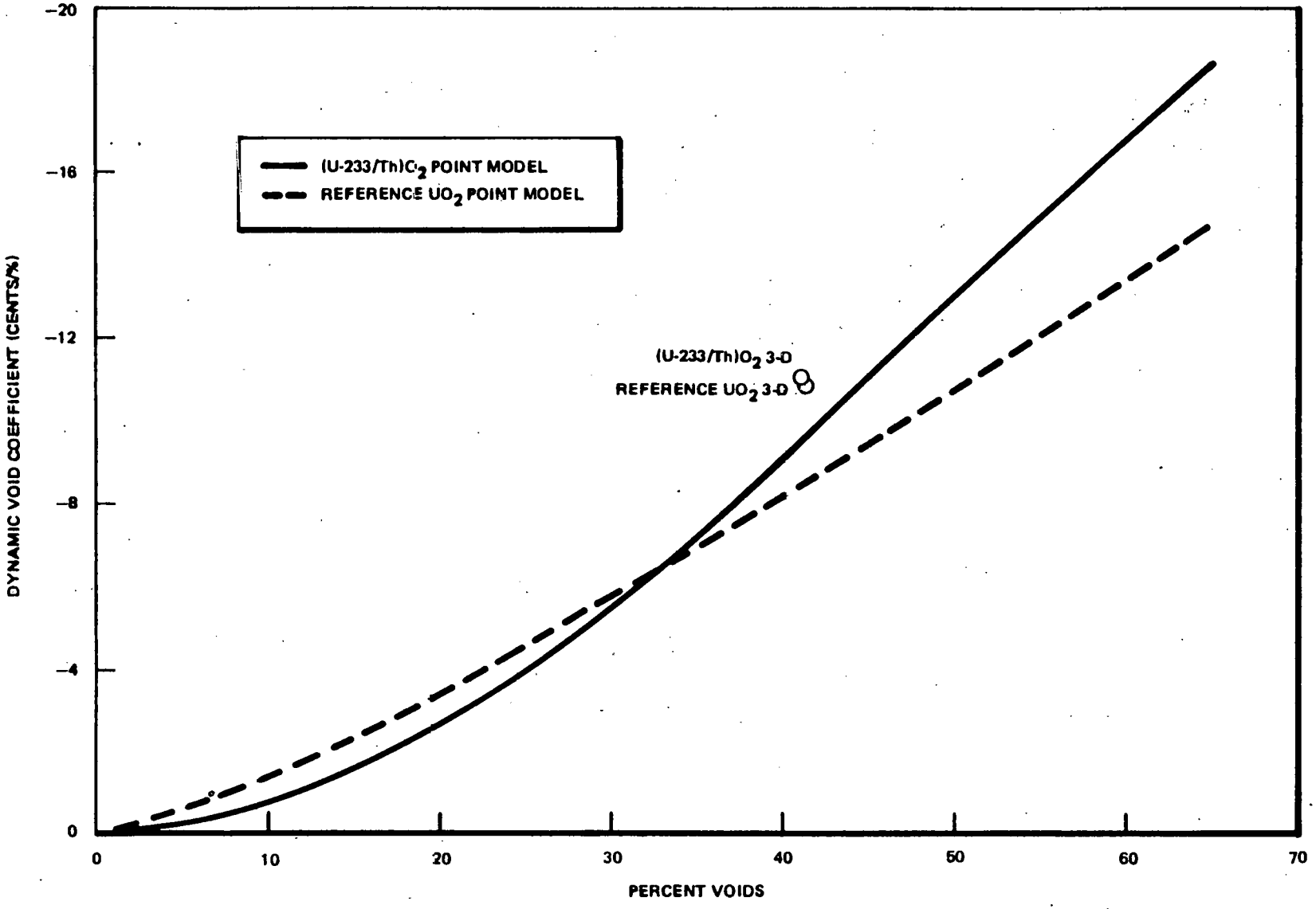

Figure 5-6. Dynamic Void Coefficient versus Percent Voids at End of Equilibrium Cycle

equilibrium cycle in the $(U\text{-}233/Th)O_2$ and UO_2 fuel designs. The DVC(E) is equal to SVC(E)V/β, thereby indicating the amount of reactivity that will be inserted per percent change in steam voids in each reactor. The thorium reactor DVC is -11¢/%V at 40% voids, it is 9% more negative than that of the reference UO_2 reactor and causes greater positive reactivity insertions due to void collapses and greater negative reactivity insertions due to void formations. Greater insertion of dynamic reactivity cause by void collapse in the $(U\text{-}233/Th)O_2$ reactor impacts transient responses while the magnitude affects reactor stability.

Figure 5-7 shows the variation of the point DVC as a function of exposure during the equilibrium cycle for the thorium and reference UO_2 fuels. The plots are used to determine the largest negative DVC for each fuel through the equilibrium cycle. The $(U\text{-}233/Th)O_2$ fuel's largest DVC is -12.5¢/%V as compared to the UO_2 DVC which is -11.5¢/%V. The maximum point DVCs are utilized in combination with the three-dimensional DVCs as input to core stability analyses.

5.3.4 Doppler Reactivity Coefficient and Dynamic Doppler Coefficient

The Doppler coefficient of reactivity is defined as:

$$\text{Doppler Coefficient} = \frac{dk}{dT}$$

where

k = infinite lattice neutron multiplication factor, and
T = fuel temperature.

The Doppler coefficient is a measure of reactivity change due to fuel temperature change.

The dynamic Doppler coefficient of reactivity is defined as:

$$\text{Dynamic Doppler Coefficient} = \frac{1}{k}\frac{dk}{dT} \times \frac{1}{\beta}$$

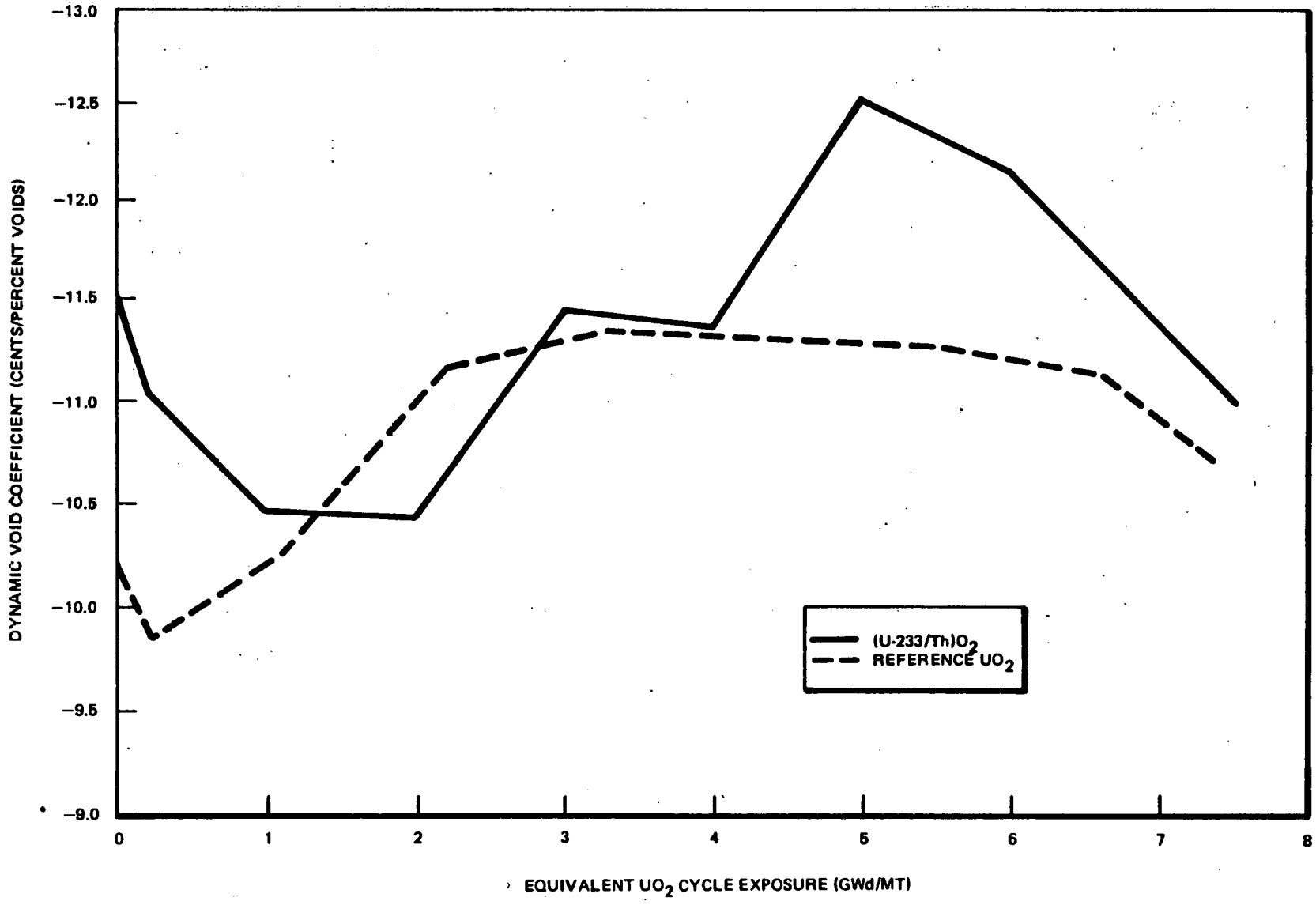

Figure 5-7. Equilibrium Cycle Dynamic Void Coefficient at Core Average Voids

where

k = infinite lattice neutron multiplication factor;
T = fuel temperature; and
β = effective delayed neutron fraction.

Because the dynamic Doppler feedback is prompt, a more negative Doppler feedback can offset the effects of a reduced delayed neutron fraction.

Figure 5-8 gives the Doppler reactivity coefficient (DC) for both the $(U\text{-}233/Th)O_2$ and reference UO_2 designs. The thorium DC is more negative for the full range of fuel temperatures observed by the fuel during normal and transient reactor operations. Thus, when the thorium DC is divided by β and k to obtain the dynamic Doppler coefficient (DDC) shown in Figure 5-9, the DDC becomes two to three times more negative than the reference UO_2 fuel design value.

Greater negative reactivity insertion, associated with the same fuel temperature increase in the thorium fuel as compared to the reference UO_2 fuel, favorably impacts accidents and abnormal transient responses. Relative to the reference UO_2 reactor, rod drop and rod withdrawal error accidents respectively result in less energy being deposited in the fuel and greater CPR margins, since the thorium reactor DDC will inhibit all power increases. Similarly, the thorium reactor power increase due to voids collapsing is mediated, relative to the reference UO_2 reactor, which in combination with improved scram response leads to increased CPR margins for all of the most limiting abnormal operational transients.

5.3.5 Reactor Prompt Period

Another parameter important to measuring relative core response is the infinite reactor prompt period. For an infinite reactor which is prompt critical, the reactor prompt period is given by:

$$T = \text{Reactor Prompt Period} = \frac{\ell^*}{\rho-\beta};\ \rho>\beta$$

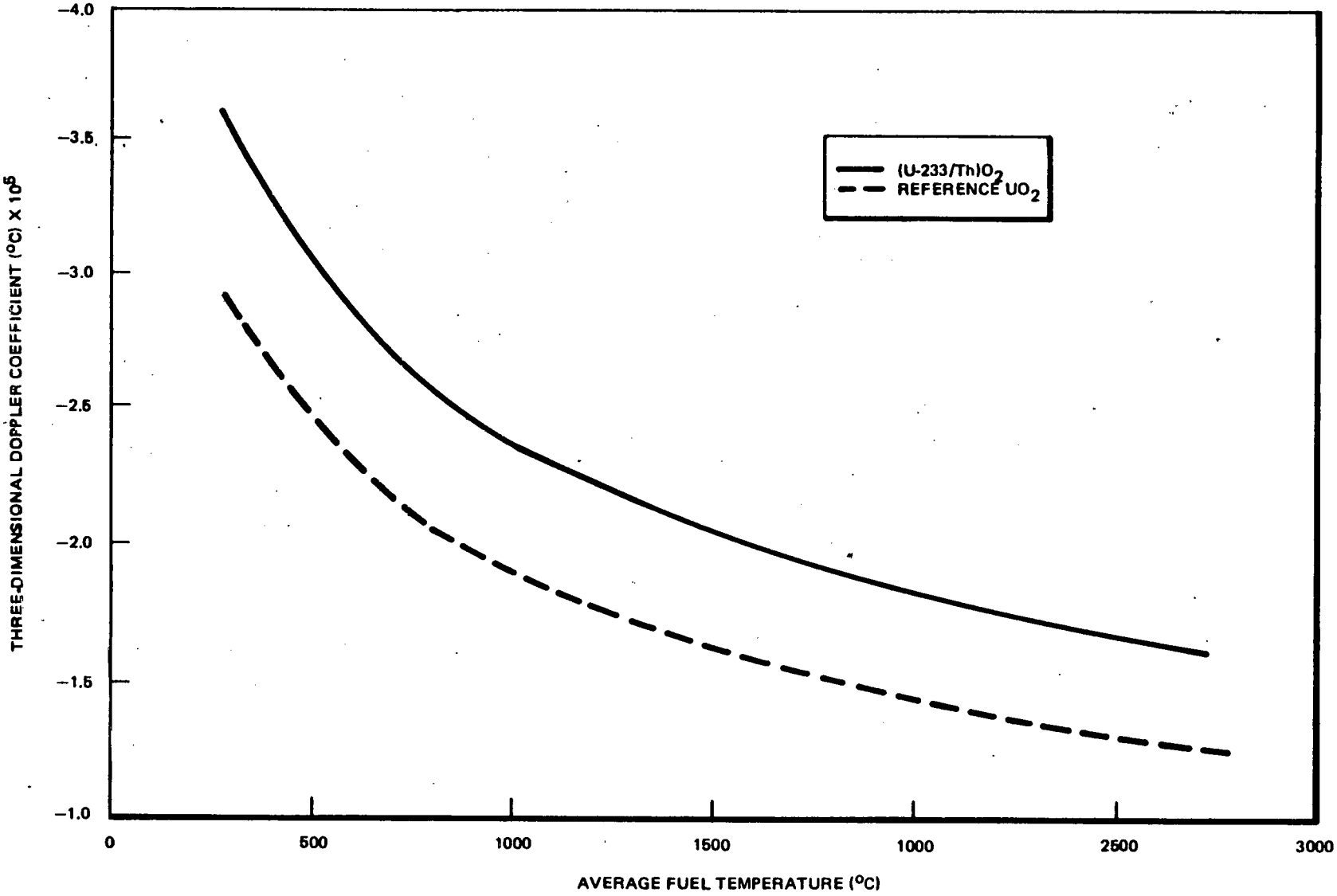

Figure 5-8. Three-Dimensional Doppler Coefficient versus Temperature at EOEC

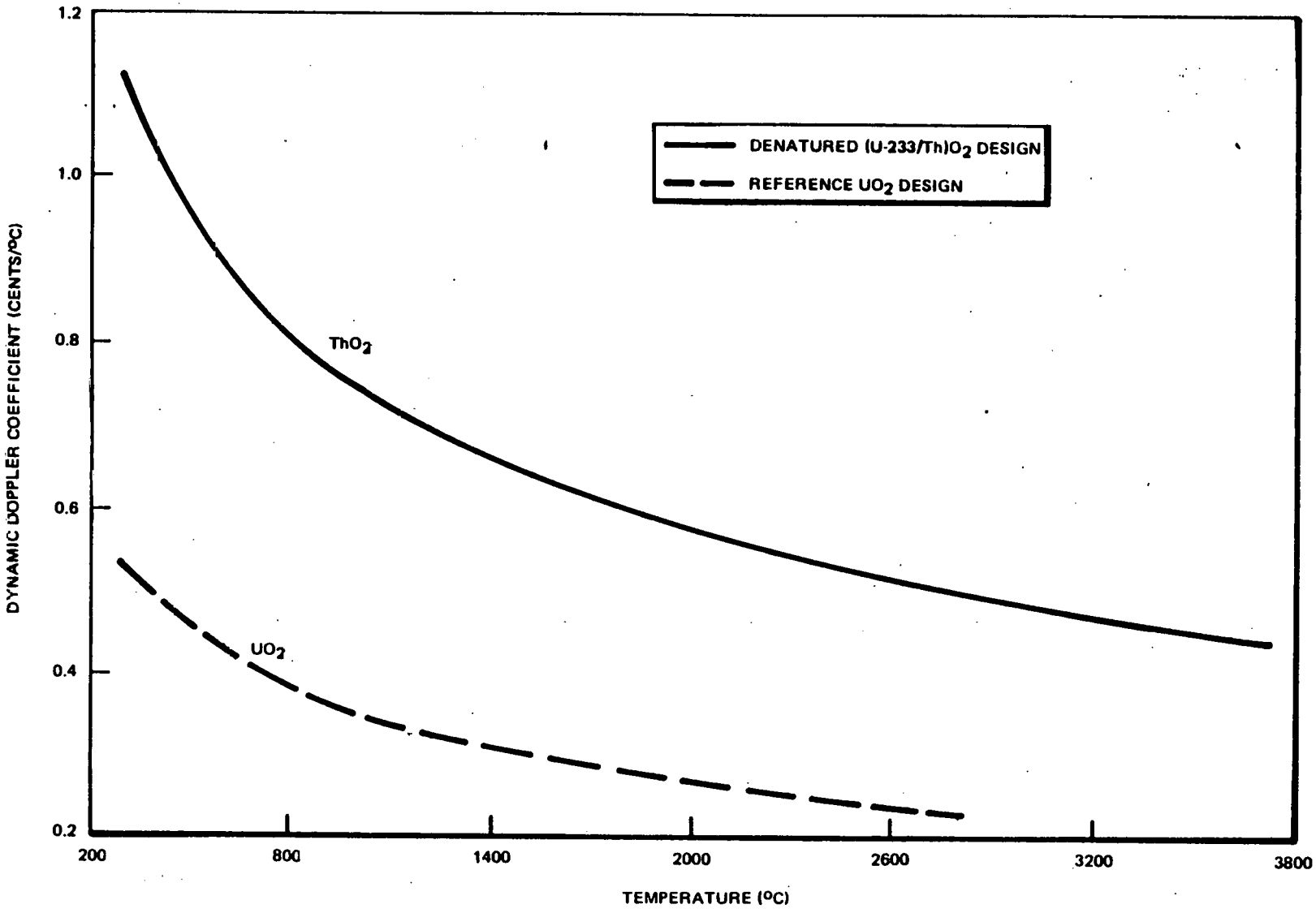

Figure 5-9. Three-Dimensional Dynamic Doppler Coefficients versus Temperature at EOEC

where:

ℓ^* = neutron generation time;
ρ = reactivity insertion, $\Delta k/k$; and
β = effective delayed neutron fraction.

The neutron generation time, ℓ^*, does not change dramatically with fuel types (see Table 5-3), but β does. At beginning of life, a fuel design with U-235 as the fissile material typically will have a β of about 0.006, but a fuel bundle with U-233 as the fissile material will have a β of about 0.003. With a smaller β, the reactivity insertion required to bring the reactor to prompt critical is reduced. Thus, the smaller the β term, the shorter the prompt period and the faster the system responds to reactivity changes.

Table 5-3
NEUTRON GENERATION TIME

Fuel Type	Neutron Generation Time* (ℓ^*), μsec
Reference UO_2	40.1
Denatured (U-233/Th)O_2	38.9

*At 16.5 GWd/MT.

6. BWR OPERATING CHARACTERISTICS

Denatured (U-233/Th)O_2 fuel utilization in BWRs would improve thermal margins and cold shutdown but may reduce the reactor's operating flexibility. Table 6-1 summarizes the major parameters that impact BWR operations for both reactor types and identifies the advantages/disadvantages of the thorium fuel design. Each parameter, in turn, is evaluated in detail below as to the effect it may have on BWR operation.

6.1 ENERGY EQUIVALENCE AND REACTIVITY MARGINS

6.1.1 Hot Excess Reactivity and Cycle Energies

An objective in the design of a denatured (U-233/Th)O_2 fuel assembly was to match the amount of excess reactivity throughout the equilibrium cycle with the reference UO_2 bundle, thereby achieving energy equivalence and exchangeability with the UO_2 bundle. Bundles are "energy equivalent" when the reactor cycle energy remains constant regardless of which bundle type is used while maintaining the same reload batch size, capacity factor, and operating strategy. Figure 6-1 gives the reactivity shape as a function of exposure for both the (U-233/Th)O_2 and the reference UO_2 bundles. The hot excess reactivity of both designs, derived from Figure 6-1, is given as a function of exposure in Figure 6-2. The two plots have similar shapes with the thorium bundle possessing about the same excess reactivity as the UO_2 bundle at the beginning of the equilibrium cycle. The thorium fuel end-of-equilibrium cycle (EOEC) burnup is equal to 8243 MWd/MT and the reference UO_2 burnup is 7361 MWd/MT. These burnups result in cycle energies of 1020 and 1004 GWd, respectively. This indicates that a more optimized (U-233/Th)O_2 design would require less enrichment and also possibly a lower burnable poison concentration or a reduced number of poison rods, which could further increase thermal margins (due to improved bundle local power distributions).

Table 6-2 gives beginning-of-equilibrium cycle (BOEC) core reactivity parameters for the denatured (U-233/Th)O_2 designs from the three-dimensional analyses. The "hot" eigenvalue is evaluated with all of the control blades fully withdrawn

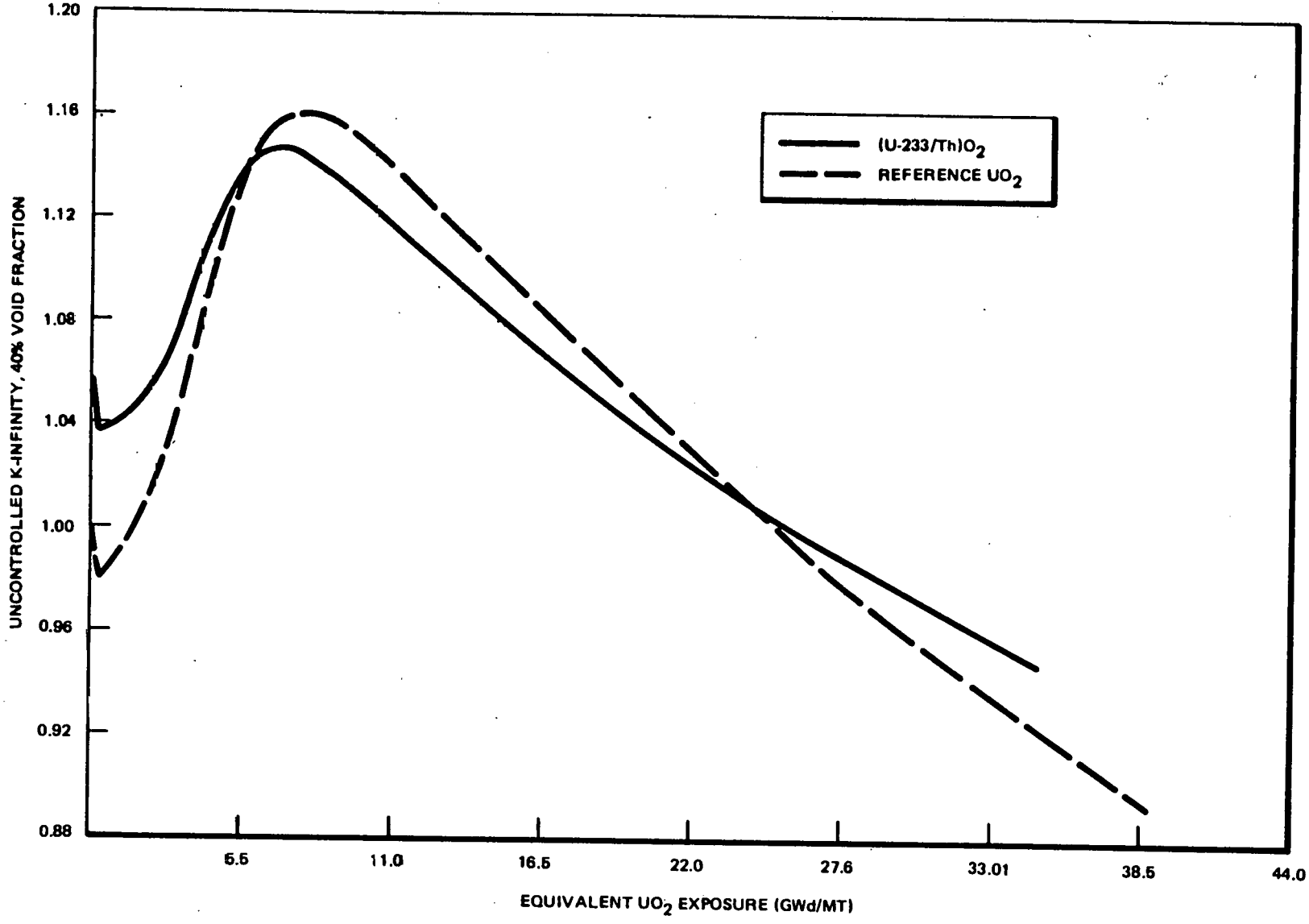

Figure 6-1. Bundle Reactivity Versus Exposure

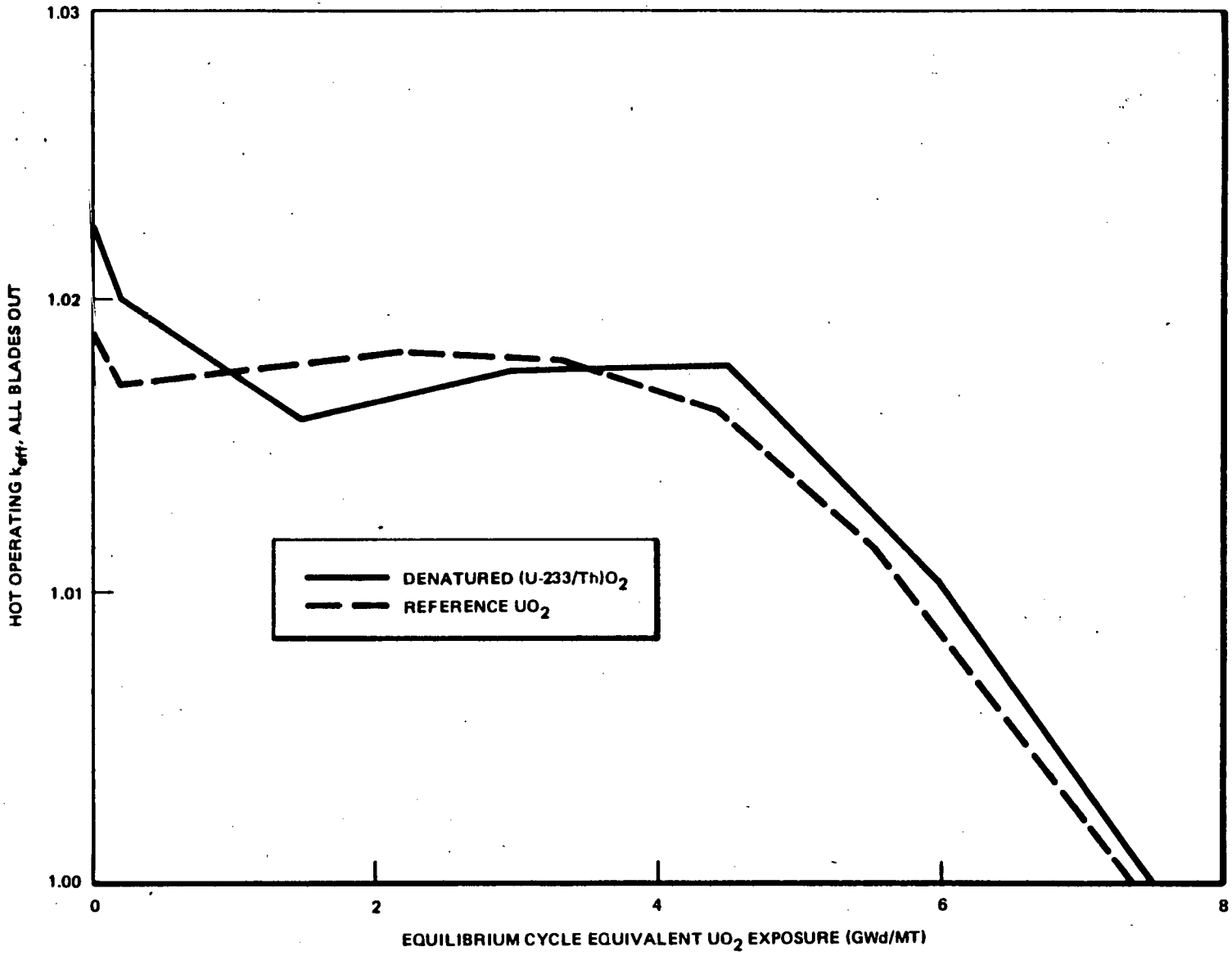

Figure 6-2. Equilibrium Cycle Hot Excess Reactivity

Table 6-1

BWR/6 EQUILIBRIUM PARAMETERS

	Reference UO_2	Denatured $(U\text{-}233/Th)O_2$	% Advantage
Cycle burnup, MWd/MT	7361	8243	---
Cycle energy, GWD	1004	1020	1.6
MCPR*	1.4	1.47	5.3
MLHGR*	10.5	9.4	10.5
Axial P/A*	1.20	1.18	1.4
Radial P/A*	1.30	1.28	1.5
Hot BOC excess reactivity	1.9	2.4	
Cold shutdown margin	1.1	4.7	327.0

*Haling, consistent power-exposure, end of cycle.

Table 6-2

COMPARISON OF REFERENCE UO_2 AND DENATURED $(U\text{-}233/Th)O_2$ BEGINNING-OF-EQUILIBRIUM CYCLE (BOEC) REACTIVITY PARAMETERS

	Reference UO_2	Denatured $(U\text{-}233/Th)O_2$
BOEC hot eigenvalue	1.0188	1.0244
BOEC hot excess reactivity	1.88%	2.44%
BOEC cold eigenvalue	0.9887	0.9534
BOEC cold shutdown margin	1.13%	4.66%

and the "cold" eigenvalue is evaluated at 20°C, zero voids, with all but the most reactive control blade fully inserted (i.e., the most reactive control blade is fully withdrawn). The hot excess reactivity is defined as the difference between the observed hot uncontrolled eigenvalue and the cold eigenvalue.

6.1.2 Cold Shutdown Margin

Cold shutdown margin given for both designs in Figure 6-3 as a function of equilibrium exposure, is required to be 1.0% or greater. The increased (4.66%) cold shutdown margin of the denatured (U-233/Th)O_2 design is brought about by its smaller hot-to-cold (uncontrolled) reactivity swing caused by the positive effects of U-233. Thus, either the number of burnable poison rods or the Gd_2O_3 poison concentration of the existing burnable poison rods could be reduced. Reduction of burnable poison in the thorium design would lead to improved performance and reduction of fissile inventory requirements, but also could result in too much hot excess reactivity.

The key to the large cold shutdown of the denatured (U-233/Th)O_2 design is the reduced sensitivity of this design to changes in moderator voids and temperatures. Table 6-3 shows several infinite lattice neutron multiplication factors at 16.5 GWd/MT for both the denatured (U-233/Th)O_2 and the reference UO_2 designs. From the three uncontrolled k-infinities in Table 6-3, it is apparent that the thorium design is both less sensitive to changes in the in-channel voids and to changes in the moderator/fuel temperatures than is the reference UO_2 design. Where k-infinity increases by 5.3% going from the hot uncontrolled state to the cold uncontrolled state for the reference UO_2 design, it increases by only 1.6% for the denatured (U-233/Th)O_2 design. Figure 6-4 shows beginning-of-life (zero exposure) controlled infinite lattice neutron multiplication factors at several fuel and moderator temperatures for both designs. Again it is clear that the denatured (U-233/Th)O_2 design is less sensitive to changes in temperature or hydrogen to heavy metal ratio.

The cold controlled and uncontrolled k-infinities in Table 6-3 also demonstrate that the blade worths for the two designs are nearly identical. The delta k-infinity cold uncontrolled to cold controlled is 0.171 for the UO_2 design and 0.166 for the thorium design.

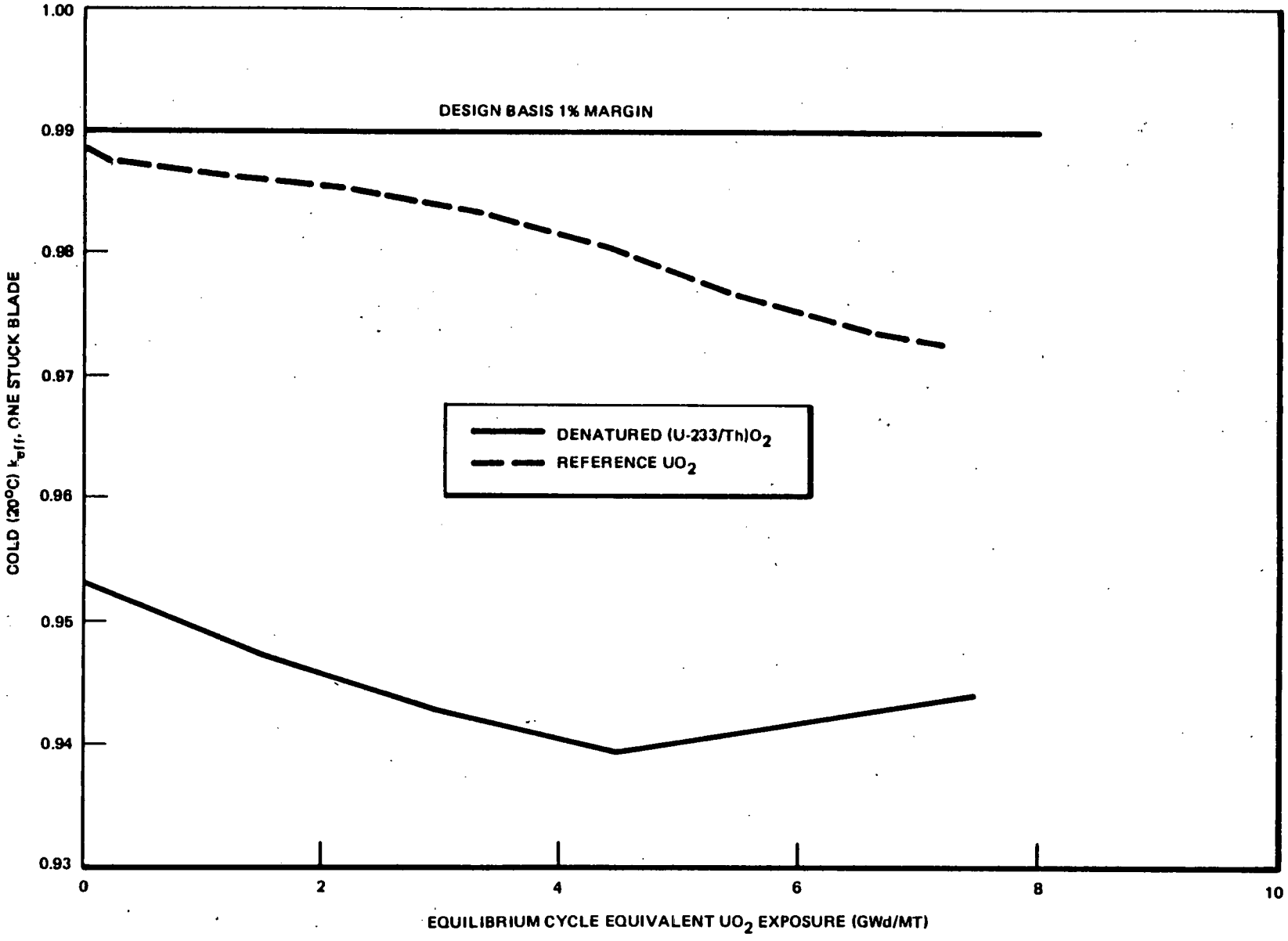

Figure 6-3. Equilibrium Cycle Cold Shutdown Margin

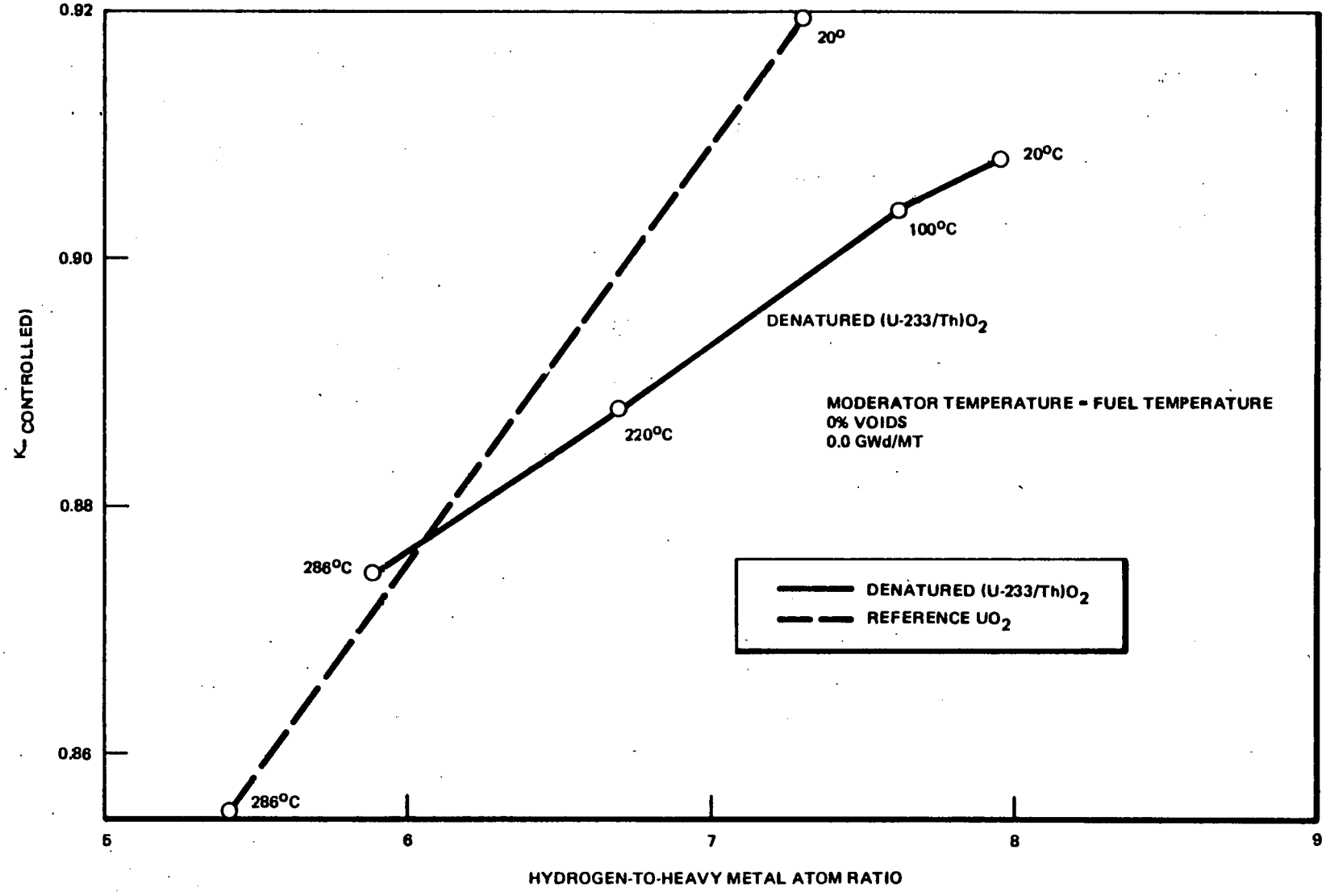

Figure 6-4. Controlled K_∞ Versus Temperature

Table 6-3

INFINITE LATTICE NEUTRON MULTIPLICATION FACTORS (K_∞) AT 16.5 GWD/MT

Lattice Conditions	UO_2	$(U\text{-}233/Th)O_2$
Hot, 40% voids, uncontrolled*	1.08688	1.08156
Hot, 0% voids, uncontrolled*	1.11492	1.09106
Cold, 0% voids, uncontrolled**	1.14496	1.09862
Cold, 0% voids, controlled**	0.97426	0.93259

*610°C fuel temperature and 286°C moderator temperature.

**20°C fuel and moderator temperatures.

6.2 THERMAL MARGINS

Thermal margins for the $(U\text{-}233/Th)O_2$ fuel design are greater than those of the reference UO_2 design. This is a direct consequence of the lesser sensitivity of U-233's fissioning rate to changes in the moderator-to-fuel ratio (void dependence) due to its larger epithermal fission resonance integral and smaller capture-to-fission ratio relative to U-235. The thorium design has an edge peaked rod power distribution, a flatter axial power shape, and reduced local power peaking, relative to the reference UO_2 fuel design.

The following thermal margins of greatest importance in affecting the safety and operational flexibility of the BWR:

a. Maximum Linear Heat Generation Rate or Peak kW/ft - The maximum linear heat generation rate (MLHGR) or the peak kW/ft, is determined by the overall reactor global peak-to-average power. Peak kW/ft determines peak central fuel temperature which affects the release of fission products inside the cladding and the strain on the cladding from pellet-clad interaction. Local, axial, and radial power distributions all contribute to the peak kW/ft.

b. Minimum Critical Power Ratio - The minimum critical power ratio (MCPR) is the power to which a fuel assembly could be taken without experiencing transition boiling, divided by the peak power at which the fuel assembly is designed to operate. Transition boiling would cause rapid temperature oscillations on the surface of the fuel elements, which would increase the Zircaloy corrosion rates. Therefore it is desirable to make the MCPR as large as possible. Because of detailed local flow and mixing characteristics within a fuel assembly, MCPR can be influenced by local power distribution.

6.2.1 Fuel Rod Power Distribution

The power distribution within a fuel rod is an important parameter in determining appropriate thermal limits for a given fuel type. The rod power shape, coupled with the thermal conductivity of the fuel, determines the heat flux from the rod, the fuel centerline temperature, and ultimately the maximum allowable linear heat generation rate for the fuel rod. From the viewpoint of thermal limits, it is desirable to have the rod power distribution peaked to the outside edge of the fuel rod.

Figures 6-5 through 6-8 illustrate the relative power distributions in a 3.0% U-235 UO_2 rod and a 3.0% fissile denatured $(U/Th)O_2$ rod at various exposures. These figures demonstrate that: at all exposures, both the UO_2 and $(U/Th)O_2$ power distributions peak at the edge of the rod; for both UO_2 and $(U/Th)O_2$, the power distributions become more edge peaked with exposure; and, for all cases, the $(U/Th)O_2$ power shape is slightly more edge peaked than that of the UO_2 fuel rod. These trends are as expected. The majority of fissions in both the UO_2 and $(U/Th)O_2$ rods occur in the thermal range and as the thermal flux is highest at the edge of the rod and lowest at the center, the power shape would be expected to be similar in shape. Because Th-232 thermal absorption cross-section is two to three times larger than that of U-238, the thermal flux in a $(U/Th)O_2$ rod will fall off more rapidly than that in a UO_2 rod with the power shape behaving similarly.

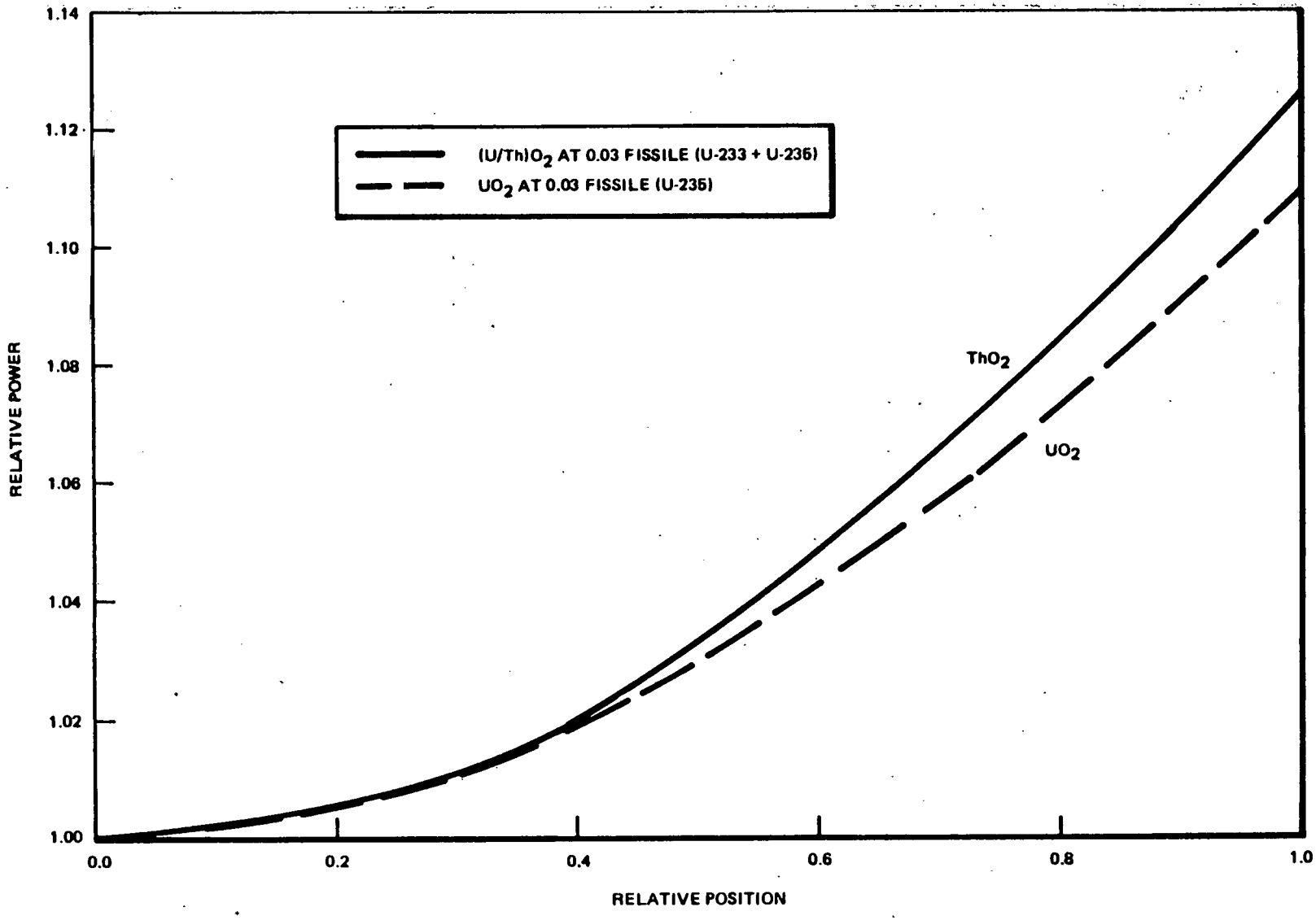

Figure 6-5. Power Shapes in UO_2 and Denatured $(U/Th)O_2$ Rods at 0.0 GWd/MT

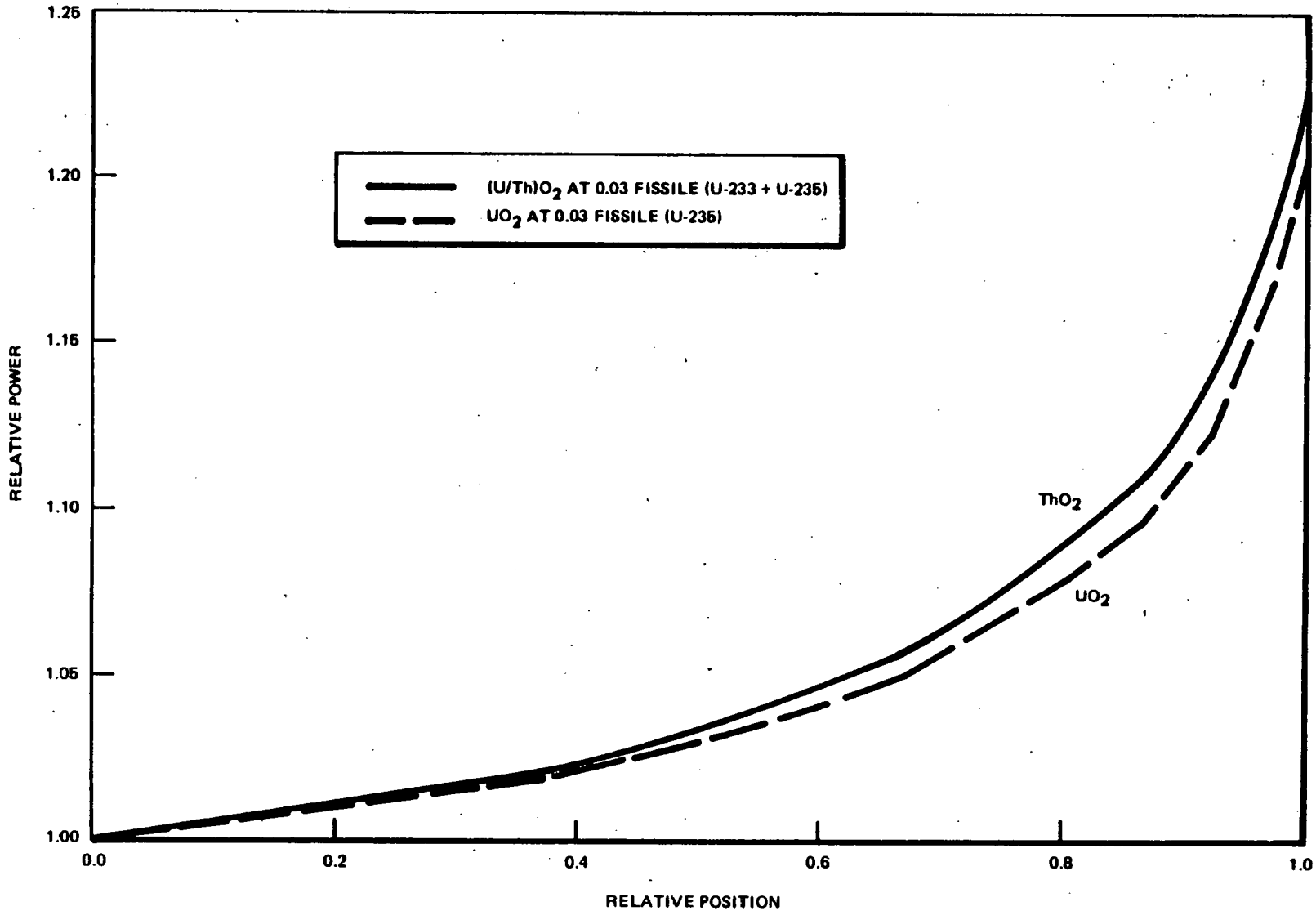

Figure 6-6. Power Shapes in UO_2 and Denatured $(U/Th)O_2$ Rods at 5.2 GWd/MT

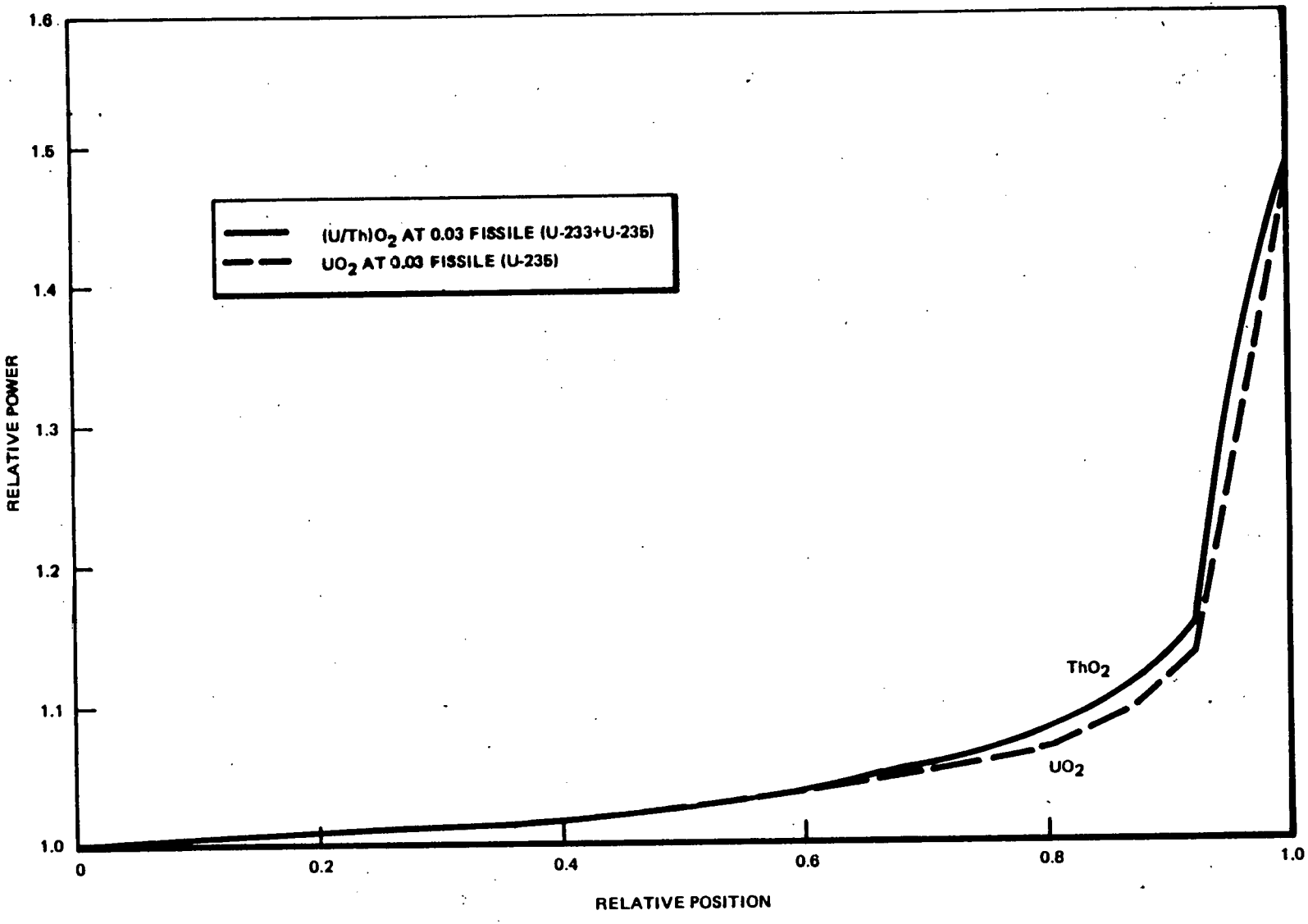

Figure 6-7. Power Shapes in UO_2 and Denatured $(U/Th)O_2$ Rods at 15.6 GWd/MT

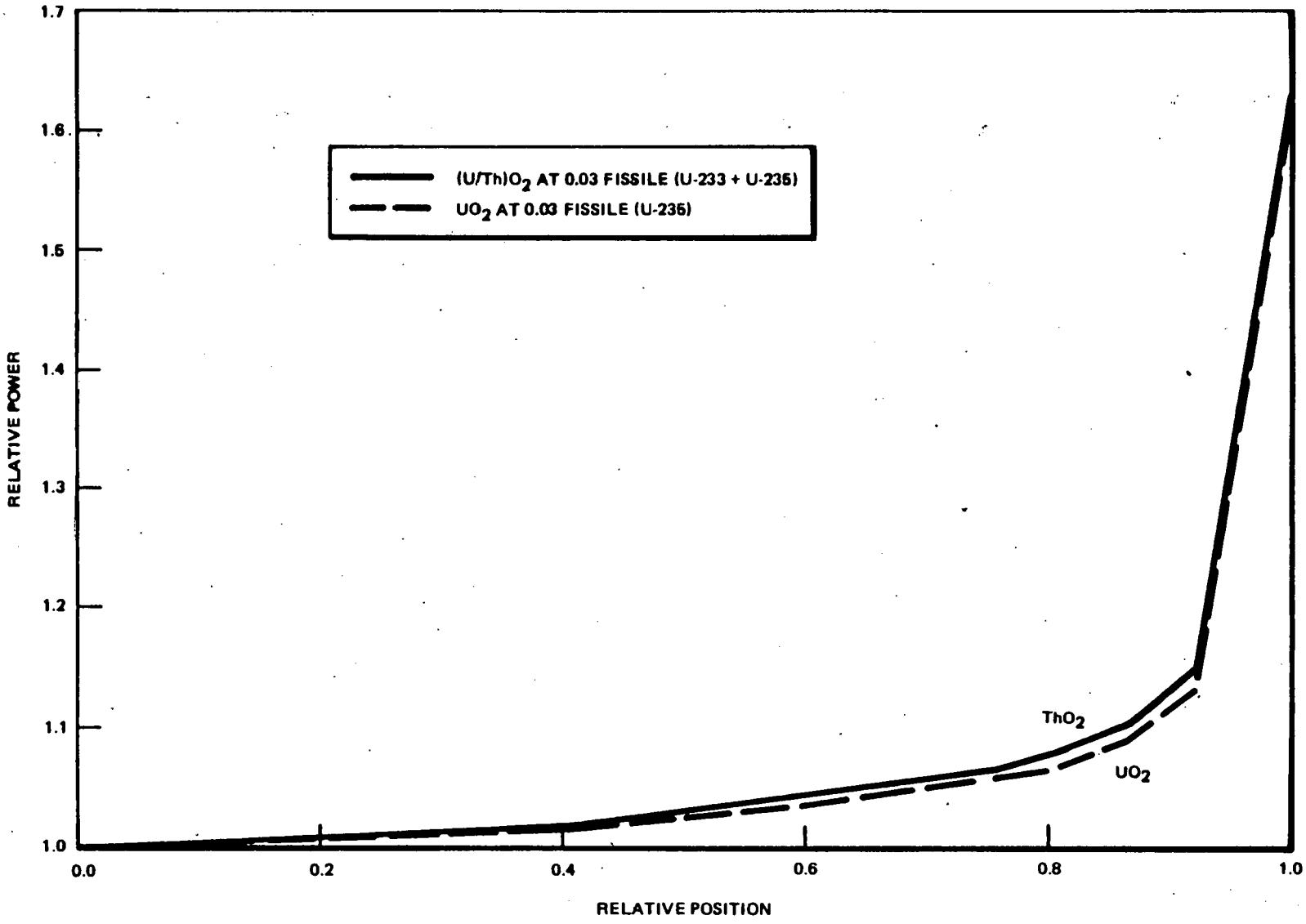

Figure 6-8. Power Shapes in UO_2 and Denatured $(U/Th)O_2$ Rods at 42 GWd/MT

The large increase in relative power at the edge of the UO_2 rod with increasing exposure is due to plutonium buildup with its large thermal fission cross-section. A similar increase in the edge power of the $(U/Th)O_2$ rod is expected as it is denatured with U-238 leading to plutonium buildup. At the same time, thermal absorptions in Th-232 result in conversion to U-233, which also contributes to the increase in relative power at the edge of the $(U/Th)O_2$ rod. In addition, U-233, the principal fissile component of the $(U\text{-}233/Th)O_2$ fuel, also is produced at a greater rate near the surface of the rod from resonance absorptions in the Th-232. The coupled effects of Pu-239 and U-233 production on the surface and greater thermal flux depression causes power to peak more toward the edge of the $(U/Th)O_2$ rod than for the UO_2 rod.

6.2.2 Axial Power Shape

Using the established equilibrium cycle, several important performance parameters are compared in Table 6-1. All of the parameters shown in the table improve for the $(U\text{-}233/Th)O_2$ design, relative to the reference UO_2 design. Evaluation of these parameters is based on an EOEC consistent power-exposure (or "Haling") shape which is shown in Figure 6-9. The EOEC target distributions do not include the effects of detailed control blade movements through the cycle; however, they should be achievable in practical reactor operation. As is apparent, the thorium design has a flatter axial power shape than the UO_2 design. This is due mainly to thorium's smaller steam void reactivity coefficient.

6.2.3 Local Power Peaking

Figure 6-10 gives the maximum local power peaking observed in the $(U\text{-}233/Th)O_2$ and the reference UO_2 bundle as a function of exposure. Local peaking in the thorium bundle is reduced, relative to the UO_2 assembly, due to less dependence of the thorium design on local fuel-to-moderator ratios and less burnable poison. At later exposures, the thorium bundle has higher local power peaking in the bundle corner rods due to the higher conversion rate of Th-232 to U-233 in these rods since they are in a highly thermalized spectrum due to the smaller local fuel-to-moderator ratio observed by corner rods, relative to interior rods. But the peaking in the corner rods does not impact the MCPRs due to lower local steam voiding near the rods.

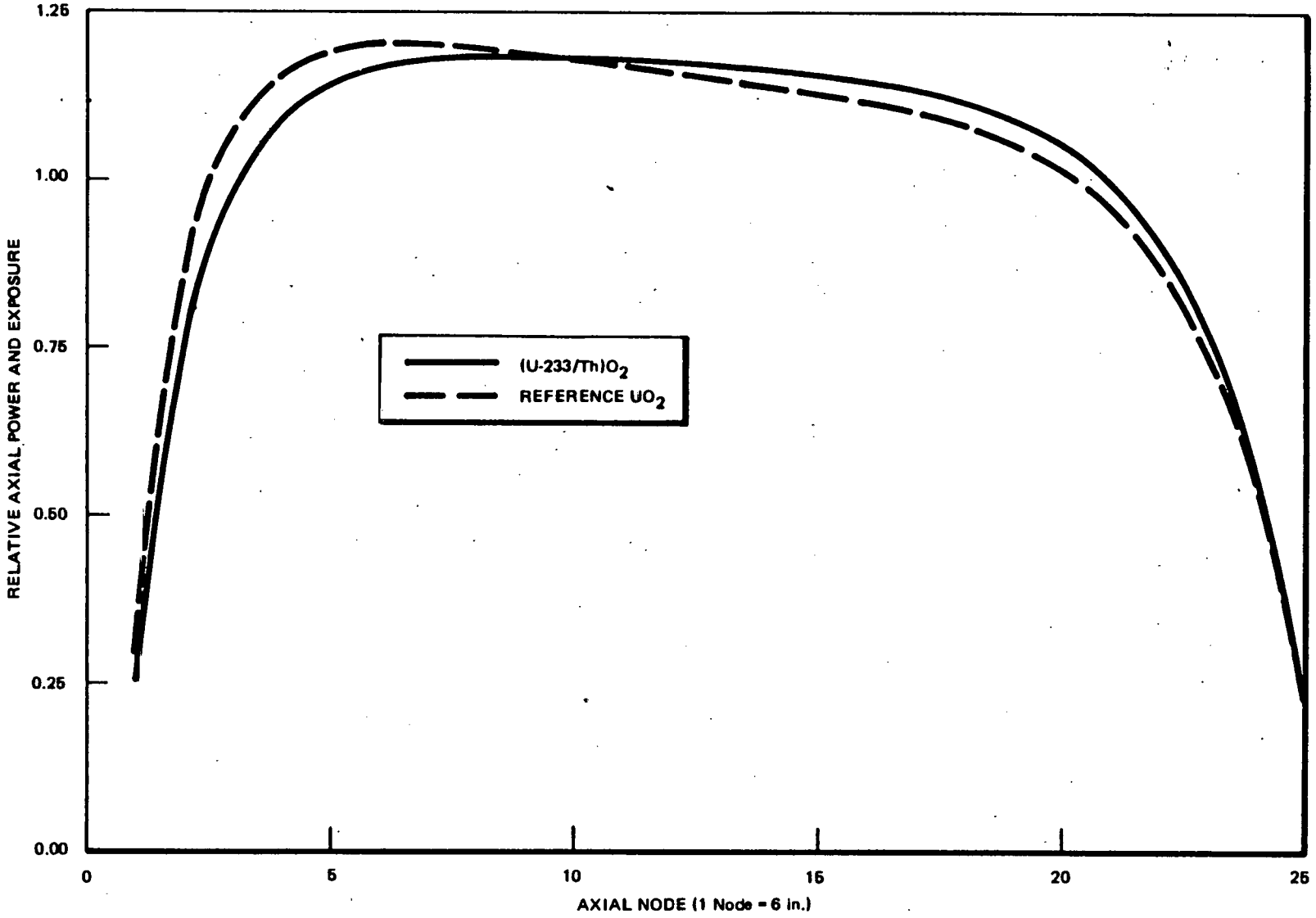

Figure 6-9. Power and Exposure Shape, EOEC (Haling)

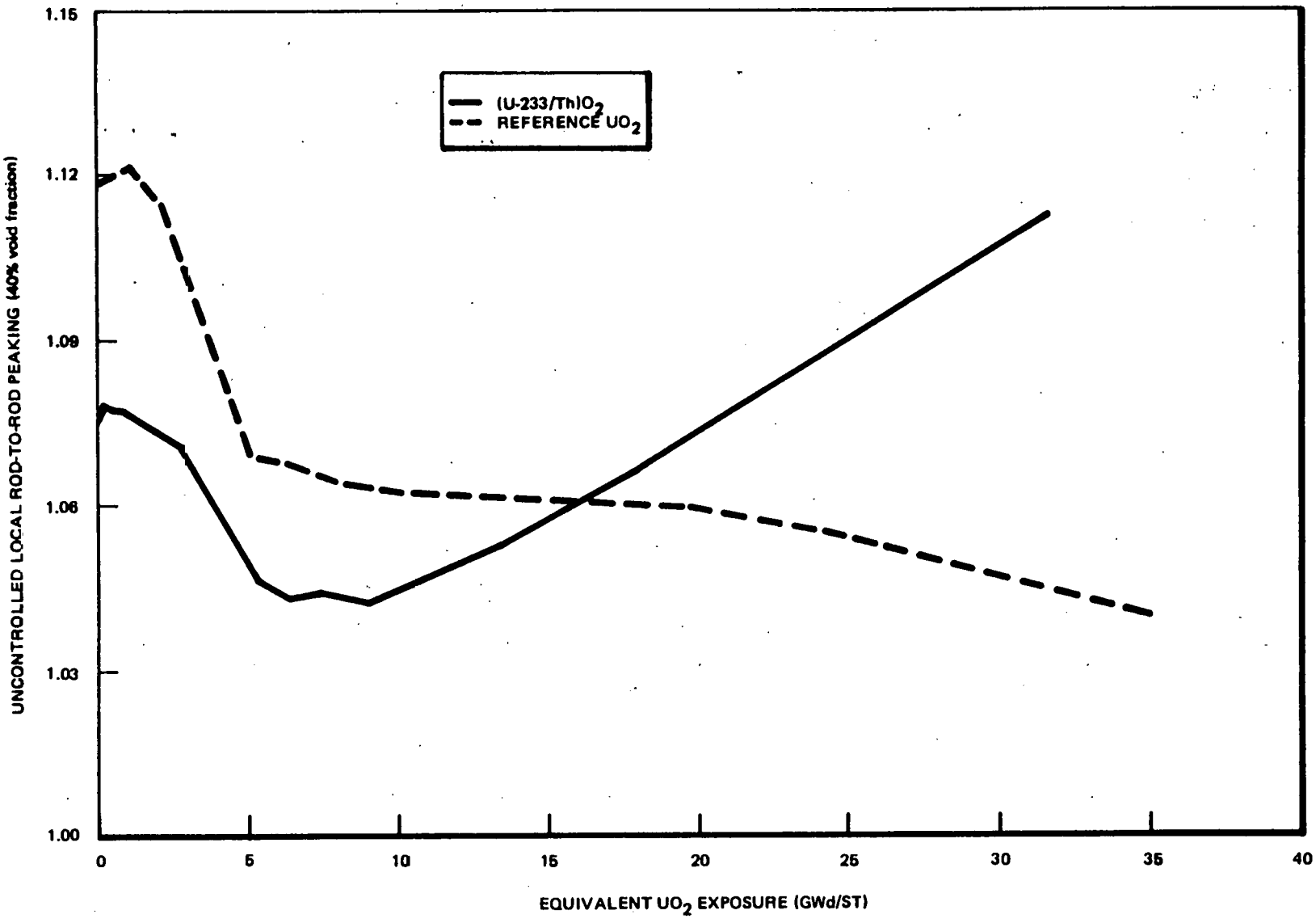

Figure 6-10. Local Power Peaking versus Exposure

The (U-233/Th)O_2 flatter axial power shape and its lower local power peaking relative to the UO_2 design contribute to lower peak linear heat generation rates (LHGRs) and greater minimum critical power ratios (MCPRs). Table 6-4 gives the MLHGRs and MCPRs as a function of exposure for both fuel designs. The control blade patterns for the (U-233/Th)O_2 minimized the use of shallow control blades which is desirable from a reactor operation viewpoint, but which may not produce the optimum patterns from a power peaking viewpoint. Once an acceptable combination of MHLGR, MCPR, and core reactivity was reached, no additional attempt was made to improve the thermal margins with other blade patterns. Therefore, the (U-233/Th)O_2 control blade patterns are non-optimal with potential for further improvement relative to the more thoroughly optimized UO_2 reference design. The importance of this data is that it demonstrates the capability of realistically operating a BWR core with the denatured (U-233/Th)O_2 fuel while meeting standard UO_2 design limits and matching or exceeding the performance of the reference UO_2 core.

6.3 REACTOR OPERABILITY

Reactor operability can be evaluated by examining the reactor flow control line and stability. Figure 6-11 shows the flow control lines for the denatured (U-233/Th)O_2 and reference UO_2 designs; stability is discussed in Section 10. As seen in the figure, the flow control lines for the two designs are similar, with that of the (U-233/Th)O_2 design being slightly flatter. As flow is reduced in a BWR, voiding is increased, resulting in a negative reactivity insertion due to the negative steam void reactivity coefficient. The (U-233/Th)O_2 steam void reactivity coefficient is less negative and the Doppler reactivity coefficient is more negative than those for UO_2. Thus, with decreasing flow, one would expect that the power of a (U-233/Th)O_2-fueled BWR would decrease less than that of a UO_2-fueled BWR. For load following purposes, it is desirable to have a steep flow control line; thus, the flatter flow control line for (U-233/Th)O_2 will affect BWR load following capability.

Table 6-4

EQUILIBRIUM CYCLE CORE PROPERTIES FOR DENATURED (U-233/Th)O_2 [1] AND REFERENCE UO_2 [2] FUEL BUNDLE DESIGNS

Cycle Exposure (GWd/MT)	Maximum Axial Peak-to-Average Power		Maximum Radial Peak-to-Average Power		Maximum Global Peak-to-Average Power		Maximum Linear Heat Generation Rate (Kw/ft)		Minimum Critical Power Ratio	
	UO_2	$(U/Th)O_2$	UO_2	$(U/Th)O_2$	UO_2	$(U/Th)O_2$	UO_2	$(U/Th)O_2$	UO_2	$(U/Th)O_2$
0.0	-	1.25	-	1.40	-	1.92	-	11.85	-	1.34
0.2	1.25	1.18	1.37	1.35	1.85	1.77	12.16	10.98	1.32	1.40
1.1	1.22	1.24	1.37	1.38	1.84	1.82	12.02	11.45	1.32	1.36
2.2	1.24	1.18	1.36	1.40	1.85	1.69	12.12	10.57	1.32	1.34
3.3	1.25	1.30	1.31	1.29	1.82	1.81	11.97	11.37	1.36	1.43
4.4	1.27	1.21	1.35	1.37	1.82	1.91	11.88	12.01	1.34	1.35
5.5	1.22	1.26	1.33	1.32	1.79	1.85	11.77	11.53	1.36	1.42
6.6	1.21	1.24	1.33	1.36	1.75	1.80	11.37	11.22	1.37	1.37
7.2	1.29	-	1.33	-	1.84	-	12.13	-	1.37	-
7.3	-	1.19	-	1.34	-	1.65	-	10.27	-	1.41
8.0	-	1.21	-	1.31	-	1.56	-	9.79	-	1.44
Average [3]	1.24	1.23	1.34	1.35	1.82	1.79	11.90	11.18	1.34	1.39

(1) Twenty-two shallow rods were used during the cycle.
(2) Eighty-eight shallow rods were used during the cycle.
(3) Exposure-weighted average.

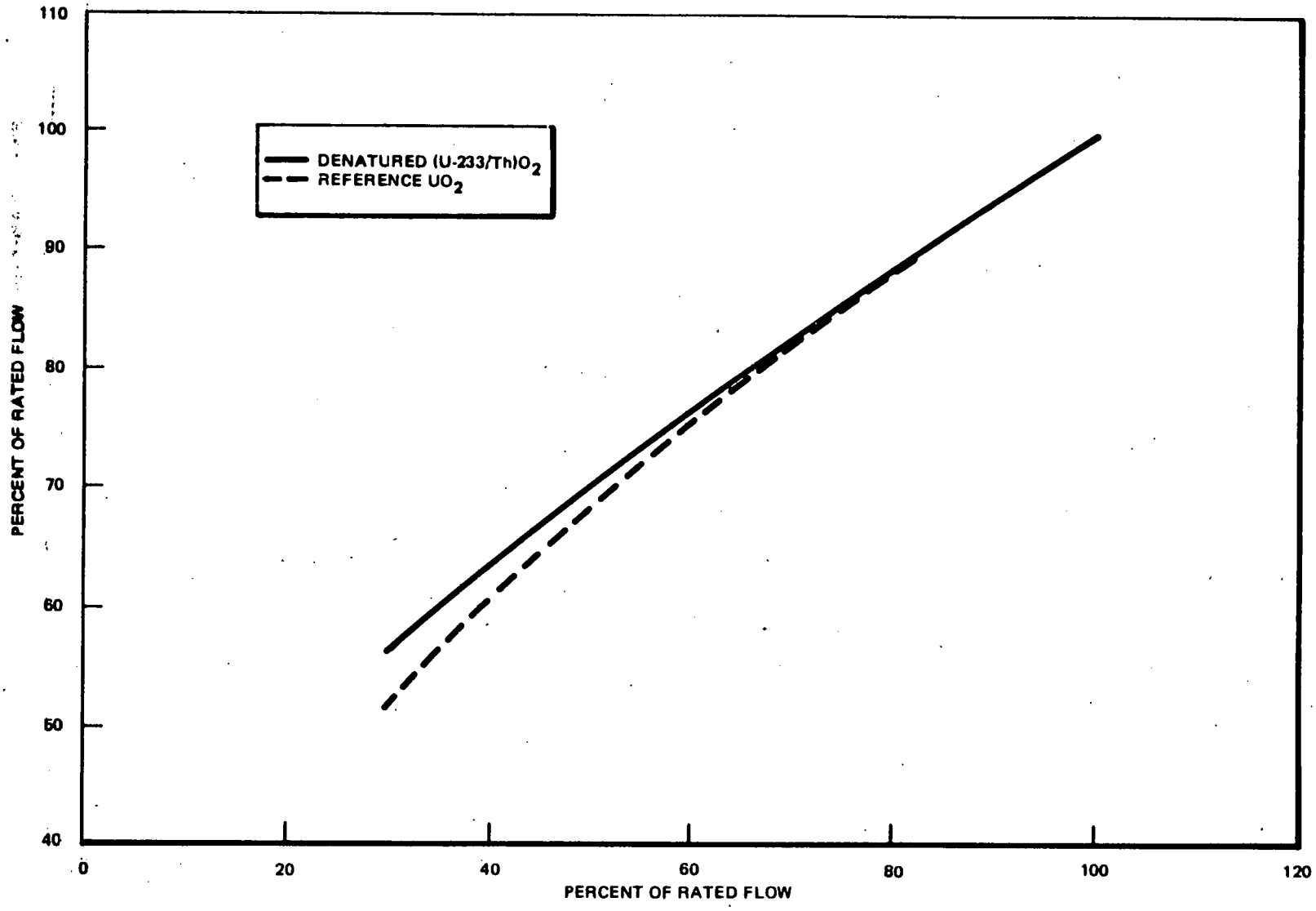

Figure 6-11. Flow Control Line for the Reference UO_2 and (U223/Th)O_2 Designs, EOEC

7. THERMAL/MECHANICAL ANALYSES

Thermal/mechanical (T/M) analyses were performed for both the denatured $(U\text{-}233/Th)O_2$ and reference UO_2 fuels to determine: (1) best estimate case parameters for input to abnormal transient and loss-of-coolant-accident (LOCA) evaluations, and (2) the fuel rod thermal/mechanical performance. T/M analyses utilize numerous physical properties of the fuel composition. Therefore, thorium physical parameters are incorporated into the T/M analyses to obtain performance representative of a thorium-fueled reactor.

7.1 THORIUM PHYSICAL PROPERTIES

Several physical properties of the $(U\text{-}233/Th)O_2$ fuel are required to perform T/M analyses. If the corresponding UO_2 parameter values conservatively approximated the thorium values, the UO_2 values of those parameters were utilized. The $(U\text{-}233/Th)O_2$ parameters that cannot be simulated sufficiently by UO_2 parameters or models are listed below along with their respective formulations. All thorium properties for the $(U\text{-}233/Th)O_2$ fuel were determined using References 12 through 14.

7.1.1 Fuel Melting Temperature

$$Tm = 5832 - 5.76\ E$$

where

Tm = melting temperature, °F
E = Exposure, GWd/STM*

*STM = Standard ton metal

7.1.2 Fuel Modulus of Elasticity

$$E = 3.1497 \times 10^{7} (1. - 0.0192(100-\rho)) (1.1021 - 8.3764 \times 10^{-5} T - 1.5892 \times 10^{-10} T^{2})$$

where

E = elastic modulus, psi
ρ = fuel density, %TD
T = temperature, °F

7.1.3 Fuel Theoretical Density

$$\rho th = 10.2 \text{ gm/cm}^3$$

7.1.4 Fuel Thermal Expansion

$$E_{t_{r,\theta,z}} = -1.182 \times 10^{-4} + 5.728 \times 10^{-6} T + 1.619 \times 10^{-10} T^{2}$$

where

E_t = directional thermal strain, in/in
T = temperature, °F

7.1.5 Fuel Enthalpy

$$H = -20.8032 + 0.061926T + 3.1796 \times 10^{-6} T^{2} + 615.926/T$$

where

H = ehthalpy, referenced to 298°K, cal/gm $(Th,U)O_2$
T = temperature, °K

7.1.6 Fuel Thermal Conductivity

$$K = \frac{3739.9}{524.8+T} + 2.9158 \times 10^{-12} (T+460)^3$$

where

T = temperature in °F

K = thermal conductivity in Btu/hr-ft-°F, for 95% TD 75% ThO_2-25% UO_2

7.2 ANALYSIS

7.2.1 Transient and Accident Fuel Performance

Thermal/mechanical analyses were performed for both the (U-233/Th)O_2 and the reference UO_2 fuel designs using the methods described in Subsection 4.3 to determine their relative performance characteristics under transient and accident (LOCA) conditions. The analyses were performed assuming current BWR/6 fuel rod geometry, fuel duty, and manufacturing specifications. The inputs to the analyses were consistent with established design procedures with the exception of certain fuel properties listed in Subsection 7.1 which are used for the (U-233/Th)O_2 analysis.

Parameters that impact transient and accident evaluations are thermal conductivity, stored energy, rod internal gas pressures, and fuel specific heat. Figure 7-1 gives a comparison of the thorium and UO_2 thermal conductivities. Figure 7-2 shows the relative difference in stored energies as a function of exposure. Figure 7-3 gives the relative internal gas pressures in the (U-233/Th)O_2 fuel. Figure 7-4 shows specific heat, relative to the reference UO_2 fuel.

7.2.2 Thermal/Mechanical Performance

Thermal/mechanical analyses were performed for both the (U-233/Th)O_2 and the reference UO_2 fuels to assess their adequacy with respect to current fuel rod

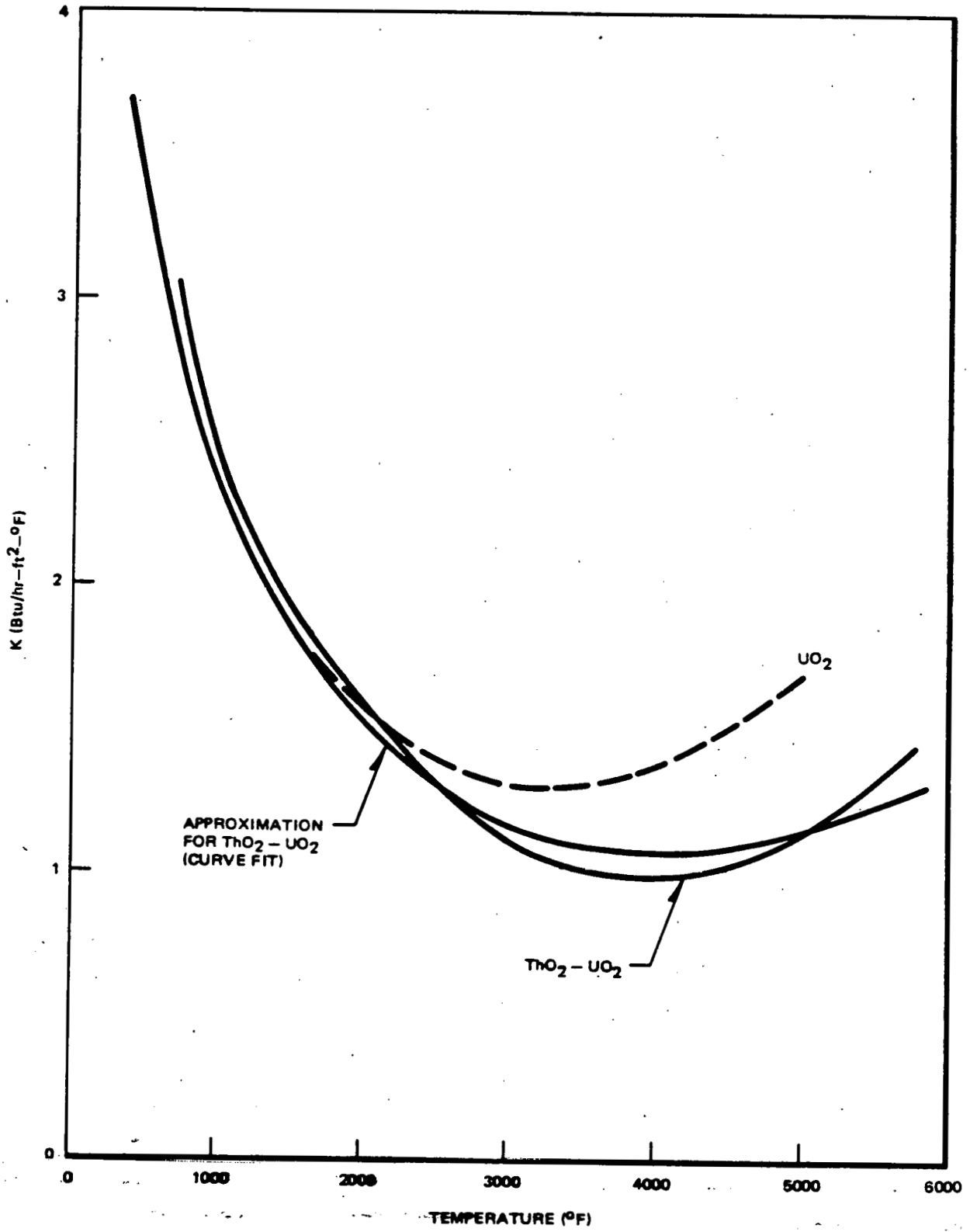

Figure 7.1. Thermal Conductivity versus Temperature for UO_2 and A (0.25 U - 0.75 Th)O_2 Mixture

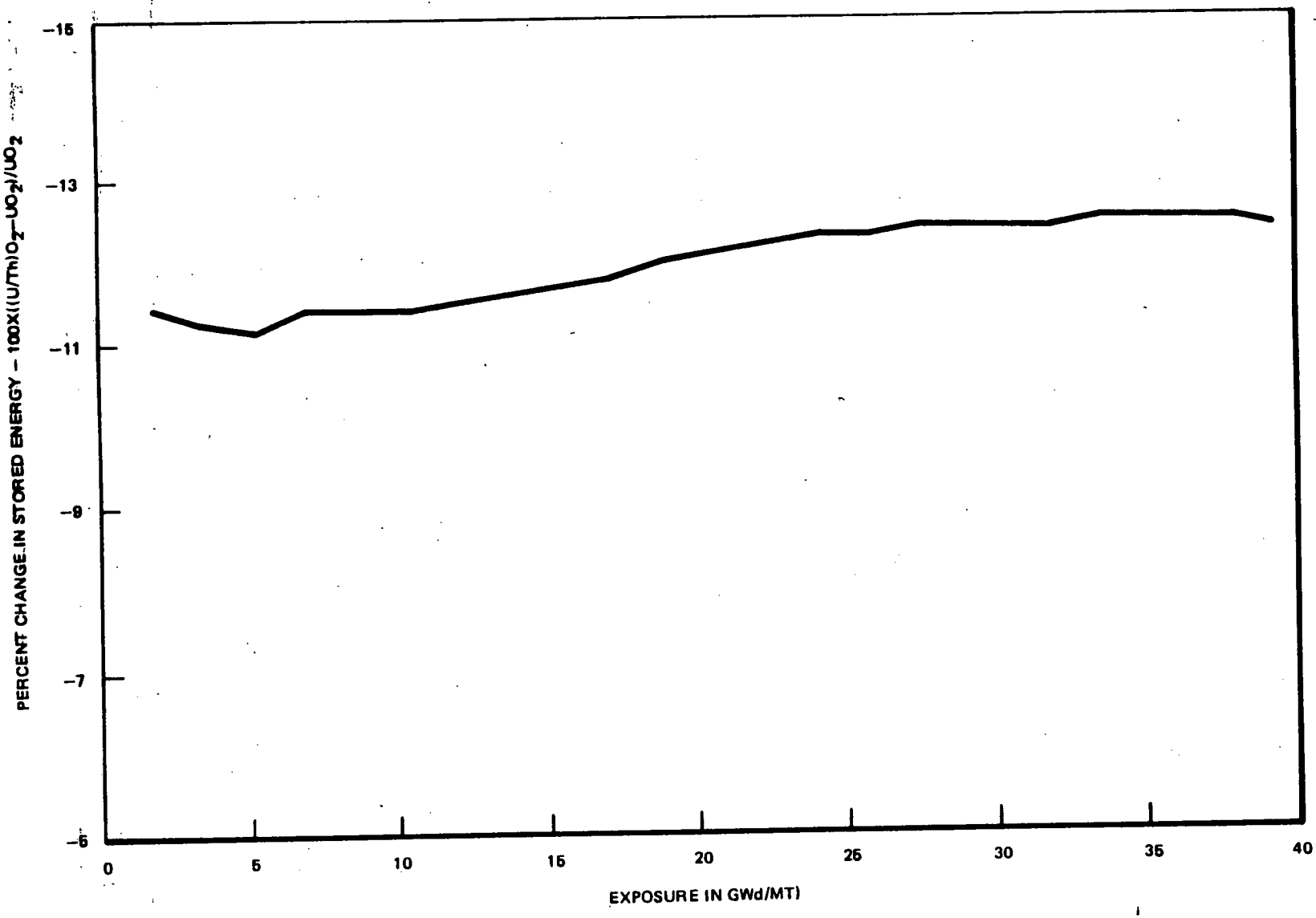

Figure 7-2. Change in Stored Energy versus Exposure for $(U/Th)O_2$ Relative to UO_2

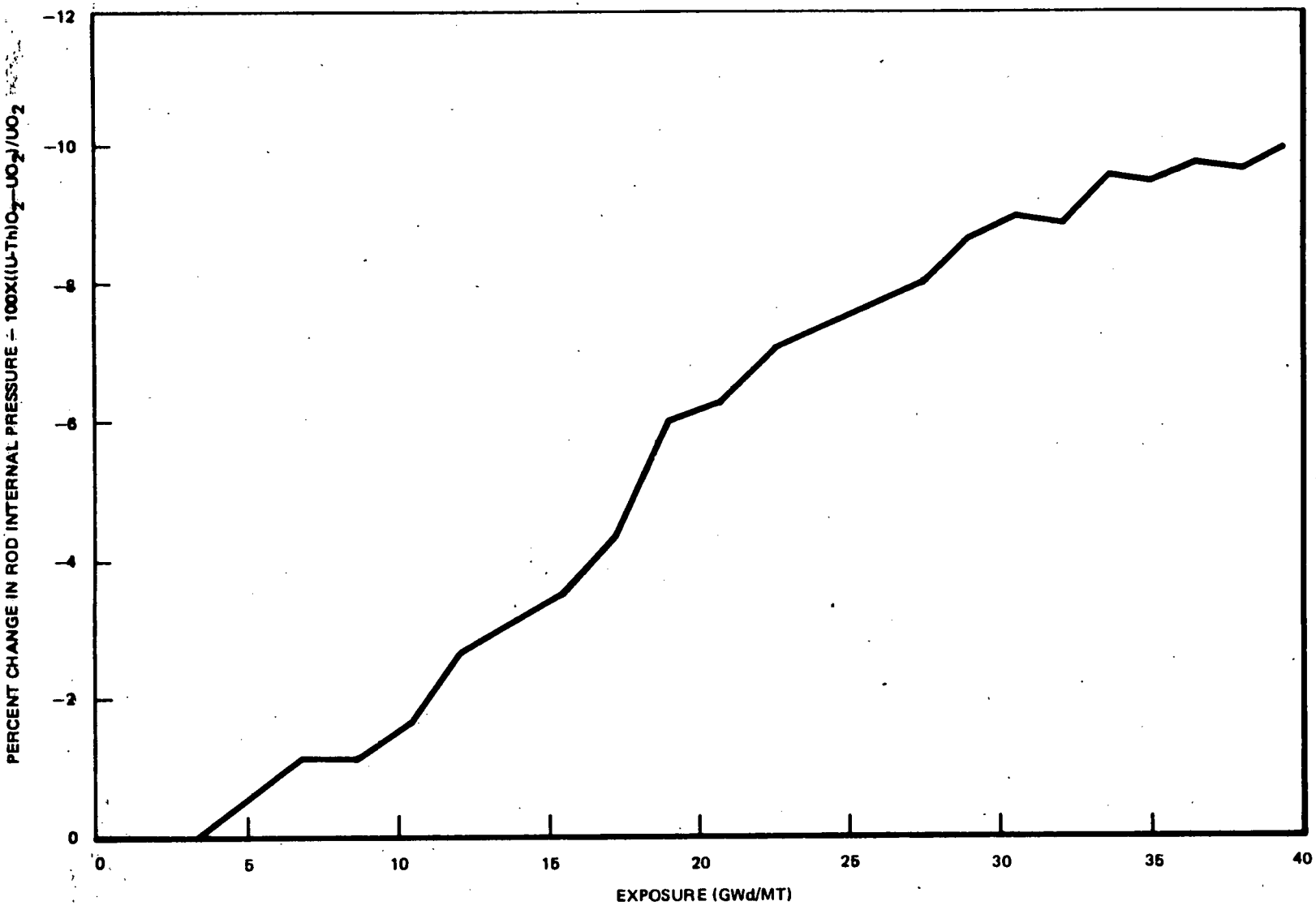

Figure 7-3. Change in High Power Rod Internal Pressure versus Exposure for $(U/Th)O_2$ Relative to UO_2

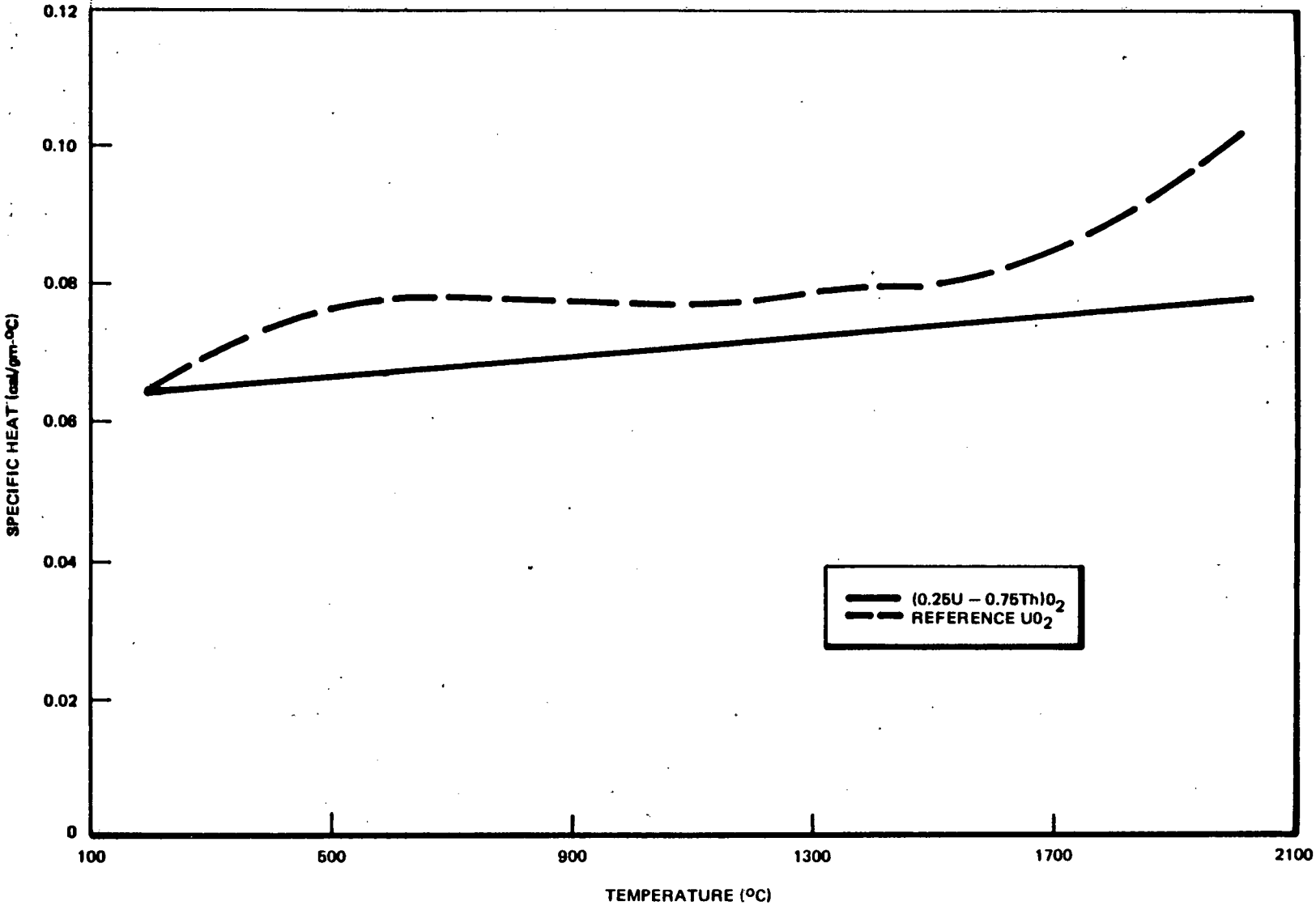

Figure 7-4. Specific Heat versus Temperature for UO_2 and a (0.25 U - 0.75 Th)O_2 Mixture

thermal mechanical design limits. Standard design procedures were used along with the (U-233/Th)O_2 fuel properties listed in Subsection 7.1.

Results of these analyses indicate that the (U-233/Th)O_2 fuel rod design would meet current fuel thermal design limits. Relative to the UO_2 fuel, the thorium fuel has a greater thermal margin to melting, less local cladding strain, and less cladding fatigue and creep rupture damage. Although the (U-233/Th)O_2 peak internal rod pressure is slightly higher than that seen in the UO_2 rod, it remains well below the design limit.

7.3 RESULTS AND CONCLUSIONS

The thermal conductivities of (U-233/Th)O_2 and UO_2, in their respective bundle designs, are nearly identical at temperatures up to 1600°F. Above 1600°F, the thermal conductivity of (U-233/Th)O_2 is slightly lower than that of UO_2. Relative to the UO_2 fuel, the (U-233/Th)O_2 fuel has 11% less stored energy, 9% lower internal rod pressures, and a slightly lower specific heat at normal operating conditions. The (U-233/Th)O_2 fuel design would meet current T/M fuel performance limits.

8. ACCIDENTS

Accidents are defined as hypothesized events that affect one or more of the radioactive material barriers and are not expected during the course of plant operations. The accident types considered are as follows:

a. Mechanical failure of various components leading to the release of radioactive material from one or more barriers. The components referred to here are not components that act as radioactive material barriers. Examples of mechanical failures are breakage of the coupling between a control rod drive and the control rod, failure of a crane cable, and failure of a spring used to close an isolation valve.

b. Overheating of the fuel barrier. This includes overheating as a result of reactivity insertion or loss of cooling. Other radioactive material barriers are not considered susceptible to failure resulting from any potential overheating situation.

c. Arbitrary rupture of any single pipe up to and including complete severance of the largest pipe in the nuclear system process barrier. Such rupture is assumed only if the component to rupture is subjected to significant pressure.

The following are considered to be unacceptable safety results for design basis accidents:

a. Radioactive material release to an extent that exceeds the guideline values of 10CFR100;

b. Catastrophic failure of fuel cladding, including fragmentation of fuel cladding (loss-of-coolant accident) and excessive fuel enthalpy (control rod drop accident);

c. Nuclear system stresses in excess of those allowed for accidents by applicable codes;

d. Containment stresses in excess of those allowed for accidents by applicable industry codes when containment is required; and

e. Overexposure to radiation of plant operations personnel in the control room.

For purposes of analysis, accidents that result in radioactive material release are categorized as follows:

a. From the fuel with the reactor coolant pressure boundary and containment initially intact;

b. Directly to the containment;

c. Directly to the drywell with the containment initially intact;

d. Directly to the drywell with the containment not intact; and

e. Outside the containment.

The effects of the various accident types are investigated for a variety of plant conditions. The accidents resulting in potential radiation exposures greater than any other accident considered under the same general accident assumptions are designated "design basis accidents" and are described in detail.

To increase conservatism in the analyses, an additional, unrelated unspecified fault in some active component or piece of equipment is assumed to occur simultaneously with or during the accident. Such a fault is assumed to result in the maloperation of a device that is intended to mitigate the consequences of the accident. The assumed result of such an unspecified fault is restricted to such events as an electrical failure, instrument error, motor stall, breaker freeze-in, or valve maloperation. Highly improbable failures, such as pipe breaks, are not assumed to occur coincidentally with the assumed accident. Other failures to be considered are in addition to those caused by the accident itself.

In the analyses of the design basis accidents, analysis assumptions are made to account for a variety of single additional failures. These assumptions are

sufficiently conservative to include the range of effects from any single additional failure. Thus, no single additional failure of the types to be considered exists that could worsen the computed radiological effects of the design basis accidents.

8.1 ROD DROP ACCIDENT

8.1.1 Description of Event

A rod drop accident (RDA) assumes that the highest worth control blade falls from its fully inserted position, limited only by the acceleration due to gravity, until it is fully ejected from the reactor core. The sequence of events for this accident in the standard BWR/6 plant is given in Table 8-1.

Table 8-1
SEQUENCE OF EVENTS FOR ROD DROP

Sequence of Events	Approximate Elapsed Time
Reactor is operating at 50% control rod density pattern.	
Rod worth minimizer is not functioning; maximum worth control blade becomes decoupled.	
Operator selects and withdraws the control rod drive of the decoupled maximum worth rod to its fully withdrawn position.	
Blade sticks in the fully inserted position.	
Blade becomes unstuck and drops at nominal measured velocity plus 3σ.	0
Reactor goes prompt critical and initial power burst is terminated by Doppler.	<1 sec
APRM 120% power signal scrams reactor.	
Scram terminates accident.	<5 sec

The prompt reactivity insertion causes an increase in the neutron power, and deposits energy inside the fuel with the quantity being limited by negative Doppler reactivity feedback. With the condition that no out of sequence rod may be moved, the postulated rod drop should not result in peak enthalpies in excess of 280 cal/gm for any possible plant operation or core exposure (the design basis limit).

8.1.2 Analysis

In the RDA analysis, the maximum incremental control blade worths should be less than 1.0% in reactivity (i.e., delta K-effective). Assuming this criterion is met, the dynamic Doppler coefficient (DDC) becomes the controlling reactivity parameter during a rod drop. This condition holds for both reactor types; the largest thorium blade worth is less than 25% delta K-effective. Since the $(U\text{-}233/Th)O_2$ fueled reactor's DDC is two to three times more negative than the UO_2 reactor value, it will limit the neutron power rise associated with a rod drop to a lower peak value than is observed in the reference UO_2 fuel, thereby decreasing the amount of total energy deposited in the thorium fuel during the accident relative to the reference UO_2 fuel.

8.1.3 Results and Conclusions

A denatured $(U\text{-}233/Th)O_2$ fueled reactor will satisfy rod drop licensing requirements. The reference UO_2-fueled reactor meets safety and licensing requirements for the rod drop accident. Therefore, since consequences from the accident are less severe in a thorium-fueled reactor than in the reference UO_2-fueled reactor, the $(U\text{-}233/Th)O_2$-fueled reactor will also meet these safety and licensing constraints.

8.2 ROD WITHDRAWAL ERROR

Current BWRs are designed with a rod withdrawal limiter (RWL) system which limits the distance that a control blade or gang of control blades can be continuously withdrawn by the operator. This system has a setpoint which insures that a rod or rod block cannot be withdrawn to the point of causing fuel damage. The use

of this system means that the rod withdrawal error and ganged rod withdrawal error are no longer safety considerations, but are important from a BWR operational viewpoint.

The current rod withdrawal limiter setpoints range from 1 to 2 feet based on generic "worst case" UO_2 analyses. The control blade stroke limits insure that the minimum critical power ratio (MCPR) will never be reduced by more than 0.13 due to the movement of any single control blade or block of control blades. As the current setpoints are based on UO_2-fueled cores, it is necessary to verify that these values are adequate to protect the fuel in a denatured $(U\text{-}233/Th)O_2$ fueled core.

8.2.1 Description of Event

The rod withdrawal error (RWE) accident results from a procedural error by the operator in which a single control rod or a gang of control rods is withdrawn continuously until the RWL system function of the rod control and information system blocks further withdrawal. The sequence of events is given in Table 8-2. It is assumed that the withdrawal error occurs with the maximum worth control rod, thereby inserting the greatest amount of positive reactivity. Due to the reactivity insertion, the local power in the vicinity of the withdrawn control rod will increase and potentially could cause localized fuel failures due to either achieving critical heat flux or by exceeding the 1% plastic strain limit imposed on the cladding as the transient failure threshold.

Table 8-2

SEQUENCE OF EVENTS FOR ROD WITHDRAWAL ERROR

Elapsed Time	Event
0	Core is operated in a typical control rod pattern on limits.
0	Operator withdraws a single rod or gang of rods continuously.
∿1 sec	The local power in the vicinity of the withdrawn rod (or gang) increases. Gross core power increases.
∿6 sec*	RWL blocks further withdrawal.
∿25 sec	Core stabilizes at slightly higher core power level.

*For a 1.5-foot RWL incrementsl withdrawal block. Time would be longer for a larger block, since rods are withdrawn at approximately 3 inches/second.

8.2.2 Analysis

The consequences of a rod withdrawal error are calculated utilizing the three-dimensional, coupled nuclear-thermal-hydraulic computer program. This model calculates the change in power level, power distribution, core flow and critical power ratio under steady-state conditions, as a function of control blade position. For this transient, the time for reactivity insertion is greater than the fuel thermal time constant and core-hydraulic transport times, so that the steady-state assumption is adequate.

The reactor core is assumed to be on MCPR and MLHGR technical specification limits prior to RWE initiation. A statistical analysis of the change in minimum critical power ratio (ΔMCPR) response to ganged rod withdrawals initiated from a wide range of operating conditions (exposure, power, flow, rod patterns, xenon conditions, etc.) has been performed to establish allowable rod withdrawal increments applicable to all BWR/6 plants. These rod withdrawal increments were determined such that the design basis ΔMCPR (difference between technical specification MCPR limit and safety MCPR) for rod withdrawal errors initiated from the technical specification operating limit and mitigated by the rod withdrawal limiter system withdrawal restrictions provides a 95% probability at the 95% confidence level that any randomly occurring rod withdrawal error will not result in a larger ΔMCPR. Minimum critical power ratio was verified to be the limiting thermal performance parameter establishing the allowable withdrawal increments. Cladding 1% plastic strain limits were always a less limiting parameter.

Based on these generic studies, the allowable rod withdrawal distances for the rod block monitor system were established as shown below:

Power Range (% of Rated)	Allowable Withdrawal Distance
70% to 100%	1.0 ft
20% to 70%	2.0 ft
0% to 20%	No restrictions*

*The BPWS function of the RCIS provides control of rod withdrawals below the 20% power setpoint and allows a maximum withdrawal distance of 9 feet.

To demonstrate that a rod withdrawal error in a BWR fueled with denatured $(U\text{-}233/Th)O_2$ will not result in localized or gross fuel damage, the RWE analysis was conducted at the most reactive point in the equilibrium cycle at 100% power conditions. The most reactive control rod and control rod gang were then withdrawn in 2-foot increments until the fully withdrawn position was attained.

8.2.3 Results and Conclusions

a. Results

The MCPR values associated with each notch position are plotted versus feet withdrawn of the control blade in Figure 8-1. From this plot, the maximum slope for MCPR versus blade position was determined for both single and gang control rod withdrawals. Using these values, it was determined that the maximum ΔMCPR which would result from a 1-foot withdrawal was 0.058 for a single control rod and 0.071 for a control rod gang. Because the technical specification MCPR is 1.23, neither of these ΔMCPRs would result in an MCPR below the safety limit MCPR of 1.07.

b. Conclusions

The worst case single control rod withdrawal error and ganged rod withdrawal error for a BWR fueled with denatured $(U\text{-}233/Th)O_2$ can be mitigated by the current rod withdrawal limiter system for UO_2-fueled BWRs. The RWL system removes the RWE from a safety consideration and makes it an operational consideration. By conforming to the generic design bases for RWE, $(U\text{-}233/Th)O_2$ places no additional operational restrictions on the BWR.

8.3 LOSS-OF-COOLANT ACCIDENT

8.3.1 Description of Event (Table 8-3)

Severe breaks in cooling system components, if unmitigated, would lead to loss of cooling to the fuel and a release of radioactive fission products

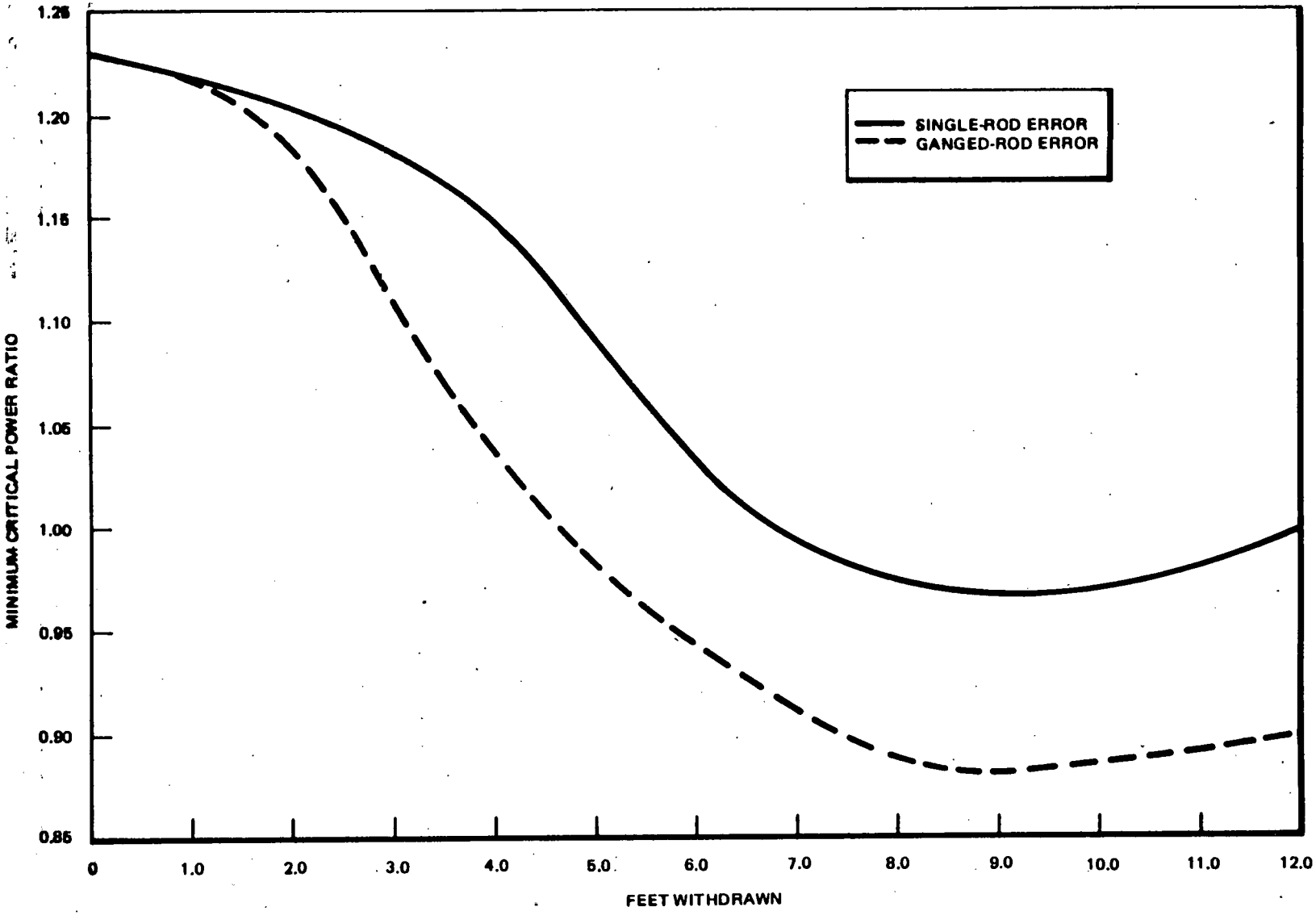

Figure 8-1. MCPR versus Control Blade Position for the RWE and GRWE

Table 8-3

SEQUENCE OF EVENTS FOR LOCA

Event begins — sudden circumferential severance of one recirculation line.
Reactor scrams.
Following pipe break and scram, the main steam isolation valves close on a low-level signal, at time zero plus ∿1 second. The low-low water level or high drywell signal will initiate operation of the core spray system and the LPCI system (RHR mode) at time zero plus ∿30 and 45 seconds, respectively.
The operator, after checking that all rods are inserted, determines plant conditions by surveying annunciators. After observing the ECCS initiation signals are present, he monitors that both core spray and LPCI have commenced operation. He also checks that the diesel generators have started in the standby condition.
The operator manually initiates containment spray and monitor drywell pressure.
The operator, after carefully monitoring the reactor water level, determines if any of the ECCS pumps can be taken out of service.
When time and conditions permit, the operator puts the residual heat removal service water into operation.

directly into the containment. In order to prevent loss of cladding integrity, thereby meeting safety and licensing requirements, the peak cladding temperature (PCT) should be limited to 2200°F for the duration of the loss-of-coolant accident (LOCA).

The worst credible accident, a design basis accident (DBA) for BWRs, which is the loss of the reactor core coolant through a double-ended guillotine break in one of the recirculation loops, is assumed after 2000 days of continuous full-power operation. A complete loss of normal power occurs simultaneously with the pipe break, which results in the longest delay time for the emergency core cooling systems to become operational.

Complete loss of cooling to the fuel is assumed subsequent to depressurization of the reactor vessel. The temperatures in the fuel and cladding rise, initially due to energy stored in the fuel pellets during power operation, then due to decay heat from fission product and actinide decays. Some heat removal is realized when the hot channel wets due to the high pressure core spray and the PCT falls immediately when coolant from the core spray, which has been collecting in the lower plenum, reaches the bottom of the active fuel length in the hottest channel (i.e., reflood).

8.3.2 Analysis

Analyses of the LOCA were performed for both the (U-233/Th)O_2 and reference UO_2 reactors using the method referenced in Subsection 4.6. Results of these analyses are plotted in Figure 8-2. PCT is displayed as a function of time following the complete severance of one recirculation loop pipeline. Analyses were performed for the thorium-fueled reactor using both the 13.4 kw/ft maximum assumed UO_2 LHGR and 12.88 kw/ft, which is the (U-233/Th)O_2 peak LHGR, taking credit for reduced local peaking.

The PCT of fuel in the (U-233/Th)O_2 reactor (if peak LHGR = 13.4 kw/ft) rises approximately 180°F higher than the PCT in the reference UO_2 reactor by the time of reflood (188 seconds) but remains below the 2200°F safety limit. Early in the event, when no cooling is assumed, the UO_2 fuel PCT rises faster than the thorium fuel PCT since the UO_2 stored energy at the onset of the LOCA is approximately 10% greater than the thorium stored energy (see Subsection 7.2-1). As the LOCA proceeds, the decay heat becomes the controlling parameter of the PCT for both fuels.

As the decay heat becomes the controlling factor of PCTs, the thorium PCT rises above the reference UO_2 PCT due to the thorium bundle's lower local power peaking. While the lower local power peaking of the (U-233/Th)O_2 fuel increases thermal margins during steady state power operation relative to the reference UO_2 margins, it penalizes the thorium fuel performance during a LOCA. Since the peak power rod of a thorium bundle assembly is nearer in power to its surrounding neighbors than in the reference UO_2 bundle, a smaller amount of the peak rod's heat energy can be radiated to the surrounding lower power rods.

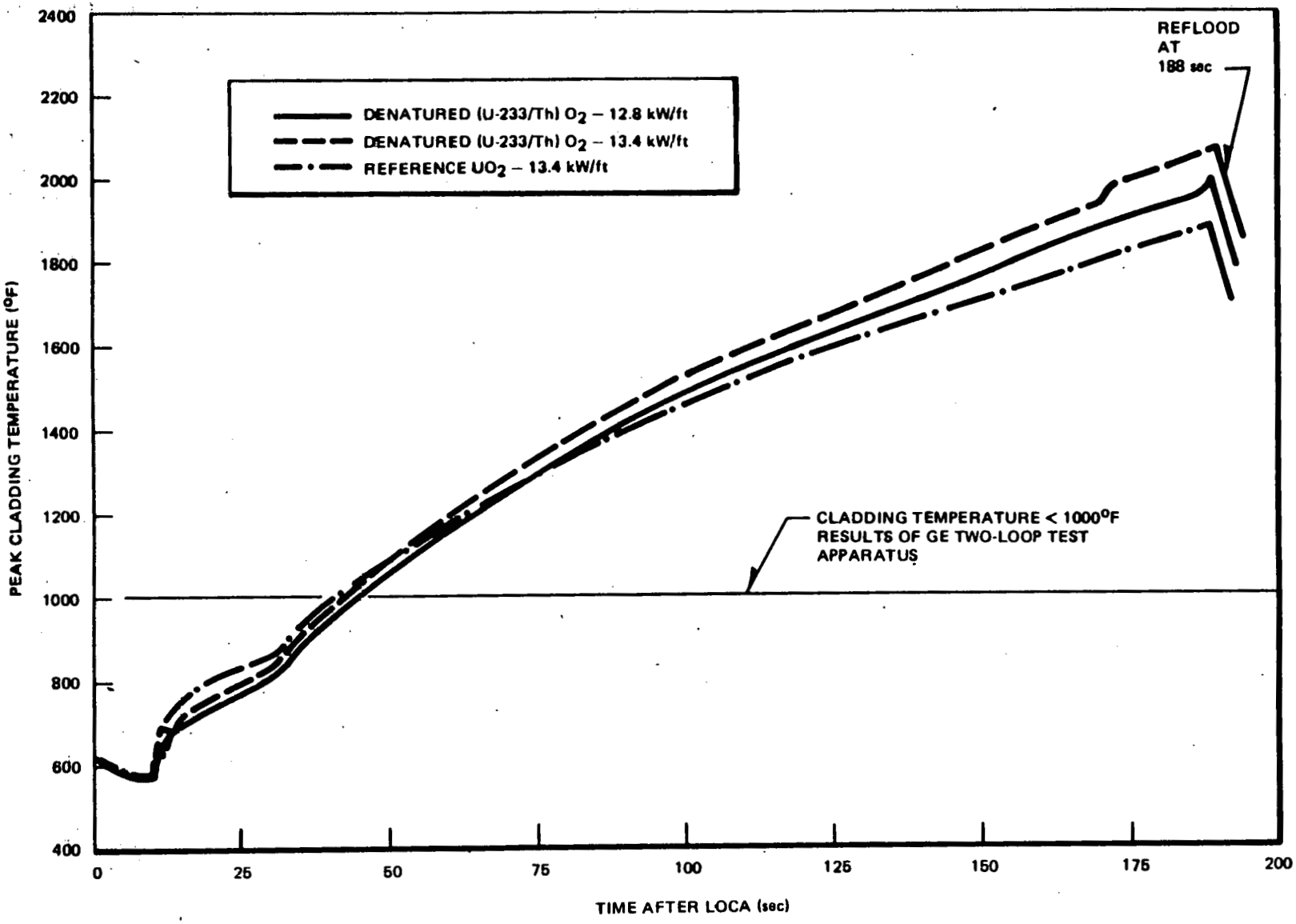

Figure 8-2. Peak Cladding Temperature versus Time After a LOCA

Therefore, the thorium bundle peak rod, not able to release as much decay heat to its neighbors as the UO_2 peak rod does, retains more energy than the UO_2 peak rod and attains a PCT approximately 180°F above the reference UO_2 fuel PCT by the time of reflood, but remains below the 2200°F design limit (i.e., no fuel failures will occur).

Poor compatibility with the existing input format for the analysis methods precluded the incorporation of a $(U\text{-}233/Th)O_2$ fuel decay heat function. Use of the UO_2 decay heat data is expected to give conservative PCTs. Decay heat data for U-233 is presented in Table 8-4. Note that, for the period of interest, 0 to 200 seconds, the U-233 decay heat is less than that of U-235, which implies that the decay heat of the reference UO_2 fuel should be greater at all times during the LOCA.

Table 8-4

SOME COMPARISONS OF U-233, U-235, AND Pu-239 DECAY HEATING FROM LASL MEASUREMENTS

Cooling Time (seconds)	F(t,T) in MeV/Fission		
	U-235	U-233	Pu-239
10	8.10	-	-
20	6.93	6.43	6.48
50	5.61	5.34	5.37
10^2	4.67	4.54	4.49
$5x10^2$	2.92	2.95	2.89
10^3	2.26	2.31	2.21
$5x10^3$	0.911	0.980	0.797
10^4	0.460	0.591	0.457
10^5	0.0454	0.0466	0.0467

8.3.3 Results and Conclusions

Analyses which ignore the reduced short term decay heat of $(U\text{-}233/Th)O_2$ fuel indicated that a $(U\text{-}233/Th)O_2$-fueled reactor core PCT is less than the design basis limit of 2200°F, but slightly greater than for UO_2 fuel. Therefore, all LOCA licensing requirements can be met by a thorium-fueled reactor. Also, it is likely that the use of the actual $(U\text{-}233/Th)O_2$ decay heat, which is less than the corresponding UO_2 fuel values as a function of time, will result in a PCT(t) which is lower than or equal to that of the reference UO_2 at corresponding times.

The 2200°F limit lies approximately 1000°F above existing PCT measurements, thus indicating the large degree of conservatism which results from mandatory assumptions imposed by the NRC in LOCA analyses. Viewed in the proper perspective, a 180°F difference in PCT between the two reactor types is minimally significant when it is compared to 1000°F of conservatism.

9. ABNORMAL OPERATIONAL TRANSIENTS

9.1 GENERAL DESCRIPTION

An abnormal operational transient is defined as any event that can be reasonably expected during the normal or planned mode of plant operations. These transients are the result of single equipment failures or single operator errors. The following types of operational single failures and operator errors are identified.

a. The undesired opening or closing of a single valve (a check valve is not assumed to close against normal flow);

b. The undesired starting or stopping of any single component;

c. The malfunction or maloperation of any single control device;

d. Any single electrical failure; and

e. Any single operator error.

Operator error is defined as an active deviation from written operating procedures or nuclear plant standard operating practices. A single operator error is the set of actions that is a direct consequence of a single erroneous decision.

The five types of single errors or single malfunctions are applied to the various plant systems for a variety of plant conditions to discover events that directly result in undesired parameter variations. Once discovered, each event is evaluated for the threat it poses to the integrity of the radioactive material barriers. Figure 9-1 shows the general method of identifying and evaluating abnormal operational transients. Eight nuclear system parameter variations are listed as posing potential deleterious effects to the nuclear steam supply system (NSSS). The parameter variations are as follows:

a. Nuclear system pressure increase threatens to rupture the nuclear system process barrier from internal pressure. Also, a pressure increase collapses the voids in the moderator. This causes an

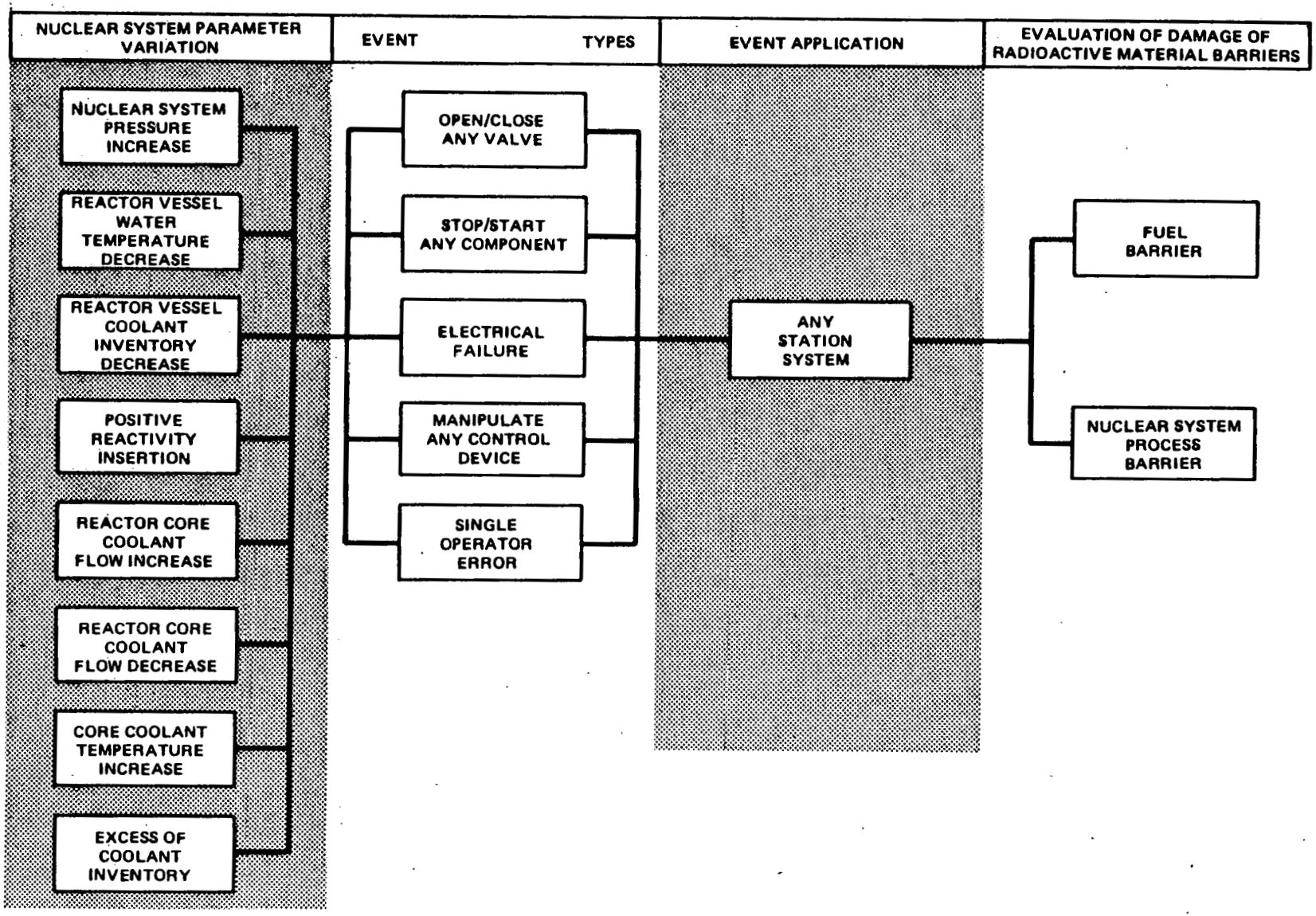

Figure 9-1. Method of Identifying and Evaluating Abnormal Operational Transients

insertion of positive reactivity which may result in fuel cladding damage because of the consequent overheating.

b. Reactor vessel water (moderator) temperature decrease results in an insertion of positive reactivity as density increases. Positive reactivity insertions threaten the fuel cladding as described in a above.

c. Positive reactivity insertion is possible from causes other than nuclear system pressure or moderator temperature changes. Such reactivity insertions threaten the fuel cladding as described in a above.

d. Reactor vessel coolant inventory decrease threatens the fuel as the coolant becomes unable to adequately remove the heat generated in the core.

e. Reactor core coolant flow decrease threatens to overheat the cladding as the coolant becomes unable to adequately remove the heat generated in the core.

f. Reactor core coolant flow increase reduces the void content to the moderator, resulting in a positive reactivity insertion. The consequent overheating may cause fuel cladding damage.

g. Core coolant temperature increase could result in fuel cladding damage from overheating.

h. Excess of coolant inventory could result in damage resulting from excessive carryover.

These eight parameter variations include all of the effects within the nuclear system caused by abnormal operational transients that threaten the integrity of the reactor fuel barrier or reactor coolant pressure boundary. The variation of any one of these parameters may cause a change in another. However, for purposes of analysis, threats to barrier integrity are evaluated by groups,

according to the parameter variation originating the threat. For example, positive reactivity insertions resulting from sudden pressure increases are evaluated in the group of threats stemming from nuclear system pressure increases.

Table 9-1 lists the abnormal operating transients which may occur during the operational lifetime of a BWR. These events can be grouped into three classifications, determined by their expected frequency of occurrence.

a. Incidents of Moderate Frequency - These are incidents that may occur during a calendar year for a particular plant.

b. Infrequent Incidents - These are incidents that may occur during the life of a particular plant.

c. Limiting Faults - These are occurrences that are not expected to occur but are postulated because their consequences would include the potential for the release of significant amounts of radioactive material.

9.1.1 Unacceptable Results for Incidents of Moderate Frequency

The following are considered to be unacceptable safety results for incidents of moderate frequency:

a. A release of radioactive material to the environs that exceeds the limits of 10CFR20.

b. A fuel cladding failure.

c. A nuclear system stress in excess of that allowed for transients by applicable industry codes.

Table 9-1

ABNORMAL OPERATIONAL TRANSIENTS

- Generator load rejection - turbine control valve
- Turbine trip
- Turbine trip with failure of generator breakers to open
- Main steam isolation valve closure (scram on 10% closure)
- Pressure regulator failure (open)
- Pressure regulator failure (closed)
- Excess coolant inventory
- Loss of feedwater heater
- Shutdown cooling (RHRS) malfunction - decreasing temperature
- Inadvertent start of HPCS pump
- Inadvertent opening of a safety/relief valve
- Loss of feedwater flow
- Loss of auxiliary power
- Trip of two recirculation pumps
- Recirculation pump seizure
- Recirculation flow control failure with decreasing flow
- Recirculation flow control failure with increasing flow
- Core coolant temperature increase

9.1.2 Unacceptable Results for Infrequent Incidents

The following are considered to be unacceptable safety results for infrequent incidents:

a. Excessive fuel damage that might preclude resumption of normal operation after a considerable outage time.

b. Excessive release of radioactivity that will interrupt or restrict public use of those areas beyond the exclusion radius.

c. Generation of a condition that results in a consequential loss of function of the reactor coolant system.

d. Generation of a condition that results in a consequential loss of function of the containment barrier.

9.1.3 Unacceptable Results for Limiting Faults

The following are considered to be unacceptable safety results for limiting faults.

a. Radioactive material release which results in dose consequences that exceeds the guideline values of 10CFR100.

b. Catastropic failure of fuel cladding, including fragmentation of fuel cladding and excessive fuel enthalpy.

c. Nuclear system stresses in excess of those allowed for accidents by applicable codes.

d. Containment stresses in excess of those allowed for accidents by applicable industry codes when containment is required.

e. Radiation exposure to plant operations personnel in the control room in excess of 5 Rem whole body, 30 Rem inhalation and 75 Rem skin.

A conservative criterion for incidents of moderate frequency is that 99% of the fuel rods in the core should not be expected to experience boiling transition (see Reference 16). This criterion is met by demonstrating that incidents of moderate frequency do not result in a minimal critical power ratio (MCPR) less than 1.07 for reload cores. This criterion is conservative, since there is considerable data which illustrates that significant fuel failure will not be caused by short term operation in transition boiling.

The MCPR during significant abnormal events is calculated using a transient core heat transfer analysis computer program. The computer program is based on a multinoide, single channel thermal-hydraulic model which requires simultaneous solution of the partial differential equations for the conservation of mass, energy, and momentum in the bundle, and which accounts for axial variation in power generation. The primary inputs to the model include a physical description of the bundle, and channel inlet flow and enthalpy, pressure and power generation as functions of time.

A detailed description of the analytical model may be found in Appendix C of Reference 17. The initial condition assumed for all full-power transient MCPR calculations is that the bundle is operating at or above the MCPR limit of 1.23 for the initial core and subsequent reload cores. Maintaining MCPR greater than 1.07 for reload cores is a sufficient, but not necessary condition to ensure that no fuel damage occurs.

9.1.4 Reactor Coolant Pressure Boundary Performance

The significant areas of interest for internal pressure damage are the high pressure portions of the reactor coolant pressure boundary (the reactor vessel and the high pressure pipelines attached to the reactor vessel). The overpressure below which no damage can occur is defined as the pressure increase over design pressure allowed by the applicable ASME Boiler and Pressure Vessel Code[18] for the reactor vessel and the high pressure nuclear system piping. Because this ASME code permits pressure transients up to 10% over design pressure, the design pressure portion of the reactor coolant pressure boundary meets the design requirement if peak nuclear system pressure remains below 1375 psig (110% x 1250 psig).

9.1.5 Initial Power/Flow Operating Constraints

The analyses basis for the transient safety analyses is the thermal power at rated core flow (100%) corresponding to 104.2% nuclear boiler rated steam flow. This operating point is the apex of a bounded operating power/flow map which, in response to any classified abnormal operational transients, will yield the minimum pressure and thermal margins of any operating point within the bounded map.

9.2 LIMITING TRANSIENTS

Table 9-2 lists the most potentially limiting transients that may be encountered during the operation of the reference UO_2-fueled BWR reactor. The transients listed in the table were simulated, using the methods described in Subsections 4.4 and 4.5, for both the denatured (U-233/Th)O_2 and the reference UO_2-fueled reactors. Relevant initial reactor conditions that are assumed at the onset of all the transients are given in Table 9-3.

The transients that have been the most limiting in UO_2-fueled BWRs should also be the most limiting in a (U-233/Th)O_2-fueled reactor. The dynamic void coefficient (DVC), dynamic Doppler coefficient (DDC), and scram reactivity are the controlling reactivity parameters in UO_2-fueled reactors. The limiting transients for the reference UO_2 reactor are those that cause the largest positive reactivity insertions from a reduction in the core average void fraction, which is directly related to the DVC. Since the (U-233/Th)O_2 controlling parameters are also the DVC, DDC and scram reactivity, the transients that insert the greatest amount of void reactivity into the reactor system should also be the most limiting transients in a thorium-fueled reactor.

The limiting transients can also be classified according to the physical mechanism that controls the insertion of void reactivity to the reactor system during the transient. The events may be classified as either pressurization transients or core inlet temperature reduction transients. Both classes cause the insertion of positive void reactivity through the reduction of the core average voids, thereby increasing the reactor power due to greater moderation of neutrons.

Table 9-2

POTENTIAL LIMITING TRANSIENTS

Event	Classification
Load rejection without turbine bypass	Infrequent occurrence
Pressure regulator downscale failure	Moderately frequent occurrence
Feedwater controller failure	Moderately frequent occurrence
Loss of feedwater heating	Moderately frequent occurrence
Main steam isolation valve closure, with scram on high neutron flux	Upset conditions
Main steam isolation valve closure, with scram on high pressure	Emergency conditions

Table 9-3

INITIAL CONDITIONS FOR TRANSIENTS AND ACCIDENTS

Thermal Power, MWt	
Analysis value (104.2% NBR*)	3729
Feedwater flow, lb/sec	4489
Core flow, lb/sec	28889
Turbine steam flow, lb/sec	4489
Vessel core pressure, psig	1045
Vessel dome pressure, psig	1056
MCPR operating limit	1.23
MCPR safety limit for incidents of moderate frequency	1.07
High flux trip, % NBR (122 x 1.042)	127.2
High pressure scram setpoint, psig	1095
Vessel level trips, feet above separator skirt bottom	
Level 8	5.89
Level 4	4.04
Level 3	2.165
Level 2	1.739
APRM** simulated thermal power trip scram setpoint, % NBR	118.8
Safety/relief valve capacity, % NBR	108.5 @ 1210 psig
Recirculation pump trip delay time, sec	0.14
Safety/relief valve pressure setpoints, psig	
Safety function	1175,1185,1195,1205,1215
Relief function	1125,1135,1145,1155
Safety/relief valve reclosure setpoints, % of closure setpoints	98

*NBR - Nuclear boiler rated.
**APRM - Average power range monitor.

Increased pressurization of the reactor core in a BWR can occur if normal steam flow from the vessel dome through the steamlines to the turbine is reduced by complete or partial closure of the turbine control valve, turbine stop valve, main steam isolation valves, or safety relief valves. As core pressures rise above the local thermodynamic saturation pressures that correspond to the coolant-moderator temperatures in voided regions, voids collapse and the boiling boundary moves upward in the core, thereby decreasing the core average void fraction. The potential resultant increases in neutron power and local heat fluxes can decrease fuel thermal margins (e.g., MCPR).

Core inlet temperature reductions can occur if the feedwater flow rate is increased or its temperature is reduced. As the coolant-moderator temperature at the boiling boundary falls below the saturation temperature that corresponds to the local pressure, the boundary shifts upward. Since void formation will now be initiated nearer the core coolant exit, the core average void fraction will decrease from its pre-transient value. The resultant increase in neutron power and local heat fluxes reduces the fuel thermal margins.

9.3 ABNORMAL OPERATIONAL TRANSIENTS

Statistical analysis of the equilibrium cycle thermal/mechanical performance for a (U-233/Th)O_2-fueled BWR/6 indicated that the safety limit MCPR is 1.07, the value for a UO_2-fueled BWR. Maintaining the MCPR above the safety limit is sufficient to guarantee compliance with the criterion that 99.9% of the fuel rods in a core not experience transition boiling during an abnormal operating transient of moderate frequency. If, in addition, the reactor coolant system design safety pressure limit (1375 psig) is not exceeded during the transient, then the reactor meets all safety and licensing requirements for transient events.

The design pressure limit is not exceeded due to any of the transients considered. Also, evaluation of the MCPR change for the feedwater controller failure, load rejection without bypass, pressure regulator downscale failure, and loss of feedwater heater indicates that no abnormal operating transient

will cause MCPR of a BWR fueled with denatured $(U\text{-}233/Th)O_2$ or UO_2 to fall below the safety limit value (1.07). Table 9-4 summarizes the MCPR results of the transients that were analyzed.

The $(U\text{-}233/Th)O_2$ and the reference UO_2 reactor designs are expected to meet safety and licensing requirements for abnormal transients. Details of the transient evaluations follow.

9.3.1 Load Rejection without Turbine Bypass (LRNBT)

9.3.1.1 Description of Event

Electrical grid disturbances that result in a significant loss of load on the generator causes the fast closure of the turbine control valves (TCVs). The TCVs are required to close rapidly to prevent overspeed damage to the turbine-generator rotor. The closure, combined with failure of all of the turbine bypass valves to open, causes a sudden reduction in steam flow from the pressure vessel, which results in a nuclear system pressure increase and a reactor scram. Table 9-5 lists the sequence of events for this low probability transient. The event chain applies to both the denatured $(U\text{-}233/Th)O_2$ and the reference UO_2 reactors.

When a load rejection occurs, the TCVs are assumed to close in 0.15 seconds to prevent turbine overspeed, simultaneously tripping the reactor scram circuit. Immediately, the reactor neutron power and heat flux begin to decrease due to insertion of negative scram reactivity. TCV closure, along with failure of the turbine bypass valves, reverses the flow of steam in the steam pipelines and initiates a pressure wave that travels back through the steamlines to the pressure vessel. The sudden increase in the vessel pressure collapses voids, thereby decreasing the core average void fraction, which inserts positive void reactivity. The subsequent rise of the neutron power and heat flux is mediated and reversed by Doppler reactivity feedback and scram reactivity when the increasing control blade worth becomes the controlling reactivity parameter. As the reactor power level decreases, safety/relief valves S/RVs open to relieve system pressure and continue to open and close periodically to relieve decay heat.

Table 9-4

ABNORMAL OPERATIONAL TRANSIENT MCPRs
FOR $(U233/Th)O_2$ AND UO_2 FUELS

	Reference UO_2 Fuel		Denatured $(U\text{-}233/Th)O_2$	
Transient	ΔMCPR	MCPR*	ΔMCPR	MCPR*
Feedwater control failure	0.046	1.184	0.039	1.191
Load rejection without bypass	0.029	1.201	0.004	1.226
Pressure regulator downscale failure	0.046	1.184	0.038	1.192
Loss of feedwater heater	0.113	1.117	0.097	1.133

*MCPR = Operating limit MCPR (1.23) - ΔMCPR of transient. The greater this value, the better. The safety limit minimum is 1.07.

Table 9-5

SEQUENCE OF EVENTS FOR GENERATOR LOAD REJECTION WITHOUT BYPASS

Time (sec)	Event
(-) 0.015 (approx.)	Turbine generator detection of loss of electrical load.
0.0	Turbine-generator power load unbalance devices trip to initiate turbine control valve fast closer.
0.0	Turbine bypass valves fail to operate.
0.0	Fast control valve closure initiates scram trip.
0.0	Fast control valve closure initiates a recirculation pump trip.
0.07	Turbine control valves closed.
1.1	Safety/relief valves open due to high pressure.
∿5.1	Vessel water level trip initiates trip of feedwater turbines.
∿8.5	Safety/relief valves close.
∿9.3	Group safety/relief valves open again to relieve decay heat.
>10.0 (est.)	Group safety/relief valves close again.

9.3.1.2 Assumptions, Conditions and Uncertainties

Initial conditions are detailed in Subsection 9.2 prior to the load rejection without bypass. All systems utilized for protection in this event were assumed to have the poorest allowable response (e.g., relief setpoints, scram stroke time and nuclear characteristics). Expected plant behavior is, therefore, expected to reduce the actual severity of the transient.

9.3.1.3 Analysis

Analyses of the LRNBT abnormal operational transient were performed for both the (U-233/Th)O_2 and the reference UO_2 reactors using the methods described in Subsection 4.4. The behavior of various reactor parameters during the transient are plotted as a function of time for the thorium-fueled and UO_2-fueled reactors in Figures 9-2 and 9-3, respectively. Parameters that are representative of reactor performance are discussed in detail to explain the differences observed between the transient responses of (U-233/Th)O_2 and the reference UO_2 reactors.

a. Reactivity

Figure 9-4 shows the variation of the net reactivity in both fuel types as a function of time following the load rejection. As seen in the figure, the (U-233/Th)O_2 net reactivity insertion is always less than that of the reference UO_2.

The fuel designs' net reactivities have scram, void, and Doppler components which are presented in Figures 9-5, 9-6, and 9-7, respectively. Due to the smaller delayed neutron fraction of the (U-233/Th)O_2 design, its individual reactivity parameters are more sensitive to reactor core environment perturbations than those of the UO_2 design. Thus, relative to the UO_2 BWR the (U-233/Th)O_2 BWR has:

(1) A greater negative scram reactivity insertion rate;

(2) Greater positive void reactivity insertion rate (due to >DVC) from core pressurization caused by the fast TVC closure; and

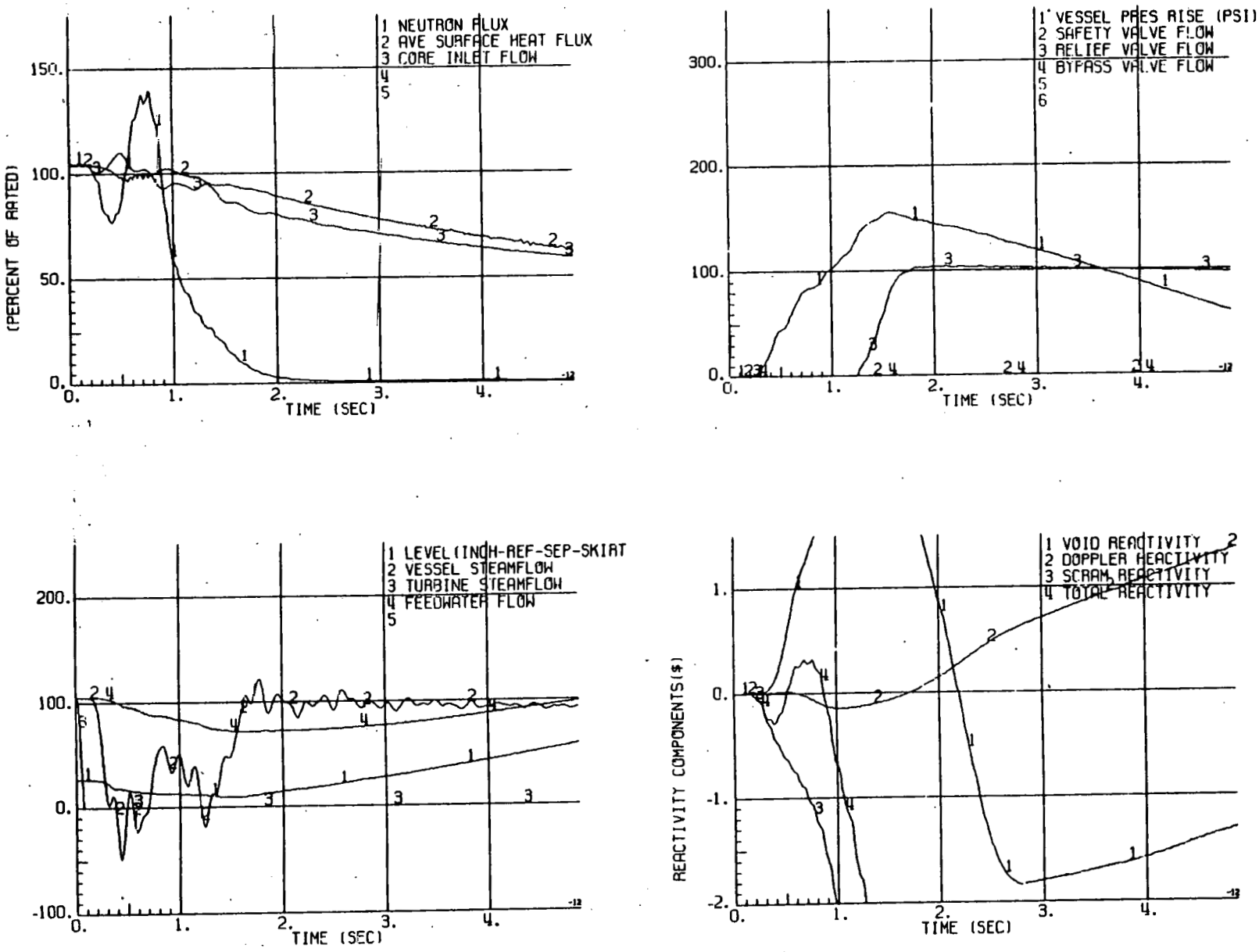

Figure 9-2. $(U/Th)O_2$ Reactor Parameters versus Time after a Generator Load Rejection without Bypass

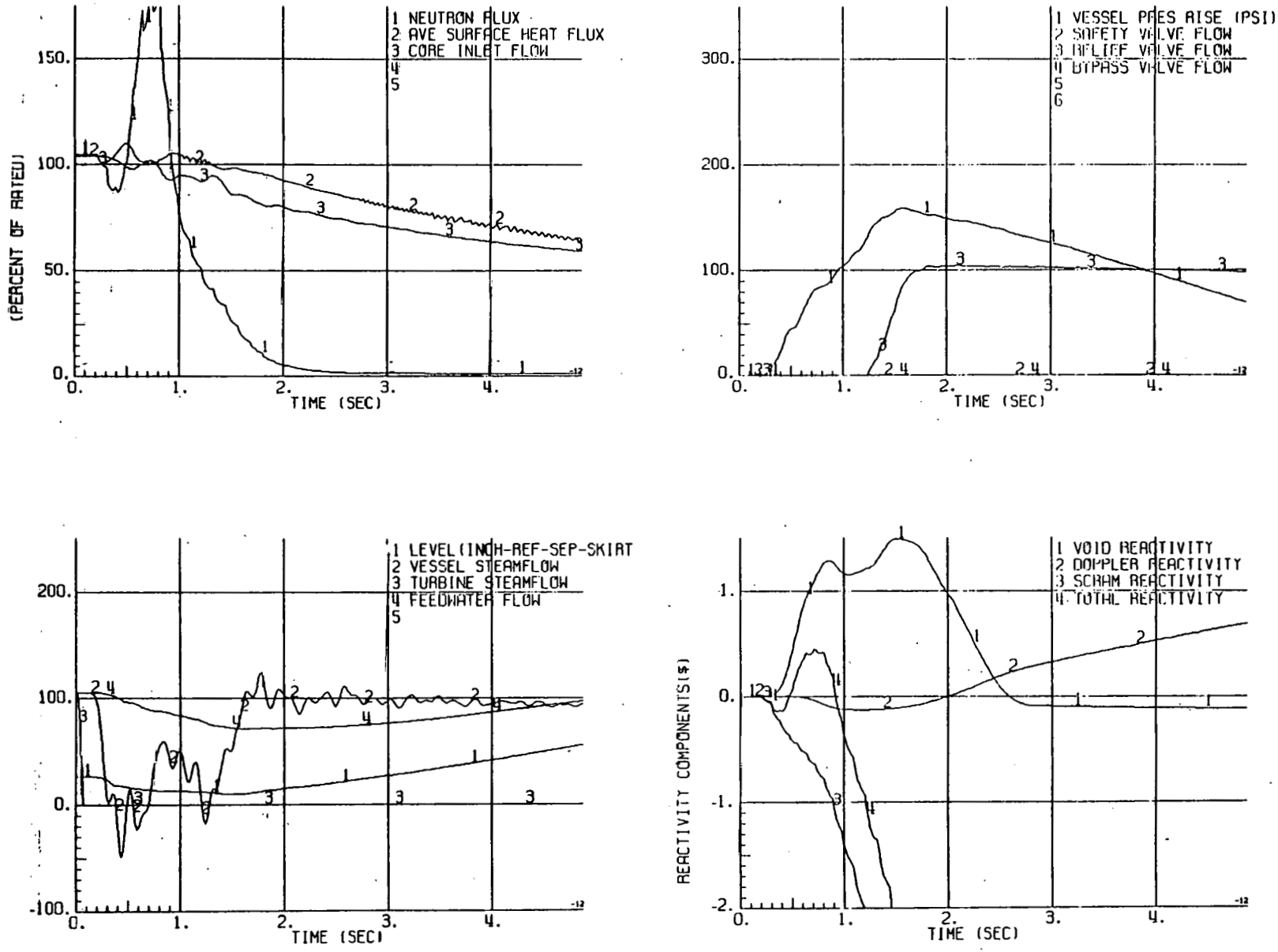

Figure 9-3. UO_2 Reactor Parameters versus Time after a Load Rejection without Bypass

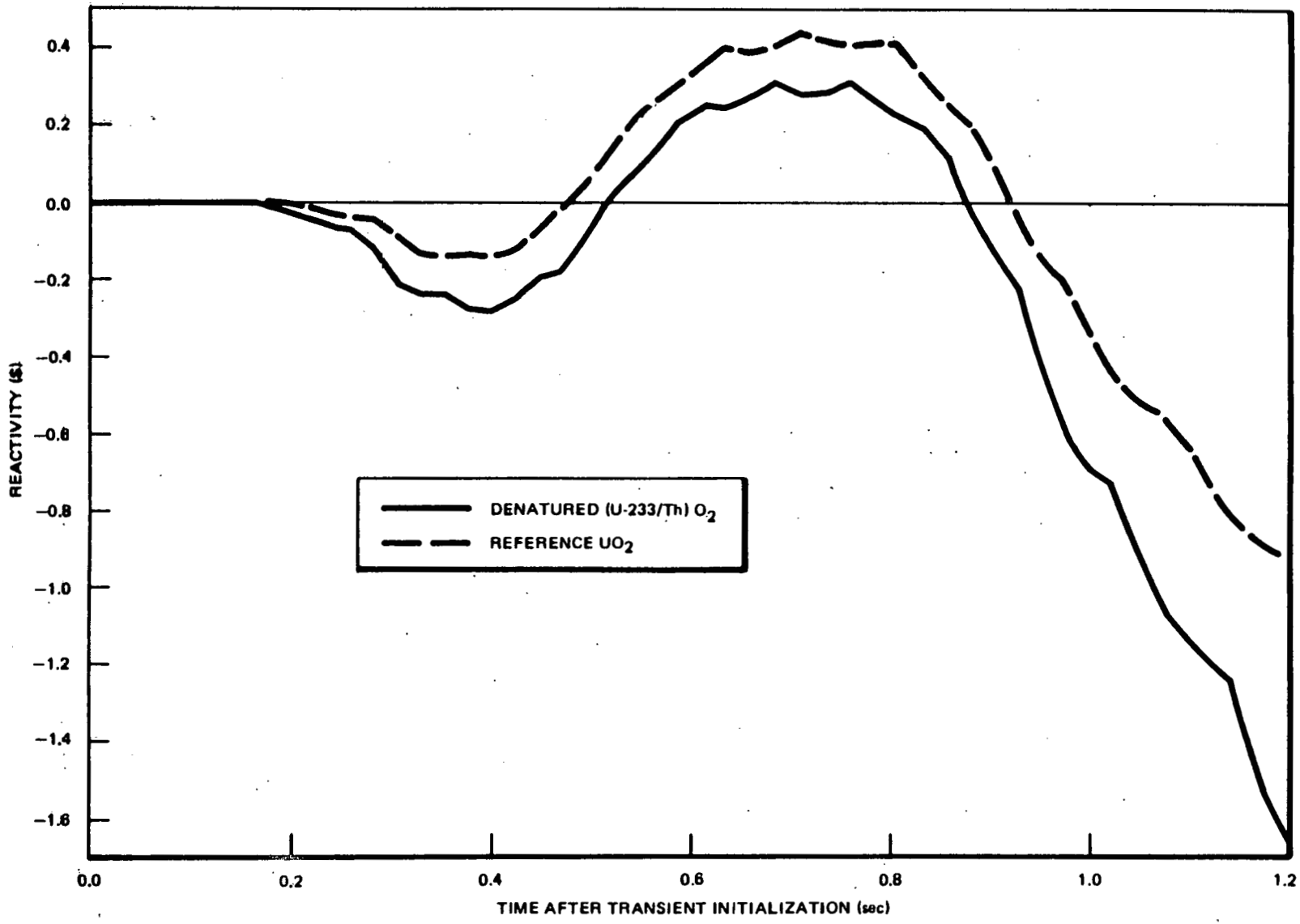

Figure 9-4. Net Reactivity versus Time after Load Rejection without Bypass

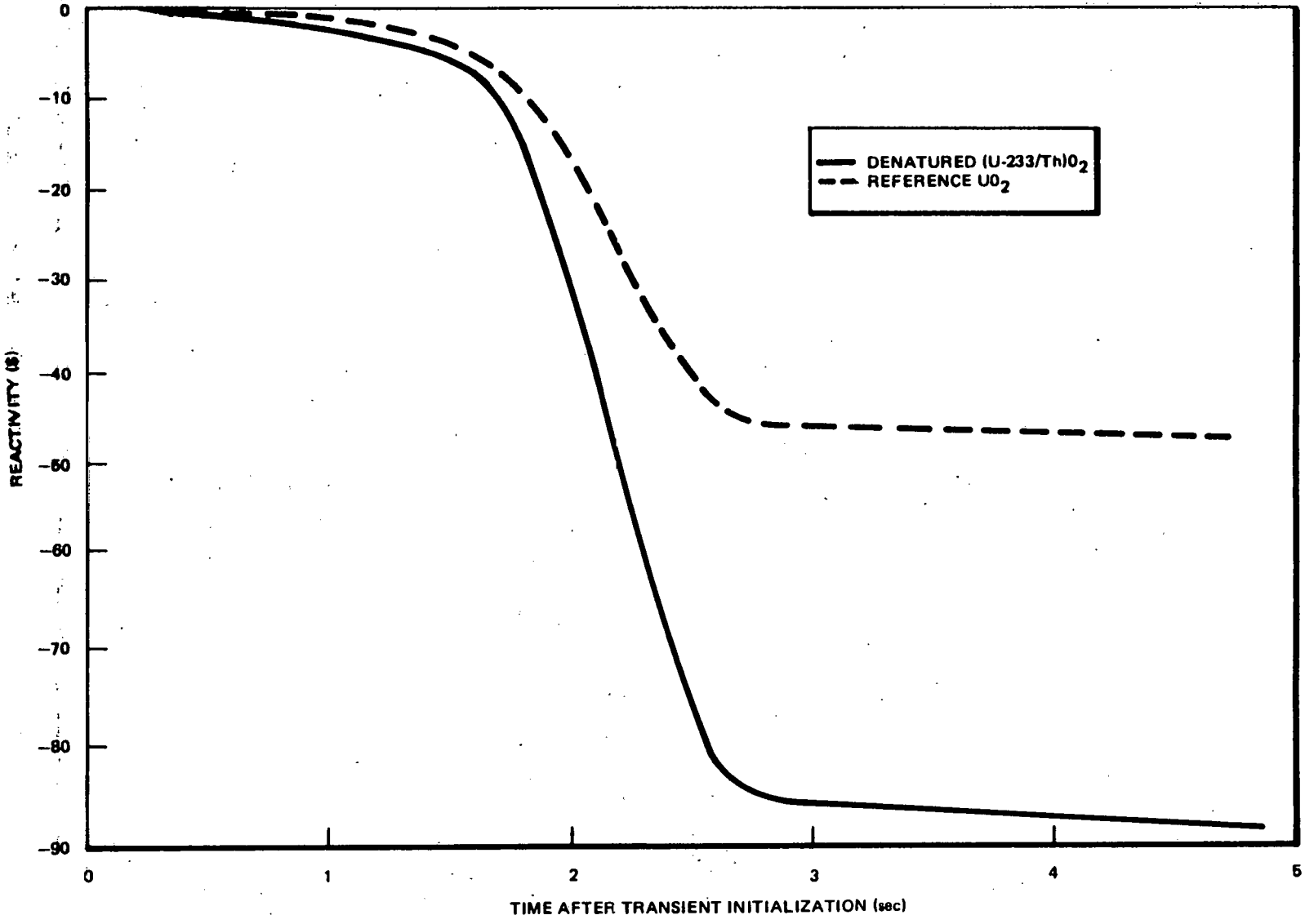

Figure 9-5. Scram Reactivity versus Time after Load Rejection without Bypass

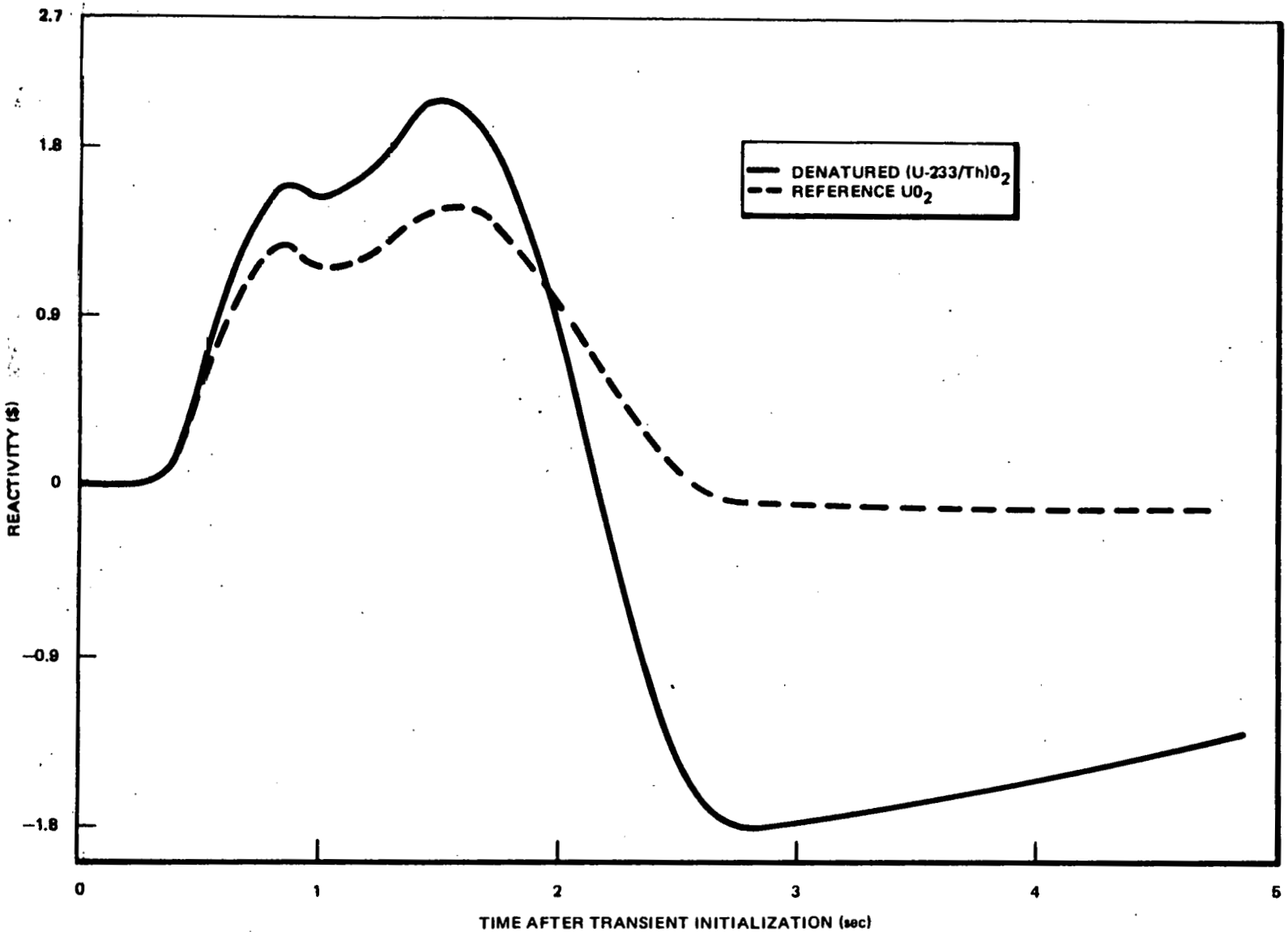

Figure 9-6. Void Reactivity versus Time after Load Rejection without Bypass

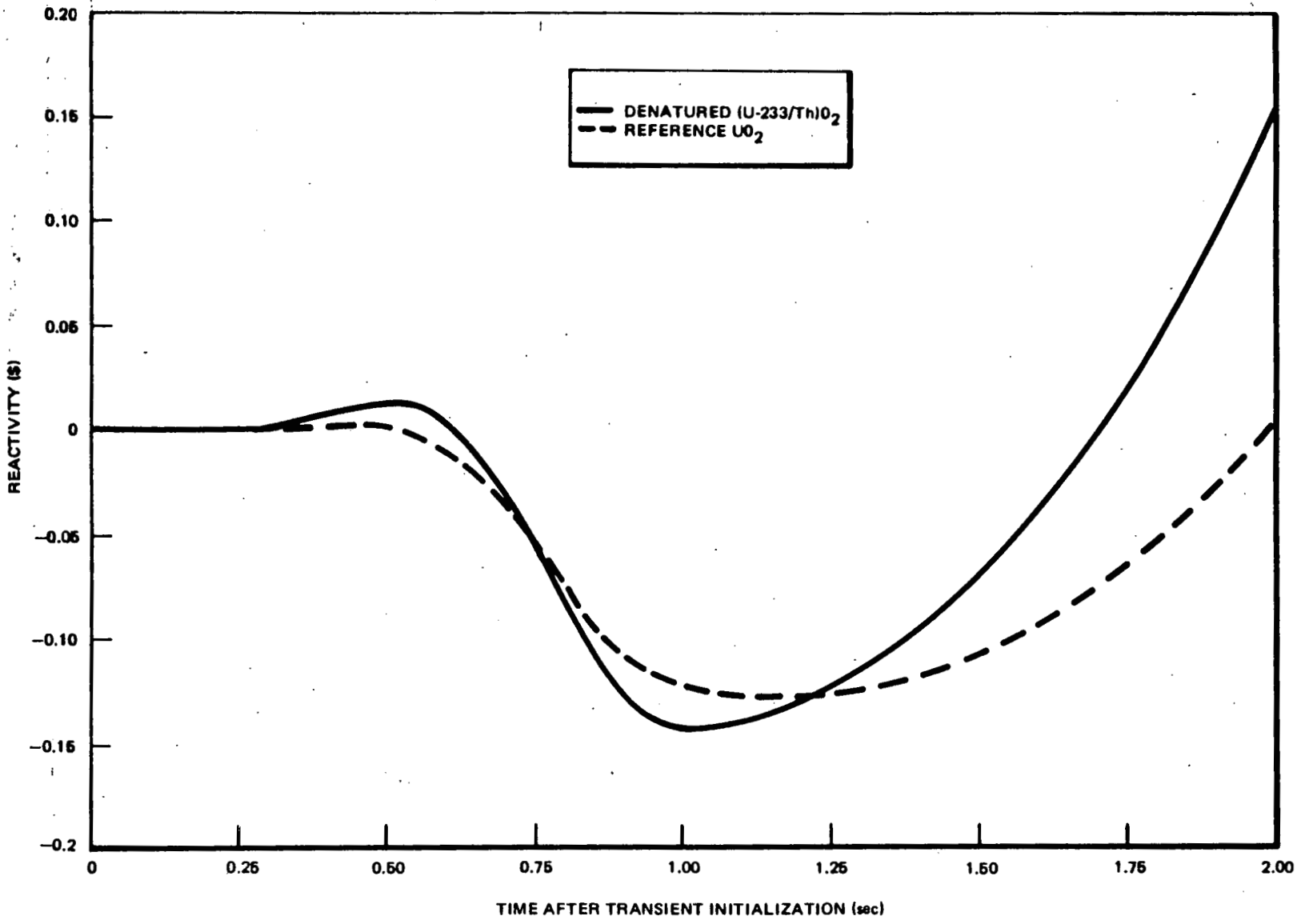

Figure 9-7. Doppler Reactivity versus Time after Load Rejection without Bypass

(3) Greater negative Doppler reactivity insertion rate (due to >DDC) from increasing fuel temperatures as the reactor power rises due to the positive reactivity insertion from (2) above.

By close examination of these individual reactivity components, it is observed that the scram reactivity is the controlling factor of net reactivity in both fuel types during the LRNBT transient. Since the thorium design scram curve is superior to that of the UO_2 design, the net positive reactivity insertion of the (U-233/Th)O_2 fuel design is less than that of the reference UO_2 desgn.

b. Neutron Flux, Heat Flux and System Pressures

Figures 9-8 through 9-11 illustrate the behavior of the neutron flux, heat flux, maximum core pressure, and maximum steamline pressure during the LRNBT transient. The increase in neutron flux for the (U-233/Th)O_2-fueled BWR is roughly half that of the UO_2-fueled BWR. Similarly, the heat flux and system pressure increases are lower for the (U-233/Th)O_2 design than for the UO_2 design. Thus, thermal and pressure margins are expected to increase in the (U-233/Th)O_2-fueled BWR relative to the reference UO_2-fueled BWR for a LRNBT transient.

9.3.1.4 Results and Conclusions

a. Results

The LRNBT is considered to be an event of infrequent occurrence. To meet infrequent event safety and licensing requirements, it is only necessary to demonstrate that the transient does not result in a maximum system pressure greater than or equal to $\geq$1375 psig. Peak pressure and MCPRs for the LRNBT are given in Table 9-6 for both reactor designs.

As seen in the table, both reactor designs meet design requirements for the LRNBT since the peak vessel pressures are less than 1375 psig.

Table 9-6

LRNBT MCPRs AND PEAK PRESSURES

Fuel Type	Operating Limit MCPR	Largest ΔMCPR During Event	Smallest MCPR During Event	Peak Vessel Bottom Pressure (psig)
Reference UO_2	1.23	0.029	1.191	1233
Denatured $(U\text{-}233/Th)O_2$	1.23	0.004	1.226	1229

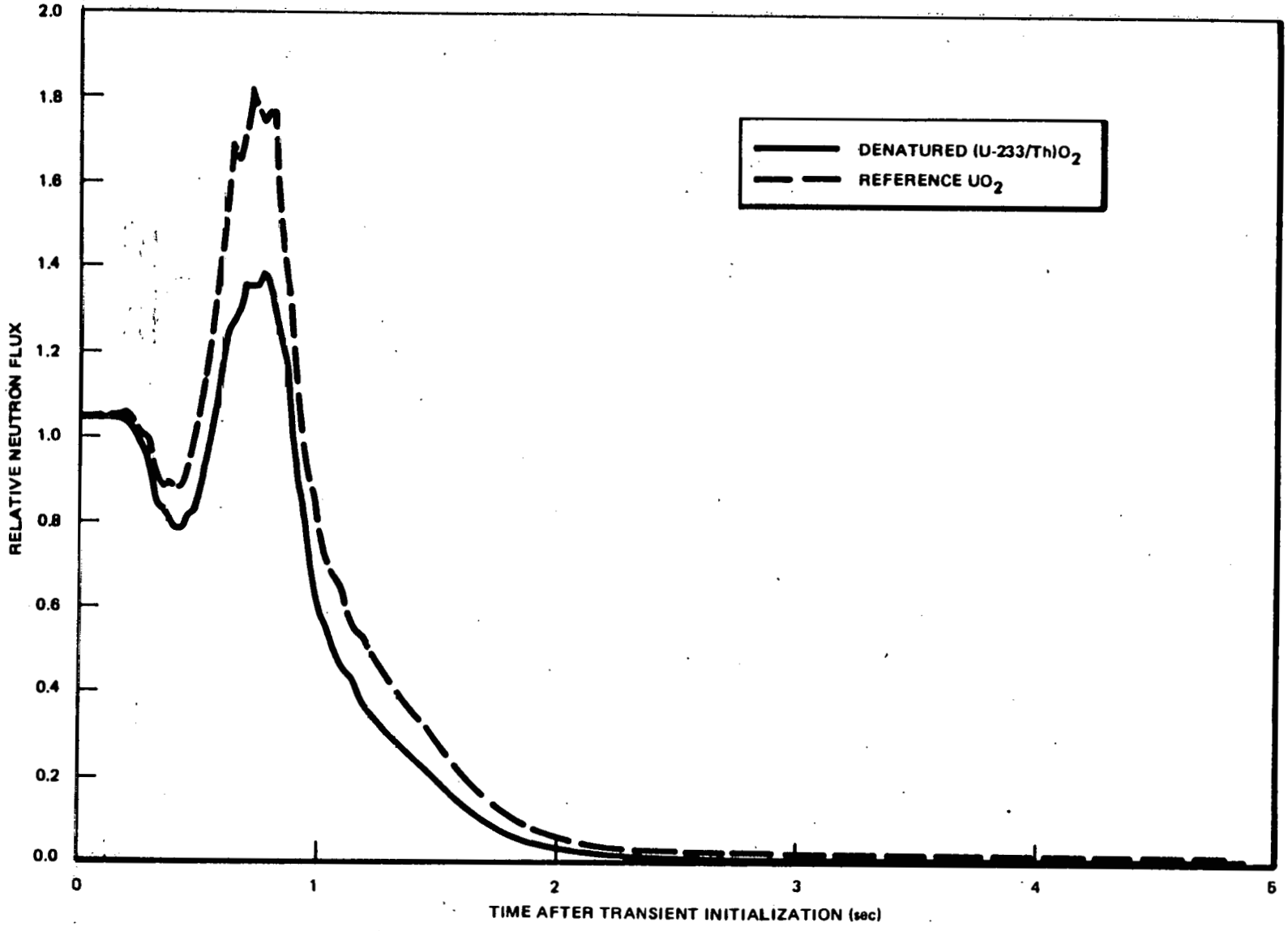

Figure 9-8. Relative Neutron Flux versus Time after Load Rejection without Bypass

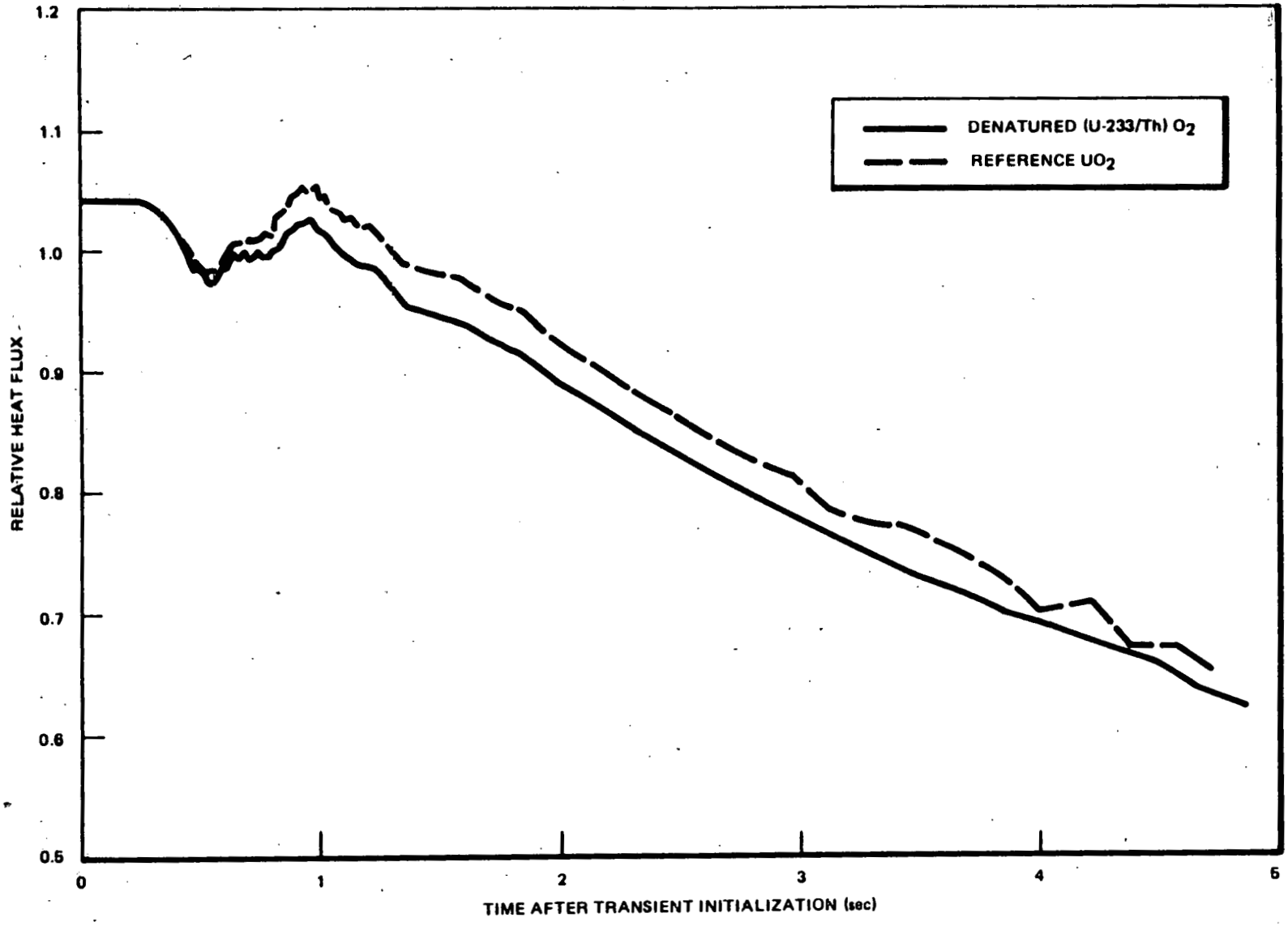

Figure 9-9. Relative Heat Flux versus Time after Load Rejection without Bypass

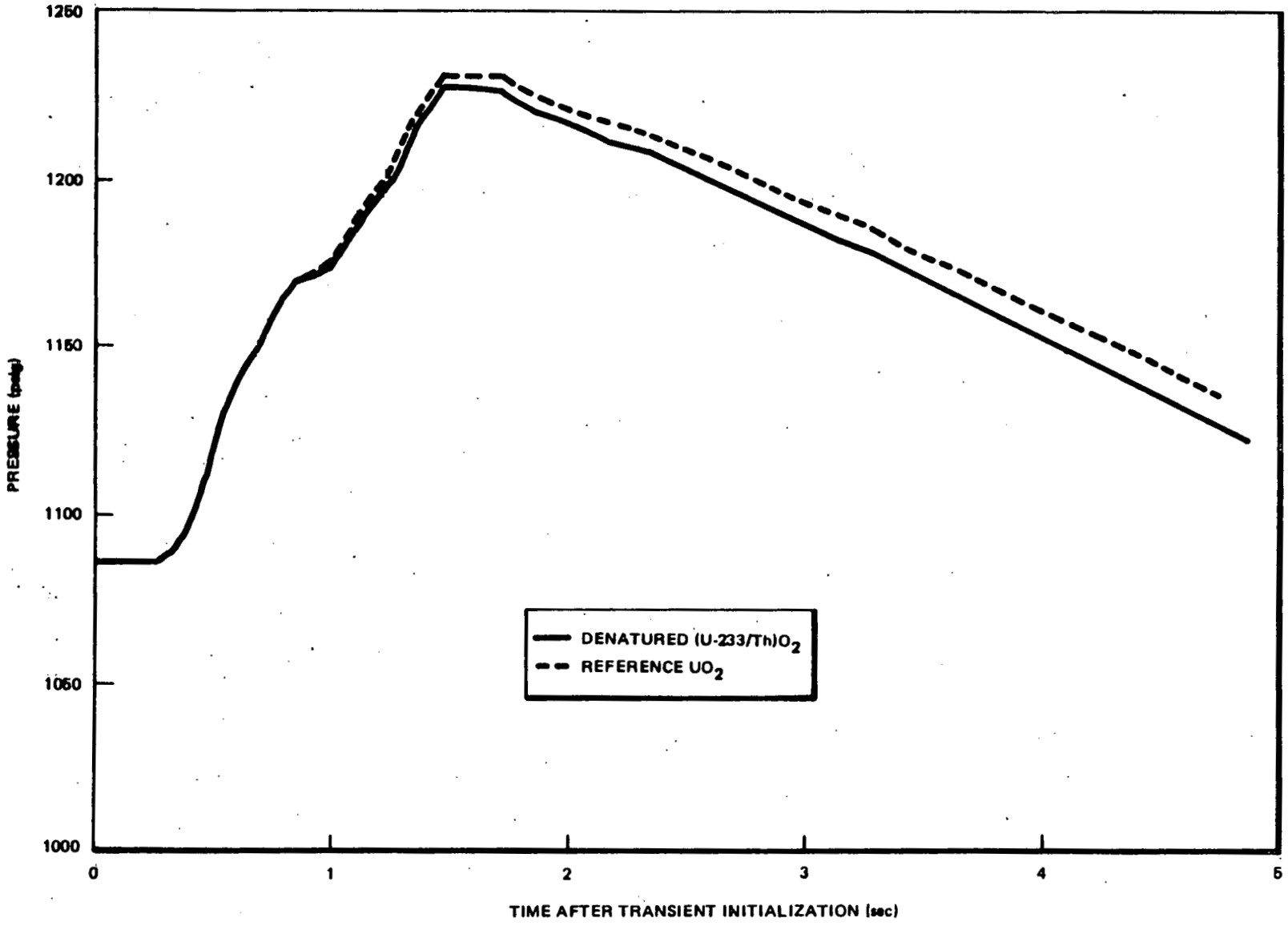

Figure 9-10. Maximum Core Pressure versus Time after Load Rejection without Bypass

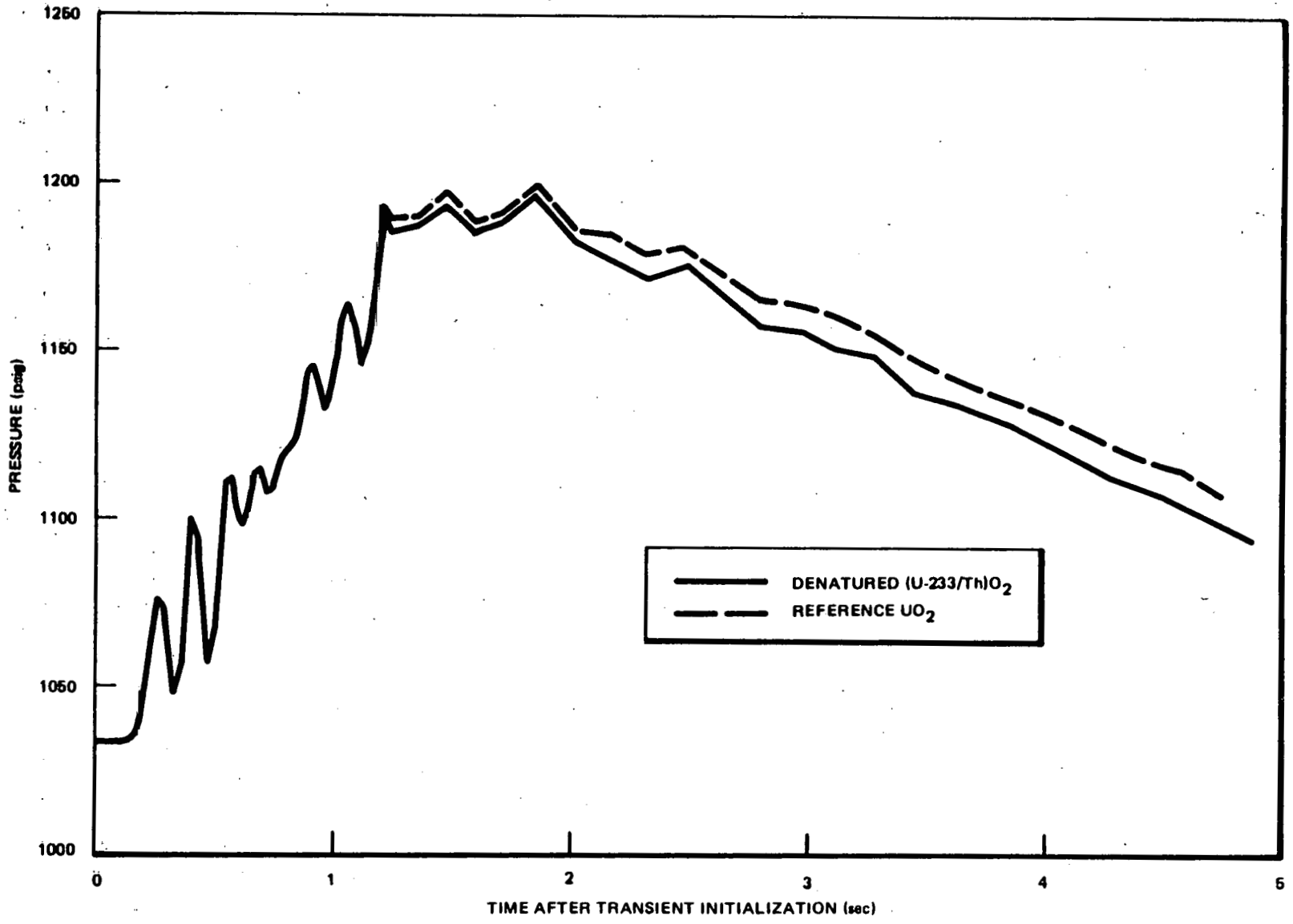

Figure 9-11. Maximum Steamline Pressure versus Time after Load Rejection without Bypass

b. Conclusions

The (U-233/Th)O_2-fueled BWR shows better performance during a LRNBT abnormal operational transient than that seen for the reference UO_2-fueled BWR. Use of thorium fuel results in greater thermal and pressure margins than are seen in the UO_2 reactor due to the superior scram curve of the (U-233/Th)O_2 design relative to that of the UO_2 design.

Both reactor types should meet current safety and licensing requirements of the LRNBT transient with the (U-233/Th)O_2 BWR being less limiting than the reference UO_2 BWR.

9.3.2 Pressure Regulator Downscale Failure (PRDF)

9.3.2.1 Description of Event

Failure of both steam pressure regulators, PRDF, will cause TCV fast closure which causes a nuclear system pressure increase and a reactor scram at the high neutron flux setpoint. Table 9-7 lists the sequence of events; the event chain applies to both the denatured (U-233/Th)O_2 and the reference UO_2 reactors.

Two identical pressure regulators are provided to maintain primary system control. They independently sense pressure just upstream of the main turbine stop valves and compare it to two separate setpoints to create proportional error signals that produce each regulator output. The output of both regulators feeds into a high value gate where the regulator with the highest output controls the main turbine control valves. The lowest pressure setpoint gives the largest regulator output. The backup regulator is set 5 psi higher, giving a slightly smaller error and a slightly smaller effective output of the controller.

A single failure is postulated to occur which erroneously causes the controlling regulator to close the main turbine control valves, thereby increasing the reactor system reactor pressures. The backup regulator assumes control, but a single failure occurs which causes a downscale failure of the pressure regulator demand to zero (e.g., high value gate downscale failure). The failure of

Table 9-7

SEQUENCE OF EVENTS FOR PRESSURE REGULATOR DOWNSCALE FAILURE

Time (sec)	Event
0.0	Simulate zero steam flow demand to main turbine and bypass valves.
0.0	Turbine control valves start to close.
1.1	Neutron flux reaches high flux scram setpoint and initiates reactor scram.
2.4	Recirculation pump drive motors are tripped due to high dome pressure.
2.4	Safety/relief valves open due to high pressure.
∿6.1	Vessel water level (L8) trip initiates main turbine and feedwater turbine trip.
∿6.2	Main turbine stop valves close.
∿9.3	Safety/relief valves close.
∿9.7	Group safety/relief valves open again to relieve decay heat.
>15.0 (est.)	Group safety/relief valves close.

the backup regulator causes full closure of the TCVs as well as an inhibit of steam bypass flow that together initiate a pressure wave that travels back through the steamline to the pressure vessel and causes an increase in core pressures. Voids collapse due to the pressure increase, thereby decreasing the core average void fraction which inserts positive void reactivity. This causes the neutron flux to rise until scram is initiated on sensed high neutron flux level. Unlike the LRNBT event, scram does not occur at the same time as the TCV full closure. This results in higher peak neutron fluxes, heat fluxes, and system pressures for the PRDF event than for the LRNBT event due to core pressurization. Reactor power decreases as S/RVs open to relieve the system high pressure and then open and close periodically to relieve decay heat pressurization of the primary system.

9.3.2.2 Assumptions, Conditions and Uncertainties

Initial conditions prior to the PRDF are detailed in Subsection 9.2. All systems utilized for protection in this event were assumed to have the poorest allowable response (e.g., relief setpoints, scram stroke time and nuclear characteristics). Expected plant behavior is, therefore, expected to reduce the actual severity of the transient.

9.3.2.3 Analysis

Analyses of the PRDF transient were performed for both the denatured (U-233/Th)O_2 and the reference UO_2 reactors using the methods described in Subsection 4.4. The behavior of various parameters during the transient are plotted as a function of time for the thorium-fueled and UO_2-fueled reactors in Figures 9-12 and 9-13, respectively. Parameters that are representative of reactor performance are discussed in detail to explain the (U-233/Th)O_2 and reference UO_2 reactors' transient responses.

a. Reactivity

Figure 9-14 illustrates the variation of the net reactivity in both fuel types as a function of time following the PRDF. The net reactivities have similar shape and magnitude until scram occurs at approximately 1.25 seconds after the PRDF, with the UO_2 design net

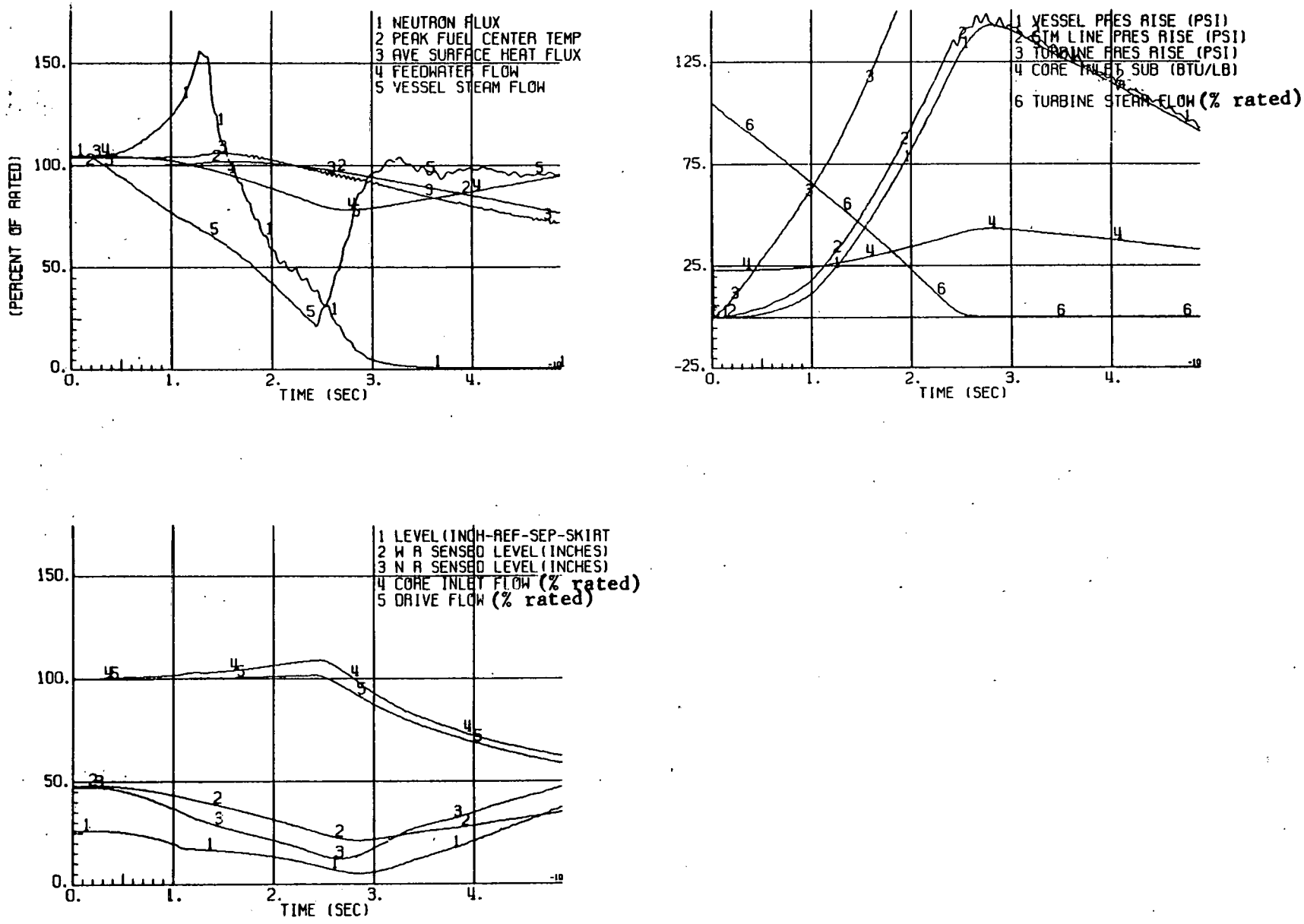

Figure 9-12. $(U/Th)O_2$ Reactor Parameters versus Time after a Pressure Regulator Downscale Failure

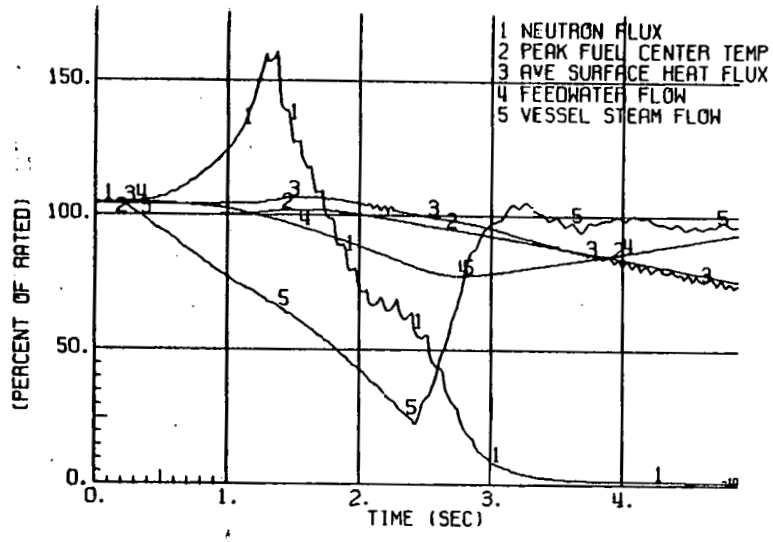

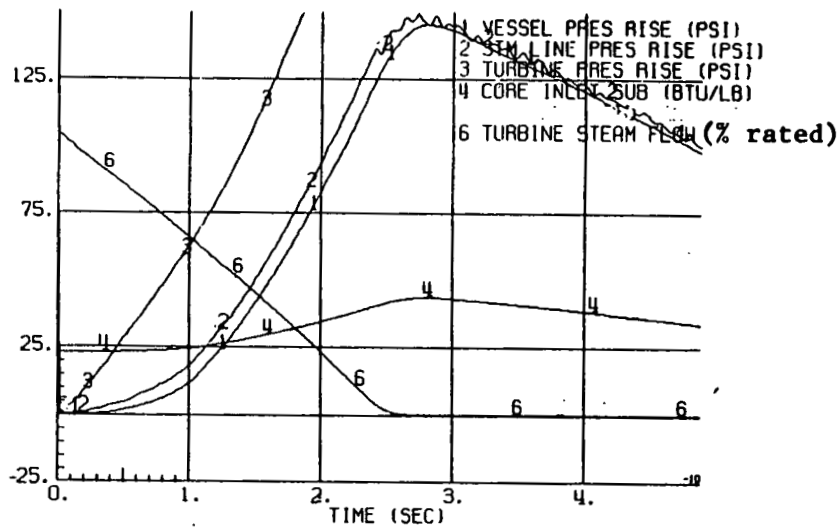

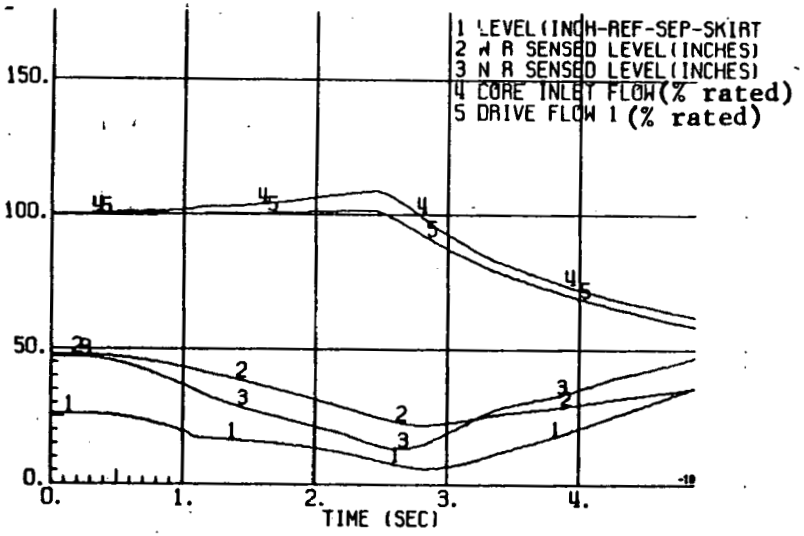

Figure 9-13. UO_2 Reactor Parameters versus Time after a Pressure Regulator Downscale Failure

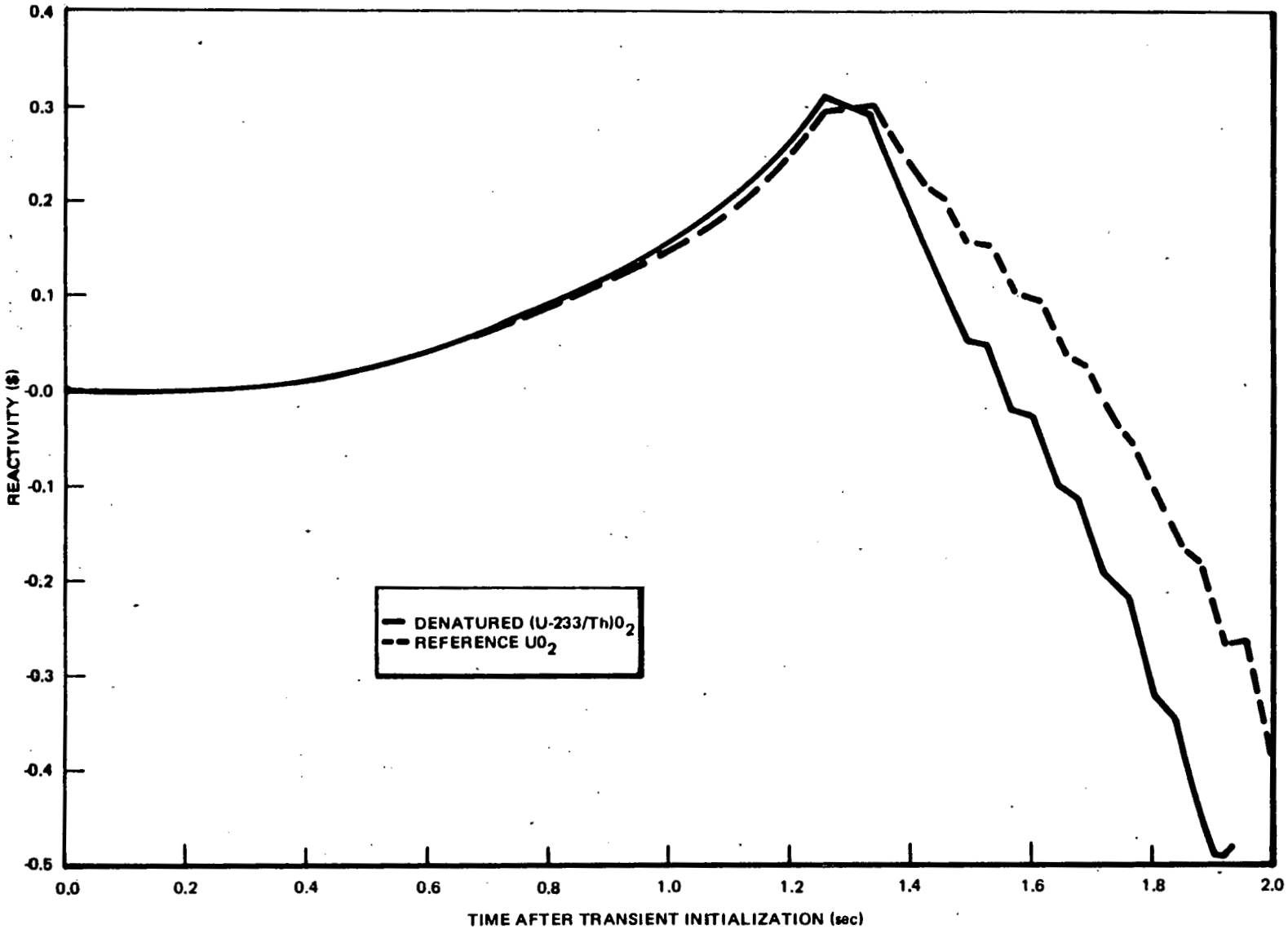

Figure 9-14. Net Reactivity versus Time after PRDF

reactivity being slightly higher than that of the $(U\text{-}233/Th)O_2$ design.

Figures 9-15 and 9-16 illustrate the void and Doppler reactivity components during the PRDF. During pressurization of the cores, the net reactivities are entirely composed of void and Doppler constituents until scram on high neutron flux at approximately 1.25 seconds following the PRDF. As was discussed in the analysis of the LRNBT, the $(U\text{-}233/Th)O_2$ reactivity components are more sensitive than the UO_2 components are to perturbations in the reactor core environment. But the corresponding increase in void reactivity and decrease in Doppler reactivity of the $(U\text{-}233/Th)O_2$ fuel relative to the UO_2 fuel cancel one another, thereby producing approximately the same net reactivity insertion as is seen in the UO_2 fuel design. Subsequent to scram, the thorium net reactivity decreases faster than the UO_2 reactivity due to the superior scram response of the $(U\text{-}233/Th)O_2$ design.

b. Neutron Flux, Heat Flux and System Pressure

Figures 9-17 through 9-20 illustrate the behavior of the neutron flux, heat flux, maximum reactor core pressure, and maximum steamline pressure during the PRDF transient. As seen in Figure 9-17, the neutron fluxes are nearly identical through much of the core pressurization, with the UO_2 flux rising slightly above that of $(U\text{-}233/Th)O_2$ about one second after the PRDF. This behavior results from the similar net reactivity insertion rates of the two fuel types during pressurization. Since the net reactivity insertion rates are almost identical, secondary effects of other nuclear parameters, such as average neutron lifetimes, the time-dependent delayed neutron precursor concentrations, and the respective delayed neutron decay constants, are observed. The complex interaction of these parameters are not quantified as to their effect on the neutron flux in this study, but were explicitly accounted for in the methods utilized to model these transients.

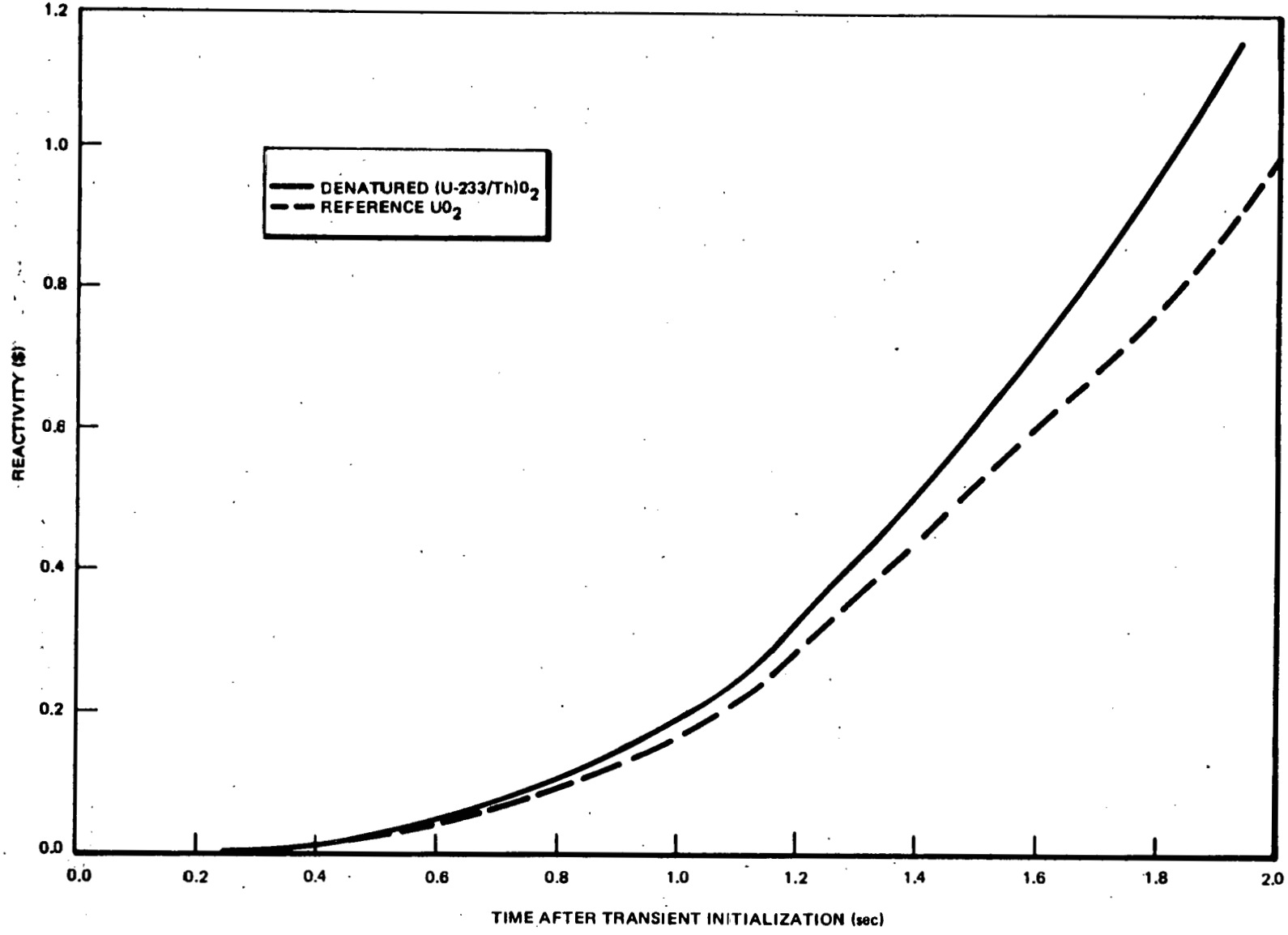

Figure 9-15. Void Reactivity versus Time after PRDF

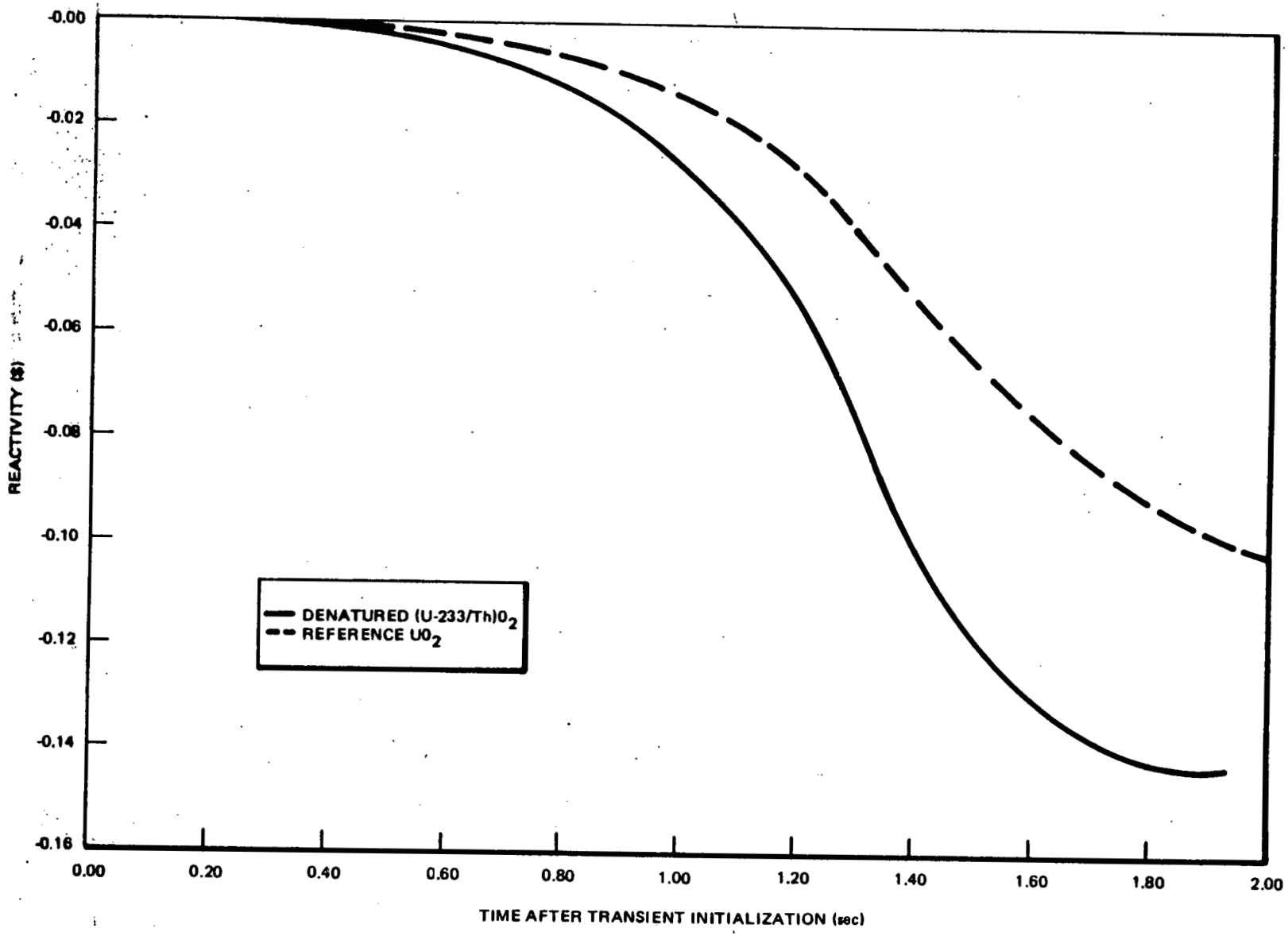

Figure 9-16. Doppler Reactivity versus Time after PRDF

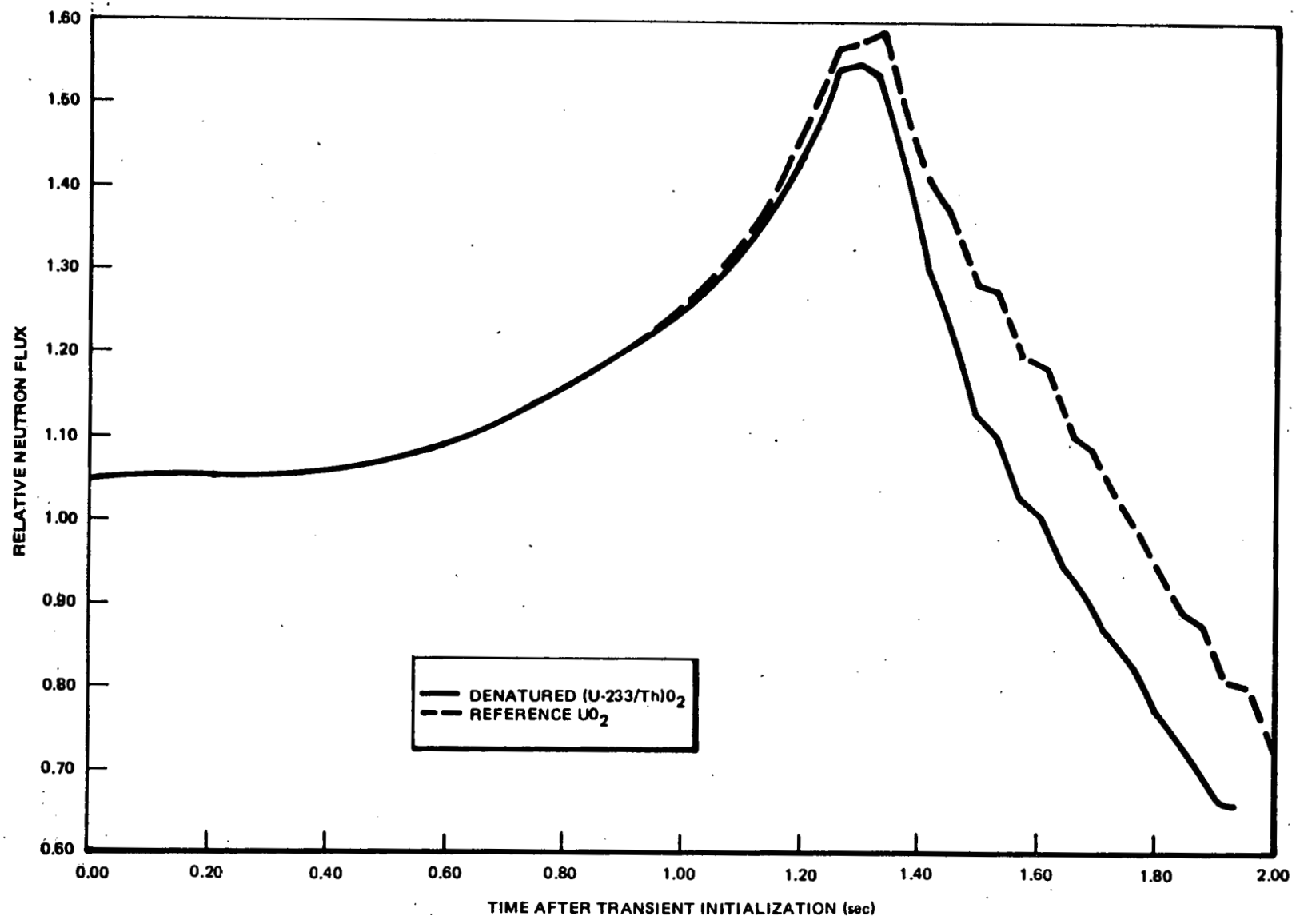

Figure 9-17. Relative Neutron Flux versus Time after PRDF

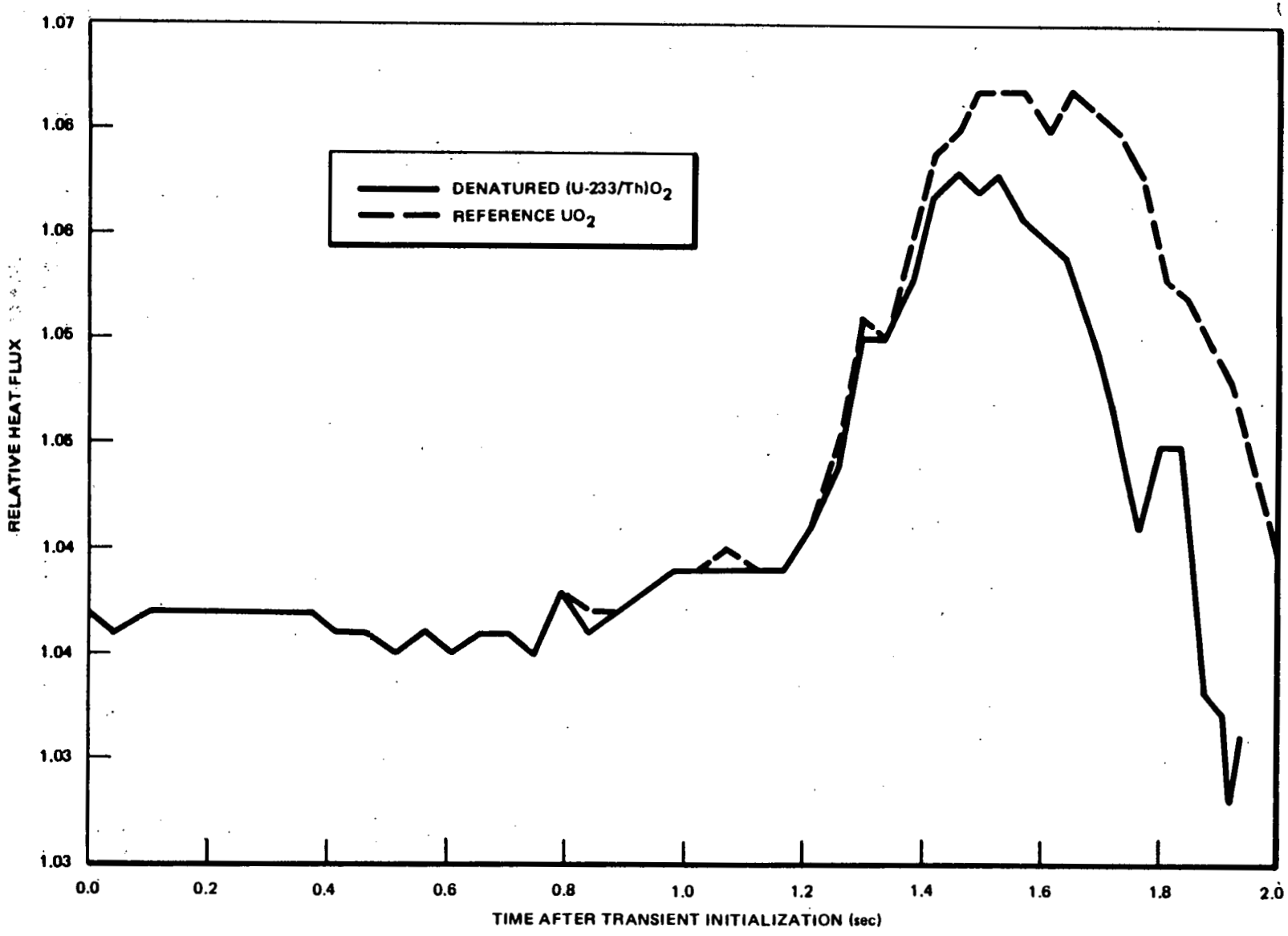

Figure 9-18. Relative Heat Flux versus Time after PRDF

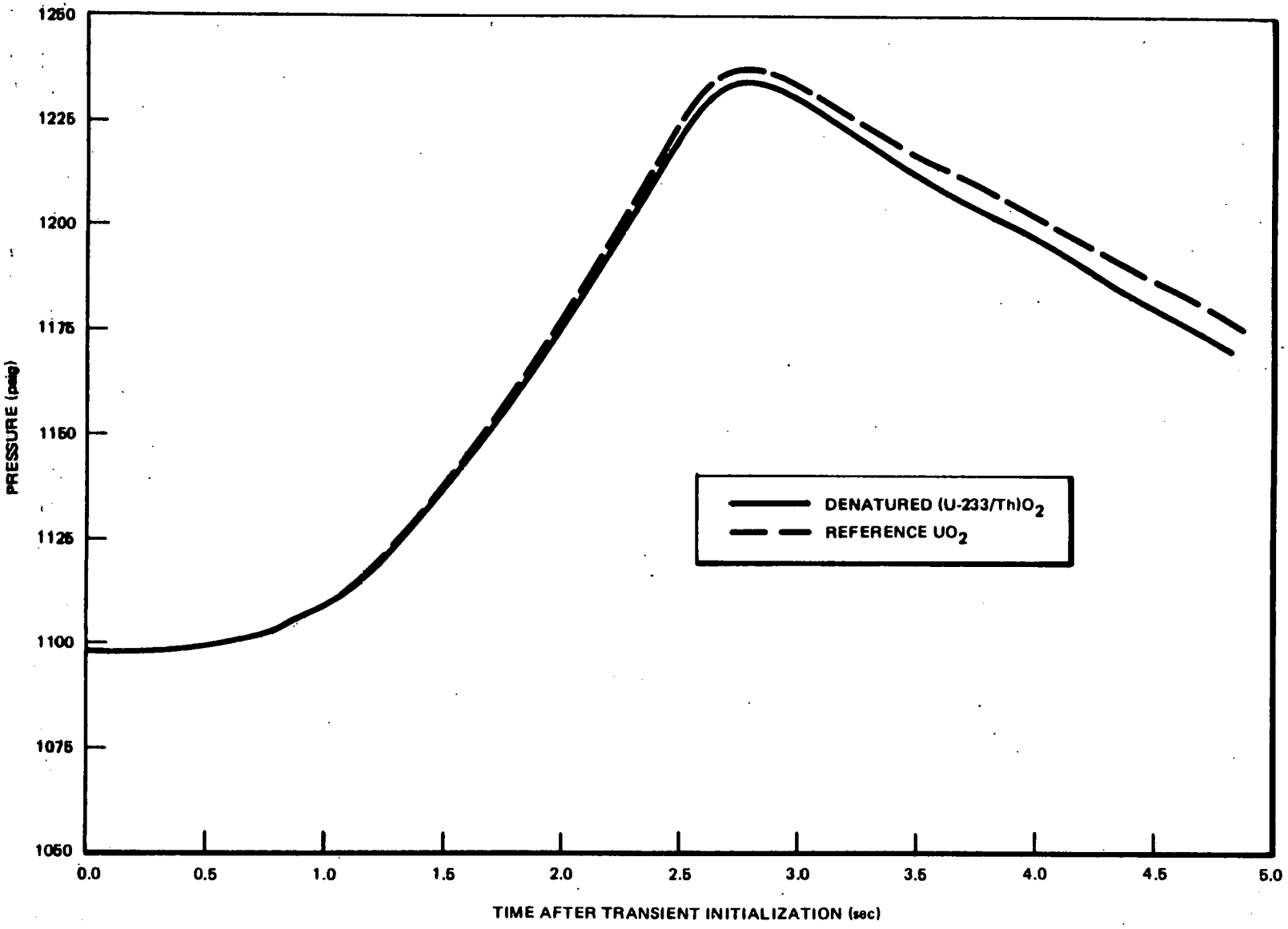

Figure 9-19. Reactor Pressure versus Time after PRDF

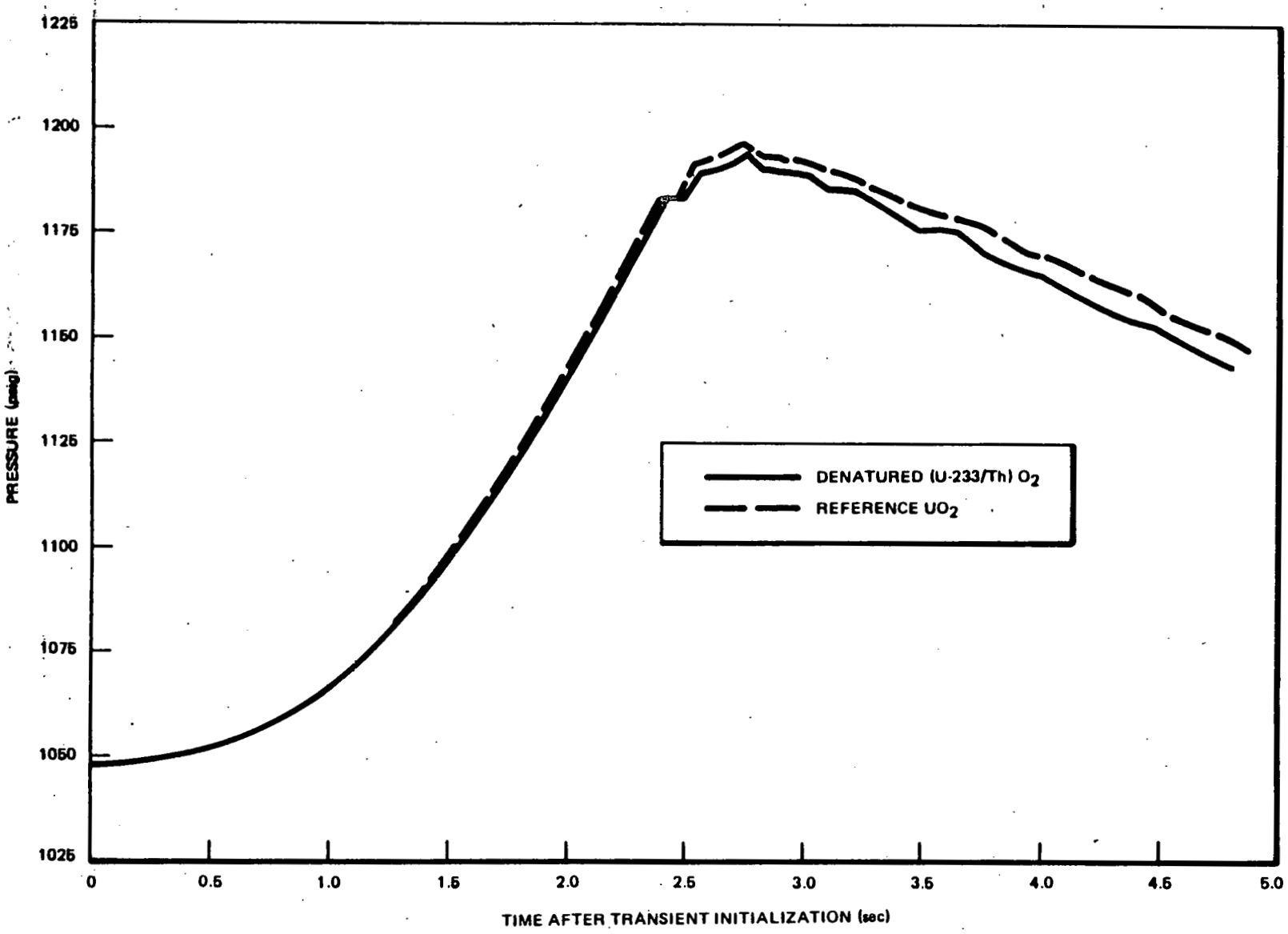

Figure 9-20. Steamline Pressure versus Time after PRDF

Subsequent to scram, the (U-233/Th)O_2 neutron flux decreases faster than the UO_2 flux due to the superior scram response observed for the (U-233/Th)O_2 design. Correspondingly, the peak heat flux and peak reactor pressure are lower for the (U-233/Th)O_2 design than for the UO_2 design. Therefore, thermal and pressure margins should improve for the (U-233/Th)O_2 BWR relative to the reference UO_2 BWR for a PRDF transient.

9.3.2.4 Results and Conclusions

a. Results

The PRDF is considered to be an event of moderate occurrence; therefore, it is necessary to demonstrate that the transient does not result in a MCPR equal to or less than 1.07 and that the maximum reactor system pressure observed during the event is less than 1375 psig for the reactor designs to meet safety and licensing requirements.

The MCPR and peak reactor pressure expected during a PRDF are given in Table 9-8 for both reactor designs. Both reactor fuel designs meet design requirements for the PRDF since the smallest MCPRs are greater than the safety limit (1.07), and peak vessel pressures are less than 1375 psig.

b. Conclusions

The (U-233/Th)O_2-fueled BWR demonstrates better performance during a PRDF abnormal operational transient than that seen for the reference UO_2-fueled BWR. The effect of the greater DVC of the thorium fuel, relative to that of the UO_2 fuel, is offset by its greater DDC. Thus, any significant difference in the response of the two fuel designs to a PRDF results from differences in the scram reactivity insertion rates of the reactors. Because of the superior scram response of the thorium fuel compared to that of the UO_2 fuel, greater thermal and pressure margins are observed for the (U-233/Th)O_2 fuel design than for the UO_2 fuel design. Both fuel types are expected to meet current safety and licensing requirements for

Table 9-8

PRDF, MCPRs AND PEAK PRESSURES

Fuel Type	Operating Limit MCPR	Largest ΔMCPR During Event	Smallest MCPR During Event	Peak Vessel Bottom Pressure (psig)
Reference UO_2	1.23	0.046	1.184	1226
Denatured $(U\text{-}233/Th)O_2$	1.23	0.038	1.192	1223

the PRDF transient event, with the denatured (U-233/Th)O_2 BWR being less limiting than the reference UO_2 BWR.

9.3.3 Feedwater Controller Failure (FWCF)

9.3.3.1 Description of Event

The loss of feedwater flow rate control, FWCF, can result in an increased rate of feedwater flow into the pressure vessel. The increased flow increases the core inlet subcooling which decreases the core average void fraction, thereby increasing the reactor power until the reactor scrams on high sensed water level in the pressure vessel. Table 9-9 lists the sequence of events; the event chain applies to both the denatured (U-233/Th)O_2 and the reference UO_2 reactors.

At the start of the transient, the feedwater controller is forced to its upper limit, 130% NBR flow. The increased flow of water into the pressure vessel causes a corresponding rise of the vessel water level, but virtually no change is observed in the core inlet flow which is determined primarily by the recirculation pump speed. Due to the increased liquid coolant inventory, the bulkwater region temperature decreases which increases the core inlet subcooling. The reduction in core inlet coolant temperature forces the boiling boundary upward, thereby decreasing the core average void fraction which inserts positive reactivity and increases the reactor power. The power continues to rise until the water level exceeds the high-water level trip reference elevation. At this point, the feedwater pumps and the main turbine are tripped and the reactor is scrammed. The turbine bypass system and several relief valves open to relieve pressure, then the relief valves close to re-establish pressure control during shutdown.

9.3.3.2 Assumptions, Conditions and Uncertainties

Initial conditions prior to the FWCF are detailed in Subsection 9.2. Important factors (such as reactivity coefficients, scram characteristics, magnitude of the feedwater temperature change) are assumed to be at the worst configuration. Therefore, any deviations observed in the actual plant operation reduce the severity of the event.

Table 9-9

SEQUENCE OF EVENTS FOR FEEDWATER CONTROLLER FAILURE

Time (sec)	Event
0.0	Initiate simulated failure of 130% upper limit at system design pressure of 1065 psig on feedwater flow.
11.6	L8 vessel level setpoint initiates reactor scram and trips main turbine and feedwater pumps.
11.7	Recirculation pump trip actuated by stop valve position switches.
11.7	Main turbine bypass valves opened due to turbine trip.
13.2	Safety/relief valves open due to high pressure.
18.4	Safety/relief valves close.
>20.0 (est.)	Water level dropped to low water level setpoint (Level 2).
>50.0 (est.)	RCIC and HPCS flow into vessel (not simulated).

9.3.3.3 Analysis

Analyses of the FWCF transient were performed for both the denatured (U-233/Th)O_2 and the reference UO_2 reactors using the methods described in Subsection 4.4. The behavior of various parameters during the transient for the thorium and reference UO_2-fueled reactors are given in Figures 9-21 and 9-22, respectively. Parameters that are representative of reactor performance are discussed in detail to explain the transient response of the (U-233/Th)O_2 and the reference UO_2 fuel designs.

a. Reactivity

Figure 9-23 shows the variation of the net reactivity in both fuel types as a function of time following the feedwater controller failure. The FWCF causes a slow insertion of positive net reactivity through the reduction of the core inlet coolant temperature as described in the description of the event. As seen in the figure, the net reactivities have approximately the same shape and magnitude until scram occurs on the high water level trip setpoint.

Figures 9-24 and 9-25 give the void and Doppler constituents of reactivity which together compose the net reactivities until scram occurs. As was discussed in previous sections, the (U-233/Th)O_2 reactivity components are more sensitive to changes in the core environment than are the UO_2 components. But, as in the PRDF analysis, changes in the reactivity components of the thorium fuel relative to the UO_2 components cancel one another, Thus, the net reactivities behave in the same manner until the reactor scram. Thereafter, since the thorium design scram curve is superior to the UO_2 design scram curve, the net reactivity insertion of the (U-233/Th)O_2 fuel design is less than that of the reference UO_2 design.

b. Neutron Flux, Heat Flux and Reactor Pressure

Figures 9-26 through 9-28 illustrate the behavior of the neutron flux, heat flux, and maximum reactor core pressure during the FWCF

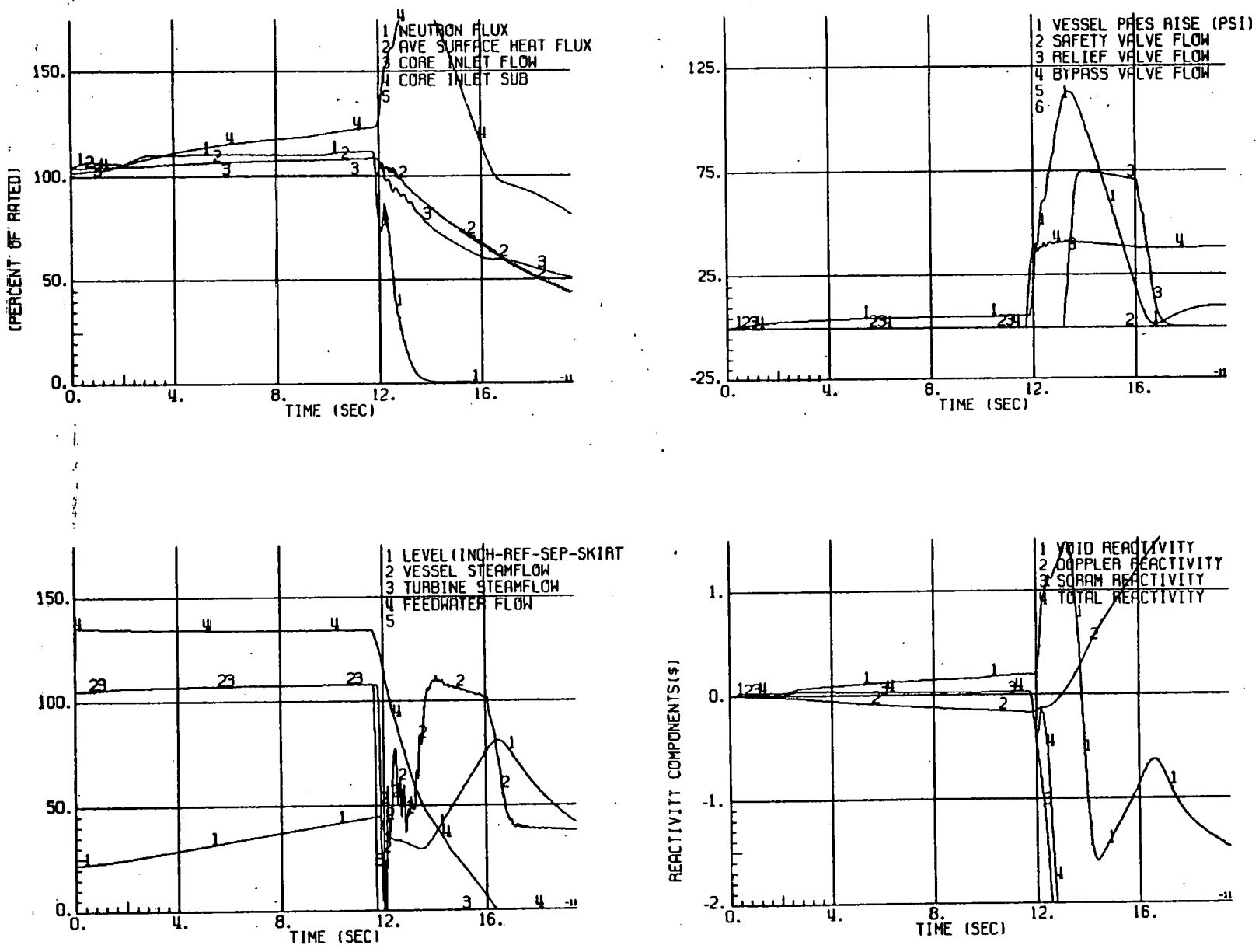

Figure 9-21. $(U/Th)O_2$ Reactor Parameters versus Time after a Feedwater Controller Failure

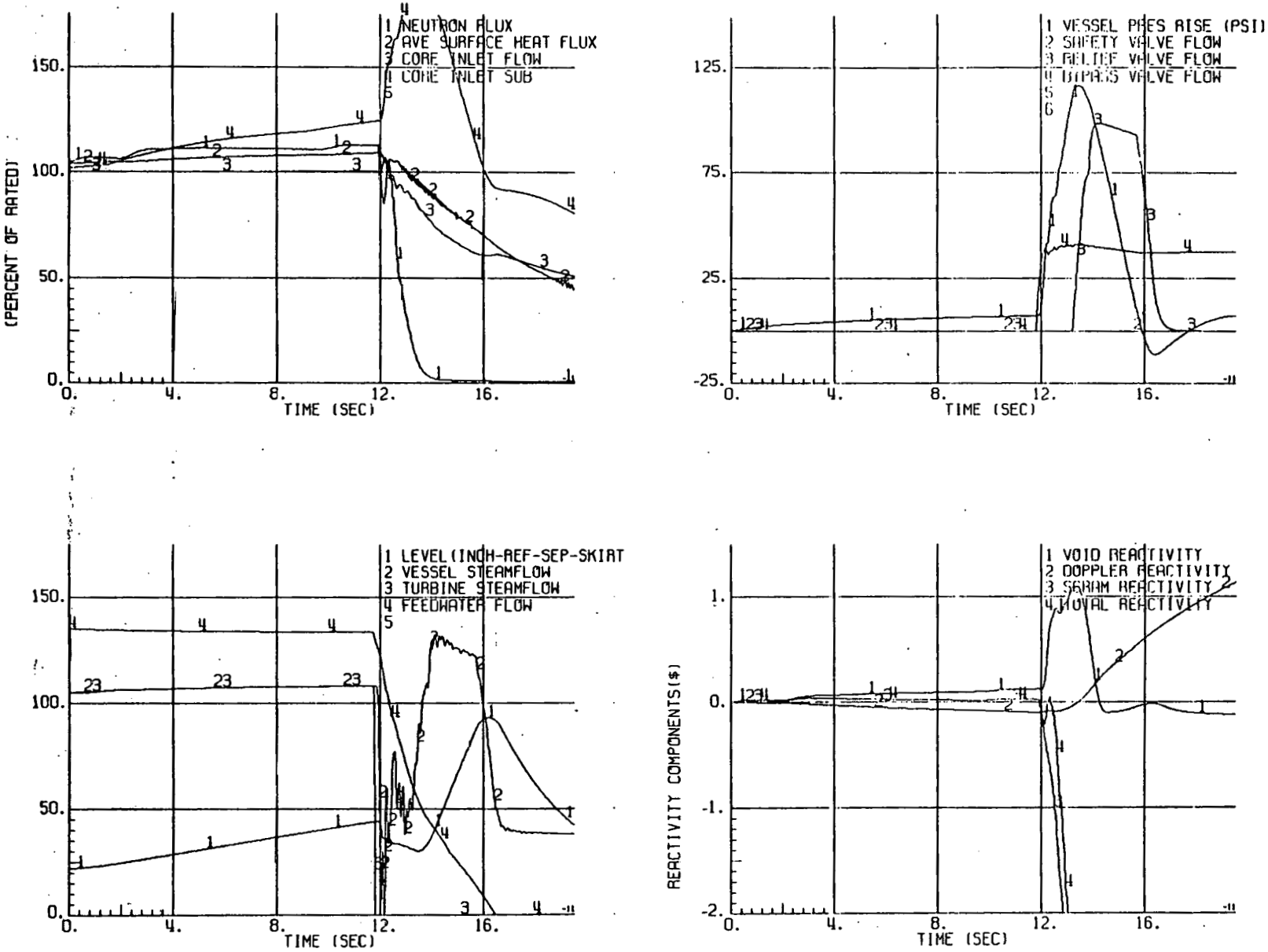

Figure 9-22. UO_2 Reactor Parameters versus Time after a Feedwater Controller Failure

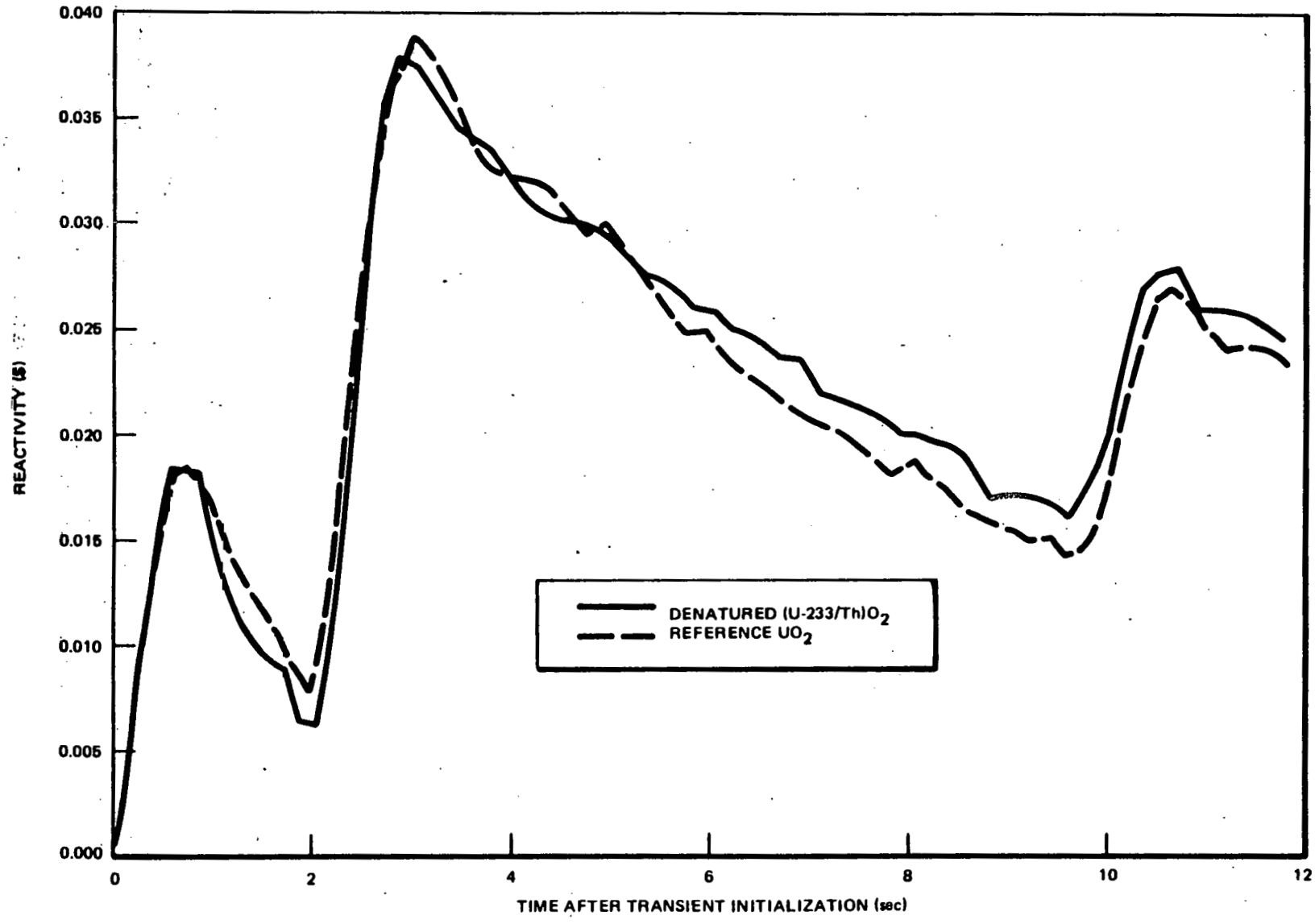

Figure 9-23. Net Reactivity versus Time after FWCF

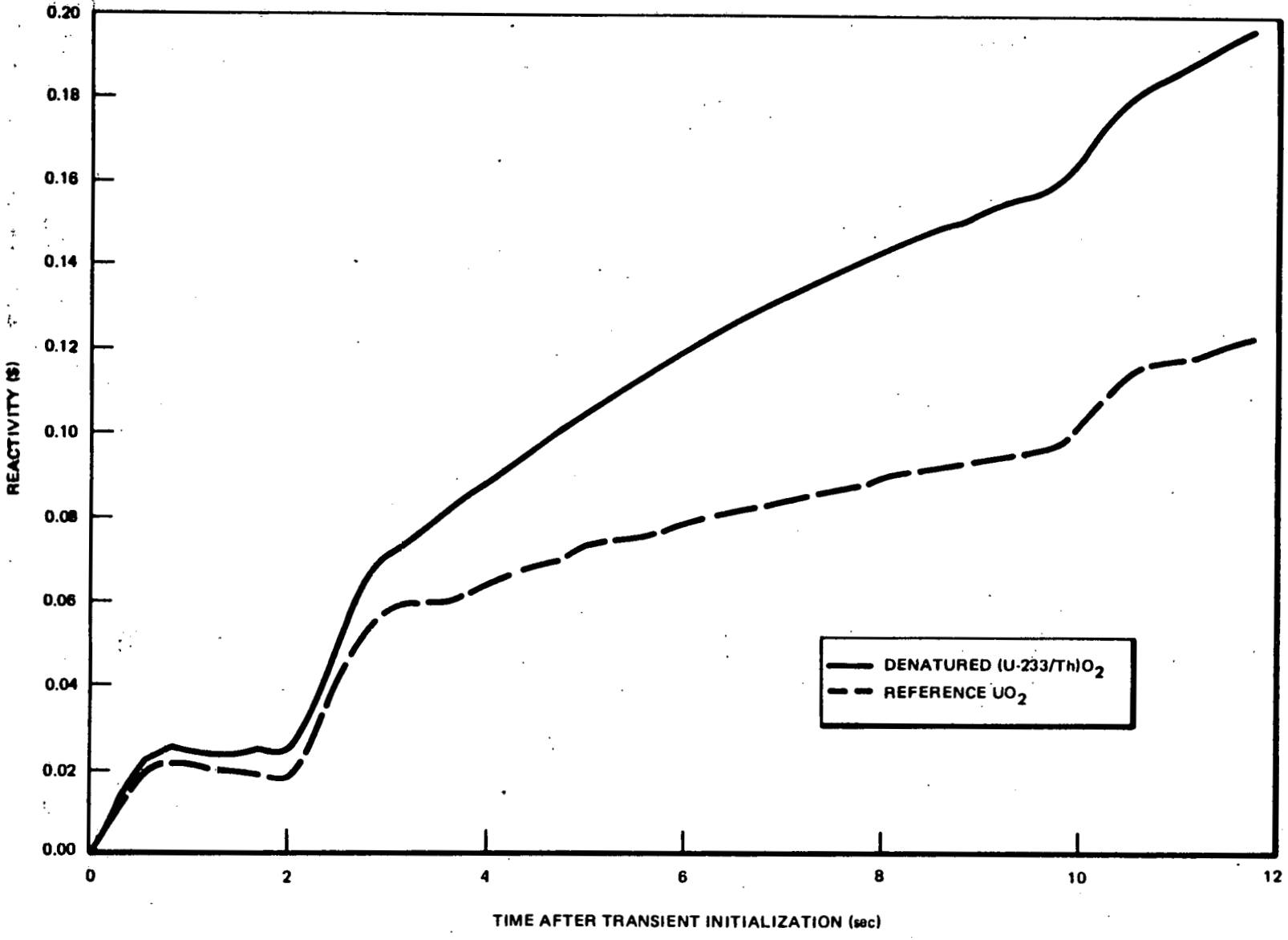

Figure 9-24. Void Reactivity versus Time after FWCF

THIS PAGE

WAS INTENTIONALLY

LEFT BLANK

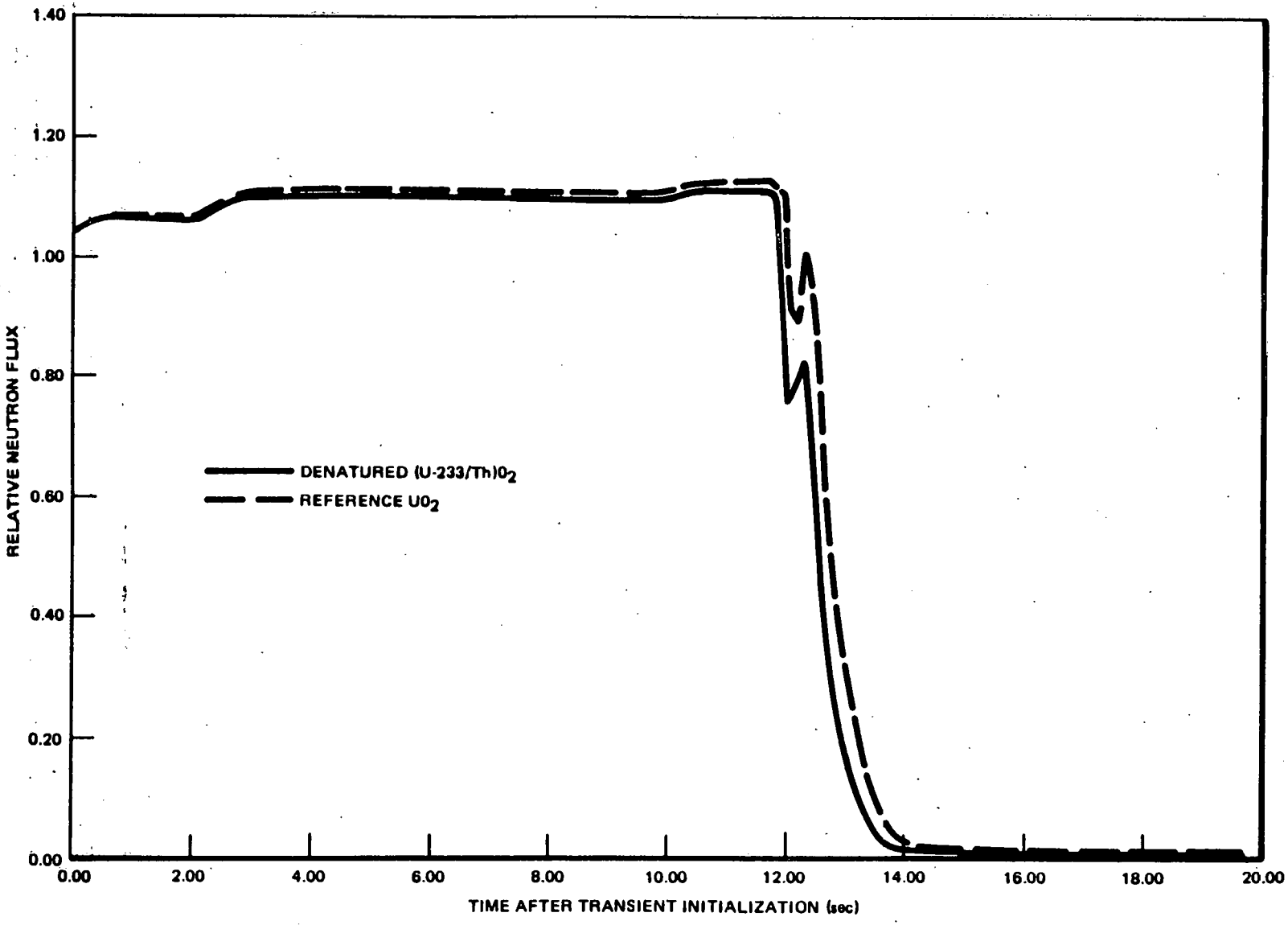

Figure 9-26. Relative Neutron Flux versus Time after FWCF

THIS PAGE

WAS INTENTIONALLY

LEFT BLANK

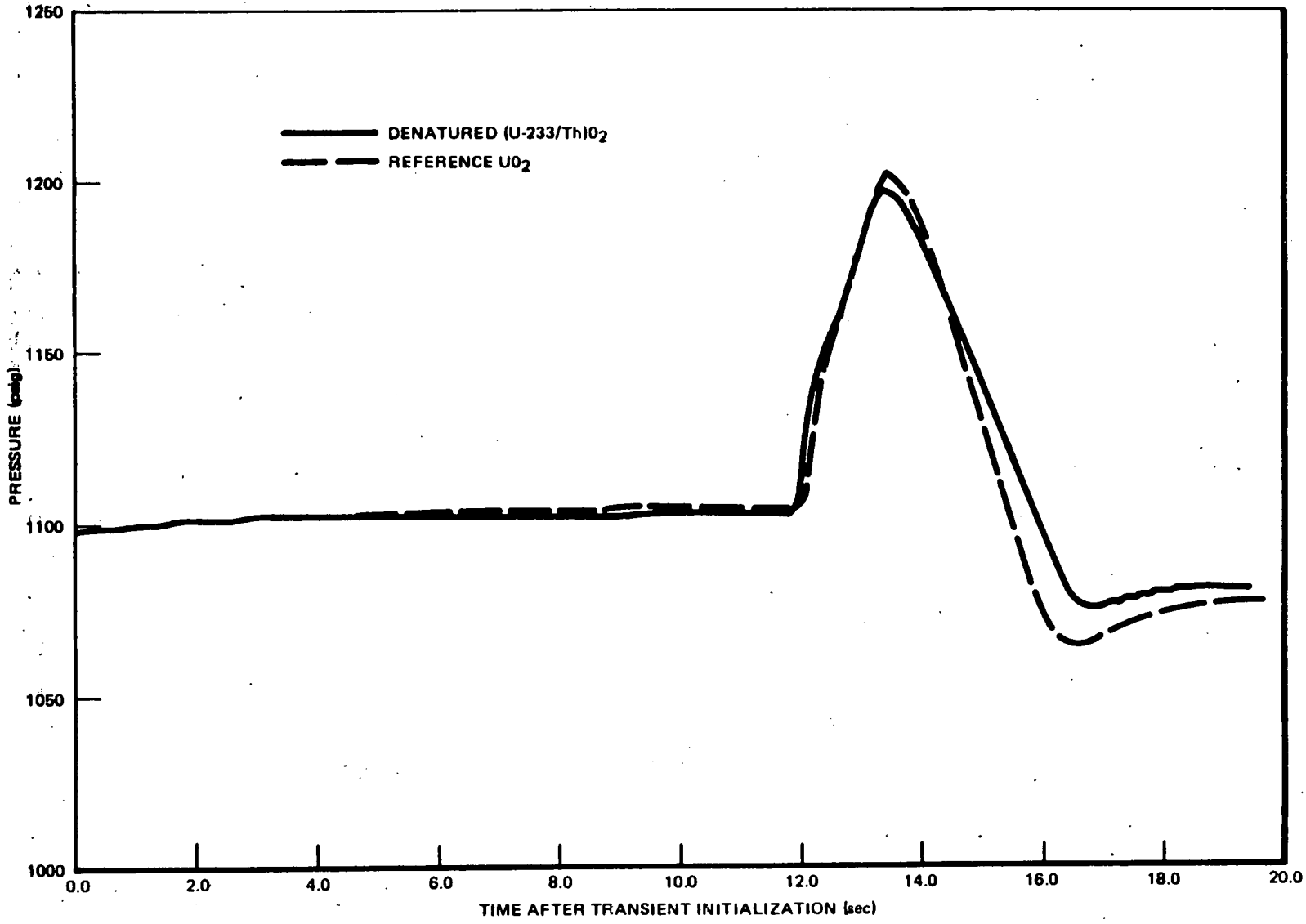

Figure 9-28. Maximum Core Pressure versus Time after FWCF

transient. The neutron flux of the (U-233/Th)O_2 fuel and the flux of the UO_2 fuel rise at about the same rate until the scram on the high water level trip setpoint. This is expected since the net reactivities of the fuels are nearly identical prior to scram. Subsequent to scram, the neutron flux of the (U-233/Th)O_2 fuel decreases faster than for the UO_2 fuel due to the superior scram curve of the thorium design as compared to the UO_2 scram curve. Consequently, the heat flux and reactor pressure rises are lower for the thorium design than for the UO_2 design. Thus, thermal and pressure margins are expected to increase in the (U-233/Th)O_2-fueled BWR relative to the reference UO_2-fueled BWR for a FWCF transient.

9.3.3.4 Results and Conclusions

a. Results

The FWCF transient is considered to be an event of moderate occurrence. Therefore, it is necessary to demonstrate that the MCPR does not fall below 1.07 and that the maximum reactor system pressure does not exceed 1375 psig during the transient for the fuel designs to meet safety and licensing requirements.

The MCPRs and peak reactor pressures expected during the FWCF for both reactor designs are given in Table 9-10. Both the (U-233/Th)O_2 and the UO_2 reactor fuel designs meet safety and licensing requirements for the FWCF since the smallest MCPRs are greater than the safety limit (1.07) and the peak vessel pressures are less than 1375 psig.

b. Conclusions

The (U-233/Th)O_2-fueled BWR demonstrates better performance than that seen for the reference UO_2-fueled BWR during a FWCF abnormal operational transient. The effect of the greater thorium DVC, relative to that seen for UO_2, is offset by its greater DDC. Thus,

Table 9-10

FWCF, MCPRs AND PEAK PRESSURES

Fuel Type	Operating Limit MCPR	Largest ΔMCPR During Event	Smallest MCPR During Event	Peak Vessel Pressure (psig)
Reference UO_2	1.23	0.046	1.184	1192
Denatured $(U\text{-}233/Th)O_2$	1.23	0.039	1.191	1187

the controlling reactor parameter with respect to performance is scram reactivity. Because of the superior scram response of the thorium fuel, compared to that of the UO_2 fuel, greater thermal and pressure margins are observed for the (U-233/Th)O_2 fuel design than for the reference UO_2 design. Both reactor types are expected to meet current safety and licensing requirements for the FWCF transient event with the denatured (U-233/Th)O_2 BWR being less limiting than the reference UO_2 BWR.

9.3.4 Loss of Feedwater Heating (LFWH)

9.3.4.1 Description of Event

The loss of feedwater heating can result in a decrease of 100°F in the feedwater temperature at the vessel inlet. The cooler feedwater flow gradually increases the core inlet subcooling, which reduces the core average void fraction. This reduction results in a slow, pseudo-steady-state power and heat flux increase that is terminated when the reactor scrams on simulated high heat flux. Tables 9-11 and 9-12 list the sequence of events for a LFWH in the denatured (U-233/Th)O_2 and the reference UO_2 reactors, respectively.

A feedwater heater may be lost in at least two ways: (1) if steam extraction line to the heater is blocked, or (2) if steam is bypassed around the heater. The first case produces a gradual cooling of the feedwater. In the second case, the steam bypasses the heater and no feedwater heating occurs. In both cases, the reactor vessel receives cooler feedwater.

The maximum number of feedwater heaters that can be tripped or bypassed by a single event represents the most severe transient for analysis considerations. This event incurs a loss of up to 100°F of the feedwater heating capability of the plant and causes an increase in core inlet subcooling. Due to the decrease in the core inlet coolant temperature, the boiling boundary moves upward in the core, which decreases the core average void fraction, thereby inserting positive reactivity and increasing the reactor power.

Table 9-11

SEQUENCE OF EVENTS FOR 100°F LOSS OF FEEDWATER HEATER FOR THE $(U/Th)O_2$ REACTOR

Time (sec)	Event
0	Initiate a 100°F temperature reduction into the feedwater systems.
5	Initial effect of unheated feedwater starts to raise core power level and steam flow.
7	Turbine control valves start to open to regulate pressure.
92	APRM initiates reactor scram on high thermal power.
134	Narrow range sensed water level reaches Level 3 setpoint.
134	Recirculation pump trip initiated due to Level 3 trip.
>150 (est.)	Wide range sensed water level reaches Level 2 setpoint.
	HPCS/RCIC flow enters vessel (not simulated).
	Reactor variables settle into limit cycle.

Table 9-12

SEQUENCE OF EVENTS FOR 100°F LOSS OF FEEDWATER HEATER FOR THE UO_2 REACTOR

Time (sec)	Event
0	Initiate a 100°F temperature reduction into the feedwater systems.
5	Initial effect of unheated feedwater starts to raise core power level and steam flow.
7	Turbine control valves start to open to regulate pressure.
44	APRM initiates reactor scram on high thermal power.
90	Narrow range sensed water level reaches Level 3 setpoint.
90	Recirculation pump trip initiated due to Level 3 trip.
>110 (est.)	Wide range sensed water level reaches Level 2 setpoint.
	HPCS/RCIC flow enters vessel (not simulated).
	Reactor variables settle into limit cycle.

The core inlet subcooling increases at a relatively slow rate, which causes the neutron power and heat flux to increase in a pseudo-steady-state fashion. The rise in power continues until the reactor scram system is initiated on a simulated high heat flux trip setpoint. After the scram, the water level drops to the low level setpoint which trips the coolant recirculation pumps.

9.3.4.2 Assumptions, Conditions, and Uncertainties

Initial conditions are detailed in Subsection 9.2 prior to the LFWH. Important factors (such as reactivity coefficients, scram characteristics, magnitude of the feedwater temperature change) are assumed to be at the worst configuration. Therefore, any deviations observed in the actual plant operation reduce the severity of the event.

9.3.4.3 Analysis

Analyses of the LFWH transient were performed for both the denatured (U-233/Th)O_2 and the reference UO_2 reactors using the methods described in Subsection 4.5. The behavior of various parameters during the transient in the thorium and the reference UO_2-fueled reactors are given as functions of time in Figures 9-29 and 9-30, respectively. Parameters that are representative of reactor performance are discussed in detail to explain the transient response of the (U-233/Th)O_2 and the reference UO_2 fuel designs.

a. Reactivity

Figure 9-31 shows the variation of the net reactivity in both fuel types as a function of time following the LFWH. This transient is characterized by a relatively slow insertion of positive reactivity from void collapse caused by gradual cooling of the core inlet coolant. As seen in Figure 9-31, the net reactivity insertion rate that is observed for the (U-233/Th)O_2 fuel design increases at approximately one-half of that seen for the reference UO_2 design until each reactor scrams on the high heat flux setpoint. Examination of the various reactivity constituents explains the differences observed in the net reactivity behavior of the fuel designs.

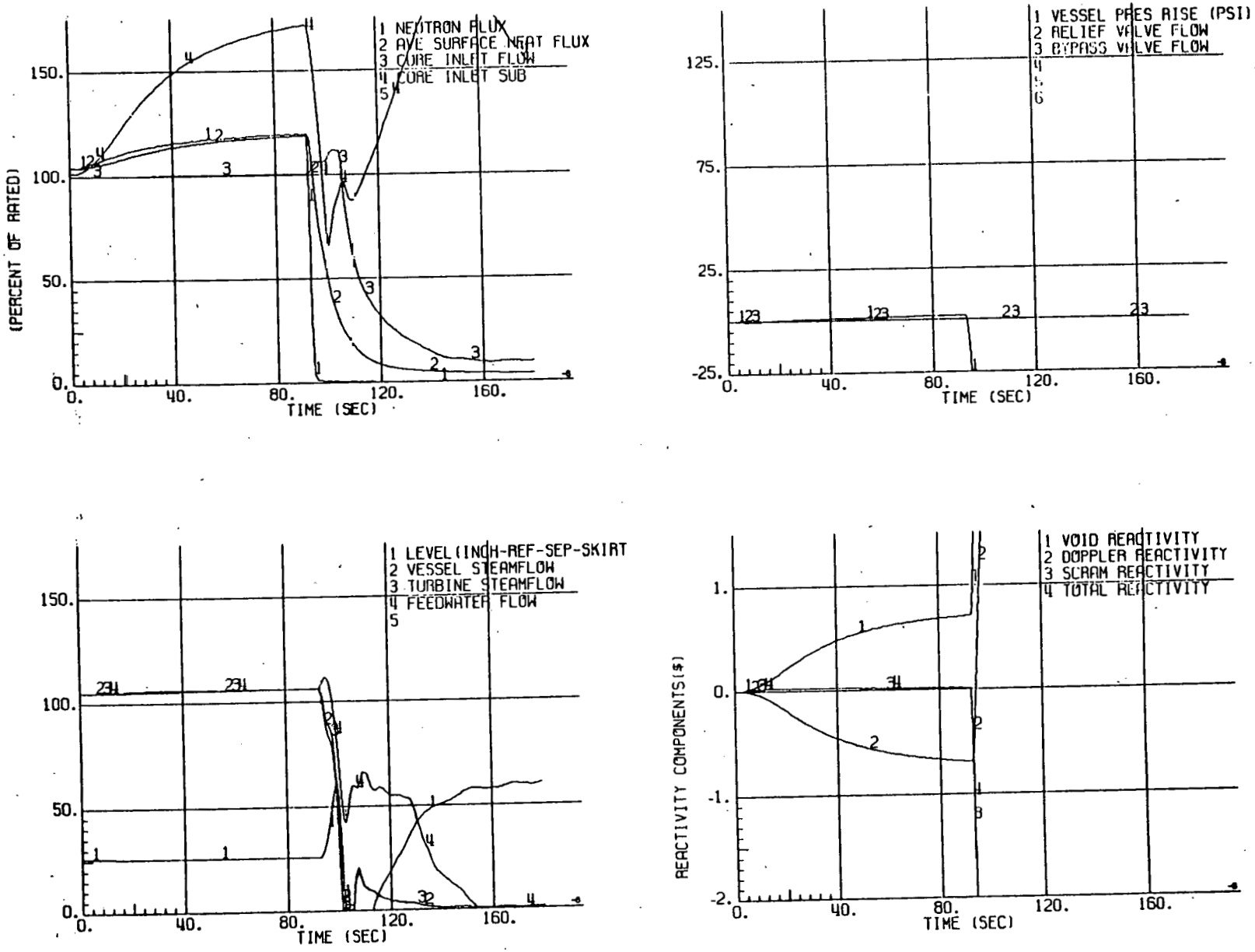

Figure 9-29. $(U/Th)O_2$ Reactor Parameters versus Time after a Loss of Feedwater Heating

THIS PAGE

WAS INTENTIONALLY

LEFT BLANK

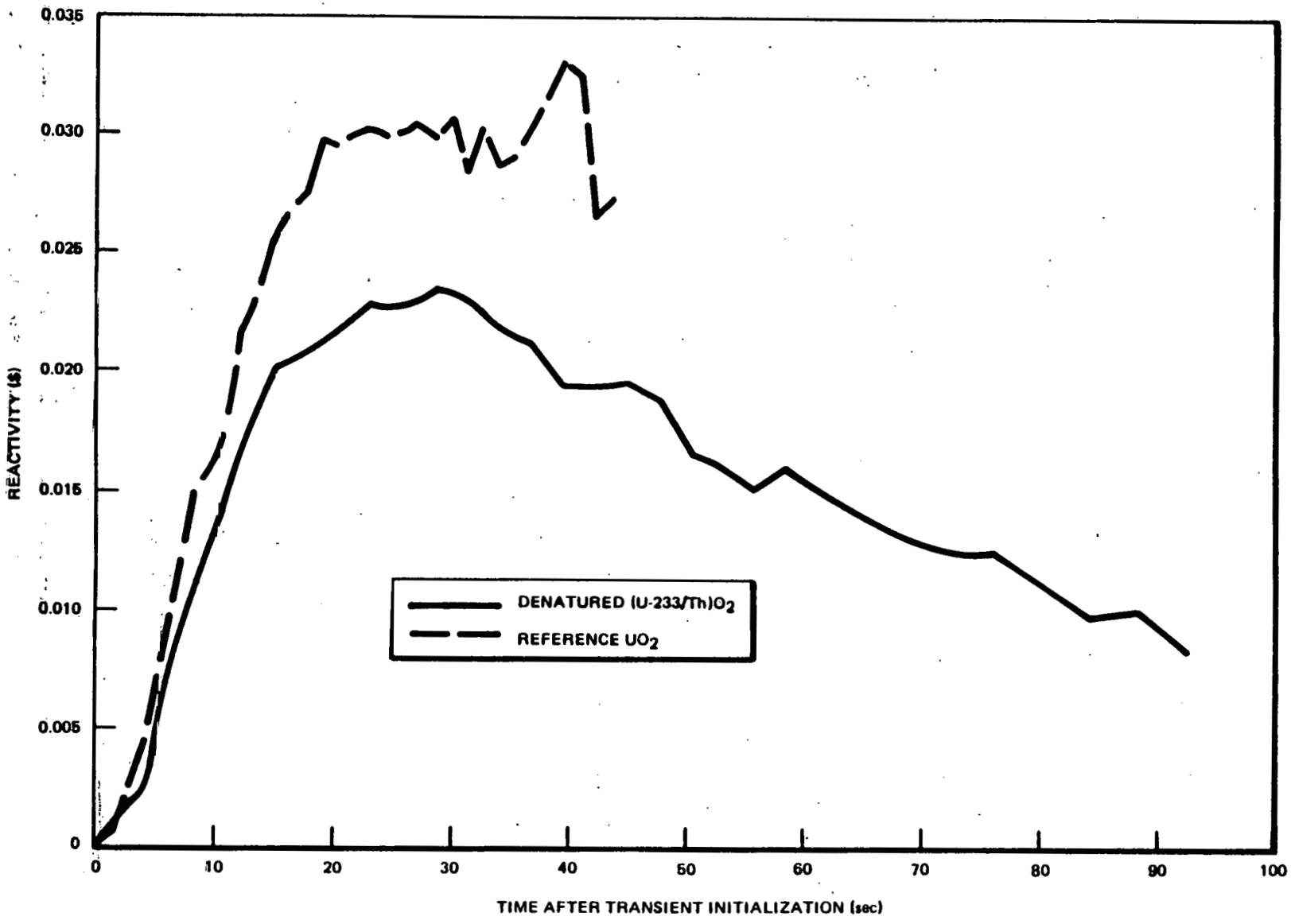

Figure 9-31. Net Reactivity versus Time after LFWH

Figures 9-32 and 9-33 illustrate the behavior of the void and Doppler reactivity components which together compose the net reactivity until scram occurs. As is seen, the slow increase in subcooling of the core inlet coolant causes an increase in both void and Doppler reactivities. As was mentioned in previous transient analysis sections, the $(U\text{-}233/Th)O_2$ reactivity components are more sensitive than the UO_2 components are to perturbations in the core environment. But the corresponding increase in the void reactivity of the thorium fuel relative to that of the UO_2 fuel is more than offset by the greater Doppler reactivity insertion of the $(U\text{-}233/Th)O_2$ design as compared to the reference UO_2 design. Therefore, the net reactivity of the thorium fuel increases at a slower rate than in the UO_2 fuel. This behavior continues until scram on the high heat flux level trip setpoint. Due to the smaller rate of positive reactivity insertion observed for the $(U\text{-}233/Th)O_2$ fuel (relative to that of the UO_2 fuel), the thorium-fueled reactor scrams at a later time than the UO_2-fueled reactor.

b. Neutron Flux, Heat Flux and Vessel Pressure

Figures 9-34 and 9-35 present the behavior of the neutron flux and heat flux during the LFWH transient. Following the net reactivity behavior, the neutron flux of the $(U\text{-}233/Th)O_2$ fuel rises at approximately half the rate of the increase in the UO_2 fuel. Corresponding, the heat flux of the thorium design also increases at approximately half of the rate seen in the reference UO_2 design. Therefore, since scram occurs at a fixed high heat flux level trip setpoint, the thorium fuel case scrams later than the UO_2 case. The peak heat flux is the primary determinant of thermal margins. Therefore, since both cases scram on identical slowly increasing heat fluxes, their peak heat fluxes, attained subsequent to scram, are approximately equal. Thus, the smallest thermal margins for the reactors during the LFWH transient should be very similar.

Figure 9-36 shows the behavior of the reactor pressure as a function of time during the LFWH transient for both reactor types. It

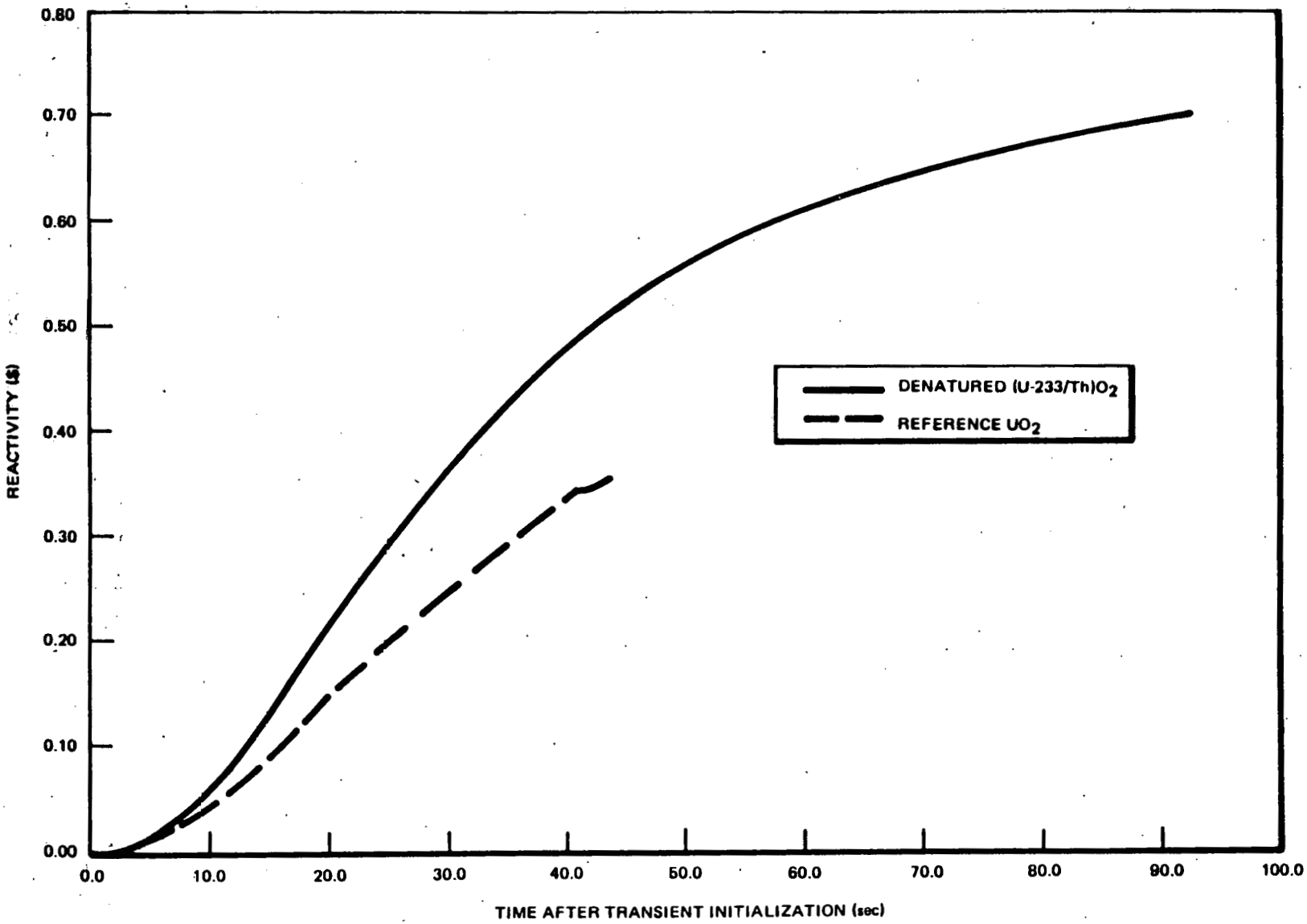

Figure 9-32. Void Reactivity versus Time after LFWH

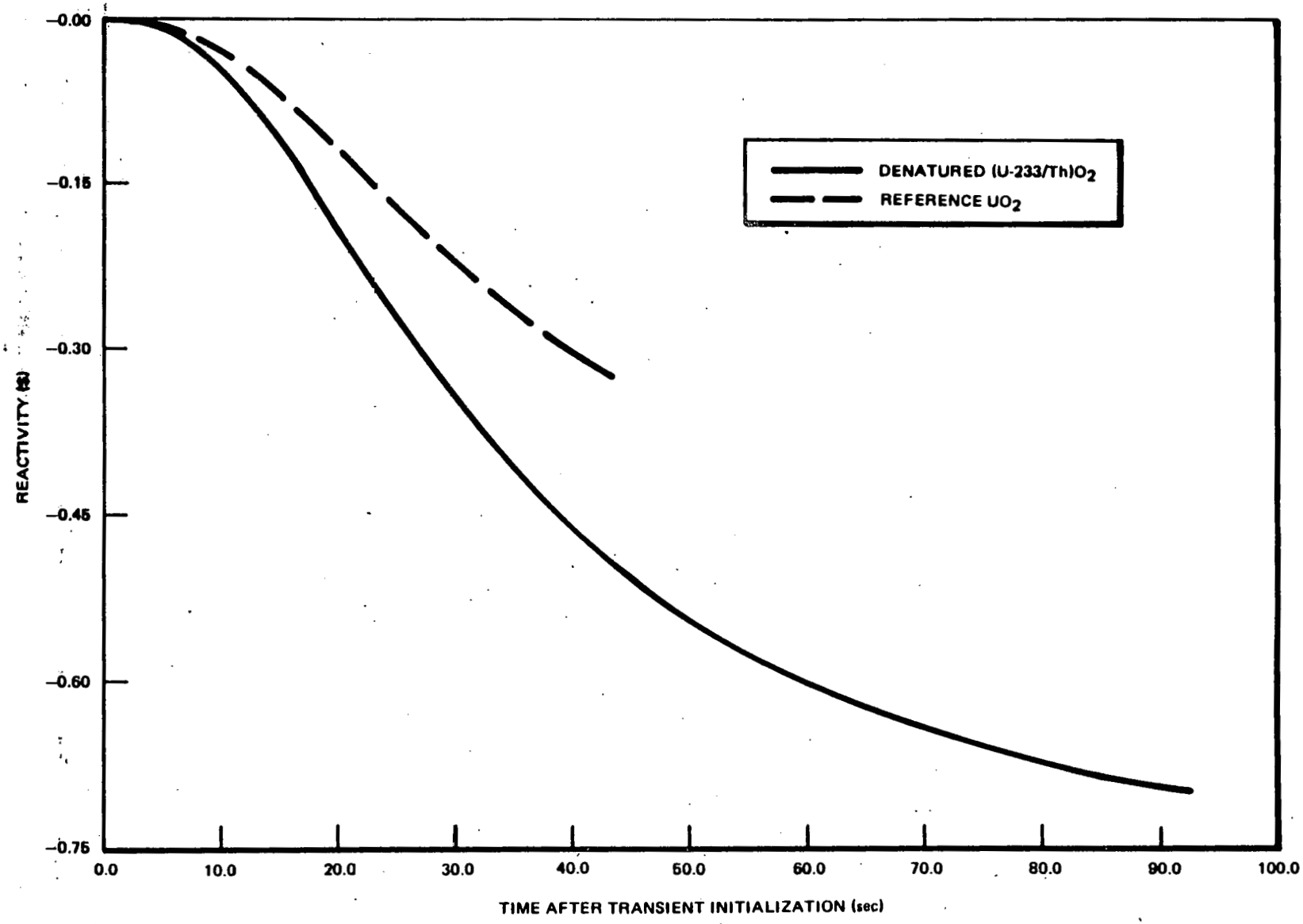

Figure 9-33. Doppler Reactivity versus Time after LFWH

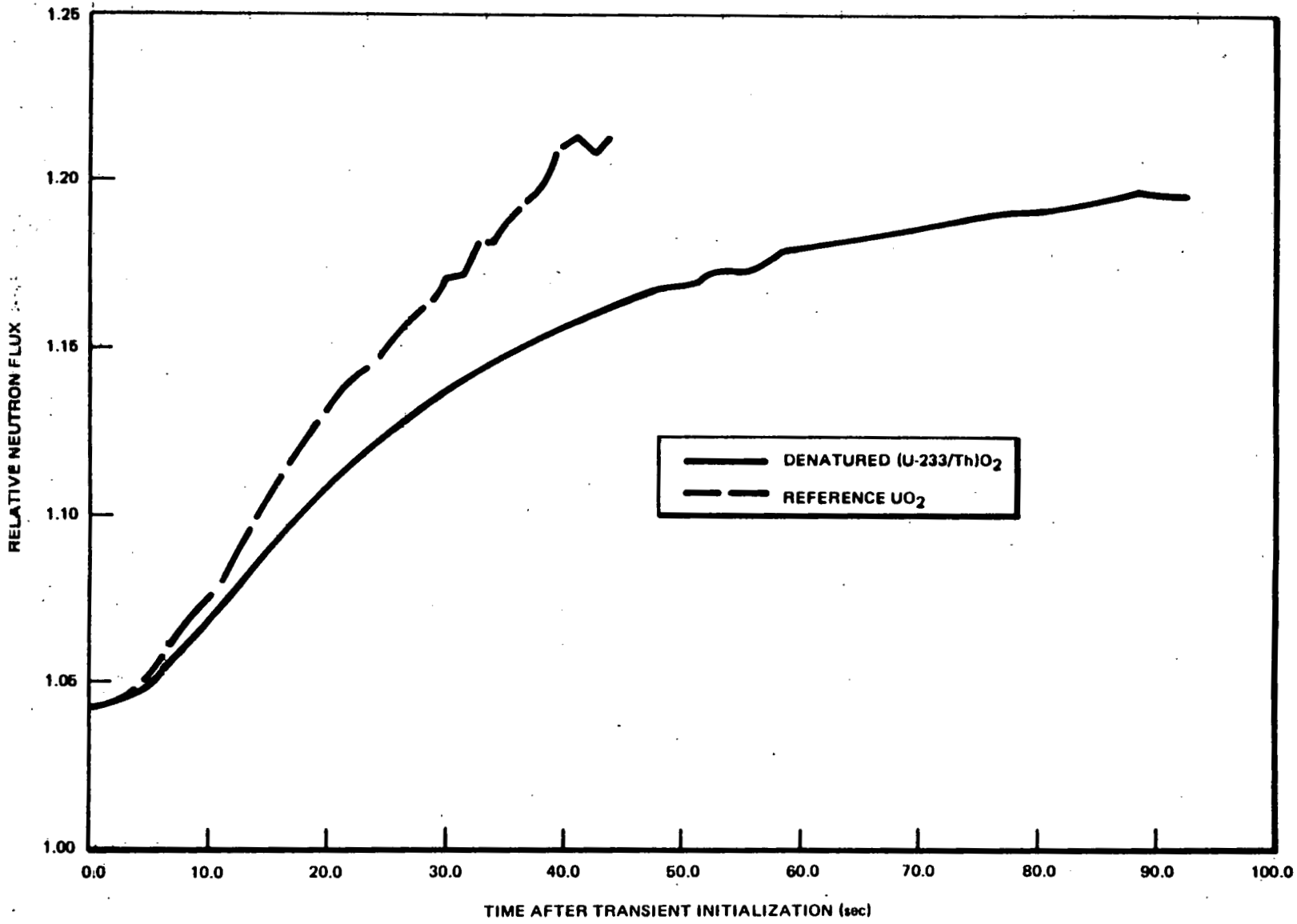

Figure 9-34. Relative Neutron Flux versus Time after LFWH

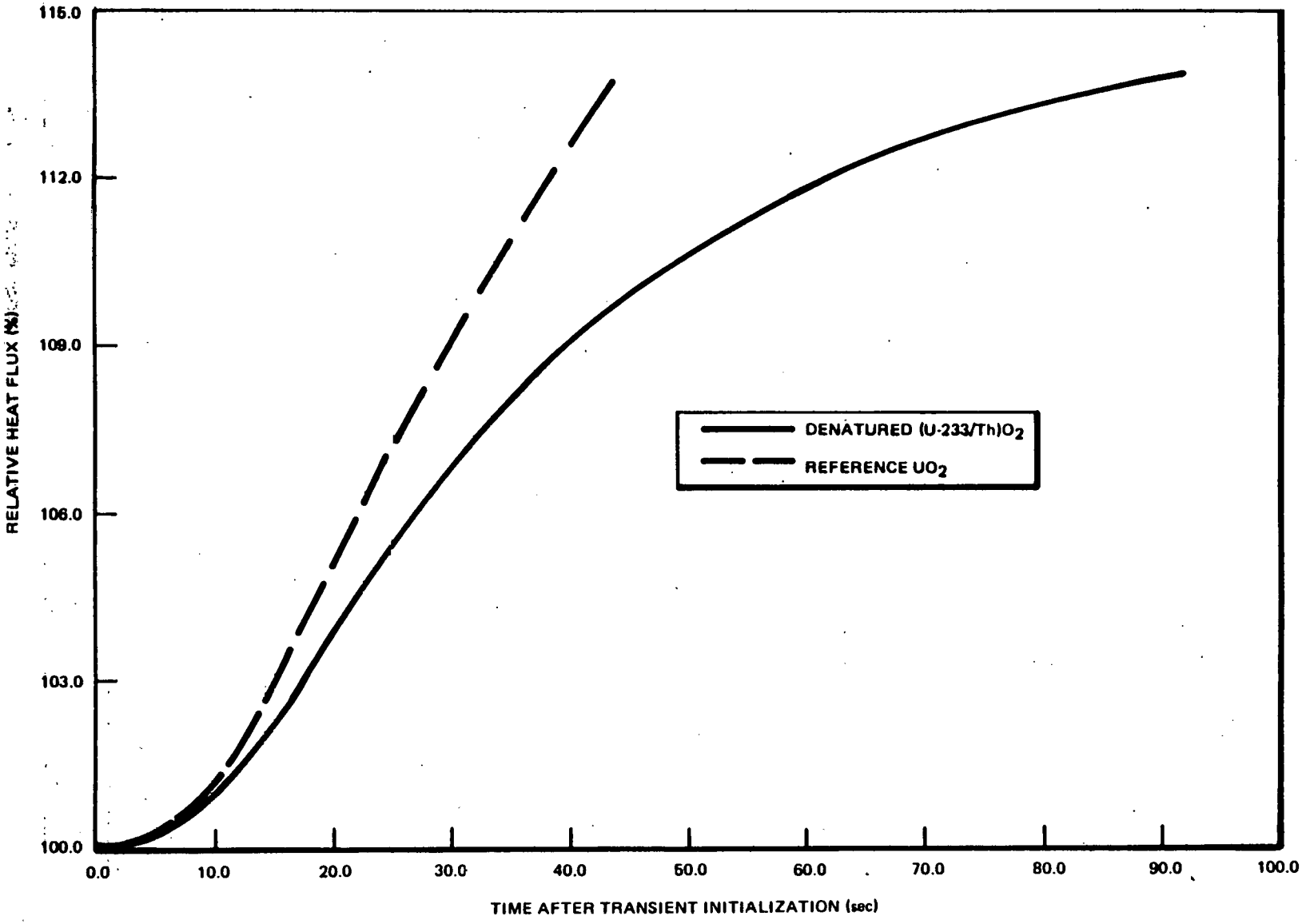

Figure 9-35. Relative Heat Flux versus Time after LFWH

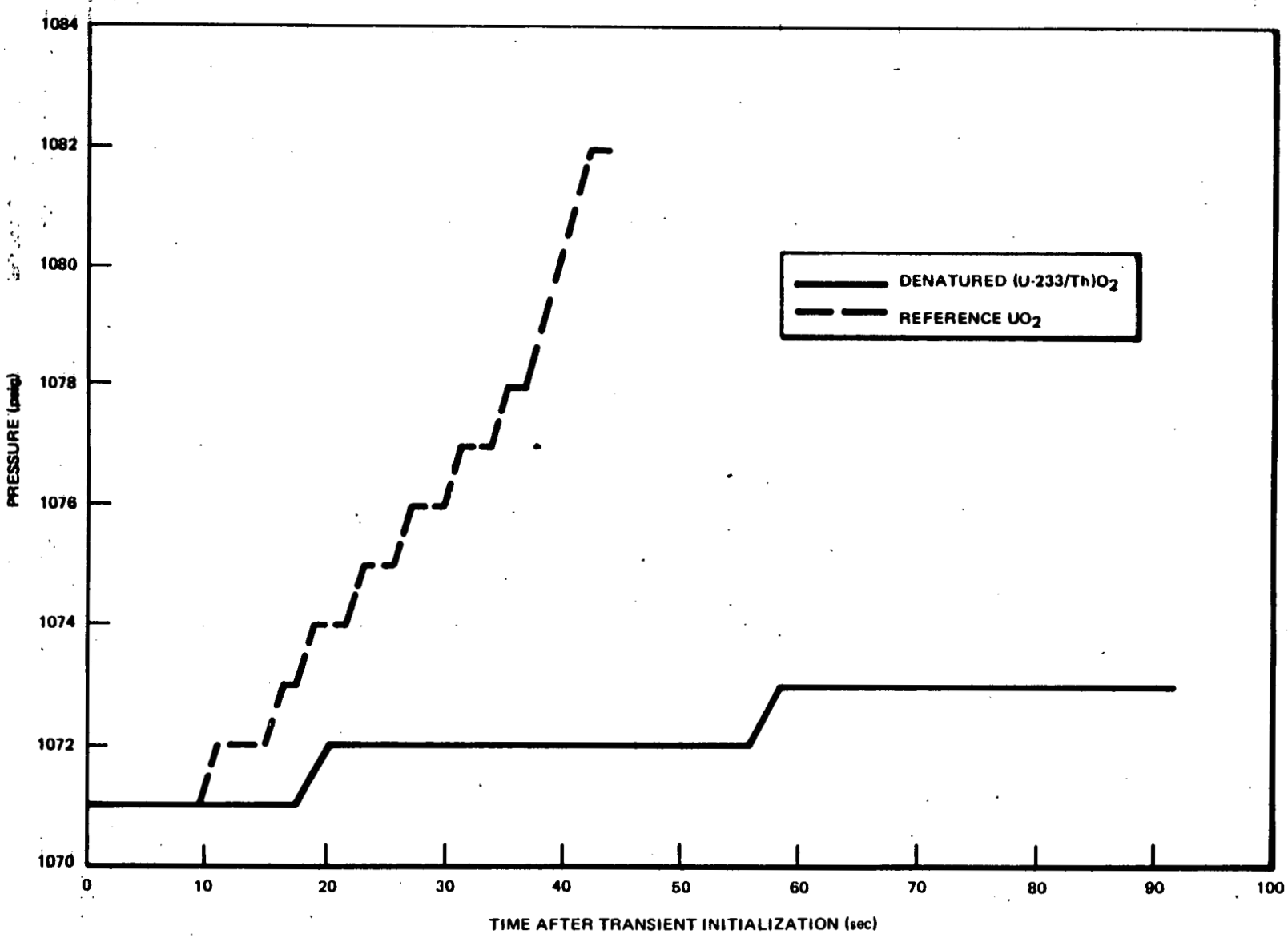

Figure 9-36. Reactor Pressure versus Time after LFWH

was determined above that the time of scram during a LFWH does not significantly affect thermal margins because the peak heat flux that occurs during the event is the main determinant of the reactor thermal margins. However, peak reactor pressures are proportional to the rate that heat is transferred to the coolant. The heat flux of the (U-233/Th)O_2 fuel increases more slowly with time than the heat flux of the UO_2 fuel. Therefore, use of (U-233/Th)O_2 fuel should result in an increased peak pressure margin relative to that of the UO_2 case during the LFWH transient.

9.3.4.4 Results and Conclusions

a. Results

The LFWH is considered to be an event of moderate occurrence. Therefore, for the thorium and reference UO_2 designs to meet safety and licensing requirements, it is necessary to demonstrate that the transient does not result in an MCPR less than or equal to the safety limit (1.07), and that the maximum reactor system pressure observed during the event be less than 1375 psig.

The MCPR and peak reactor pressure that are expected during a LFWH are given in Table 9-13 for both the (U-233/Th)O_2 and the reference UO_2 reactor designs. Both reactor fuel designs meet safety and licensing requirements for the LFWH since the smallest MCPRs are greater that the safety limit and peak vessel pressures are less than 1375 psig. Also note that this transient results in the smallest thermal margins of the transients considered in this study for both fuel designs.

b. Conclusions

The (U-233/Th)O_2-fueled BWR demonstrates better performance during a LFWH abnormal operational transient than that seen for the reference UO_2-fueled BWR. The LFWH is the most limiting of the transients

Table 9-13

LFWH, MCPRs AND PEAK PRESSURES

Fuel Type	Operating Limit MCPR	Largest ΔMCPR During Event	Smallest MCPR During Event	Peak Vessel Pressure (psig)
Reference UO_2	1.23	0.113	1.117	1095
Denatured $(U\text{-}233/Th)O_2$	1.23	0.097	1.133	1091

considered in this study. Relative to the UO_2 reactor design, the greater DDC of the thorium reactor design more than offsets its greater DVC which results in a slower rise of neutron flux and heat flux. Thus, greater thermal and pressure margins are realized for the (U-233/Th)O_2-fueled reactor than for the UO_2 reactor. Both reactor types are expected to meet current safety and licensing requirements for the LFWH transient event with the denatured (U-233/Th)O_2 BWR being less limiting than the reference UO_2 BWR.

9.3.5 Main Steam Isolation Valve Closure, MSIV Closure (Flux Scram and Pressure Scram)

The MSIV closure along with reactor scram on the high neutron flux or on the high pressure setpoints are considered to be "upset" and "emergency" conditions, respectively, for BWR systems. A reactor design is acceptable, with respect to these events if the peak vessel pressure during an upset transient remains below the ASME code limit, 1375 psig, 110% of the vessel design pressure.

9.3.5.1 Description of Event

Closure of the main steam isolation valves (MSIV closure) results in large reactor system pressure increases. Pressurization reduces the core average void fraction, which inserts positive reactivity, thereby increasing the reactor power. If scram is not initiated by the MSIV closure, the reactor will scram on a high neutron flux level trip setpoint or, failing this, it will scram on high pressure. Tables 9-14 and 9-15 list the sequence of events for a MSIV closure with flux scram and pressure scram, respectively; the event chains apply to both the denatured (U-233/Th)O_2 and the reference UO_2 reactors.

Various steamline and nuclear system malfunctions or operator actions (e.g., low steamline pressure, high steamline radiation, low water level in pressure vessel, or manual action) can initiate MSIV closures. As the MSIVs close, position switches on the valves normally initiate a reactor scram

Table 9-14

SEQUENCE OF EVENTS FOR MAIN STEAM ISOLATION VALVE CLOSURE, FLUX SCRAM

Time-(sec)	Event
0	Closure of all main steam isolation valves initiated.
0.3	MSIVs reached 90% open; failure of direct position scram assumed.
1.6	Neutron flux reached the high APRM* flux scram setpoint and initiated reactor scram.
2.1	Reactor dome pressure reached the setpoint of recirculation pump trip
2.3	Reactor dome pressure reached the Group 1 safety/relief valves pressure setpoint (power-actuated mode). Only half of valves in this group were assumed functioning.
2.3	Steamline pressure reached the Group 1 safety/relief valves pressure setpoint (spring-action mode). Valves which were not opened in this power-activated mode were opened.
2.4	Recirculation pump/motor initiated to coastdown.
2.7	All safety/relief valves opened in either power-actuated mode or spring action mode due to high pressure.
3.0	MSIVs completely closed.
3.0	Vessel bottom pressure reached its peak value.
>10 (est)	Safety/relief valves opened in their spring-action mode closed.
>20 (est)	Wide-range sensed water level reached L2 setpoint. HPCS and RCIC flow entered reactor vessel. Safety valves closed and reopen cyclicly.

*APRM = Average power range monitor

Table 9-15

SEQUENCE OF EVENTS FOR MAIN STEAM ISOLATION VALVE CLOSURE, PRESSURE SCRAM

Time-(sec)	Event
0	Closure of all main steam isolation valves initiated.
0.3	MSIVs reached 90% open; failure of direct position scram assumed.
2.1	Neutron flux reached the high APRM* flux scram setpoint and initiated reactor scram.
2.1	Reactor dome pressure reached the setpoint of recirculation pump trip.
2.3	Reactor dome pressure reached the Group 1 safety/relief valves pressure setpoint (power-actuated mode). Only half of valves in this group were assumed functioning.
2.3	Steamline pressure reach the Group 1 safety/relief valves pressure setpoint (spring-action mode). Valves which were not opened in this power-activated mode were opened.
2.4	Recirculation pump/motor initiated to coastdown.
2.7	All safety/relief valves opened in either power-actuated mode or spring action mode due to high pressure.
3.0	MSIVs completely closed.
3.0	Vessel bottom pressure reached its peak value.
>10 (est)	Safety/relief valves opened in their spring-action mode closed.
>20 (est)	Wide-range sensed water level reached L2 setpoint. HPCS and RCIC flow entered reactor vessel. Safety valves closed and reopened cyclicly.

*APRM = Average power range monitor

when the valves in three or more main steamlines are less than 90% open and the reactor pressure is above 600 psig. For these analyses, it is assumed that the initial scram trip fails. The core average void fraction is reduced due to the pressurization of the reactor system which causes an increase of the reactor neutron power, heat flux, and steaming rate that aid the pressure rise until scram is initiated by high neutron flux or high pressure trip. Throughout the reactor pressure increase, S/RVs open to relieve the high pressure then continue to open and close periodically to remove decay heat.

9.3.5.2 Assumptions, Conditions and Uncertainties

Initial conditions prior to the MSIV closure are detailed in Subsection 9.2. All systems utilized for protection in this event were assumed to have the poorest allowable response (e.g., relief valve setpoints, scram stroke time and nuclear characteristics). Therefore, any deviations observed in the actual operation reduce the severity of the event.

9.3.5.3 Analysis

Analyses of the MSIV closures were performed for both the denatured (U-233/Th)O_2 and the reference UO_2 reactors using the method described in Subsection 4.4. The behavior of various parameters during the transients in the thorium and the reference UO_2-fueled reactors are given as functions of time in Figures 9-37 through 9-40.

As in previous transients analyzed in this study, the larger DVC and larger DDC of the thorium fuel relative to the UO_2 fuel cancel one another. Therefore, net reactivities of the two fuel designs are similar for both the MSIV closure on flux scram and pressure scram until scram occurs. Then, the net reactivity, neutron flux and heat flux decrease faster in (U-233/Th)O_2 fuel than in the reference UO_2 fuel due to the superior scram response of the (U-233/Th)O_2 design relative to the UO_2 design. The steam production rate in the thorium fuel design will be lower than in the UO_2 design; therefore, lower peak reactor pressures are seen in the thorium reactor than are seen in the UO_2 reactor.

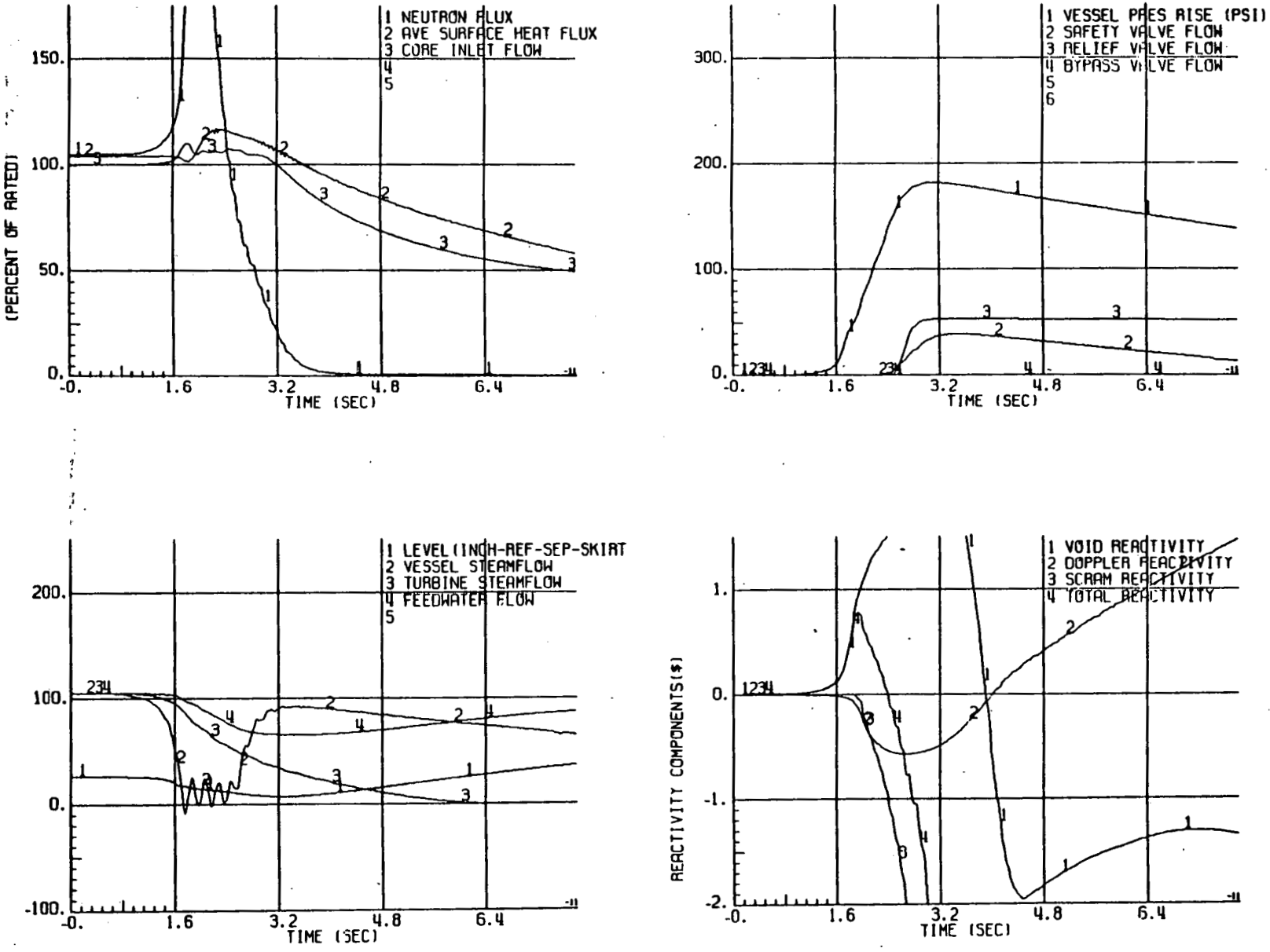

Figure 9-37. $(U/Th)O_2$ Reactor Parameters versus Time after a Main Isolation Valve Closure (Flux Scram)

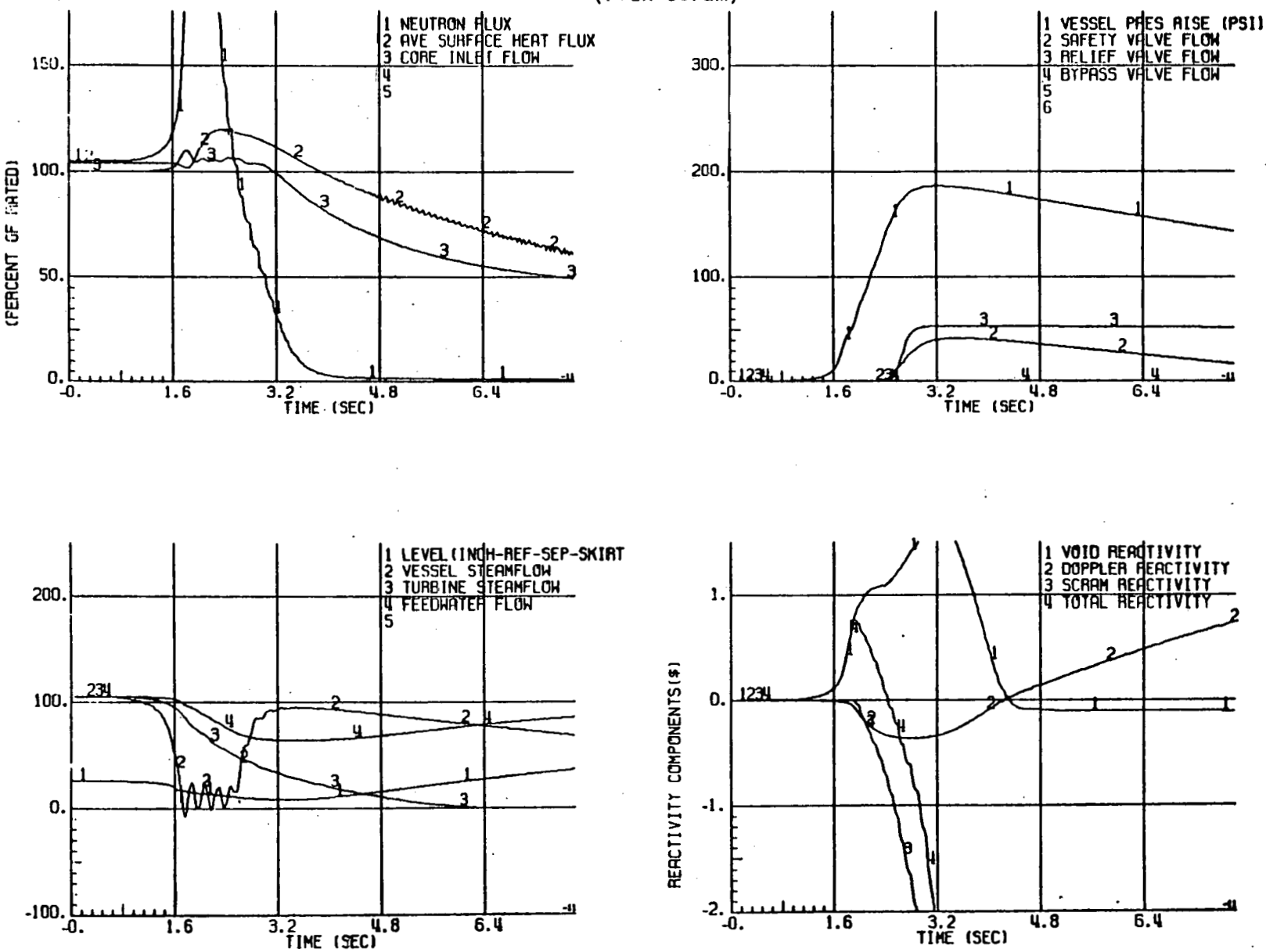

Figure 9-38. UO_2 Reactor Parameters versus Time after a Main Steam Isolation Valve Closure (Flux Scram)

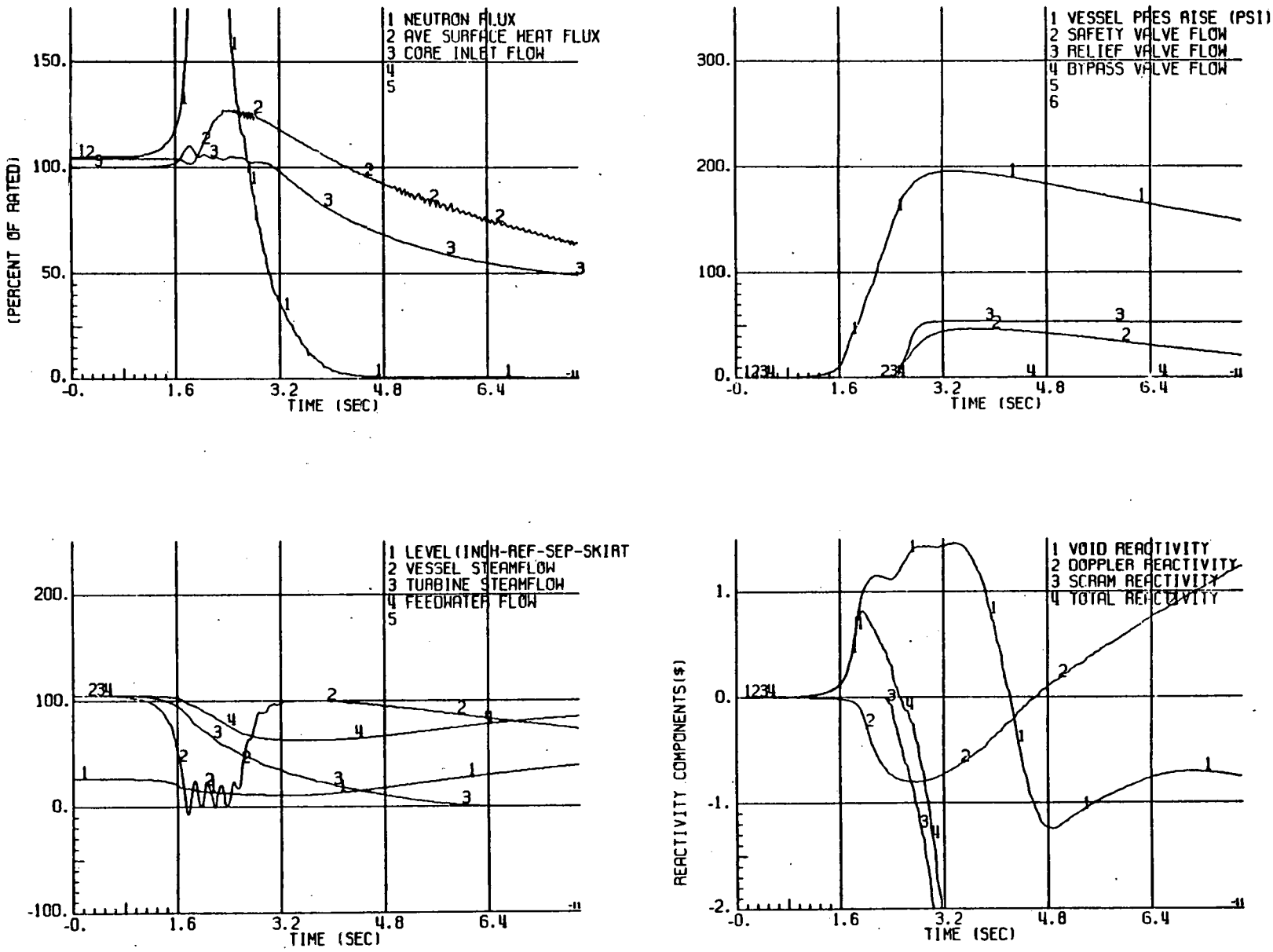

Figure 9-39. $(U/Th)O_2$ Reactor Parameters versus Time after a Main Steam Isolation Valve Closure (Pressure Scram)

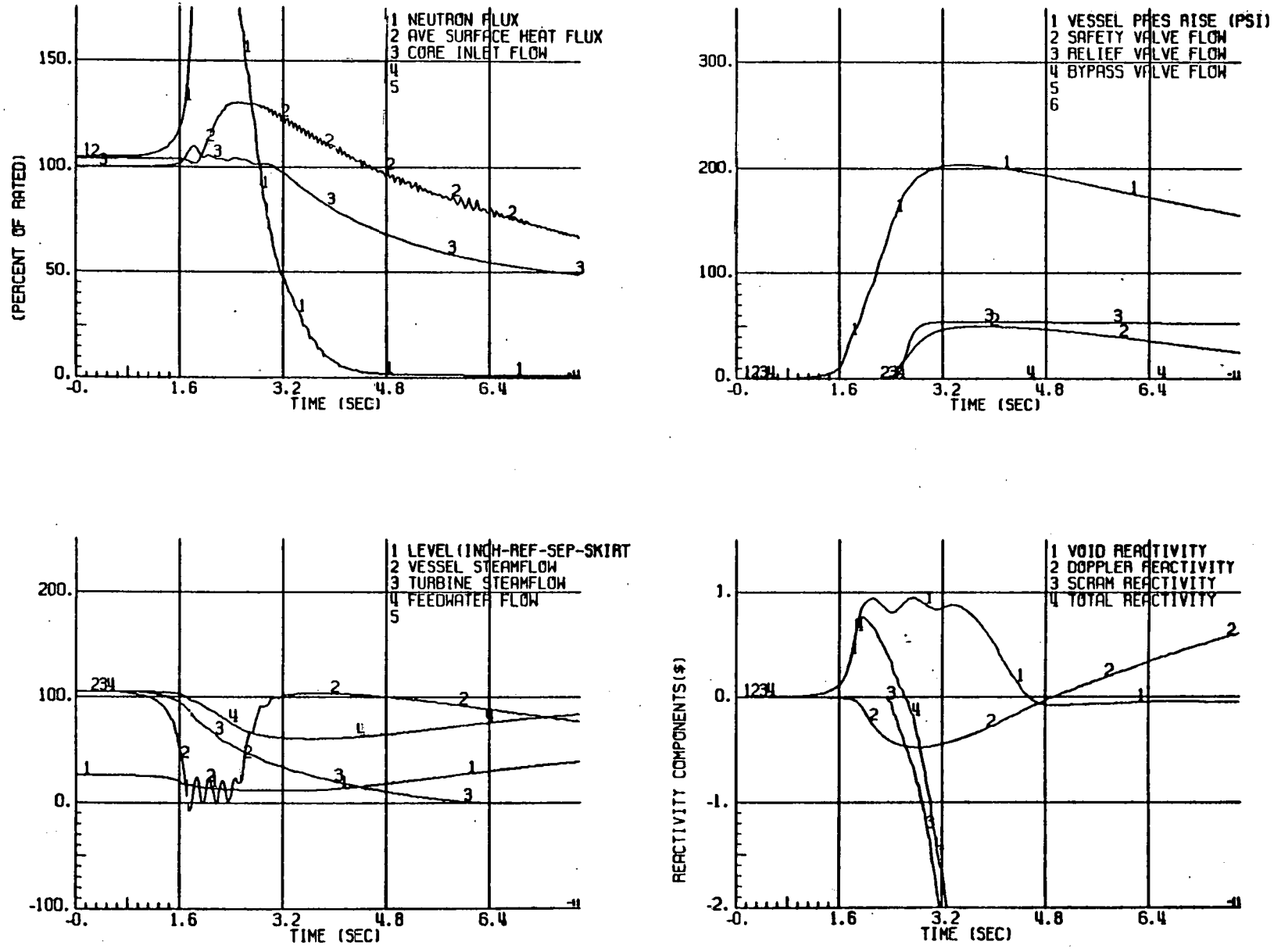

Figure 9-40. UO_2 Reactor Parameters versus Time after a Main Steam Isolation Valve Closure (Pressure Scram)

9.3.5.4 Results and Conclusions

a. Results

As discussed above, the MSIV closure with scram on high neutron flux and high pressure trip levels are "upset" and "emergency" conditions, respectively, for the reactor primary containment boundary. Therefore, performance of the reactor system is satisfactory if the peak reactor vessel pressure observed is less than 1375 psig.

Peak pressures observed during the MSIV closures for both reactor types are listed in Table 9-16. The MSIV closure transient with flux scram or pressure scram results in peak vessel pressures less than 1375 psig for the denatured $(U\text{-}233/Th)O_2$ and the reference UO_2 reactors. Thus, the necessary overprotection is provided by both reactor types.

b. Conclusions

The $(U\text{-}233/Th)O_2$-fueled BWR demonstrates better performance during a MSIV closure with reactor scram on the high flux or high pressure trip setpoints than that seen for the reference UO_2-fueled BWR.

The greater DVC of the thorium design relative to that of the UO_2 design is offset by its greater DDC. When the reactors scram, the neutron flux and heat flux of $(U\text{-}233/Th)O_2$ fuel decrease faster than those of the UO_2 fuel due to the superior scram curve of the $(U\text{-}233/Th)O_2$ design relative to the reference UO_2 design. Thus, the peak vessel pressures observed in the thorium-fueled reactor are less than those seen in the UO_2-fueled reactor. Both reactor types are expected to meet pressure protection requirements for the MSIV closure, with flux scram or pressure scram with the $(U\text{-}233/Th)O_2$ BWR being less limiting than the reference UO_2 BWR.

Table 9-16

MSIV CLOSURE PEAK REACTOR PRESSURES

Fuel Type	Scram Type	Peak Vessel Pressure (psig)
UO_2	Flux	1269
UO_2	Pressure	1284
Denatured $(U\text{-}233/Th)O_2$	Flux	1264
Denatured $(U\text{-}233/Th)O_2$	Pressure	1277

10. BWR STABILITY

10.1 GENERAL DESCRIPTION

10.1.1 Stable Conditions

Reactor power level stability in a BWR is determined by the sensitivity of the neutron power to change in core voiding and the resulting perturbations in reactivity. A stable reactor's neutron power will fluctuate around:

(1) A constant power level (as is shown by Figure 10-1); or

(2) A steadily increasing or decreasing power level (as illustrated in Figure 10-2).

Note that during stable operation, immediately following a small reactivity insertion, the second peak in power is smaller than the first as the power fluctuation damps out. Thus, it is apparent that the condition for stable operation is that the decay ratio, defined as the second peak/first peak, must be less than 1.0.

10.1.2 Stability Analysis

In general, any factor which increases the rate of heat transfer from the fuel to the coolant decreases reactor stability. A more negative dynamic void coefficient increases the decay ratio, thereby decreasing stability. The secondary effects of flatter axial profiles, lower specific heat, greater gap conductance, and greater conductivity also reduce stability.

10.2 ANALYSIS

Thermal-hydraulic stability analyses were performed for the $(U\text{-}233/Th)O_2$-fueled and reference UO_2-fueled reactors using the methods described in Subsection 4.7. The results of these analyses are summarized in Figure 10-3. In this figure, the shaded area represents regions of instability. The intersecting curves shown for each design represent the natural circulation and the 105% rod power/flow lines which bound the power/flow operating states.

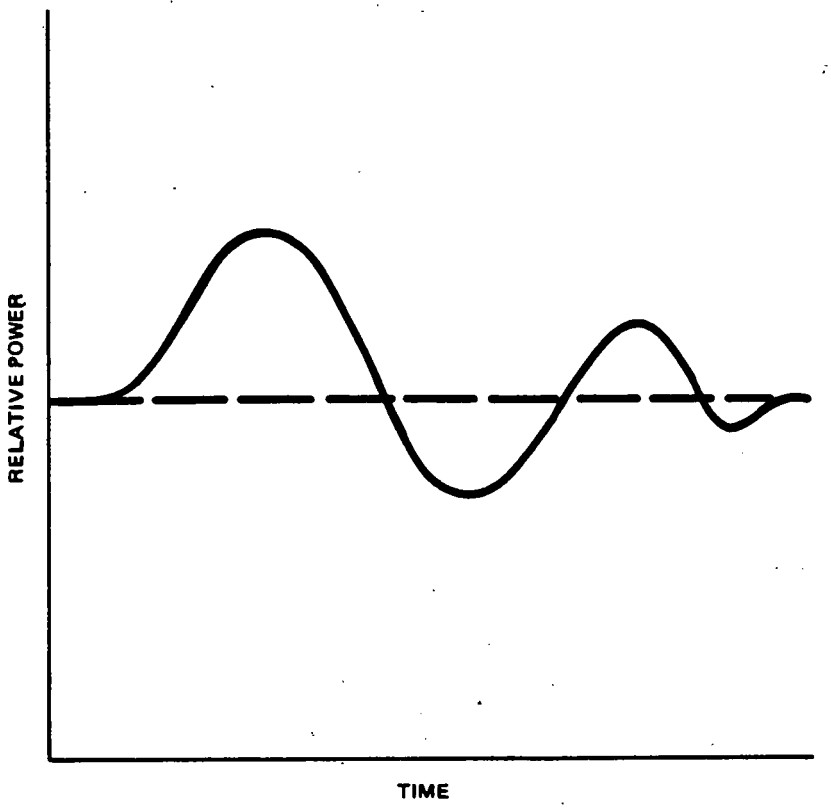

Figure 10-1. Stable Steady Power Operation

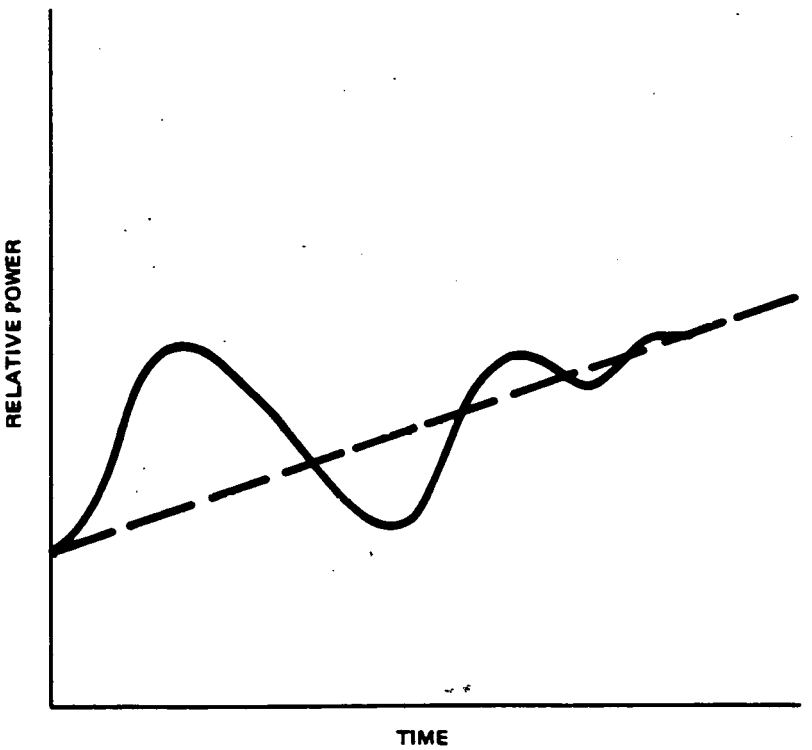

Figure 10-2. Stable Power Increase

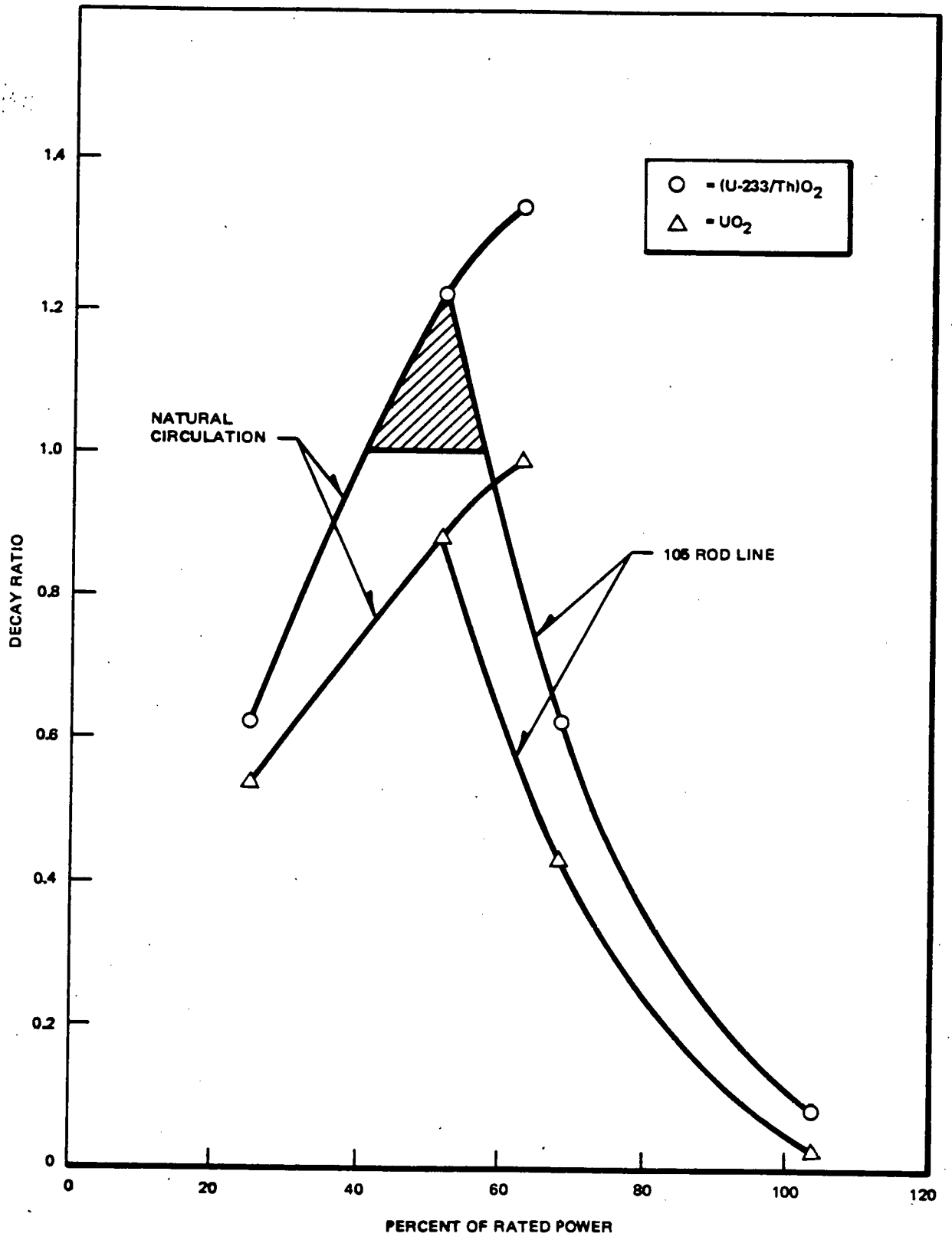

Figure 10-3. Decay Ratio versus Percent of Rated Reactor Power

The natural circulation line represents various power levels at the conservatively assumed constant natural circulation flow rate of 30% of rated flow. The 105% rod line represents various power/flow conditions along the power/flow line which results in 105% power at 100% of rated flow.

10.3 RESULTS AND CONCLUSIONS

10.3.1 Results

As shown in Figure 10-3, the $(U\text{-}233/Th)O_2$-fueled BWR is unstable at certain power/flow conditions and is definitely less stable than the reference UO_2-fueled BWR. The primary cause for the reduced stability of the $(U\text{-}233/Th)O_2$ design is its smaller delayed neutron fraction and resultant more negative dynamic void reactivity coefficient. Other minor factors which will contribute to the reduced stability of $(U\text{-}233/Th)O_2$ include its flatter axial power shape, larger thermal conductivity, and lower specific heat relative to UO_2; these factors were not specifically considered in these analyses. Also not specifically considered was the substantially more negative dynamic Doppler coefficient of reactivity, which may have a stabilizing effect.

10.3.2 Conclusions

While a denatured $(U\text{-}233/Th)O_2$-fueled BWR has been determined to be less stable than the reference UO_2-fueled BWR, this is not a safety concern. Mitigation of any oscillations (should they ever be encountered at this very unlikely operating condition) is adequately provided by the APRM flux scram. The identified power/flow regions of instability could also be avoided by altering the standard BWR operating map to exclude these operating conditions. Thus, while the relative instability of the $(U\text{-}233/Th)O_2$ design is not a safety concern, it will potentially affect the operational flexibility of the BWR, especially in the startup and load following modes.

11. ASSESSMENT OF ALTERNATE FUEL DESIGNS

In addition to the detailed safety evaluation of the denatured (U-233/Th)O_2-fueled reactor, qualitive studies were performed to assess the safety and licensing performance of two other thorium fuel designs: denatured (U-235/Th)O_2 and (Pu/Th)O_2. The denatured (U-235/Th)O_2 and the (Pu/Th)O_2 fuel assemblies considered here were developed under the 1975 ERDA program, "Appraisal of BWR Plutonium Burners for Energy Center," and the 1977 DOE/ORNL program, "Assessment of Utilization of Thorium in BWRs," respectively. These were scoping studies with the objective of determining BWR potential for utilizing alternative (i.e., other than UO_2) fuels. While the limited scope of these programs precluded performance of detailed three-dimensional multicycle BWR simulator calculations to verify the interchangeability of these designs with the reference UO_2 fuel assembly, it is believed that these designs match the reference design well enough to allow meaningful comparisons of their nuclear parameters and their expected effect on accidents, abnormal transient response, BWR operability, and stability.

11.1 FUEL DESIGN DESCRIPTIONS

The alternate fuel evaluations are based on point model and infinite lattice predictions of various nuclear parameters. Indications are that a (U-235/Th)O_2-fueled BWR will behave in a manner substantially the same as the reference UO_2 design with little or no impact on accident or abnormal operating response. There could, however, be some (probably very small) decrease in thermal margins and stability. The impact of (Pu/Th)O_2 fuel on the BWR must be evaluated, especially in the abnormal operating transient, stability, and thermal limits areas, all of which could be adversely affected relative to the reference UO_2 design.

11.1.1 Denatured (U-235/Th)O_2 Assembly Design

The (U-235/Th)O_2 fuel assembly design is identical to the reference UO_2 assembly with the exception of its fuel composition. The (U-235/Th)O_2 fuel rods are arranged in an 8x8 array that includes two water filled rods. In this design, the 62 fueled rods contain UO_2 and ThO_2 with the fissile content varied among them to reduce local power peaking in the fuel bundle assembly.

The fissile material in this design is U-235 in a denatured combination with U-235 consisting of 20% $(U\text{-}235)O_2$ and 80% $(U\text{-}238)O_2$ by weight. Four fuel rod fissile compositions were utilized to flatten local power. The UO_2 fuel contents range from a high of 20% of the $(U/Th)O_2$ fuel composition to a low of 13.04%, with corresponding fissile contents of 4% and 2.608% by weight, respectively.

11.1.2 $(Pu/Th)O_2$ Assembly Design

The $(Pu/Th)O_2$ fuel assembly design, like the $(U\text{-}235/Th)O_2$ design, is identical to the reference UO_2 assembly with the exception of its fuel composition. The $(Pu/Th)O_2$ fuel rods are arranged in an 8x8 array that includes two water rods and several $(Pu/Th)O_2$-Gd_2O_3 poison rods. The 62 fueled rods contain PuO_2, ThO_2 and Gd_2O_3, with the fissile content varied among them to reduce local power peaking in the fuel bundle assembly.

The fissile material in this design is Pu-239 and Pu-241 in a combination with the fertile isotopes Pu-240, Pu-242, and Th-232.

11.2 NUCLEAR CHARACTERISTICS

As the denatured $(U\text{-}235/Th)O_2$ bundle assembly was designed without burnable poison, comparisons of the alternate designs to the reference UO_2 and denatured $(U\text{-}233/Th)O_2$ assemblies were made at an exposure beyond the poison burnout point. This exposure point (16.5 GWd/MT) was also chosen because it approximates the average fuel bundle exposure of a BWR equilibrium cycle core where the parameters are the most limiting concerning abnormal operating transient responses.

From the relative variation of various point model and infinite lattice predicted nuclear characteristics between fuel designs, probable performance of alternately fueled reactors during normal operation and expected abnormal events may be determined. Table 11-1 gives the point model reactivity coefficients at the core average void fraction and 16.5 GWd/MT for the two alternate bundle assembly designs as well as for the denatured $(U\text{-}233/Th)O_2$ and the reference UO_2

Table 11-1

POINT MODEL REACTIVITY COEFFICIENTS AT CORE AVERAGE VOIDS AND 16.5 GWd/MT

Coefficient	Reference UO_2	Denatured $(U\text{-}233/Th)O_2$	Denatured $(U\text{-}235/Th)O_2$	$(Pu/Th)O_2$
Steam void reactivity x 10^4	-11.3	-7.0	-12.0	-10.1
Dynamic void reactivity (¢/% voids)	-8.4	-9.2	-8.8	-12.4
Doppler reactivity x 10^5	-0.112	-0.157	-0.168	-0.125
Dynamic Doppler reactivity (¢/°F @ T_f = 610°C)	-0.205	-0.506	-0.304	-0.370

bundle designs. Figures 11-1 through 11-4 show the variation of these parameters as functions of void fraction or fuel temperature. The delayed neutron fraction, β, and infinite lattice neutron multiplication factors and control blade worths are given in Tables 11-2 and 11-3, respectively. The impact of these parameters on BWR thermal margins, accident performance, transient response, operability, and stability will be discussed briefly in following sections.

Table 11-2

DELAYED NEUTRON FRACTIONS (β) AT CORE AVERAGE VOIDS AND 16.5 GWd/MT

Design	β
Reference UO_2	0.00546
Denatured $(U233/Th)O_2$	0.00311
Denatured $(U235/Th)O_2$	0.00552
$(Pu/Th)O_2$	0.00331

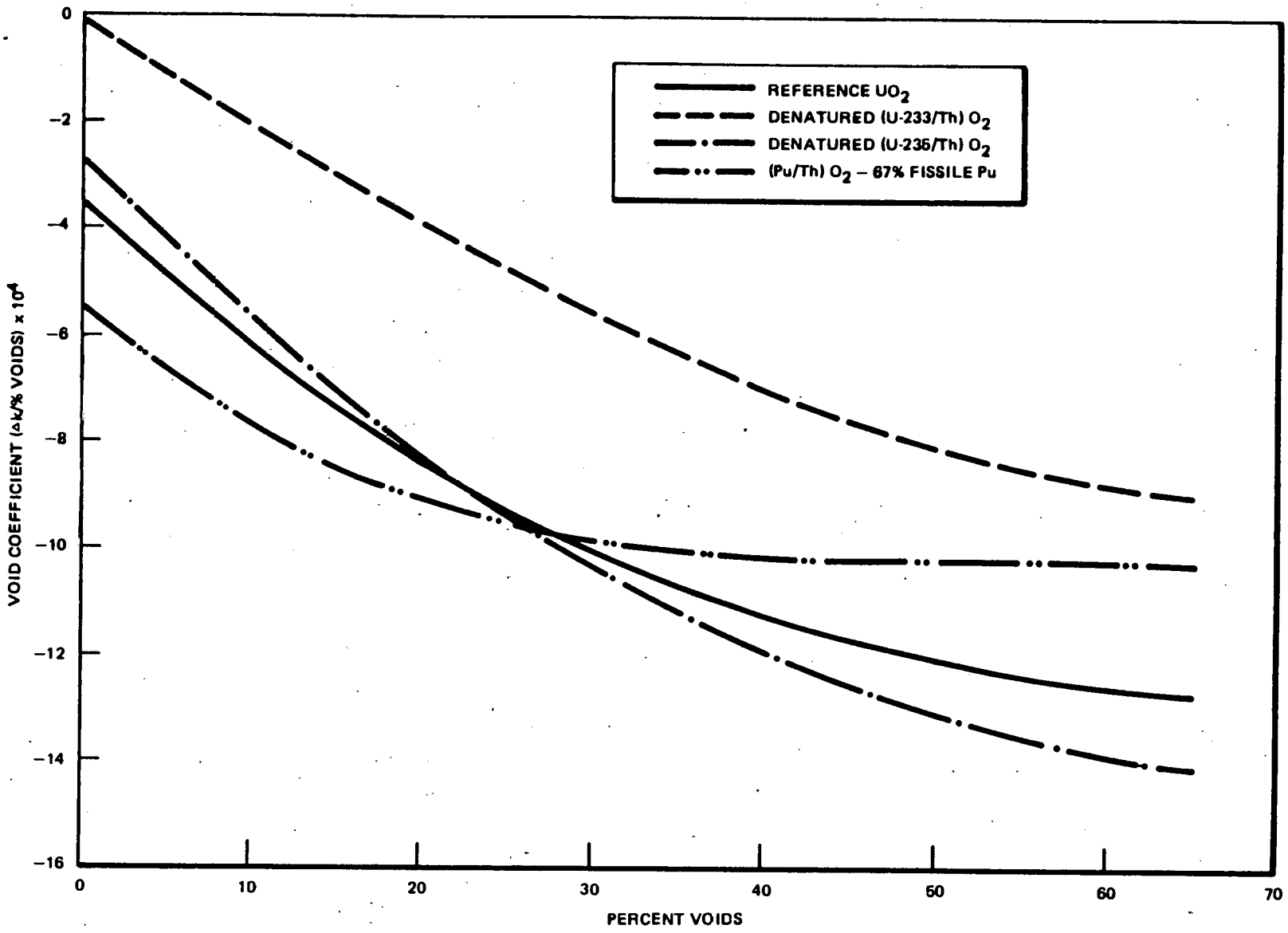

Figure 11-1. Point Model Void Coefficient versus Percent Voids

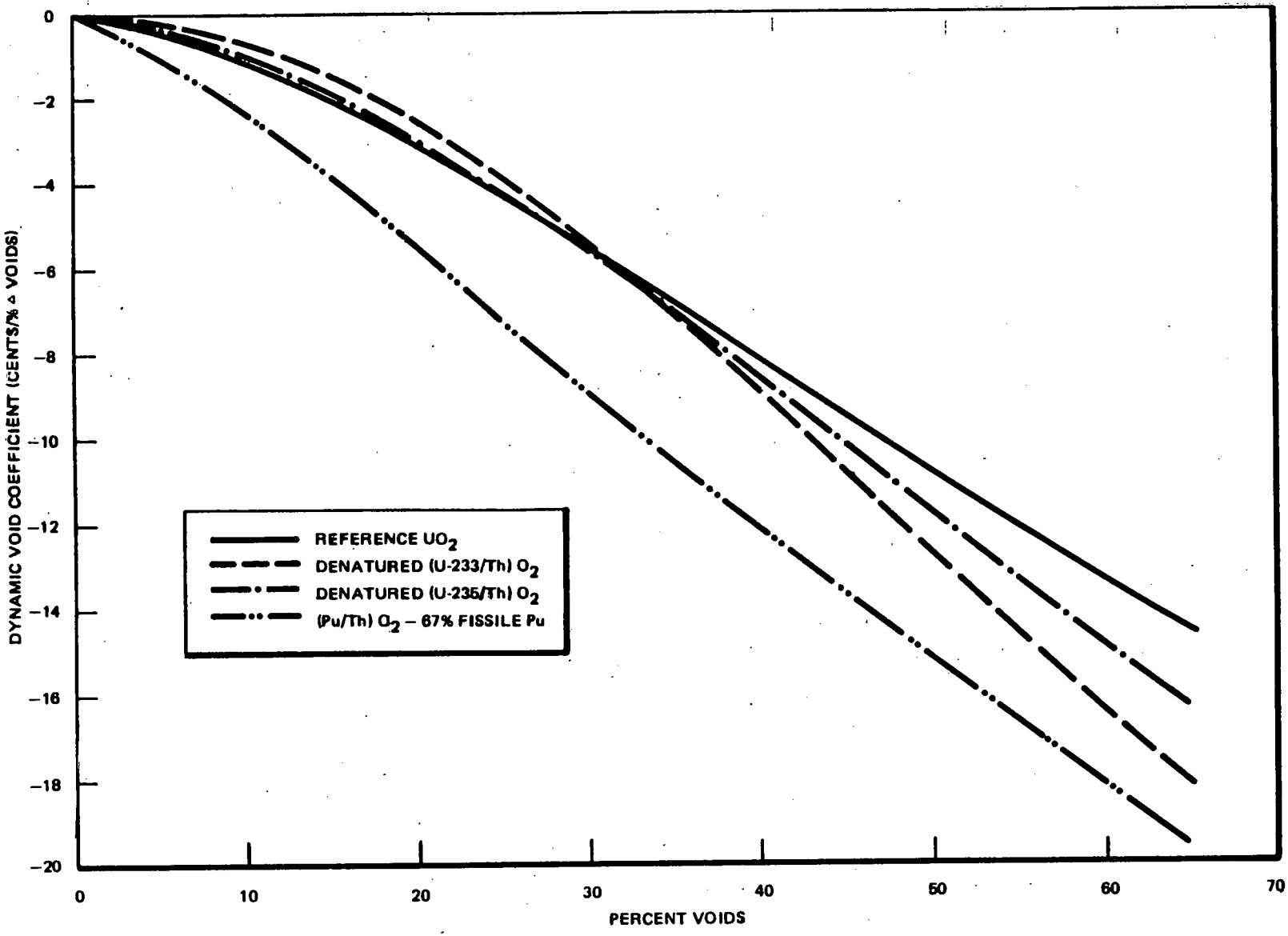

Figure 11-2. Point Model Dynamic Void Coefficient versus Percent Voids

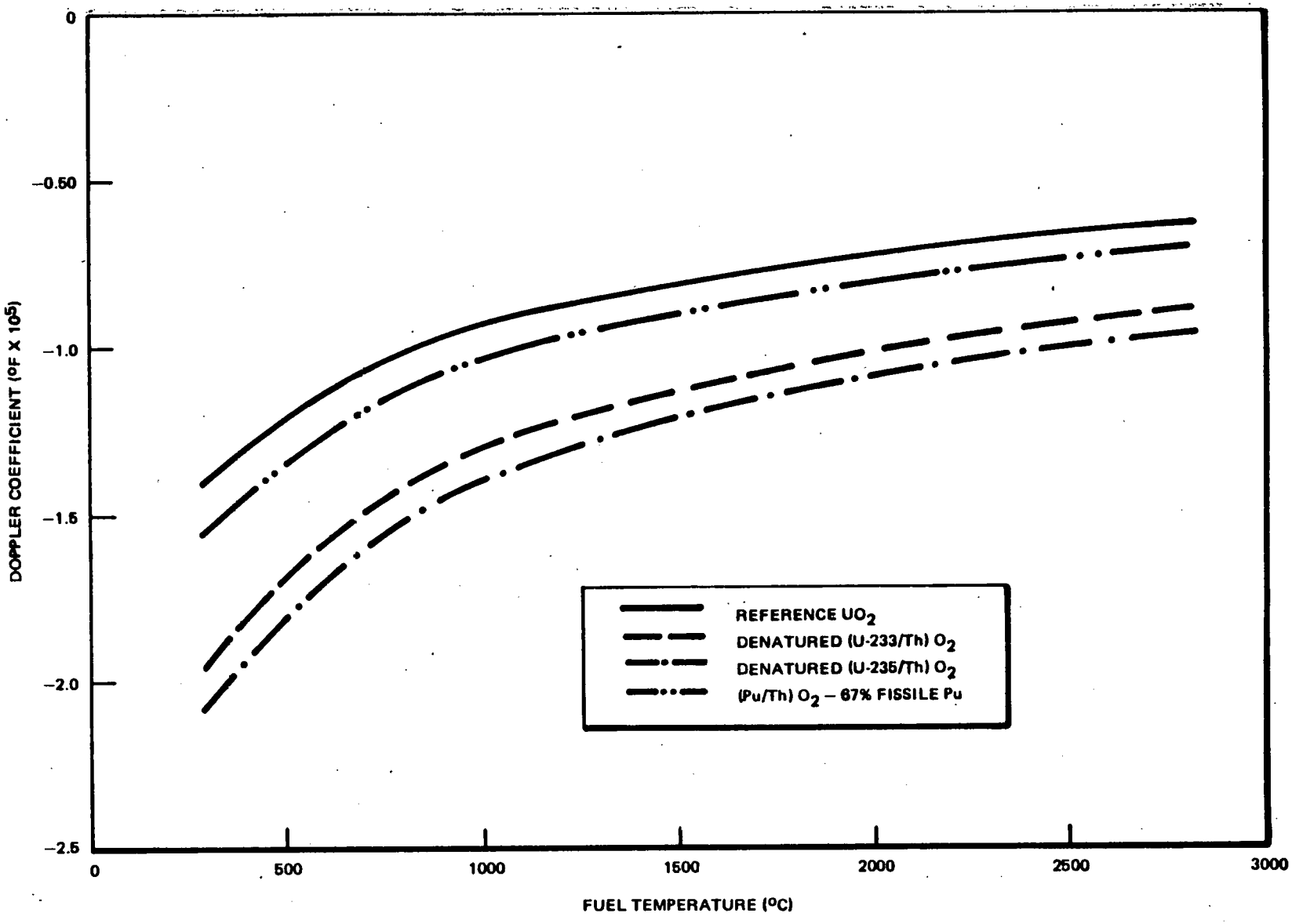

Figure 11-3. Point Model Doppler Coefficient versus Average Fuel Temperature

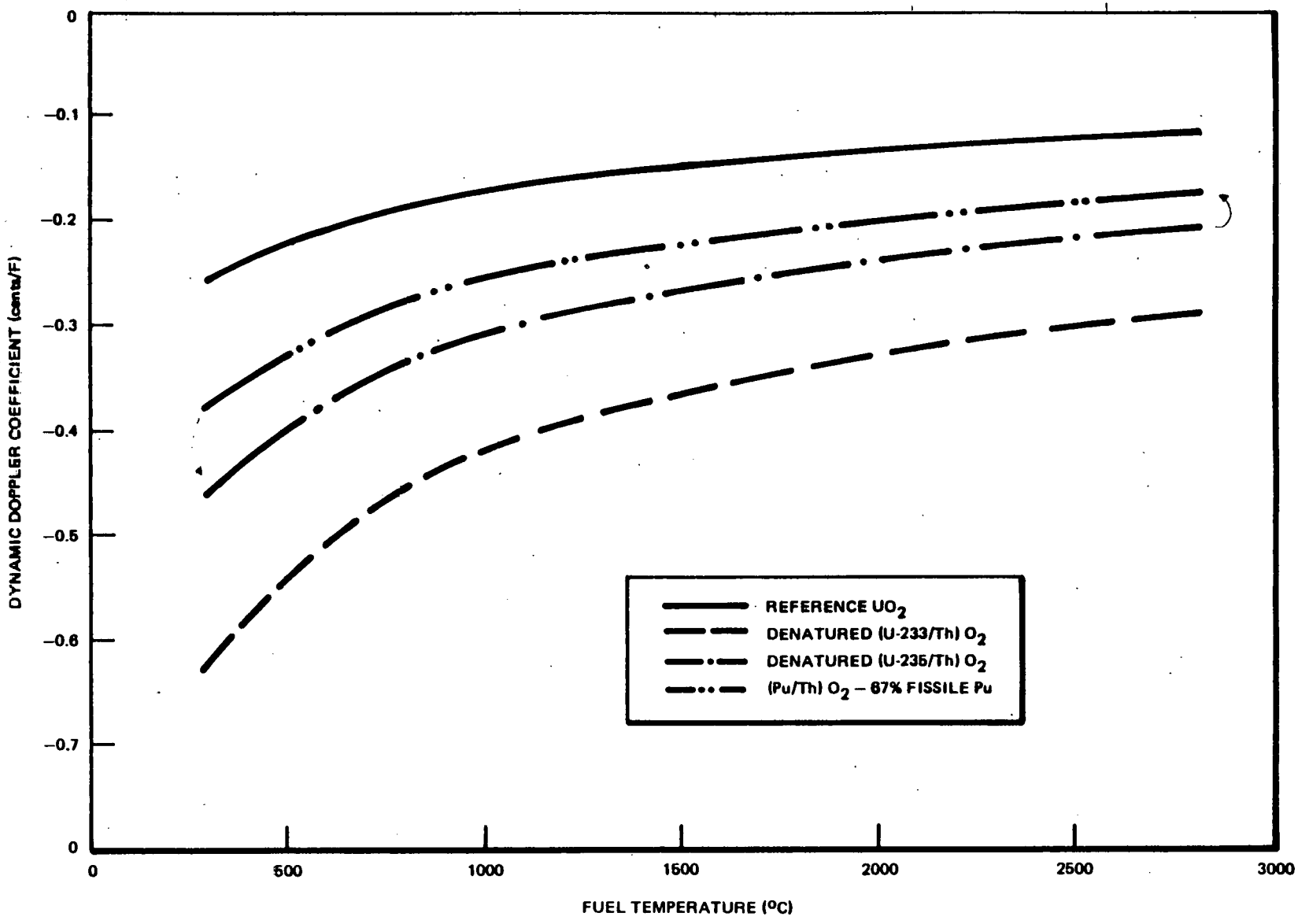

Figure 11-4. Point Model Dynamic Doppler Coefficient versus Fuel Temperature

Table 11-3

INFINITE LATTICE NEUTRON MULTIPLICATION FACTORS AND CONTROL BLADE PARAMETERS AT 16.5 GWd/MT

Conditions	Reference UO_2	Denatured $(U233/Th)O_2$	Denatured $(U235/Th)O_2$	$(Pu/Th)O_2$
Hot[1], 40% voids, uncontrolled	1.08564	1.08156	1.08479	1.08242
Hot, 40% voids, controlled	0.83845	0.83081	0.83054	0.88578
Cold[2], 0% voids, uncontrolled	1.13895	1.09862	1.14781	1.12484
Cold, 0% voids, controlled	0.95637	0.93259	0.97441	0.98240
Δk^∞ blade, hot	-0.2472	-0.2508	-0.2543	-0.1966
$\Delta k^\infty/k^\infty$ blade, hot	-0.2277	-0.2318	-0.2344	-0.1817
Blade reactivity[3], hot	-41.69	-74.59	-42.44	-54.95
Δk^∞ blade, cold	-0.1736	-0.1660	-0.1734	-0.1424
$\Delta k^\infty/k^\infty$ blade, cold	-0.1524	-0.1511	-0.1511	-0.1266
Blade reactivity, cold	-27.90	-48.62	-27.35	-38.30

(1) Hot conditions indicate a moderator temperature of 286°C and a fuel temperature of 610°C.
(2) Cold conditions indicate that moderator and fuel temperatures are equal at 20°C.
(3) Blade reactivity is in dollars [i.e., $(1/\beta)$ $(\Delta k^\infty/k^\infty)$ blade].

11.3 CORE PERFORMANCE AND THERMAL MARGINS

11.3.1 Input on Thermal Margin

BWR thermal margins such as the maximum linear heat generation rate (MLHGR) and the minimum critical power ratio (MCPR), depend to a significant degree on fuel bundle local (i.e., rod-to-rod) power distributions. In turn, the local power distributions are strongly dependent on the number and content of burnable poison rods in a fuel assembly. The fact that not all of the fuel bundle designs being considered were designed with burnable poison rods makes it difficult to draw definite conclusions about the thermal margins. In general, it is believed that a denatured (U-235/Th)O_2-fueled BWR would have thermal margins very similar to the reference UO_2 BWR. A (Pu/Th)O_2-fueled BWR would probably have reduced thermal margins. The very large thermal fission cross-sections of Pu-239 and Pu-241 cause a thermal flux depression across the fuel bundle which makes it difficult to design a flat local power distribution.

11.3.2 Cold Shutdown Margin

Designing for adequate cold shutdown margin should not be difficult for the denatured (U-235/Th)O_2 fuel design. A similar number of burnable poison rods with similar concentration of poison as used in the reference UO_2 design should prove acceptable. In the case of (Pu/Th)O_2, the effectiveness of the burnable poison (Gd_2O_3) is reduced due to the large (relative to U-235) thermal fission cross-sections of Pu-239 and Pu-241. Therefore, to obtain adequate cold shutdown margin for this design may require the use of more burnable poison rods or poison rods of higher concentration.

11.4 ACCIDENT RESPONSE

11.4.1 Rod Drop Accident and Rod Withdrawal Error

Judging the impact of these fuel designs on the rod drop accident and rod withdrawal error is difficult without knowing the three-dimensional power and void distributions. A primary factor in determining the impact of these

accidents is the control blade worth associated with a particular fuel design. In Table 11-3, it is seen that the hot blade worths of the reference UO_2 design and the denatured (U-235/Th)O_2 design are very similar. This, coupled with the more negative Doppler reactivity coefficient (Table 11-1) of the (U-235/Th)O_2 design, indicates that the denatured (U-235/Th)O_2-fueled BWR would meet the design basis safety criteria for these accidents. As shown in Table 11-3, the (Pu/Th)O_2 blade worths are significantly lower than those of the reference UO_2 design, indicating that the consequences of these accidents should be less severe for the (Pu/Th)O_2 design than for the reference case.

11.4.2 Loss-of-Coolant-Accident

In the study, it was found that the consequences of a loss-of-coolant-accident (LOCA) were not greatly impacted by the introduction of denatured (U-233/Th)O_2 fuel in a BWR. As both of these alternate designs are predominately thorium, it is expected that the LOCA results would not change radically relative to the reference UO_2 case.

11.5 TRANSIENT RESPONSE

Abnormal operating transients for a BWR are of two general types: (1) rapid core pressurization leading to positive reactivity insertion due to void collapse, and (2) slow but continuous reactivity insertion resulting in a pseudo-steady-state rise in core neutron flux and power. The limiting pressurization type transients are the load rejection without bypass, pressure regulator downscale failure, and the main steamline isolation valve closure. The feedwater controller failure and the loss of feedwater heating are the limiting pseudo-steady-state power increase transients.

11.5.1 Pressurization Type Transients

In all pressurization type transients, the dominant factor is the dynamic void reactivity coefficient. As core pressurization results in void collapse, the negative void reactivity coefficient of a BWR results in a positive reactivity insertion. The more negative the dynamic void reactivity coefficient associated

with a particular fuel type, the larger the positive reactivity insertion will be. The point model dynamic void reactivity coefficients (DVCs) for the four fuel types being considered are given in Table 11-1. In actual transient analyses, the three-dimensional (i.e., whole-core) DVC would be used; however, the trends illustrated by the point model values would also hold true in the three-dimensional case.

As seen in Table 11-1, the DVC for the denatured (U-235/Th)O_2 design is not substantially different than that of the reference UO_2 design. This, coupled with the fact that the dynamic Doppler reactivity coefficient (DDC) for the denatured (U-235/Th)O_2 design is significantly more negative than that of the UO_2 design (Doppler feedback tends to mitigate the impact of pressurization transients to some extent), indicates that the response of a BWR fueled with denatured (U-235/Th)O_2 to pressurization transients would be no more severe than that for the reference UO_2 plant.

The point model DVC of the (Pu/Th)O_2 design is approximately 48% more negative than that of the reference UO_2 design and the DDC is approximately two times as negative as the reference UO_2 value. These reactivity characteristics would result in a more severe response to pressurization transients for a (Pu/Th)O_2 fueled BWR. However, these transients would not be limiting.

11.5.2 Loss of Feedwater Heater

Under the current BWR design basis, the most limiting abnormal operating transient is the loss of feedwater heating (LFWH). This is a "slow" transient brought on by a gradual decrease in the feedwater inlet temperature following the feedwater heater failure. As feedwater temperature is reduced, core average voiding is also reduced leading to a positive reactivity insertion. This transient continues until ended by a scram induced by exceeding the estimated high heat flux trip level.

As in the pressurization type transients, a primary controlling factor in the LWFH transient is the void reactivity coefficient. Because the LFWH transient is a slow pseudo-steady-state event, the Doppler reactivity coefficient is of

more importance in this instance than in the more rapid transients. The importance of the Doppler feedback was demonstrated by the denatured (U-233/Th)O_2 case. The dynamic void reactivity coefficient for denatured (U-233/Th)O_2 is roughly 10% more negative than that of the reference UO_2 case. However, the denatured (U-233/Th)O_2 dynamic Doppler reactivity coefficient is nearly three times as large as that for UO_2, which resulted in improved response for the denatured (U-233/Th)O_2-fueled BWR during a LFWH transient relative to the reference UO_2 BWR.

Both the dynamic void reactivity and dynamic Doppler reactivity coefficients are slightly more negative for the denatured (U-235/Th)O_2 case than they are for the reference UO_2 case. Noting this and recalling the results of the denatured (U-233/Th)O_2 LFWH analysis, one would expect that the response to a LFWH transient would be a very similar for the denatured (U-235/Th)O_2 and reference UO_2-fueled BWRs.

While the dynamic Doppler reactivity coefficient for (Pu/Th)O_2 is roughly a factor of two times more negative than that for UO_2, its 48% more negative dynamic void reactivity coefficient would likely result in a more severe response to the LFWH transient. As the LFWH is typically the most limiting BWR transient, the worsened response to this transient may require additional safety system hardware to allow (Pu/Th)O_2 use in the BWR. A possible "fix" might be the addition of hardware which would initiate reactor scram at a preset feedwater inlet temperature and/or feedwater inlet temperature change.

11.6 BWR OPERABILITY

11.6.1 Power/Flow Control Line

The impact of a particular fuel design on BWR operability can to a large degree be determined by examining the effects of the fuel type on the power/flow control line and nuclear thermal-hydraulic stability. The most dominant factor in the determination of the power/flow control line is the steam void reactivity coefficient. A more negative steam void reactivity coefficient will result in a steeper flow control line, which in turn will enhance the load following capabilities of the BWR. In Table 11-1, it is seen that the

denatured (U-233/Th)O_2 steam void reactivity coefficient is substantially (~38%) less negative than that for the reference UO_2 design. However three-dimensional BWR simulator studies have shown that the flow control line for the denatured (U-233/Th)O_2-fueled BWR is only slightly flatter than that for the reference UO_2 BWR. Based on this result and noting that the steam void reactivity coefficients for both the denatured (U-235/Th)O_2 and (Pu/Th)O_2 design are much closer to the reference UO_2 design than those for the denatured (U-233/Th)O_2 design, one would not expect either of these fuel designs to have a large impact on the BWR flow control line.

11.6.2 Stability

Stability of a BWR is strongly affected by the magnitude of the dynamic void reactivity coefficient, with a more negative value leading to reduced stability. From Table 11-1, it is seen that the denatured (U-235/Th)O_2 dynamic void coefficient is only slightly (~5%) more negative than that of the reference UO_2 design and lies between the UO_2 and denatured (U-233/Th)O_2 values. Stability analyses for the denatured (U-233/Th)O_2-fueled BWR showed that stability would be somewhat reduced relative to the reference UO_2 plant; therefore, it appears that denatured (U-235/Th)O_2 would reduce BWR stability, but to a lesser degree than does (U-233/Th)O_2. The 48% more negative dynamic void coefficient of the (Pu/Th)O_2 fuel would have a significant detrimental impact on BWR stability. If the decreased stability is not too severe, it could be avoided by restricting the power/flow operating range of a (Pu/Th)O_2-fueled BWR.

12. RESEARCH, DEVELOPMENT, AND DEMONSTRATION REQUIREMENTS

The actions and associated estimated costs that would be necessary for successful implementation of thorium-based fuels in BWRs are summarized in Table 12-1.

Table 12-1

RD&D Requirements	Approximate Resources
Fuels	$ 20M - 30M
• Property measurements	
• Lead test assemblies	
• Segmented rod programs, including ramp tests	
• Fission gas	
• Fuels methods modification as needed	
Manufacturing Development	$ 20M - 200M
Nuclear	$ 5M - 6M
• Improved Th-232 cross-section	
• Critical experiments (high-temperature)	
• Gamma scan, isotopics, burnup measurements on LTAs	
• Cold shutdown measurements	
• Nuclear methods modification as needed	
Licensing	$ 2M - 5M
• Methods improvements	
• Analysis based on fuels and nuclear measurements	
• NRC review and acceptance	
Full-Scale Demonstration (Four Reloads in Sequence)	$ 10M - 15M
• Fuel measurements (confirmation of reliability)	
• Nuclear measurements (gamma scan, criticality)	
• Transient and stability measurements (pressure transient, pressure oscillation)	
TOTAL REQUIRED:	$ 60M - 260M

The total cost of implementation of thorium/U-233/U-238 fuels in the BWR would range between 60 and 260 million dollars, depending on the amount of detailed effort required in each phase.

13. REFERENCES

1. H. E. Williamson, "Assessment of Utilization of Thorium in BWRs," January 1978 (NEDG-24073).

2. H. E. Williamson, "Appraisal of BWR Plutonium Burners for Energy Centers," January 1976 (GEAP-11367).

3. J. A. Woolley, "Three-Dimensional BWR Core Simulator" (NEDO-20953-A).

4. C. L. Martin, "Lattice Physics Methods," July 1976 (NEDO-20913).

5. J. M. Sorensen, "CHAST06 Core Heatup Analysis Model Technical Description," November 1977 (NEDO-23728).

6. "One-Dimensional Core Transient Model," October 1978 (NEDO-24154).

7. R. B. Linford, "Analytical Methods of Plant Transient Evaluations For The General Electric Boiling Water Reactor," February 1973 (NEDO-10802).

8. Perry Nuclear Power Plant Units 1 and 2 Preliminary Safety Analysis Report.

9. E. B. Johansson, G. A. Potts and R. A. Rand, "GESTR - A Model For the Prediction of GE BWR Fuel Rod Thermal/Mechanical Performance," March 1978 (NEDO-23785).

10. "Stability and Dynamic Performance of The General Electric Boiling Water Reactor," January 1977 (NEDO-21506).

11. BNL-325, 3rd Edition.

12. J. H. Kittel, et al., "Properties of Fuels for Alternate Fuel Cycles," May 1977 (ANL-AFP-38).

13. Joanne K. Fink, Martin G. Chasanon, and Leonard Leibowitz, "Thermophysical Properties of Thorium and Uranium System for Use In Reactor Safety Analysis," June 1977 (ANL-GEN-FSD-77-1).

14. J. Belle and R. M. Berman, "Properties of Thoria and Thoria-Urania: A Review," June 1978 (WAPD-TM-1340).

15. T. R. England, R. E. Schenter, and F. Schmittroth, "Integral Decay-Heat Measurements and Comparisons to ENDF/B-IV and V," August 1978 (NUREG/CR-0305)

16. "General Electric BWR Thermal Analysis Basis (GETAB): Data, Correlation and Design Application" (NEDO-10958).

17. "General Electric Company Model For Loss-of-Coolant Analysis In Accordance With 10CFR50, Appendix K" (NED-20566).

18. ASME Boiler and Pressure Vessel Code, Section III, Class 1.

APPENDIX

SAR FOR A DENATURED (U-233/Th)O_2-FUELED STANDARD BWR

15.1.3 Generator Load Rejection - Turbine Control Valve (TCV) Fast Closure

15.1.3.1 Identification of Causes

Same as given in Appendix*. Table 15.1-1 gives sequence of events.

15.1.3.2 Analysis of Effects and Consequences

The predicted dynamic behavior has been determined using a computer simulated, analytical model of a generic direct-cycle BWR. This computer model has been verified through extensive comparison of its predicted results with actual BWR test data.

15.1.3.2.1 Methods

The nonlinear computer simulated analytical model is designed to predict associated transient behavior of this reactor. Some of the significant features of the model are:

a. A one-dimensional 24 axial node kinetic model is assumed with reactivity feedbacks from control rods (absorption), voids (moderation) and Doppler (capture) effects.

b. At each axial location the average fuel element is represented by seven (7) cylindrical nodes encased in a cladding node. This element is used to represent core average power and fuel temperature conditions, providing the source of Doppler feedback.

c. Thirty-four primary system pressure nodes are simulated:

   (1) Upper plenum pressure;
   (2) Vessel dome pressure;
   (3) Eight steamline nodal pressures;
   (4) Twenty-four reactor core nodal pressures.

d. One-dimensional nuclear parameters are obtained from a steady-state 3-D BWR core simulator. Axial void variation is determined from multinodal transient core calculations. Heat fluxes are obtained from the average fuel model and transient nuclear solution.

e. Principle controller functions such as feedwater flow, recirculation flow, reactor water level, pressure, and load demand are represented together with their dominant nonlinear characteristics.

f. The ability to simulate necessary reactor protection system functions is provided.

15.1.3.2.2 Assumptions and Conditions

Same as given in Appendix.

15.1.3.2.3 Results and Consequences

* Appendix = Perry Nuclear Power Plant Units 1 & 2
Preliminary Safety Analysis Report,
Volume 9

15.1.3.2.3.1 Generator Load Rejection with Bypass

Not analyzed since Generator Load Rejection Without Bypass is more severe.

15.1.3.2.3.2 Generator Load Rejection with Bypass Valve Failure

The most severe transient (assuming the worst single failure) for a full power Generator Load Rejection occurs if the turbine bypass valves fail to operate. Figure 15.1-1 shows that, assuming the initial reactor power level is 104.2% NBR*, the neutron flux peaks at 140% NBR and the average surface heat flux peaks at approximately 106% NBR. Since this event is classified as an infrequent incident, it is not limited by the GETAB** criteria and the MCPR*** limit is permitted to fall below the safety limit for the incidents of moderate frequency. MCPR remains above 1.07 for this event and the peak vessel bottom pressure is 1229 psig, below the design pressure limit of 1375 psig.

15.1.3.2.3.3 Consideration of Uncertainties

The full stroke closure rate of the turbine control valve of 0.15 second is conservative. Typically, the actual closure rate is closer to 0.20 seconds. Clearly, the less time for closure, the more severe the pressurization effect.

All systems utilized for protection in this event were assumed to have the poorest allowable response (e.g., the relief set points, scram stroke time and nuclear characteristics-EOEC). Expected plant behavior is, therefore, expected to reduce the actual severity of the transient.

* NBR = Nuclear Boiler Rated

** GETAB = General Electric BWR Thermal Analysis Basis

*** MCPR = Minimum Critical Heat Flux Ratio

15.1.6 Pressure Regulator Failure

15.1.6.1 Pressure Regulator Failure (Open)

Not considered since Pressure Regulator Downscale Failure is more severe.

15.1.6.2 Pressure Regulator Failure (Closed)

15.1.6.2.1 Identification of Causes

15.1.6.2.1.1 Starting Conditions and Assumptions

The reactor is initially operating at 104.2% of NBR power with vessel dome pressure at 1060 psig.

15.1.6.2.1.2 Event Description

Two identical pressure regulators are provided to maintain primary system pressure control. They independently sense pressure just upstream of the main turbine stop valves and compare it to two separate set points to create proportional error signals that produce each regulator output. The output of both regulators feeds in a high valve gate. The regulator with the highest output controls the main turbine control valves. The lowest pressure set point gives the largest pressure error and thereby largest regulator output. The backup regulator is set 5 psi higher giving a slightly smaller error and a slightly smaller effective output of the controller.

It is assumed for purposes of this transient analysis that a single failure occurs which erroneously causes the controlling regulator to close the main turbine control valves and thereby increases reactor pressure. If this occurs, the backup regulator is ready to take control.

It is also assumed for purpose of this transient analysis that a single failure occurs which causes a downscale failure of the pressure regulation demand to zero (e.g., high valve gate downscale failure). Should this occur, it could cause full closure of turbine control valves as well as an inhibit of steam bypass flow and thereby increase reactor power and pressure. When this occurs, reactor scram will be initiated when high neutron flux scram set point is reached.

The sequence of event is given in Table 15.1-2.

15.1.6.2.1.3 Identification of Operator Actions

The operator should:

a. Monitor that all rods are in.

b. Monitor reactor water level and pressure.

c. Observe turbine coastdown and break vacuum before loss of steam seals. Check turbine auxiliaries.

d. Observe that the reactor pressure relief valves open at their set point.

e. Monitor reactor outer level and continue cooldown per normal procedure.

f. Complete the scram report and initiate a maintenance survey of pressure regulator before reactor restart.

15.1.6.2.2 Analysis of Effects and Consequences

15.1.6.2.2.1 Methods

The non-linear dynamic model described briefly in Subsection 15.1.3 is used to simulate this event.

15.1.6.2.2.2 Assumptions and Conditions

Analysis of this event assumes normal functioning of plant instrumentation and controls, and plant protection and reactor protection systems. Specifically this transient takes credit for high neutron flux scram to shut down the reactor. The nature of the first failure produces a slight pressure increase in the reactor until the backup regulator gains control, since no other action is significant in restoring normal operation. If the backup regulator fails at this time, the second assumed failure, the control valves would begin to close, raising reactor pressure to the point where a flux scram trip would be initiated to shut down the reactor.

15.1.6.2.2.3 Results and Consequences

Figure 15.1-2 shows a pressure regulation downscale failure simulated at 104.2% NB rated steam flow condition, initially. Neutron flux increases rapidly because of the void reduction caused by the pressure increases. When the sensed neutron flux reaches the high neutron flux scram set point, a reactor scram is initiated. The neutron flux increase is limited to 156% NB rated value by the reactor scram. Peak fuel surface heat flux does not exceed 106% NB rated and MCPR remains above the safety limit MCPR, 1.07. Peak pressure at the safety/relief valves reaches 1181 psig. The peak nuclear system pressure reaches 1223 psig, well below the nuclear barrier transient pressure limit of 1375 psig.

15.1.6.2.2.4 Consideration of Uncertainties

All systems utilized for protection in this event were assumed to have the poorest allowable response (e.g., relief set points, scram stroke time and nuclear characteristics). Expected plant behavior is, therefore, expected to reduce the actual severity of the transient.

15.1.7 Excess Coolant Inventory

15.1.7.1 Identification of Causes

15.1.7.1.1 Starting Conditions and Assumptions

The reactor is initially operating at 104.2% NBR power level at 100% NBR core flow with the vessel dome pressure = 1060 psig.

15.1.7.1.2 Event Description

An event that can directly cause excess coolant inventory is one in which feedwater flow is increased without changing other reactor parameters. The applicable event is a feedwater controller failure to maximum flow demand, 130% NB rated. The feedwater controller is forced to its upper limit at time = 0. With the advent of the excess feedwater flow, the water level rises to the high level reference point, at which time the feedwater pumps and the main turbine are tripped and a scram is initiated. Table 15.1-3 shows the sequence of events.

15.1.7.1.3 Identification of Operator Actions

The operator should:

a. Observe that high feedwater pump trip has terminated the failure event.

b. Switch the feedwater controller from automatic to manual control in order to try to regain a correct output signal.

c. Identify causes of the failure and report all key plant parameters during the event.

15.1.7.2 Analysis of Effects and Consequences

15.1.7.2.1 Methods, Assumptions and Conditions

Same as given in Appendix.

15.1.7.2.2 Results and Consequences

Figure 15.1-3 shows the transient response to a feedwater controller failure. The high water level turbine trip and feedwater pump trip are initiated at approximately 11.6 seconds. Simultaneously, stop valve closure initiates scram. This limits the neutron flux peak to 113% NBR and average surface heat flux to 109% NBR so that the design basis is satisfied. The turbine bypass system and some of the relief valves open to limit peak steamline pressure to 1155 psig and peak vessel bottom pressure to 1187 psig, well below the design pressure limit of 1375 psig. The relief valves close in approximately 4 seconds to re-establish pressure control in the vessel during shutdown.

The water level will gradually drop to the low level reference point (Level 2) activating the RCIC/HPCS* for long term level control.

15.1.7.2.3 Considerations of Uncertainties

Same as given in Appendix.

* RCIC/HPCS • Reactor Containment Isolation Coolant / High Pressure Core Spray

15.1.8 Loss of Feedwater Heater

15.1.8.1 Identification of Causes

Same as given in Appendix with the exception that the initial power level is = 104.2 NB rated power level. Table 15.1-4 gives sequence of events.

15.1.8.2 Analysis of Effects and Consequences

15.1.8.2.1 Methods, Assumptions and Conditions

The detailed, nonlinear dynamic model described in Subsection 15.1.3 of the Appendix is used to simulate this event, since currently the 1-D transient analysis used for evaluation of the previously discussed transients is not qualified to analyze a loss of feedwater heater. The valves for both the feedwater heater time constant and the feedwater time volume between the heaters and the sporgers are adjusted to reduce the time delays since they are not critical to the calculation of this transient. The transient is simulated by programming a change in feedwater enthalpy corresponding to a 100°F loss in feedwater heating.

15.1.8.2.2 Results and Consequences

Figure 15.1-4 shows the transient response to a loss of feedwater heater, 100°F. In manual mode no compensation is provided by core flow, consequentially the power increase is greater than in the automatic mode. Scram occurs at approximately 92 seconds on high APRM simulated thermal power. Vessel steam flow increases and the initial system pressure increase is slightly larger. Peak heat flux is 119% of its initial valve and average fuel temperature increases 120°F. The increased core inlet subcooling aids core thermal margins and MCPR remains above the safety limit, 1.07. Therefore, the design basis is satisfied. Vessel and steamline pressures do not rise significantly. Therefore, the system pressures remain below the design limit 1375 psig. After the reactor scram, the water level drops to the low level trip point for recirculation pump trip.

This transient is less severe from lower power levels for two main reasons:

(1) lower initial power level will have initial values greater than the limiting initial value assumed.

(2) the magnitude of the power rise decreases with lower initial power conditions. Therefore, transients from lower power levels will be less severe.

15.1.8.2.3 Considerations of Uncertainties

Important factors (such as reactivity coefficient, scram characteristics, magnitude of the feedwater temperature change) are assumed to be at the worst configuration. Therefore, any deviations observed in the actual plant operation reduce the severity of the event.

15.1.11 Continuous Control Rod Withdrawal During Power Range Operation

15.1.11.1 Identification of Causes

15.1.11.1.1 Starting Conditions and Assumptions

The Rod Withdrawal Error (RWE) transient results from a procedural error by the operator in which a single control rod or a gang of control rods is withdrawn continuously until the Rod Withdrawal Limiter (RWL) function of the Rod Control and Information System (RCIS) blocks further withdrawal. The reactor operator has followed procedures and up to the point of the withdrawal error is in a normal mode of operation (i.e., the control rod pattern, flow setpoint, etc., are all within normal operating limits). For these conditions it is assumed that the withdrawal error occurs with the maximum worth control rod. Therefore, the maximum positive reactivity insertion will occur.

15.1.11.1.2 Event Description

While operating in the power range in a normal mode of operation the reactor operator makes a procedural error and withdraws the maximum worth control rod to its fully withdrawn position. Due to this positive reactivity insertion, the core average power will increase. More importantly, the local power in the vicinity of the withdrawn control rod will increase and potentially could cause localized fuel failures due to either achieving critical heat flux (CHF) or by exceeding the 1% plastic strain limit imposed on the cladding as the transient failure threshold.

SEQUENCE of EVENTS

Elapsed Time	Event
0	Core is operated in a typical control rod pattern on limits.
0	Operator withdraws a single rod or gang of rods continuously.
∿ 1 sec	The local power in the vicinity of the withdrawn rod (or gang) increases. Gross core power increases.
∿ 6 sec*	RWL blocks further withdrawal.
∿25 sec	Core stabilizes at slightly higher core power level.

* For a 1.5 foot RWL incremental withdrawal block. Time would be longer for a larger block since rods are withdrawn at approximately 3 inches/second.

15.1.11.1.3 Identification of Operator Actions

Under most normal operating conditions, no operator action will be required since the transient which will occur will be very mild. If the peak linear power design limits are exceeded, the nearest local power range monitors (LPRM's) will detect this phenomenon and sound an alarm. The operator must acknowledge this alarm and take appropriate action to rectify the situation.

If the rod withdrawal error is severe enough, the rod block monitor (RBM) system will sound alarms, at which time the operator must acknowledge the alarm and take corrective action. Even for extremely severe conditions (i.e., for highly abnormal control rod patterns, operating conditions, and assuming that the operator ignores all alarms and warnings and continues to withdraw the control rod) the RBM system will block further withdrawal of the control rod before fuel damage occurs.

15.1.11.2 Analyses of Effects and Consequences

15.1.11.2.1 Method, Assumptions and Conditions

The consequences of a rod withdrawal error are calculated utilizing a three-dimensional, coupled nuclear-thermal-hydraulics computer program. This model calculates the changes in power level, power distribution, core flow and critical power ratio under steady state conditions, as a function of control blade position. For this transient, the time for reactivity insertion is greater than the fuel thermal time constant and core-hydraulic transport times, so that the steady state assumption is adequate.

The reactor core is assumed to be on MCPR and MLHGR technical specification limits prior to RWE initiation. A statistical analysis of the ΔMCPR (Minimum Critical Power Ratio) response to ganged rod withdrawals initiated from a wide range of operating conditions (exposure, power, flow, rod patterns, xenon conditions, etc.) has been performed establishing allowable rod withdrawal increments applicable to all BWR/6 plants. These rod withdrawal increments were determined such that the design basis ΔMCPR (difference between technical specification MCPR limit and safety MCPR) for rod withdrawal errors initiated from the technical specification operating limit and mitigated by the rod withdrawal limiter system withdrawal restrictions provides a 95% probability at the 95% confidence level that any randomly occurring rod withdrawal error will not result in a larger ΔMCPR. MCPR was verified to be the limiting thermal performance parameter establishing the allowable withdrawal increments. Cladding 1% plastic strain limits were always a less limiting parameter.

Based on these generic studies, the allowable rod withdrawal distances for the Rod Block Monitor System were established as shown below.

Power Range (% of rated)	Allowable Withdrawal Distance
70% - 100%	1.0 feet
20% - 70%	2.0 feet
0% - 20%	No Restrictions*

* The BPWS function of the RCIS provides control of rod withdrawals below the 20% power setpoint and allows a maximum withdrawal distance of 9 feet.

15.1.11.2.2 Results and Consequences

To demonstrate that a rod withdrawal error in a BWR fueled with denatured (U-233/Th)O_2 will not result in localized or gross fuel damage the RWE analysis was conducted at the most reactive point in the equilibrium cycle at 100% power conditions. The most reactive control rod and control rod gang were then withdrawn in two foot increments until the fully withdrawn position was attained. The ΔMCPR's that resulted from each incremental control rod movement are shown in Table 15.1-5 . Using these values, it was determine that the maximum ΔMCPR which would result from a one foot withdrawal was 0.058 for a single control rod and 0.071 for a control rod gang. As the technical specification MCPR is 1.23 neither of these ΔMCPR's would result in an MCPR below the safety limit MCPR of 1.07.

TABLE 15.0-1

INITIAL CONDITIONS FOR TRANSIENTS AND ACCIDENTS

Thermal Power, MWt Analysis Value(104.2% NBR*)	3729
Feedwater Flow,lb/sec	4489
Core Flow,lb/sec	28889
Turbine Steam Flow,lb/sec	4489
Vessel Core Pressure,psig	1045
Vessel Dome Pressure,psig	1056
MCPR Operating Limit	1.23
MCPR Safety Limit For Incidents of Moderate Frequency	1.07
High Flux Trip,%NBR(122x1.042)	127.2
High Pressure Scram Setpoint,psig	1095
Vessel Level Trips,Feet Above Separator Skirt Bottom	
Level 8 (L8),feet	5.89
Level 4 (L4),feet	4.04
Level 3 (L3),feet	2.165
Level 2 (L2),feet	1.739
APRM** Simulated Thermal Power Trip Scram Setpoint,%NBR	118.8
Safety/Relief Valve Capacity,%NBR	108.5 @ 1210 psig
Recirculation Pump Trip (RPT) Delay Time,sec	.14
Safety/Relief Valve Pressure Setpoints,psig	
Safety Function	1175,1185,1195,1205,1215
Relief Function	1125,1135,1145,1155
Safety/Relief Valve Re-closure Setpoints,% of Closure Setpoints	98

*NBR- Nuclear Boiler Rated **APRM- Average Power Range Monitors

TABLE 15.1-1

SEQUENCE OF EVENTS FOR GENERATOR LOAD REJECTION WITHOUT BYPASS

TIME - SEC	EVENT
(-) 0.015 (Approx.)	Turbine generator detection of loss of electrical load.
0	Turbine-generator power load unbalance (PLU) devices trip to initiate turbine control valve fast closer.
0	Turbine bypass valves fail to operate.
0	Fast control valve closure (FCV) initiates scram trip.
0	Fast control valve closure (FCV) initiates a recirculation pump trip (RPT).
0.07	Turbine control valves closed.
1.1	Safety/Relief valves open due to high pressure.
∿5.1	Vessel water level (L8) trip initiates trip of feedwater turbines.
∿8.5	Safety/Relief valves close.
∿9.3	Group/safety/relief valves open again to relieve decay heat.
>10. (est.)	Group/safety/relief valves close again

TABLE 15.1-2

SEQUENCE OF EVENT FOR PRESSURE REGULATOR DOWNSCALE FAILURE

TIME-SEC	EVENT
0	Simulate zero steam flow demand to main turbine and bypass valves.
0	Turbine control valves start to close.
1.1	Neutron flux reaches high flux scram set point and initiates reactor scram.
2.4	Recirculation pump drive motors are tripped due to high dome pressure
2.4	Safety/Relief valves open due to high pressure.
∿6.1	Vessel water level (L8) trip initiates main turbine and feedwater turbine trip.
∿6.2	Main turbine stop valves closed.
∿9.3	Safety/Relief valves close.
∿9.7	Group/safety/relief valves open again to relieve decay heat.
>15 (est.)	Group/safety/relief valves close.

TABLE 15.1-3

SEQUENCE OF EVENTS FOR FEEDWATER CONTROLLER FAILURE

TIME - SEC	EVENT
0	Initiate simulated failure of 130% upper limit at system design pressure of 1065 psig on feedwater flow.
11.6	L8 vessel level set point initiates reactor scram and trips main turbine and feedwater pumps.
11.7	Recirculation pump trip (RPT) actuated by stop valve position switches.
11.7	Main turbine bypass valves opened due to turbine trip.
13.2	Safety/relief valves open due to high pressure.
18.4	Safety/relief valves close.
>20 (est.)	Water level dropped to low water level set point (Level 2).
>50 (est.)	RCIC and HPCS flow into vessel (not simulated).

TABLE 15.1-4

Sequence of Events for 100°F Loss of Feedwater Heater

TIME - SEC	EVENT
0	Initiate a 100°F temperature reduction into the feedwater systems.
5	Initial effect of unheated feedwater starts to raise core power level and steam flow.
7	Turbine control valves start to open to regulate pressure.
92	APRM initiates reactor scram on high thermal power.
134	Narrow range sensed water level reaches Level 3 (L3) set point.
134	Recirculation pump trip initiated due to Level 3 trip.
>150 (est.)	Wide range sensed water level reaches Level 2 (L2) set point.
	HPCS/RCIC flow enters vessel (not simulated)
	Reactor variables settle into limit cycle.

TABLE 15.1-5

Error Rod or Gang Withdrawal Increment *	ΔMCPR for Single Control Rod	ΔMCPR for Control Rod Gang
1	-0.026	-0.049
2	-0.056	-0.142
3	-0.115	-0.094
4	-0.060	-0.056
5	-0.003	-0.003
6	0.030	0.014

* Each increment represents a two foot withdrawal.

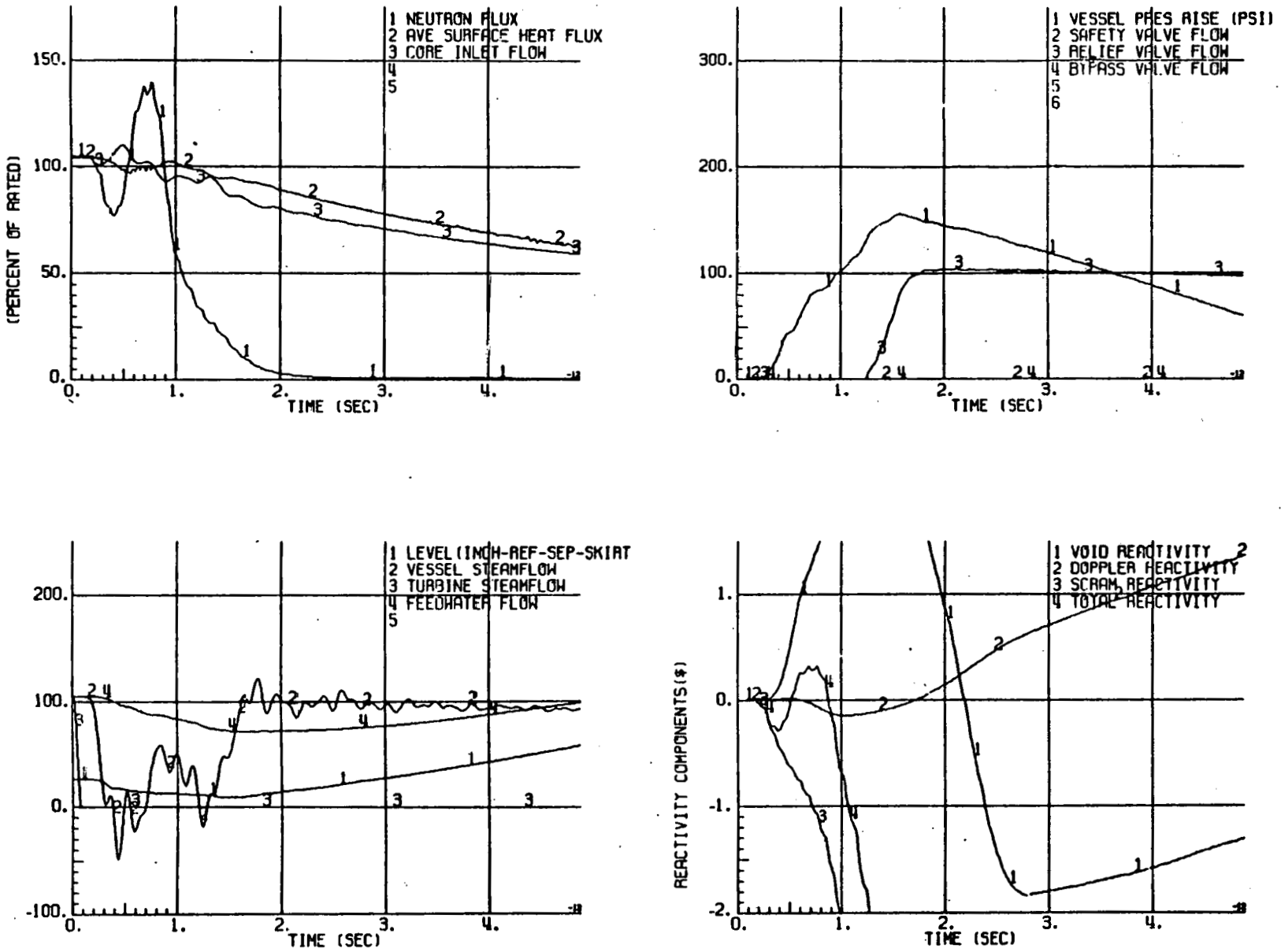

Figure 15.1-1. Generator Load Rejection, without Bypass

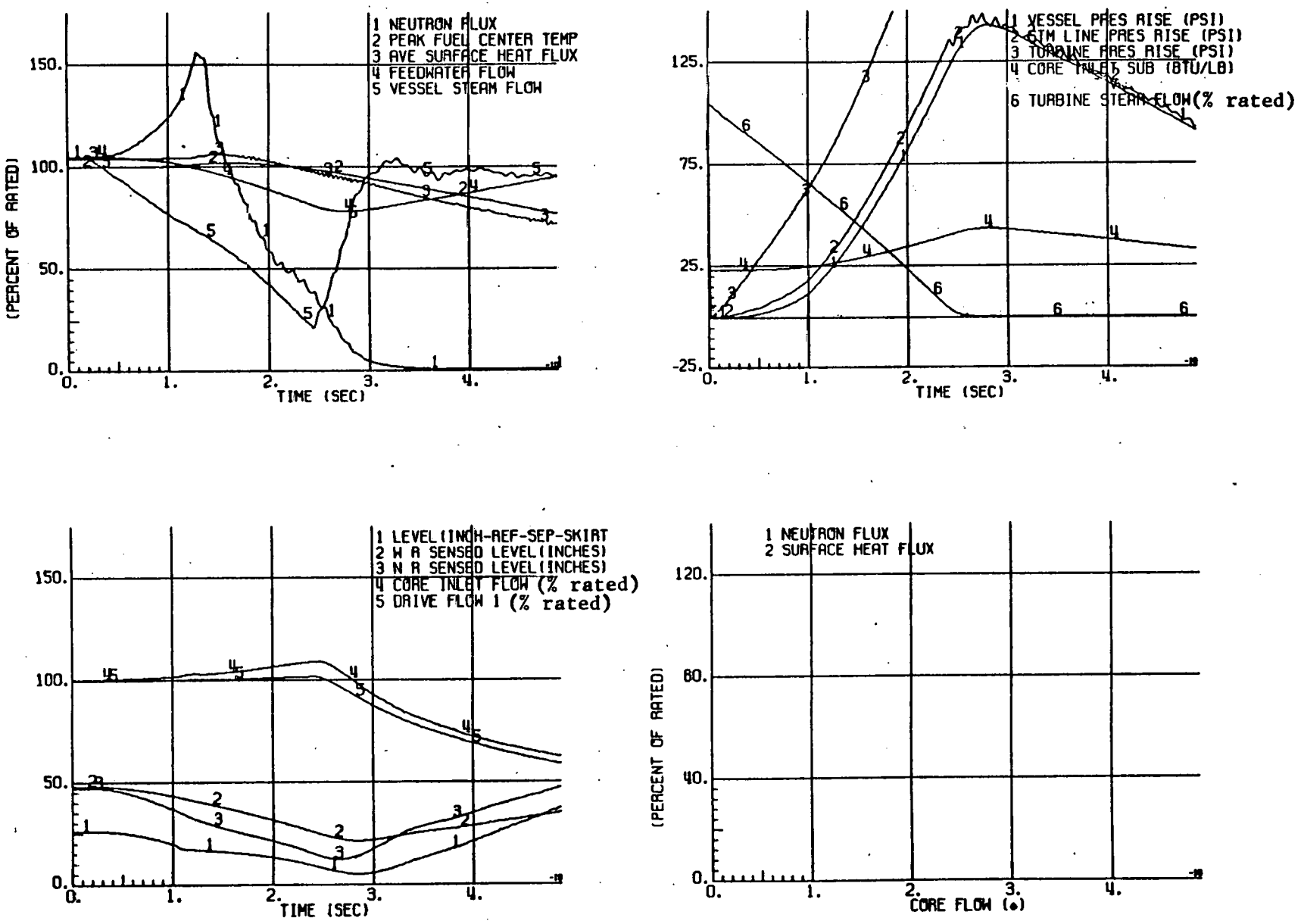

Figure 15.1-2. Pressure Regulator Downscale Failure

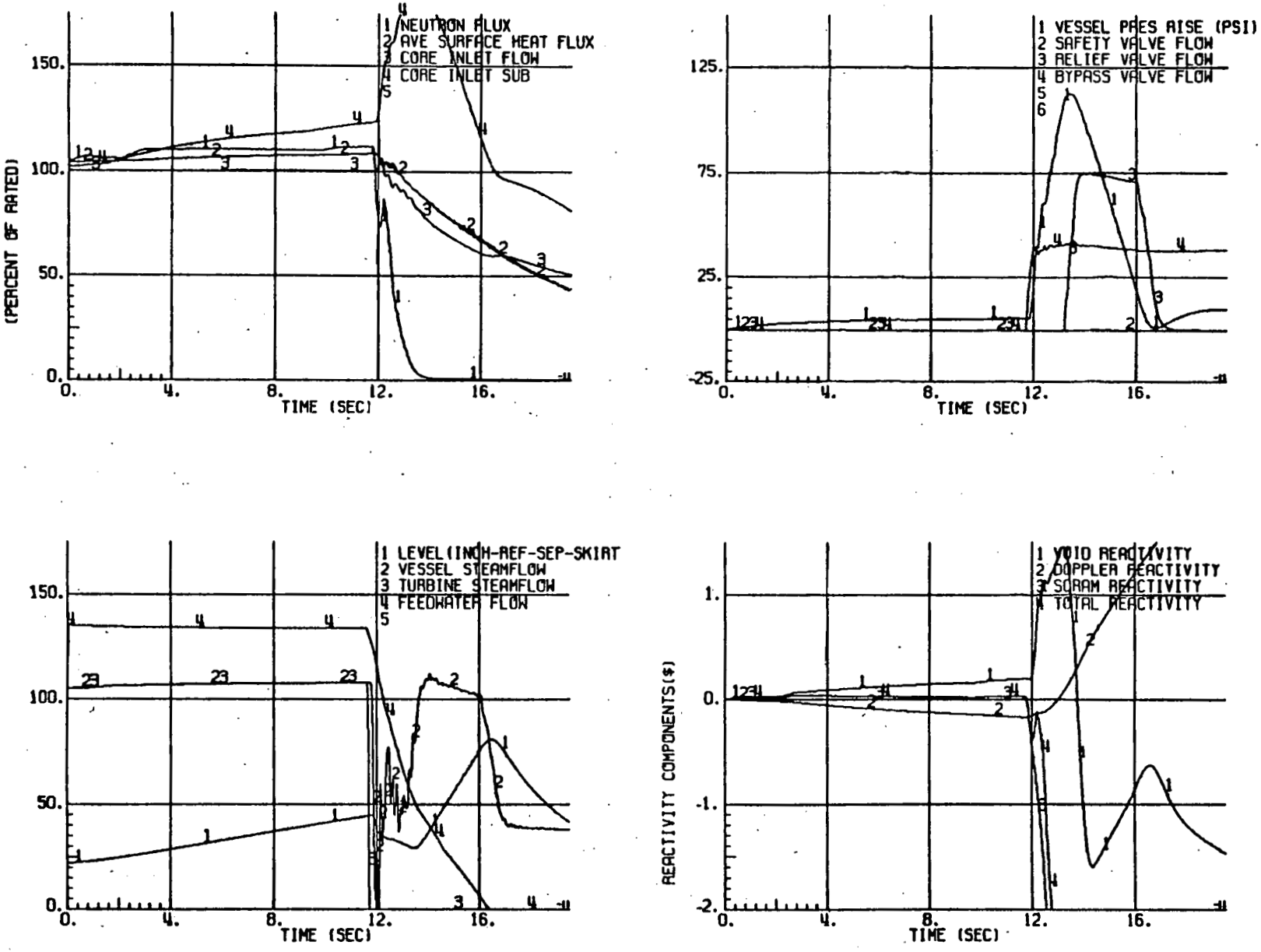

Figure 15.1-3. Feedwater Controller Failure, Maximum Demand, with High Water Level Trips

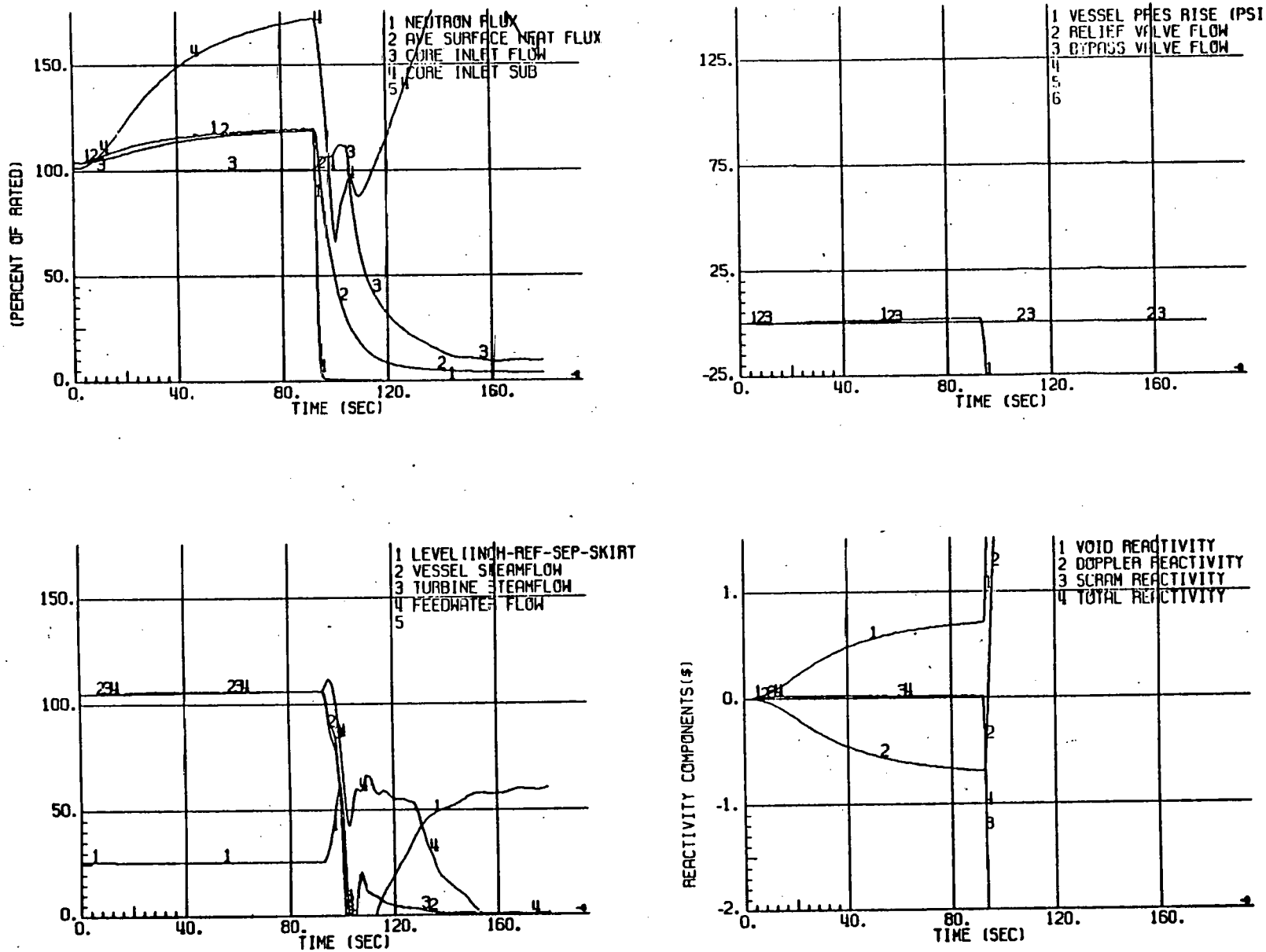

Figure 15.1-4. Loss of 100 degree F Feedwater Heating, MFC